UNIVERSITY OF CALIFORNIA, SAN DIEGO

TRANSDUCING VOLTAGE CHANGES IN BIOLOGICAL SYSTEMS TO FLUORESCENT SIGNALS VIA SMALL MOLECULES USING PHOTOINDUCED ELECTRON TRANSFER MECHANISM

A dissertation submitted in partial satisfaction of the
requirements for the degree of Doctor of Philosophy

in

CHEMISTRY

by

CLIFFORD RODEREIGH WOODFORD IV

Committee in charge:

Professor Roger Y. Tsien, Chair
Professor Patricia A. Jennings
Professor William B. Kristan Jr.
Professor Charles L. Perrin
Professor Emmanuel Theodorakis

2016

The dissertation of Clifford Rodereigh Woodford IV is approved, and it is acceptable in quality and form for publication on microfilm and electronically:

_____

_____

_____

_____

_____
Chair

University of California, San Diego

2016

DEDICATION

I am both a sentimental and private person. Sentiment has won out here.

To my parents, all things were made possible in my life through your love. To my mind, this freedom you gave me is the greatest gift I, or any person, could possibly hope to receive. I can never repay you, but here I thank you.

To my brother, you are an ideal model I look up to for living a life of joy. I am lucky to have you in my life.

To my godparents, you have been like a second set of parents. Having you in my life and receiving so much of your love is truly an incredible gift.

To my friends, it's been an unbelievably fulfilling journey, thank you for sharing it with me. To those closest to me, thank you for your support in the toughest times and making the best of times more than I could hope for.

To my advisor, the level of agency and resources you empowered me with were far more than could be expected. I don't know anyone with a more ambitious brilliant mind. You have made me into a better scientist than I could have imagined. It has truly been an honor to work under you and learn from you.

To my labmates, it takes village to raise a graduate student in the Tsien lab and I thank you for your patience, guidance, and companionship. I would not have a thesis to write without you.

EPIGRAPH

“The truest determinant of success in this field is perseverance.”

-Mike Burkart

TABLE OF CONTENTS

LIST OF SUPPLEMENTARY FILES

woodford_01_HEK_cell Epifluorescence image of a HEK cell under voltage clamp conditions, identical to Figure 2 in the main text. The movie shows a single HEK cell stained with VF2.1OMe.H, held at a potential of -60 mV under voltage clamp for 50 ms, and then systematically stepped to a new holding potential (+100 mV to -100 mV in 20 mV increments) for 50 ms before returning to -60 mV for 50 ms. There are 11 such sessions in the movie, beginning with +100 mV and proceeding through to -100 mV. In between each session, shutter closes, resulting in brief periods of total darkness. The movie replay rate is slowed down 25x (20 frames per second).

woodford_02_Neuron Epifluorescence image of a cultured rat neuron under current clamp conditions, identical to Figure 4 in the main text. The movie shows a single neurons stained with VF2.1OMe.H and held under current clamp. During the acquisition, 3 brief pulses of depolarizing current are injected to evoke 3 separate action potentials. Data is quantified in Figure 4b and c. The movie replay rate is slowed down 20x (50 frames per second).

LIST OF FIGURES

ACKNOWLEDGEMENTS

I would like to acknowledge the following people for without whom this research would not have been possible:

Dr. Roger Y. Tsien
Dr. Stephen Adams
Dr. John Lin
Dr. Elamprakash Savariar
Joan Kanter
Dr. Larry Gross
Dr. John Ngo
Dr. Evan W. Miller
Sakina Palida
Paul Steinbach
Dr. Tao Jiang
Qing Xiong
Dr. Erik Rodriguez
Rachel Levin

I would like to acknowledge my thesis committee as well.

Chapter 2, in part, is a reprint of the work as it appears in Journal of the American Chemical Society, published January 2015. The dissertation author was the primary author of this material and contributed to experimental design, execution of experiments, interpretation of data, generation of figures and editing of manuscript. Clifford R. Woodford, E. Paxon Frady, Richard S. Smith, Benjamin Morey, Gabriele Canzi, Sakina F. Palida, Ricardo C. Araneda, William B. KristanJr., Clifford P. Kubiak, Evan W. Miller, and Roger Y. Tsien Improved PeT Molecules for Optically Sensing Voltage in Neurons. Journal of the American Chemical Society **137**(5): 1817-1824 (2015).

VITA

2011	Bachelor of Science in Chemistry and Biochemistry, Trinity University
2013	Master of Science, University of California, San Diego
2016	Doctor of Philosophy, University of California, San Diego

PUBLICATIONS

Black, M.; **Woodford, C.**; Mills, N., "Anti-aromatic Dianions: Dianions of Dixanthylidene by Reduction and Attempted Excited-State Deprotonation" *J. Org. Chem.*, **2011**, *76*, 2286-2290

Woodford, C., Smith, R., Frady, E., Morey, B., Canzi, G., Kubiak, C., Araneda, R., Kristan, W., Miller, E., Tsien, R. "Improved molecular wires for sensing voltage in neurons" In Preparation

ABSTRACT OF THE DISSERTATION

TRANSDUCING VOLTAGE CHANGES IN BIOLOGICAL SYSTEMS TO FLUORESCENT SIGNALS VIA SMALL MOLECULES USING A PHOTO-INDUCED ELECTRON TRANSFER MECHANISM

by

Clifford Rodereigh Woodford IV

Doctor of Philosophy in Chemistry

University of California, San Diego, 2016

Professor Roger Y. Tsien, Chair

Neuronal networks are responsible for complicated responses to stimuli and behavior. Understanding these networks involves recording the changes in transmembrane electrical potential from small subcellular locations such as dendritic spines, to large networks of neurons. This dissertation represents a concerted effort toward the development

of small molecule probes with fluorescent intensities responsive to the transmembrane electrical potential of neurons.

Fluorescent voltage sensitive molecules termed VoltageFluors (VF) are capable of undergoing photo-induced electron transfer (PeT). Previous work demonstrated that when embedded within a membrane of interest, the local electric field modulates the extent of PeT, and thus the fluorescence intensity as well. This thesis presents efforts toward rationally improving the voltage sensitivity of VF dyes through tuning the driving force for electron transfer and optimizing the structure of bridges. Optimization led to a significant improvement in voltage sensitivity of newly developed dyes epitomized by VF2.1OMe.H with a 48% ΔF/F per 100 mV demonstrated in HEK cells. This voltage sensor was to record voltage changes across neuronal systems from leech ganglia to mouse brain slices with high fidelity as well.

In addition to sensitivity improvements, VF dyes were developed with a Cy5-like acceptor for far red fluorescence imaging in biology, The most sensitive dye in this class, VF Red, showed a 25% ΔF/F per 100 mV in HEK cells and could effectively be used with optical activity activators for all optical stimulation and recording of electrical activity in neurons.

Further improvements to recording voltage changes in biological systems included work toward reducing background fluorescence and generating a higher signal to noise ratio by generating non-fluorescent VF dyes by chemical reduction. These molecules were then subjected to selective reoxidation back to fluorescent VF dyes solely where oxidizing protein was present. Both fluorescein and cy5-based VF dyes were shown to undergo a degree of oxidation *in vitro* upon addition of oxidizing proteins. These efforts represent significant improvements to VF dyes toward improved optical sensor of voltage across many neuronal systems.

Chapter 1 Methods for Recording Activity of Neuronal Systems

1.1 The Importance of Electrical Activity in Biology

Cell signaling and communication takes many forms including, however changes in the electrical potential across the cell membrane are certainly some of the most important and ubiquitous in biology. Mature foci of research include electrical signaling in in the heart, muscle, and neuronal systems of higher order eukaryotes. Among these pursuits, neuronal systems provide the biggest challenge with regard to the spatial and temporal resolution required for effective study. Cardiac and muscle cells generally respond to slower electrical signals on the order of seconds and show very simple large patterns of activity both within cells and across cells. This simplicity provides far fewer challenges for effective probe development. As a result, developing probes for imaging membrane potential in neuronal systems has been the core effort of researchers. The ultimate challenge undoubtedly is understanding the electrical signaling of the human brain in particular. The human brain represents the most complex machine in the known world. The incredible computing power, memory storage, and information processing performed by the brain is thought to be largely the result of the byzantine architecture and rapid signaling among its neurons.

1.2 Mission and Introductory Outline

It is the goal of this thesis to focus on the development of a new class of fluorescent voltage sensitive probes towards understanding neuronal systems. Accordingly, the first part

of this introduction will outline where fluorescent voltage imaging fits within the wider context of techniques for understanding electrical signaling of neurons and offer brief explanations of a few notable methods. Second, the challenges of voltage imaging will be laid out to form a framework for critical analysis of probe capabilities. Next, the history and development of optical voltage sensitive probes themselves will be discussed in greater detail to understand the narrow context in which this work contributed. Lastly, the approach this work took as a new and promising avenue towards improved optical voltage imaging probes is laid out.

1.3 The Challenge of Recording Electrical Activity

To put the staggering complexity of the brain in a bit of context, it is composed of approximately 86 billion neurons.[1] It has been estimated that if you laid every axon down from end to end the line would extend approximately 100,000 miles. Estimates claim this vast network contains over a trillion synapses and is able to perform 1x10^16 calculations a second.[2] The subtle electrical changes that are the physical manifestations of these calculations are occurring in dendritic spines less than a micron across, integrated in neurons that may be millimeters in length, and affect networks of cells tenths of meters away. This represents a spatial scope spanning 5 orders of magnitude that must be studied to fully understand the role of the electrical signals. To compound this, the spatial information must be combined with changes in these electrical signals that can occur every millisecond to get a complete picture of the output. Along with the enormous challenges to simply gathering this data, there is an equally nuanced problem in gathering the data within the context of behavior generated by the brain, especially considering the fact that the entire network must be largely undisturbed to achieve this. Taken together, these formidable hurdles make a strong argument that understanding the brain is the greatest challenge humans have ever undertaken. The following represents our greatest attempts toward this crucial understanding.

1.4 Seminal Methods for Recording Neuronal Activity

1.4.1 Electrode-based Recordings

The importance of electrical activity in neuronal systems has been known for well over two hundred years since Luigi Galvani touched an electrode to a frog's brain and first began to scratch the surface of what he called "animal electricity."[3] True progress in understanding the nature of these electrical signals was realized by Hodgkin and Huxley's Nobel Prize winning work recording the electrical signals of the *Loligo* giant squid axon with a rudimentary electrode. Their early recordings were able to show that voltage changes across the cell membrane were largely governed by sodium and potassium ion flux and determined levels of conductivity and inactivity essential to generating electrical responses and action potentials.[4–7] They were able to use this information to generate a robust quantitative mathematical model of neuronal firing that set a foundation for understanding biological electrical activity we are continuously building on.[8]

Hodgkin and Huxley were fortunate enough to find a model system in the giant squid axon that was unusually large allowing an entire electrode to be run through the interior of the cell. Unfortunately, this setup is not feasible with the vast majority of cell types and systems. Neher and Sakmann changed this with the development of patch clamping which allowed for any cell capable of making contact with a 3-5 μm electrode tip susceptible to recording .[9] After its initial development, the technique was improved to allow for a number of different recording techniques from single ion channels to whole cells. Patch clamping has remained an essential tool for modern electrophysiologists. Electrode based recording has become increasingly more sophisticated and capable of measuring electrical activity in complex systems reliably. Intracellular approaches such as the whole cell patch clamp, voltage clamp, and current clamp pushed forward our knowledge of cell types, their firing patterns, and roles within circuits in

the brain.[10] Patch clamping techniques generally focus on a single cell and give very detailed information on cellular electrophysiology. Since the early work developing this technique, little methodological advancement has been made. It should be noted, the contribution patch clamping has made to neuroscience can hardly be understated as an explosion of discoveries were born from this technique.

Complementary to patch clamping is extracellular recordings done with both single electrodes and electrode arrays. This technique utilizes small electrodes placed close enough to a neuron to record electrical changes without damaging the neuron, which allowed for awake and behaving animals to be recorded from known regions of the brain. This method has been used to uncover the fundamental electrical underpinnings of behavior and as well as mapping activity of different brain regions. The most notable application of this technique was the Nobel Prize winning work of Hubel and Wiesel on the visual system.[11] Electrode arrays capable of detecting signals more accurately with greater spatial precision and less invasively is a continual desire of electrophysiologists. Consequently, significant methodological advancements have been made to date with regard to electrode materials and recordings. While early electrodes offered a single point of contact at a glass or metal interface, modern nanomaterials such as graphene and spatially precise manufacturing techniques have been employed to record neuronal electrical signals with continually greater spatial resolution.[12] These electrodes are capable of recording the local field potential of their environment, which is a summation of rapid action potentials and slower depolarizations and hyperpolarizations of dendrites and glial cells. Neuronal electric fields are spatially limited to within 1 nm of the membrane due to the high ionic strength and electrical conducibility inherent to these systems.[13] This often means signals are highly attenuated when recorded by extracellular electrodes. Compound this limitation with the high density of signals surrounding a single recording point, and the readout can be insurmountably convoluted for some applications.

Even with these limitations, the ability to resolve electrical activity from multiple points with an array combined with the advantage of recording in behaving animals is unquestionably valuable.

Electrodes have been an outstanding tool for recording electrical activity in neurons due in part to their inherent rapid sampling frequency. The electrical signals are generated and propagated quite rapidly, on the order of milliseconds. This is well within the recording capabilities of electrodes and their accompanying amplifiers, oscilloscopes, or modern data acquisition software. Electrodes are also able to give precise spatial information regarding the area they are recording from, an invaluable characteristic when structural information is just as important as the temporal firing pattern. Electrode versatility is further augmented by the additional ability to stimulate activity through current injection as well.

However, electrodes have two glaring inherent challenges when recording neuronal activity that have limited their application. Firstly, these tools are quite invasive as the probe must be in close proximity to the signal source. This is a major challenge for any application to human subjects outside of those with significant head trauma where electrodes can be easily placed. Additionally, the damage current electrodes impart on model organisms is non-trivial and successful application of probes requires a high level of expertise especially when recording from deeper areas of the brain such as the hippocampus. Secondly, the short recording distance also means that recording circuits or neural activity across a spatial plane is extremely limited. Unfortunately, these networks of activity are incredibly valuable in understanding brain function. Multi-electrode arrays are making these types of experiments easier, but their capabilities are still limited by probe technology and are more invasive than single electrodes.

1.4.2 Non-Invasive Recording Techniques

The need for non-invasive recording techniques capable of spanning large areas of the human brain necessitated the rise of functional magnetic resonance imaging (fMRI) and electroencephalography (EEG) among other notable techniques. These techniques allow neurobiologists access to study arguably the most interesting neuronal system, the human brain.

Less widely used for research purposes, EEG employs a similar approach to previously discussed electrode based techniques. Rather than inserting electrodes into the brain, electrodes are placed on the scalp where local field potentials are recorded on the millisecond time scale. However, the same challenges to multi-electrode array recording are seen and amplified in EEG. The advantages of accessing the human brain directly with millisecond temporal resolution are unique to non-invasive techniques and have led to important discoveries particularly in disease states such as epilepsy.

fMRI offers a completely different approach toward non-invasive brain activity imaging. MRI uses magnetic fields coupled with resonant radio wave frequency stimulation and relaxation to three dimensionally map the location of paramagnetic atoms, and hydrogen in particular. fMRI takes advantage of the proton transverse relaxation time (T_2) of water in the blood which is dependent on the oxygenation state of the local hemoglobin.[14] Increased blood oxygenation levels are correlated with increased local neural activity, thus fMRI is able to detect activity by proxy. By probing magnetic fields and radio waves and using endogenous water as a reporter, the technique is inherently non-invasive and can probe deep into the brain unlike EEG. These advantages have quickly made fMRI an important tool for diagnosis and prognosis for human disease.[15] Beyond a clear therapeutic value, fMRI is beginning to approach fundamental questions linking neural activity to cognition and behavior in ways not otherwise possible.[16] However, fMRI is not without its challenges. Magnetic resonance signals are very weak and can only record an image once every few seconds. The spatial resolution is

also quite limited to a cubic millimeter of space.[17] This precludes imaging such things as action potentials or electrical changes in single neurons, which are only visible with millisecond and micron resolution. Combine this with the tenuous relationship blood oxygen levels have with the actual electrical activity and the prospects for understanding cognition at a fundamental level are even murkier.

1.4.3 Hierarchy of Imaging Techniques

If we analogize the brain to global surveillance, patch clamping is like having a agent on the ground capable of giving incredible detail about the local terrain, including vegetation, weather, and what people in that area are doing, but doesn't have the scope to see more than a few hundred feet in any direction. Conversely, fMRI is like an SR-71 Blackbird flying high above intermittently taking pictures. They can see the large structures like cities, mountain ranges, and man-made creations such as a new factory, but can't see the details like what could be in the factory or what it's for. Ideally, neurobiologists would like a "satellite" as well to compliment these techniques. Something capable of seeing the big picture of cities and buildings, but can also zoom in with pinpoint accuracy to see individual people in those areas and their activities minute by minute. Fluorescent reporters of neuronal activity coupled with modern optical imaging techniques offer the best hope for a satellite-like tool for brain imaging. They are minimally invasive and able to report on activity of fine structures like dendrites on the micrometer and millisecond scales, while also providing a window into the activity of larger regions of the brain and circuits with simultaneous monitoring of behavior. Fluorescent probes offer an exciting middle ground relative to the other essential imaging techniques discussed earlier.

Fluorescent reporters of neuronal activity have generally focused on neurotransmitters, calcium, and voltage.

1.4.4 Fluorescent Neurotransmitter Sensors

Neurotransmitter sensors and analogs have been the most recent approach in an effort to image activity that has been ongoing for well over fifty years. They generally fall into two camps: receptors and analogs. On the receptor front, proteins like GluSnFr which binds to glutamate and undergoes a change in FRET are genetically encoded and can be targeted to specific regions of interest.[18] Another recent approach has been the use of small molecule false neurotransmitters that report upon uptake and release by vesicular monoamine transporters.[19] In addition to reporting neurotransmitter activity, small molecules may be used to stimulate neural activity as seen with two-photon photo-labile glutamate analogs.[20] Photo-uncaging of neurotransmitters to stimulate activity has been a particularly useful technique due to the minimally invasive nature combined with a high spatial and temporal control of release. While this has been an exciting new area of activity within the neuroscience community, these efforts represent a niche area of application relative to calcium and voltage sensors.

1.4.5 Calcium Sensors

By far, calcium sensors have been the most widely employed fluorescent tool for understanding electrical signaling in neurons. This is largely due to the ubiquitous calcium influx seen across neuron types upon depolarization and the high quality of sensors developed to date. The first calcium sensors pioneered by Roger Tsien were small molecules based on the selective calcium chelator EGTA.[21] This early probe was further optimized for cell internalization and improved spectral properties, allowing biologists to quantifiably monitor calcium levels without disturbing the cell membrane.[22] Importantly, the intelligent design of the probes led to rapid improvements on the original giving probes such as the fura dyes that enjoy widespread use within the neurobiological community.[23]

Small molecule calcium sensors remain a valuable asset for the modern neurobiologist, however they have limited application in spatially resolving calcium signals both within subcellular regions and in complex neuronal preparations where monitoring distinct populations of neurons is of interest. Genetically targeted calcium sensors can be modified with specific tags for trafficking to distinct locations or placed under the control of specific promoters for expression in distinct cell populations or at specific times. These probes generally undergo changes in FRET based on calcium binding to calmodulin and M13. Examples such as cameleon and FIP-CB_{SM} were the first tools to provide this capability.[24,25] Later approaches such as GCaMP and Flash-Pericam used a single circularly permuted pH sensitive green fluorescent protein that exhibited a change in fluorescence intensity when a fused calmodulin and M13 bound to calcium.[26,27] These probes, especially GCaMP, have experienced a surge of optimization engineering to improve kinetics and fluorescent wavelengths toward ideal sensors that can be widely used.[28,29]

Fluorescent calcium sensors have been an important tool for high spatial resolution of neuronal activity on a wide range of scales, however calcium signals are only part of the story neurobiologists are interested in. Changes in membrane potential remain an important aspect in neuronal signaling. Calcium changes are correlated with some of this activity, but can never tell the full story. Ideally, fluorescent voltage sensors capable of the same or better spatial resolution would fill in this much maligned gap in the neurobiologist's toolkit.

1.5 The Challenges for Effective Voltage Imaging Probes

Voltage sensors capable of optically reporting faithfully throughout a wide range of spatial and temporal regimes applicable to a vast array of relevant biological preparations remains one of the great unmet needs of neurobiologists.[30] Voltage sensitive probes have the

potential to reveal answers to questions that cannot be addressed with any other current technique.

Researchers have been attempting to develop voltage sensors for well over 50 years with varying degrees of success. With such great promise for discovery associated with voltage sensors the lack of a truly outstanding probe is a testament to the significant challenges toward development researchers face.

1.5.1 Spatial Resolution

Notably, voltage changes are acutely localized to within approximately 1 nm of the cell membrane meaning the probe sensing these changes must also be localized to within 1 nm of the cell membrane.[13] This limitation creates a surprising number of challenges. First, the cell membrane is a highly organized, and at times, delicate part of the cell. Adding exogenous probes or expressing proteins at the membrane can potentially increase permeability, phototoxicity, or alter structures leading to toxicity, thus limiting the amount of probe that can be added to an already relatively small part of the cell. In contrast, cytosolic probes like calcium sensors have a much larger space to occupy with potentially many more probes capable of reporting activity. Additionally, in complex neuronal systems the membranes of many neurons collect in neuropil with minute spatial separation. Teasing out signal from individual cells or processes is near impossible in these situations without sparse or specific labeling. It has been noted already, but is worth repeating that very small structures, such as dendrites or axons harbor a significant amount of important electrical information. The small size of these structures limit still further the amount probe available for reporting voltage changes.

1.5.2 Temporal Resolution

Coupled with the spatial constraints are the temporal restraints. The fundamental unit of information for the neuron is the action potential. These electrical spikes occur on the order

of 10 ms and often fire in bursts up to 50 Hz. Keeping in mind the Nyquist frequency, which is twice the highest signal frequency present, signaling must be sampled at a minimum frequency of 100 Hz, or an image every 10 ms to avoid aliasing and record at least a portion of every event. When you are collecting photons over such a short time, and in very small areas you are often only able to record a small number of photons. This means that collecting enough photons to generate an imaging signal above the level of noise is a major constraint.

1.5.3 Shot Noise, an Inherent Challenge to Low Light Imaging

Recording fluorescence with very low photon counts is an inherently noisy process due to shot noise first and foremost. Shot noise increases with the square root of the number of photons recorded, so fewer photons means this noise will represent a larger portion of the signal. This noise arises from the quantized, probabilistic nature that a photon of light will be absorbed and emitted by a given fluorescent probe. For instance, let us imagine a situation where on average, only 10 photons are recorded per frame. Here the shot noise will vary the photon count from 7 to 13. Let's say in the first frame of a recoding 9 photons of light may have been successfully absorbed and reemitted. In the next frame, simply by chance, perhaps 13 photons are absorbed and reemitted, and in a third frame only 8 photons are recorded. In this scenario, one could falsely believe the second frame represents some event, when in reality it just so happened that the fluorophores randomly absorbed and emitted more photons in that period of time. Additionally, in this senario a biological event could occur which would increase the level of fluorescence by 20% in a given frame. We would expect 12 photons rather than 10 to be emitted, but due to the shot noise, which can randomly generate that number of photons with a reasonable probability, it is impossible to definitively say this increase in fluorescence is due to biological activity rather than just random chance in a single trial.

This problem of shot noise resolves itself when photon counts are much higher. If we imagine 1,000 photons are being absorbed and reemitted on every frame instead, now the shot noise in each frame may vary from 970 to 1,030 photons. This range now only represents a very small deviation relative to our first example. Here if we have a biological event that increases the level of fluorescence by 20% we would expect to record 1,200 photons, well above the inherent shot noise of the signal. Here we could say with confidence that a biological event is taking place and yet we have changed nothing except the number of photons being recorded per frame of the image.

Unless we find a way to get around quantum mechanics, we are stuck with shot noise. Other forms of noise such as dark noise and read noise have become much less of a concern with modern cameras. It is important to always be mindful of these noise sources as well, but they represent a solvable engineering problem, unlike shot noise.

1.5.4 Background Noise

In addition to shot noise, another inherent source of noise comes from the biological system itself, and probe outside the region of interest. Together, these sources of noise represent the background noise. Many biological molecules have overlapping absorbance and fluorescence emission spectra to voltage sensors that are recorded in the process of recording probe signal. This background noise is known as autofluorescence. Additionally, probe that is nearby, but not reporting on the region of interest will contribute to the noise and help drown out any recording. In addition to fluorescent background, valuable light emitted from fluorescent reporters may be scattered by the preparation further limit the number of signal photons recorded.

1.6 Experimental Approaches for Improved Voltage Imaging

Of course, there are approaches to overcoming shot noise and background noise including optimizing the microscope, manipulating the biological preparation, manipulating the light used, and optimizing the probe. What follows is a cursory description of the general approaches a wide array of scientists from numerous disciplines are using to overcome these challenges.

1.6.1 Decrease Spatial and Temporal Resolution

Some of the easiest ways to improve voltage recordings to visualized signal above noise are through longer exposure times to collect more photons over a longer period of time, or collect photons from a wider area to be recorded as a single pixel. Unfortunately, these compromises limit either the spatial or temporal resolution of the image. In practice, this means the incredibly fast events like action potentials or small structures like axons may no longer be recognizable in a single recording and only slower events, or much larger structures can be recorded.

1.6.2 Signal averaging

If one is interested in the very small or very fast components of electrical signaling a second solution can be used where a number of recordings can be averaged into one single recording. This is essentially equivalent to recording more photons for a single trial, but allows for lower light levels to image deeper or with less damage to the tissue. This approach is limited because electrical signals often vary from trial to trial, so averaging is not an option in many of the most interesting experiments.

1.6.3 Increasing Photons Recorded

A third solution is to increase the number of photons that the probe is exposed to or the number of photons that are collected. This is perhaps the best solution to avoid the unpleasant

compromises required above. Much work in physics, chemistry and biology is devoted to this goal through a variety of approaches. More powerful light sources are an obvious starting point, but light is inherently damaging to both the biological sample and probe. To date, researchers have pushed laser intensities to the extreme limits of an acceptable level of damage to the biological preparation and probe being used; this is a hard limit for laser power that is difficult to overcome. Even at these high intensities, it can be quite challenging to get enough photons both to and from the voltage sensor in a wide range of applications.

Engineering Hardware and Neuronal System

The brain is not flat, and many interesting cells are found deep in the organ. This means light must pass through many millimeters of tissue to reach the probe. Unfortunately, biological samples are full of molecules that absorb and scatter light quickly, lowering the number of photons that can be recorded. Dissecting the brain so that slices of these deeper layers are exposed to the surface and thus more light is a popular solution, but this means networks that are essential for normal activity are cut away, limiting what can be learned and completely preventing any direct correlation to behavior.

Imaging these deeper areas in an intact animal is essential for some experiments. This requires complex fiber optics, mirrors, and small microscopes mounted to the organism to visualize activity in the context of a complete animal. While an ideal solution, the engineering challenges associated with this set up are very significant, and these types of experiments require years of specialized training and expertise to carry out. Much progress in making hardware capable of these types of experiments is still necessary.

Engineering Light

Additionally, rather than manipulating the microscope or neurological system being studied to record more photons, a significant amount of effort has been made in manipulating the light used for probe stimulation.

One of the most important aspects of engineering light used in voltage sensing is limiting the spatial plane the light source is exciting. Focusing sharply on solely the region of interest will limit the background fluorescence, photobleaching, and scattering that degrades the quality of the recording. Confocal microscopy is a popular option in biology, but is essentially not possible for voltage imaging because the pin hole throws away far too many valuable photons and is too inefficient. Two-photon microscopy is however a viable solution. In essence, with two-photon microscopy, rather than absorbing a single photon and radiatively relaxing back to ground state, the molecules absorb two photons of light with half the energy. The molecule then undergoes the same radiative relaxation to ground state as with one photon excitation. The key difference is that two-photon excitation is much less probable than one photon, so the chances of out of focus light being excited are negligible. Highly specialized lasers that pulse huge numbers of photons over the course of a femtosecond into the preparation followed by a quiet period are essential to keep stimulating two-photon fluorescence. These lasers use low energy long wavelengths of light that are absorbed and scattered far less than shorter wavelengths of light to probe as deep as 1 mm into the brain, a distance far deeper than could be achieved with one photon fluorescence. Of course, since the emission of the fluorophore is always one photon of shorter light wavelengths, these advantages can only be realized with the excitation light. Other approaches such as non-degenerative two-photon imaging where two wavelengths of different energy are used, or three photon imaging are more dramatic approaches that could potentially further exploit the advantages of two-photon imaging.

1.6.4 Improving Probe Wavelength, Brightness, and Targeting

Important, particularly for the focus of this thesis, is the effort on improving probes for voltage imaging. In addition to taking advantage of the long wavelengths of light used in two-photon imaging, some of these advantages can be realized by using probes that are stimulated with longer wavelengths of light for one photon excitation as well. In general, the lower the energy of visible light capable of being used, the less background noise there will be.

Improved probe brightness is an important aspect to limiting the effect of shot noise and autofluorescence; this can be achieved though a combination of increased molar absorptivity and quantum yield. A brighter probe improves photon economy and helps elevate signal above background fluorescence.

As discussed earlier, background fluorescence from probe outside of the region of interest is a potentially onerous source of noise given that many membranes beyond the plasma membrane of a cell of interest are present and may be stained. The large cytosolic volume that probe may also inhabit and other untargeted probes have the potential to drown out the relatively small signal of appropriately localized probe.

1.6.5 Improving Probe Sensitivity to Voltage

In addition, improving fluorescence sensitivity to voltage changes can help push signal over levels of noise. Considering many of the challenges to imaging voltage are inherent to the technique and many of the solutions require unappealing compromises, improving the probe sensitivity offers one of the best hopes for accessing the most challenging and interesting experiments. Improved sensitivity is always welcome as more and more subtle changes in smaller and smaller areas can be visualized. This is certainly one of the main areas of research in achieving high resolution voltage imaging and much work in this dissertation and elsewhere has been done to continuously push the capabilities of neuroscientists.

1.7 Voltage Imaging Probe Design, Development, and Evolution

1.7.1 The First Optical Probes

The earliest examples of optical voltage sensors were discovered as researchers returned to the giant squid axon to survey a library of small molecules that could potentially report voltage changes. These screens isolated the first voltage sensing probe, Merocyanine 540, which reported voltage dynamics via changes in light transmission upon staining.[31] These first molecules showed vastly different voltage sensitivities depending on the preparation they were applied to and little was known as to the exact mechanism or mechanisms of voltage sensing, making optimization particularly challenging.

This landmark discovery lead to further refinement of the methodology for testing hundreds more molecules which lead to still further more sensitive probes based on oxonol and cyanine chromophores that were able to report voltage changes through fluorescence rather than transmittance.[32,33] The benefits of small molecules that were able to transduce changes in voltage via fluorescence rather than transmittance were immediately realized by neurobiologists studying electrical activity in cultured neurons.[34] To date, fluorescence intensity has proven to be the most useful chemical phenomenon for monitoring voltage.

1.7.2 Electrochromic Small Molecule Fluorophores

Soon after the first dyes provided a foothold for researches to grasp, useful probes were then designed rather than simply screened. Electrochromism was the first phenomenon exploited for voltage sensing, whereby the emission spectrum of a fluorescent molecule was altered by the surrounding electric field based on the charge shift seen in the electron configuration of the excited state.[35] This guiding principle led to the first designed probe using a *p*-aminostyrylpyridinium chromophore initially characterized in artificial lipid bilayers and subsequently in the ever useful giant squid axon.[3637] One of the most widely used dyes, di-4-

ANEPPS arose soon after from this line of work.[38] The 8% change in fluorescence relative to baseline fluorescence (ΔF/F) per 100 mV observed was one of the most sensitive dyes made and put voltage imaging probes into the hands a wider, though still niche audience.

Concurrently, a family of styryl dyes were developed that also used an electrochromic mechanism.[39] These probes were also able to monitor electrical activity in cultured neurons similar to di-4-ANEPPS.[40] A larger palette of dyes proved to be important considering the wide range of neuronal preparations and their unique biological characteristics that altered the voltage sensitivities of electrochromic probes in unpredictable ways.[41]

The latest iteration of electrochromic dyes rigidized the styryl chromophore to eliminate complex intermolecular interactions that may have affected voltage sensitivity.[42] Further modification to a more positively charged species improved solubility and resulted in the most sensitive electrochromic dye to date with up to a 25% ΔF/F per 100 mV when tested in HEK cells.

1.7.3 FRET Probes

Outside of electrochromic dyes, one of the most promising approaches to fluorescent voltage sensing has been a voltage dependent repartitioning across the cell membrane of a FRET pair. Initially, a hydrophobic oxonol quencher capable of traversing the cell membrane combined with a GFP bound to the extracellular side of the membrane was able to sense voltage up to a 34% ΔF/F per 100 mV with a high level of brightness.[43] Later iterations used some combination of dipicrylamine quenchers with diO and GFP fluorophores with some success and gradual improvement upon the initial design.[44–46]

1.7.4 Quantum Dots

Small molecule fluorescence is used throughout modern experimental biological disciplines with great effect. However, the phototoxicity, spectral characteristics, and

photobleaching are all limitations when applied. Nanotechnology has begun to address these important challenges through fluorescent quantum dots capable of reporting voltage changes.[47] These materials are in the midst of a rapidly progressing field that could provide the next great voltage sensors. However, at the time of this writing, quantum dot voltage sensors remain an exciting intellectual curiosity with little improved utility over competing approaches.[48]

1.7.5 Second Harmonic Generation Voltage Sensitivity

Fluorescence has certainly been the dominant technique for optical reporting of voltage, but it is worth noting the use of second harmonic generation towards this end as well. Previously discussed molecules like di-4-ANEPPS whose fluorescence is sensitive to voltage also show second harmonic generations sensitive to voltage up to a 43% $\Delta F/F$ per 100 mV.[49] Additionally, probes have been developed specifically for second harmonic generation sensing of voltage as well with some success.[49] This optical technique is useful due to the lower photo damage during imaging, but suffers immensely from low signal efficiencies that lead to small photon counts, an Achilles heel of voltage sensors.

1.7.6 Voltage Sensitive Fluorescent Proteins

To this point, optical sensors of voltage have exclusively focused on small molecules and nanomaterials, however just as with calcium indicators, genetically targeted probes offer unique advantages in terms of spatial resolution that cannot be ignored.

Many have seen protein-based sensors as the future of voltage imaging due to the improved signal relative to background noise presented with targeted expression exclusively to membranes of interest. This certainly is a powerful advantage that many researchers have attempted to exploit, though efficient trafficking of probe is an important consideration with regard to background. Voltage sensitive proteins are not without their own set of challenges. They are inherently limited to neuronal systems with easily manipulated genetics. Protein-

based probes have also suffered from slow kinetics and low sensitivities which have limited their application.

There are generally 3 classes of probes that have been developed. The first uses the voltage sensing domains of other proteins fused to a FRET pair where physical movement of the protein alters the extent of FRET. The second applies a voltage sensing domain as well, but reports physical changes in this domain through changes in fluorescence intensity of a single fluorescent protein fused to this domain rather than a change of FRET. The third approach uses a modified light sensitive proton pump from microbial rhodopsins that is inherently mildly fluorescent.

1.7.7 Shaker-based Probes

In some ways, development of protein based sensors is much easier than small molecules considering the vast array of protein domains already in existence that are sensitive to voltage changes across species in the form of voltage gated ion channels and phosphatases. These domains undergo considerable conformational changes that can be recorded when coupled to a fluorescent protein. The first protein based voltage sensor took advantage of this approach using the voltage sensing domain of a shaker potassium ion channel coupled to a modified GFP whose fluorescence intensity was modified by the conformation of the fused channel domain. While it only showed a modest voltage sensitivity of 5% $\Delta F/F$ per 100 mV it was both a proof of concept and a corner stone for future development.[50]

From here, researchers continued to employ the shaker voltage sensing domain, but shifted their attention on a FRET pair reporter of conformational change rather than a single modified GFP with a modest 2% $\Delta F/F$ per 100 mV.[51]

1.7.8 Voltage Sensitive Phosphatase Containing Probes

A breakthrough was realized as the voltage sensing domain found in a phosphatase protein in the *Ciona Intestinalis* sea squirt was shown to undergo dramatic conformational changes dependent on membrane potential.[52] This sensing domain quickly replaced the less effective shaker domain. When coupled with a CFP and YFP fluorescent pair, voltage sensitivities improved from 2% to 5% ΔF/F per 100 mV.[53] Beyond improvements to the voltage sensing domain, further optimization of the FRET pair from CFP and YFP to mKO and UKG fluorophores proved to be an important innovation. The mKO and UKG proteins used in this new probe called Mermaid were far less sensitive to pH and showed much more FRET sensitivity to changes in the phosphatase conformation leading to a 13% ΔF/F per 100 mV with improved wavelengths and stability.[54]

Similar to previous probes, Mermaid suffered from slow kinetics that limited application for studying fast electrical signals such as action potentials. To remedy this, a series of new constructs were developed that still used the *Ciona Intestinalis* phosphatase, but rather than using a FRET pair focused on fusing a circularly permuted GFP in a similar fashion to the GCamP proteins discussed above. This new probe termed ElectricPK exhibited kinetics an order of magnitude faster than any previous design, though exhibited only a modest sensitivity of 1.5% ΔF/F per 100 mV.[55] These modest sensitivities were greatly improved upon by modern probes while retaining the improved kinetics.

Progress in protein based voltage sensors was often more serendipitous than design. Perhaps the best example of this is the development of ArcLight, another probe using the *Ciona Intestinalis* phosphatase that is fused an ecliptic pHluorin, which is a pH sensitive GFP variant. At some point, the pHluorin acquired a A227D point mutation that generated a 14-fold enhancement in voltage sensitivity which was further optimized to give a 35% ΔF/F per 100 mV in HEK cells.[56] Simply by chance, a dramatic improvement in sensitivity was achieved

and ushered in the modern era of protein based voltage imaging. Unfortunately, with a temporal response of 17 ms, much of the fast activity was still difficult to record as it happens much faster than the associated conformational changes of ArcLight.

The latest iteration of improved protein based sensors named ASAP1 follows a similar formulat to its predecessors. Combining a chicken voltage sensing phosphatase domain with a circularly permuted GFP greatly improved the kinetics of the voltage response giving a 2ms on-rate, while exhibiting a 29% ΔF/F per 100 mV.[57] This probe represents the current state of the art for voltage sensing domains fused to fluorescent proteins for voltage imaging.

1.7.9 Microbial Rhodopsins as Voltage Sensors

More recently a second approach to voltage imaging through an entirely different class of sensors has been developed. Microbial rhodopsins have evolved as light driven ion pumps that provide energy for the organisms. These proteins have been engineered to essentially run in reverse where voltage dependent conformational changes lead to correlating changes in fluorescence.

The first example of a microbial rhodopsin employed as a voltage sensor was Arch, a protein from *Halorubrum sodomense*. Early optimization gave fast kinetics and a voltage sensitivity of 40% ΔF/F per 100 mV.[58] These promising characteristics for a first generation probe gave hope that perhaps an ideal sensor could be developed from this new family of proteins. Within a couple years, the voltage sensitivity of a second generation termed QuasAr had more than doubled the voltage sensitivity to a 90% ΔF/F per 100 mV.

Additionally, the far red fluorescence and low bleach rate created opportunities to combine the sensor with other optical tools in the blue region for increased experimental application.[59] These probes were an incredibly promising development in a field that had only

been inching forward for decades. However, these early sensors had a few severe shortcomings typified by a very low level of brightness that greatly limited application in biological systems.

Recently, the cripplingly low brightness levels of rhodopsins have been addressed by fusing a bright fluorescent protein the sensor. While the rhodopsin may not be a bright reporter, it appears capable of acting as a sufficient FRET quencher, where the level of FRET quenching is effectively modified by voltage. The probes MacQ-mCitrine, and most recently, Ace1Q-mNeon combine the favorable kinetics and sensitivity of rhodopsins with the brightness of modern fluorescent proteins to give greatly improved voltage sensors.[60,61] The Ace1Q-mNeon probe is perhaps the best protein based voltage sensor currently available. With a voltage sensitivity of 70% ΔF/F per 100 mV in cultured neurons, an on-rate near 2 ms, and one of the brightest fluorescent proteins in mNeon, Ace1Q-mNeon is as good, or better, than any previous probe with regard to these important parameters. As we have seen, the "best probe" rarely retains that moniker for long. It is exciting to think of what developments await in the near future for protein-based voltage sensors.

1.8 A New Mechanism for Probing Voltage through Photoinduced Electron Transfer

A promising new approach toward developing the ideal voltage imaging probe has recently been developed by taking advantage of photoinduced electron transfer (PeT). In this new class of sensors, a fluorophore is excited by a photon of light and an electron is promoted to an excited state. Upon excitation, there is a vacancy in a lower energy molecular orbital that is then occupied by a nearby electron that resided in a higher energy molecular orbital. This now reduced fluorophore relaxes to a ground state non-radiatively and returns an electron to the nearby donor.[62] This electronic process is well known to be dependent on the local electric

field.[63] Theoretical considerations concluded that molecules localized to neuronal plasma membranes that are excited by a photon and compete between PeT and fluorescent relaxation processes based on the local electric field would provide a fluorescence intensity readout of that local field. This approach was thought to potentially provide more sensitive sensors than previous attempts in voltage sensor development.[64]

The first iteration of a PeT based voltage sensor, termed VoltageFluor (VF), was realized using an aniline based electron donor, phenylene vinylene bridge to provide a conduit for electron transfer, and a fluorescein based electron acceptor and fluorophore (Figure 1.1). This setup creates a lipophilic molecules with a hydrophobic donor and bridge and hydrophilic acceptor that embeds itself within a plasma membrane to sense the localized voltage.[65] Such a design allows the VF dye to orient itself normal to the electric field generated by the neuron. In a hyperpolarized cell, upon excitation PeT is more likely as the negatively charged electron travels from the negative side of the membrane to the positive side. Conversely, in a depolarized cell PeT is less likely to occur given the electron has to travel towards the negative side of the membrane. With a less likely chance to undergo PeT, a fluorescent relaxation to ground state is much more likely. This modulation of fluorescence intensity by the local electric field can be recorded and studied in a wide range of different neuronal contexts and presents a potentially far improved platform for developing voltage sensors than previous attempts.

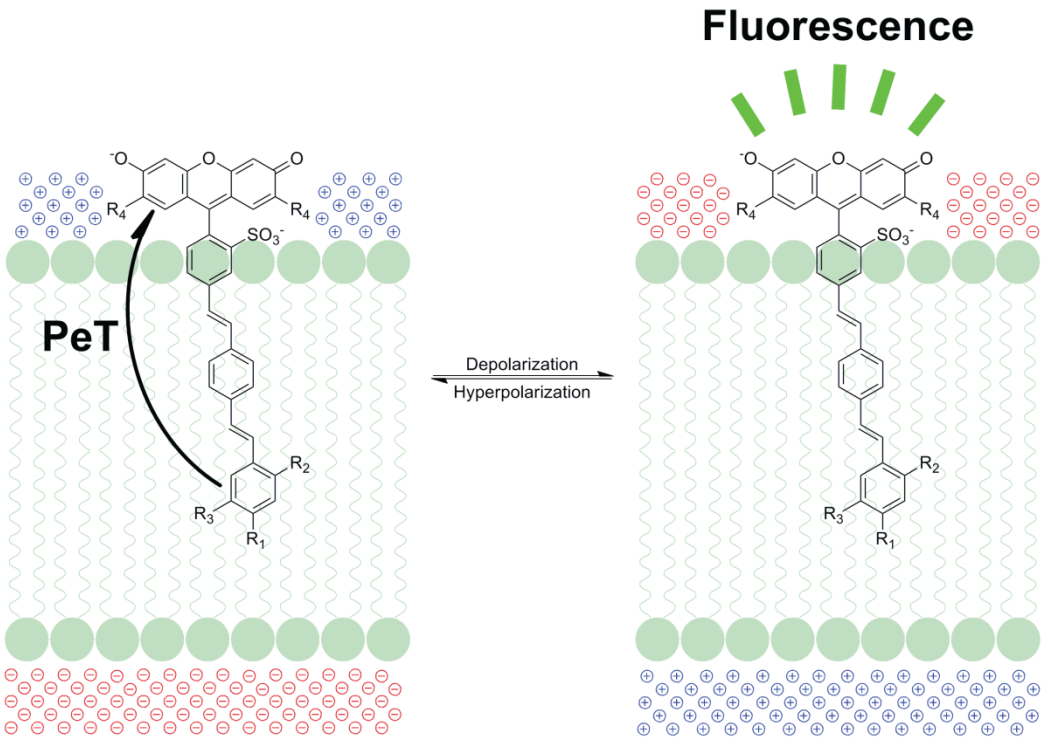

Figure 1.1 Voltage Sensing Mechanism of VoltageFluor Dyes. On the left, hyperpolarized membrane potentials (negative inside cell) promote PeT and quench fluorescence. On the right, depolarization (positive inside cell) decreases PeT and increases fluorescence.

VoltageFluor dyes provide a number of notable inherent improvements to other small molecule dyes and proteins. PeT occurs on the microsecond time scale which creates two main benefits over a slower process such as a physical reorientation of a protein. First, there is no added capacitative load since the charged species are so short lived, and second, the fluorescent signal is able to keep pace with even the most rapid electrical events. For instance, it has been shown that VF dye fluorescent changes are able to closely match electrode based recordings on a microsecond scale. Additionally, since the intensity of fluorescence rather than say, a shift in emission spectrum is affected by the membrane potential, the entire excitation and emission spectra can be used to its greatest effect. Furthermore, given that PeT can be realized through a number of different fluorophores the characteristics of the probe can be significantly altered to longer wavelengths or molecules with improved brightness for two-photon microscopy for

instance. Beyond this, there is a great potential to engineer a more targeted probe with improved affinity to specific locations. Lastly, a number of enzymatic approaches for turning on an active probe only in membranes of interest is possible. The vast potential of VF probes proved to be a fertile area of research and has given rise to numerous advancements to be discussed in the following chapters.

The initial design generated a probe with a 26% ΔF/F per 100 mV in HEK cells, and emission peak at 521 nm with an affinity for plasma membranes upon bath addition. These characteristics represent a strong foundation which the work in this thesis was built upon. The focus of this thesis is to improve upon these characteristics, specifically the voltage sensitivity, fluorescence characteristics, and targeting of VF dyes.

1.9 Bibliography

1. Azevedo, F. A. C., Carvalho, L. R. B., Grinberg, L. T., Farfel, J. M., Ferretti, R. E. L., Leite, R. E. P., Filho, W. J., Lent, R. & Herculano-Houzel, S. Equal numbers of neuronal and nonneuronal cells make the human brain an isometrically scaled-up primate brain. *J. Comp. Neurol.* **513,** 532–541 (2009).

2. Goodwin, D. & Cham, J. Your Brain by the Numbers. *Scientific American* (2012).

3. Piccolino, M. Luigi Galvani and animal electricity: two centuries after the foundation of electrophysiology. *Trends Neurosci.* **20,** 443–448 (1997).

4. Hodgkin, A. L., Huxley, A. F. & Katz, B. Measurement of current-voltage relations in the membrane of the giant axon of Loligo. *J. Physiol.* **116,** 424–448 (1951).

5. Hodgkin, A. L. & Huxley, A. F. The Components of Membrane Counductance in the Giant Axon of Loligo. *J. Physiol.* **116,** 473–496 (1952).

6. Hodgkin, A. L. & Huxley, A. F. Currents Carried By Sodium and Potassium Ions Through the Membrane of the Giant Axon of Loligo. *J. Physiol.* **116,** 449–472 (1952).

7. Hodgkin, A. L. & Huxley, A. F. The dual effect of membrane potential on sodium conductance in the giant axon of Loligo. *J. Physiol.* **116,** 497–506 (1952).

8. Hodgkin, A. L. & Huxley, A. F. A Quantitative Description of Membrane Current and its Application to Conduction and Excitation in Nerve. *J. Physiol.* **117,** 500–544 (1952).

9. Neher, E. & Sakmann, B. Single-channel currents recorded from membrane of denervated frog muscle fibres. *Nature* **260,** 799–802 (1976).

10. Hamill, O. P., Marty, A., Neher, E., Sakmann, B. & Sigworth, F. J. Improved patch-clamp techniques for high-resolution current recording from cells and cell-free membrane patches. *Eur. J. Physiol.* **391,** 85–100 (1981).

11. Hubel, D. H. & Wiesel, T. N. Receptive fields of single neurones in the cat's striate cortex. *J. Physiol.* **148,** 574–591 (1959).

12. Spira, M. E. & Hai, A. Multi-electrode array technologies for neuroscience and cardiology. *Nat. Nanotechnol.* **8,** 83–94 (2013).

13. Olivotto, M., Arcangeli, A., Carlà, M. & Wanke, E. Electric fields at the plasma membrane level: a neglected element in the mechanisms of cell signalling. *Bioessays* **18,** 495–504 (1996).

14. Thulborn, K. R., Waterton, J. C., Matthews, P. M. & Radda, G. K. Oxygenation Dependence of the Transverse Relaxation Time of Water Protons in Whole Blood at High Field. *Biochim. Biophys. Acta* **714,** 265–270 (1982).

15. D'Esposito, M., Deouell, L. Y. & Gazzaley, A. Alterations in the BOLD fMRI signal with ageing and disease: a challenge for neuroimaging. *Nat. Rev. Neurosci.* **4,** 863–872 (2003).

16. Cabeza, R. & Nyberg, L. Imaging cognition II: An empirical review of 275 PET and fMRI studies. *J. Cogn. Neurosci.* **12,** 1–47 (2000).

17. Dale, A. M., Liu, A. K., Fischl, B. R., Buckner, R. L., Belliveau, J. W., Lewine, J. D. & Halgren, E. Dynamic Statistical Parametric Mapping. *Neuron* **26,** 55–67 (2000).

18. Hires, S. A., Zhu, Y. & Tsien, R. Y. Optical measurement of synaptic glutamate spillover and reuptake by linker optimized glutamate-sensitive fluorescent reporters. *Proc. Natl. Acad. Sci. U. S. A.* **105,** 4411–6 (2008).

19. Lee, M., Gubernator, N. G., Sulzer, D. & Sames, D. Development of pH-responsive fluorescent false neurotransmitters. *J. Am. Chem. Soc.* **132,** 8828–30 (2010).

20. Furuta, T., Wang, S. S., Dantzker, J. L., Dore, T. M., Bybee, W. J., Callaway, E. M., Denk, W. & Tsien, R. Y. Brominated 7-hydroxycoumarin-4-ylmethyls: photolabile protecting groups with biologically useful cross-sections for two photon photolysis. *Proc. Natl. Acad. Sci. U. S. A.* **96,** 1193–1200 (1999).

21. Tsien, R. Y. New Calcium Indicators and Buffers with High Selectivity against Magnesium and Protons: Design, Synthesis, and Properties of Prototype Structures. *Biochemistry* **19,** 2396–2404 (1980).

22. Tsien, R. Y. A Non-disruptive Technique for Loading Calcium Buffers and Indicators into Cells. *Nature* **290,** 527–528 (1981).

23. Grynkiewicz, G., Poenie, M. & Tsien, R. Y. A New Generation Ca2+ Indicators with Greatly Improved Fluorescence Properties. *J. Biol. Chem.* **260,** 34403450 (1985).

24. Romoser, V. A., Hinkle, P. M. & Persechini, A. Detection in Living Cells of Ca2+-dependent Changes in the Fluorescence Emission of an Indicator Composed of Two Green Fluorescent Protein Variants Linked by a Calmodulin-binding Sequence: A NEW CLASS OF FLUORESCENT INDICATORS. *J. Biol. Chem.* **272,** 13270–13274 (1997).

25. Miyawaki, a, Llopis, J., Heim, R., McCaffery, J. M., Adams, J. a, Ikura, M. & Tsien, R. Y. Fluorescent indicators for Ca2+ based on green fluorescent proteins and calmodulin. *Nature* **388,** 882–887 (1997).

26. Nakai, J., Ohkura, M. & Imoto, K. A high signal-to-noise Ca(2+) probe composed of a single green fluorescent protein. *Nat. Biotechnol.* **19,** 137–41 (2001).

27. Nagai, T., Sawano, a, Park, E. S. & Miyawaki, a. Circularly permuted green fluorescent proteins engineered to sense Ca2+. *Proc. Natl. Acad. Sci. U. S. A.* **98,** 3197–3202 (2001).

28. Zhao, Y., Araki, S., Wu, J., Teramoto, T., Chang, Y.-F., Nakano, M., Abdelfattah, A. S., Fujiwara, M., Ishihara, T., Nagai, T. & Campbell, R. E. An expanded palette of genetically encoded Ca^{2+} indicators. *Science* **333,** 1888–91 (2011).

29. Ohkura, M., Sasaki, T., Sadakari, J., Gengyo-Ando, K., Kagawa-Nagamura, Y., Kobayashi, C., Ikegaya, Y. & Nakai, J. Genetically encoded green fluorescent Ca2+ indicators with improved detectability for neuronal Ca2+ signals. *PLoS One* **7,** e51286 (2012).

30. Vogt, N. In vivo voltage sensors. *Nat. Methods* **12,** 36–36 (2014).

31. Salzberg, B. M., Davila, H. V & Cohen, L. B. Optical recording of impulses in individual neurones of an invertebrate central nervous system. *Nature* **246,** 508–509 (1973).

32. Cohen, L. B., Salzberg, B. M., Davila, H. V, Ross, W. N., Landowne, D., Waggoner, A. S. & Wang, C. H. Changes in axon fluorescence during activity: Molecular probes of membrane potential. *J. Membr. Biol.* **19,** 1–36 (1974).

33. Gupta, R. K., Salzberg, B. M., Grinvald, A., Cohen, L. B., Kamino, K., Lesher, S., Boyle, M. B., Waggoner, A. S. & Wang, C. H. Improvements in optical methods for measuring rapid changes in membrane potential. *J. Membr. Biol.* **58,** 123–137 (1981).

34. Grinvald, a, Ross, W. N. & Farber, I. Simultaneous optical measurements of electrical activity from multiple sites on processes of cultured neurons. *Proc. Natl. Acad. Sci. U. S. A.* **78,** 3245–9 (1981).

35. Loew, L. M., Bonneville, G. W. & Surow, J. Charge shift optical probes of membrane potential. Theory. *Biochemistry* **17,** 4065–4071 (1978).

36. Loew, L. M. & Simpson, L. L. Charge-shift probes of membrane potential: a probable electrochromic mechanism for p-aminostyrylpyridinium probes on a hemispherical lipid bilayer. *Biophysical Journal* **34,** 353–365 (1981).

37. Loew, L. M., Cohen, L. B., Salzberg, B. M., Obaid, A. L. & Bezanilla, F. Charge-shift probes of membrane potential. Characterization of aminostyrylpyridinium dyes on the squid giant axon. *Biophys. J.* **47,** 71–7 (1985).

38. Fluhler, E., Burnham, V. G. & Loew, L. M. Spectra, membrane binding, and potentiometric responses of new charge shift probes. *Biochemistry* **24,** 5749–5755 (1985).

39. Grinvald, A., Hildesheim, R., Farber, I. C. & Anglister, L. Improved fluorescent probes for the measurement of rapid changes in membrane potential. *Biophysical Journal* **39,** 301–308 (1982).

40. Grinvald, A., Fine, A., Farber, I. C. & Hildesheim, R. Fluorescence monitoring of electrical responses from small neurons and their processes. *Biophys. J.* **42,** 195–8 (1983).

41. Waggoner, A. Dye indicators of membrane potential. *Annu. Rev. Biophys. Bioeng.* 47–68 (1979). doi:10.1146/annurev.bb.08.060179.000403

42. Kuhn, B. & Fromherz, P. Anellated Hemicyanine Dyes in a Neuron Membrane: Molecular Stark Effect and Optical Voltage Recording. *J. Phys. Chem. B* **107,** 7903–7913 (2003).

43. Gonzalez, J. E. & Tsien, R. Y. Voltage sensing by fluorescence resonance energy transfer in single cells. *Biophys J* **69,** 1272–1280 (1995).

44. Sjulson, L. & Miesenbock, G. Rational optimization and imaging in vivo of a genetically encoded optical voltage reporter. *J. Neurosci.* **28,** 5582–5593 (2008).

45. Chanda, B., Blunck, R., Faria, L. C., Schweizer, F. E., Mody, I. & Bezanilla, F. A hybrid approach to measuring electrical activity in genetically specified neurons. *Nat. Neurosci.* **8,** 1619–1626 (2005).

46. Bradley, J., Luo, R., Otis, T. S. & DiGregorio, D. A. Submillisecond optical reporting of membrane potential in situ using a neuronal tracer dye. *J. Neurosci.* **29,** 9197–9209 (2009).

47. Park, K., Deutsch, Z., Li, J. J., Oron, D. & Weiss, S. Single molecule quantum-confined Stark effect measurements of semiconductor nanoparticles at room temperature. *ACS Nano* **6,** 10013–23 (2012).

48. Marshall, J. D. & Schnitzer, M. J. Optical strategies for sensing neuronal voltage using quantum dots and other semiconductor nanocrystals. *ACS Nano* **7,** 4601–9 (2013).

49. Millard, A. C., Jin, L., Wei, M.-D., Wuskell, J. P., Lewis, A. & Loew, L. M. Sensitivity of second harmonic generation from styryl dyes to transmembrane potential. *Biophys. J.* **86,** 1169–76 (2004).

50. Siegel, M. S. & Isacoff, E. Y. A genetically encoded optical probe of membrane voltage. *Neuron* **19,** 735–741 (1997).

51. Sakai, R., Repunte-Canonigo, V., Raj, C. D. & Kn??pfel, T. Design and characterization of a DNA-encoded, voltage-sensitive fluorescent protein. *Eur. J. Neurosci.* **13,** 2314–2318 (2001).

52. Murata, Y., Iwasaki, H., Sasaki, M., Inaba, K. & Okamura, Y. Phosphoinositide phosphatase activity coupled to an intrinsic voltage sensor. *Nature* **435,** 1239–43 (2005).

53. Dimitrov, D., He, Y., Mutoh, H., Baker, B. J., Cohen, L., Akermann, W. & Kn??pfel, T. Engineering and characterization of an enhanced fluorescent protein voltage sensor. *PLoS One* **2,** 2–6 (2007).

54. Tsutsui, H., Karasawa, S., Okamura, Y. & Miyawaki, A. Improving membrane voltage measurements using FRET with new fluorescent proteins. *Nat Meth* **5,** 683–685 (2008).

55. Barnett, L., Platisa, J., Popovic, M., Pieribone, V. A. & Hughes, T. A Fluorescent, Genetically-Encoded Voltage Probe Capable of Resolving Action Potentials. *PLoS One* **7,** e43454 (2012).

56. Jin, L., Han, Z., Platisa, J., Wooltorton, J. R. A., Cohen, L. B. & Pieribone, V. A. Single Action Potentials and Subthreshold Electrical Events Imaged in Neurons with a Fluorescent Protein Voltage Probe. *Neuron* **75,** 779–785 (2012).

57. St-Pierre, F., Marshall, J. D., Yang, Y., Gong, Y., Schnitzer, M. J. & Lin, M. Z. High-fidelity optical reporting of neuronal electrical activity with an ultrafast fluorescent voltage sensor. *Nat. Neurosci.* **17,** 884–9 (2014).

58. Kralj, J. M., Douglass, A. D., Hochbaum, D. R., Maclaurin, D. & Cohen, A. E. Optical recording of action potentials in mammalian neurons using a microbial rhodopsin. *Nat. Methods* **9,** 90–5 (2012).

59. Hochbaum, D. R., Zhao, Y., Farhi, S. L., Klapoetke, N., Werley, C. A., Kapoor, V., Zou, P., Kralj, J. M., Maclaurin, D., Smedemark-Margulies, N., Saulnier, J. L., Boulting, G. L., Straub, C., Cho, Y. K., Melkonian, M., Wong, G. K.-S., Harrison, D. J., Murthy, V. N., Sabatini, B. L., Boyden, E. S., Campbell, R. E. & Cohen, A. E. All-optical electrophysiology in mammalian neurons using engineered microbial rhodopsins. *Nat. Methods* **11,** 825–33 (2014).

60. Gong, Y., Wagner, M. J., Zhong Li, J. & Schnitzer, M. J. Imaging neural spiking in brain tissue using FRET-opsin protein voltage sensors. *Nat. Commun.* **5,** 3674 (2014).

61. Gong, Y., Huang, C., Li, J. Z., Grewe, B. F., Zhang, Y., Eismann, S. & Schnitzer, M. J. High-speed recording of neural spikes in awake mice and flies with a fluorescent voltage sensor. *Science (80-.).* **350,** 1–11 (2015).

62. Marcus, R. A., Marcus, A. & Soc, D. F. On the Theory of Electron-Transfer Reactions. VI. Unified Treatment for Homogeneous and Electrode Reactions*. **43,** (1965).

63. Bixon, M. & Jortner, J. Electrlc Field Effects on the Prtmary Charge Separation in Bacterial Photosynthesis. *J. Phys. Chem.* **92,** 7148–7156 (1988).

64. Li, L. Fluorescence Probes for Membrane Potentials Based on Mesoscopic Electron Transfer. *Nano Lett.* **7,** 2981–2986 (2007).

65. Miller, E. W., Lin, J. Y., Frady, E. P., Steinbach, P. A., Kristan, W. B. & Tsien, R. Y. Optically monitoring voltage in neurons by photo- induced electron transfer through molecular wires. *Proc. Natl. Acad. Sci.* **109,** 2114–2119 (2011).

Chapter 2 Rational Design of Improved PeT Molecules

2.1 Introduction

One of the great limitations of fluorescent voltage sensitive probes are their low sensitivities to changes in membrane potential. On one hand, this seems very unlikely given the huge electric field changes felt across the plasma membrane of neurons. A resting electric field of -1.5x10^7 V/m may be abruptly flipped to a +1.x10^7 V/m field during an action potential assuming a 4 nm membrane width and a membrane potential shift from -60 mV to +40 mV. An electric field change this large should have dramatic effects on charged species within this field that could be exploitable to generate highly sensitive probes.[1] However, harnessing the huge potential of these fields is riddled with numerous hurdles discussed in Chapter 1. VF dyes represent a fundamentally new approach toward exploiting the interaction of charge with the electric field of the neuron. It is a platform that offers a general chemical strategy for voltage sensing that can be rationally improved through modulation of donor and acceptor electron affinities. This work represents the design and synthesis of a series of 10 new structurally-related VoltageFluors with sensitivities ranging from a 0% to 49%ΔF/F per 100 mV. Estimates of their driving force for PeT (ΔG_{PeT}) crucial for voltage sensitivity are performed through multiple analytical techniques and are shown to correlate with measured voltage sensitivity values. Lastly, our best dye, VF2.1OMe.H is applied in cultured cells, dissociated mammalian neurons, *ex vivo* leech ganglia, and acutely prepared rodent olfactory bulb slices to give a sense of the range of preparations VF dyes can be successfully applied to.

2.2 Results

2.2.1 Design, Synthesis, and Characterization of VoltageFluors

Our strategy for voltage sensing relies on proper orientation of a fluorophore-wire-donor construct into the plasma membrane Figure 2.1. Sulfofluoresceins were an initial choice because the persistently ionized sulfonic acid (pKa < -2) helps prevent internalization of the sensor through the cellular membrane. Sulfofluoresceins also have demonstrated utility in two-photon fluorescence imaging, leaving open possibilities for *in vivo* applications.[2]

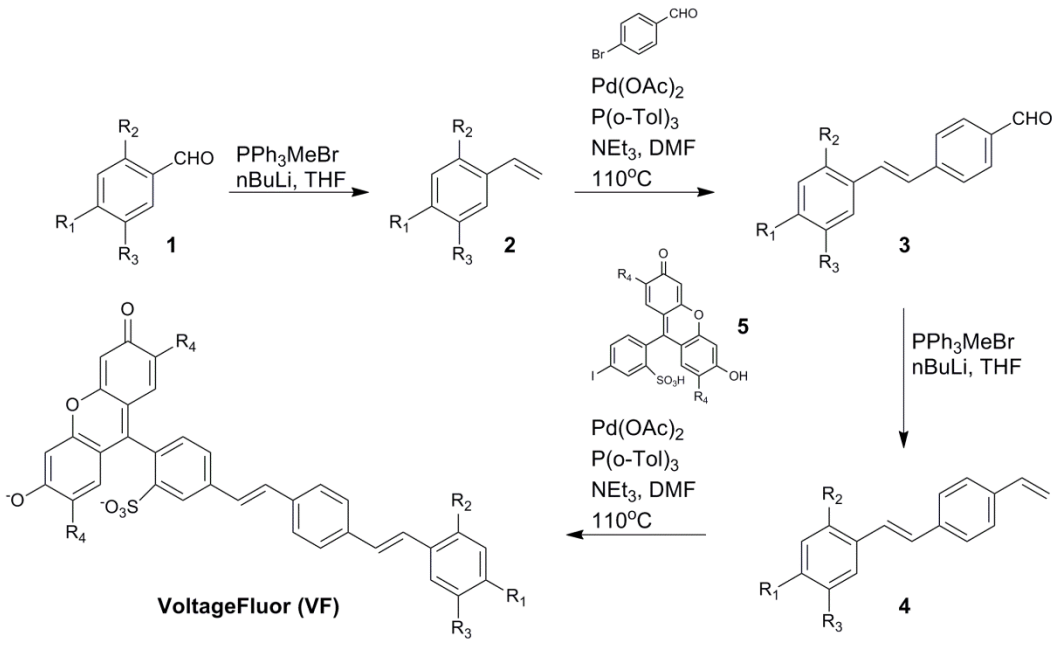

Figure 2.1 Voltage sensing mechanism and synthesis of VoltageFluor dyes. a) Hyperpolarized (left) membrane potentials (negative inside cell) promote PeT and quench fluorescence. Depolarization (positive inside cell) decreases PeT and increases fluorescence (right).

The low attenuation values and ease of chemical synthesis of phenylenevinylene (PPV) molecular wires made them an ideal choice for spacers to act as a molecular wire between the electron donor and acceptor. Our previous study showed that 2 generations of PPV spacer

provided excellent voltage sensitivity while maintaining sufficient loading and water solubility. Finally, nitrogenous donors are frequently used in PeT sensors and in this case, offer the opportunity to tune the relative energetics of PeT by modulation of the electron-richness of the aniline.[3–6] Previous studies show that, while N,N-dibutylaniline-derived VF2.4.Cl had similar voltage sensitivities as the N,N-dimethyl substituted VF2.1.Cl, the dimethyl analog had better signal-to-noise, on account of increased uptake into cellular membranes—therefore, dimethyl analogs were used throughout this study.

We sought to explore the voltage sensitivity of VF2.1.Cl through substituent changes on both the fluorophore/acceptor and donor. The modular nature of the VF dye synthesis in Figure 2.1 enabled rapid construction of several new derivatives listed in Figure 2.6. Figure 2.1 outlines the synthesis of the VF family of dyes (full details available in Supporting Information). All of the VF sensors were characterized spectroscopically in aqueous media (pH 9, 0.1% Triton X-100 to ensure complete solubility and deprotonization of the hydroxy-xanthenone) and had absorption maxima ranging from 504 nm (VF2.1OMe.H) to 522 nm (VF2.1Cl compounds) and emission profiles from between 522 nm to 538 nm in Figure 2.6. The substituent pattern on the chromophore determined the absorbance band, with unsubstituted sulfofluorescein displaying λ_{max} values centered around 506 nm, fluoro-substituted sulfofluorescein centered at 508 nm, methyl at 514 nm, and chloro at 522 nm. Additionally, each VF compound exhibited a secondary absorbance band characteristic of a conjugated phenylenevinylene molecular wire, with λ_{max} values ranging from 392 to 410 nm in Figure 2.2b and Figure 2.7. VF2.0.Cl had a secondary λ_{max} substantially blue-shifted from the other VF dyes (363 nm), owing to the lack of conjugation through the dimethylaniline. The quantum yields for the dyes ranged from 0.04 for VF2.1(OMe).Me to 0.50 for VF2.0.Cl in Figure 2.6.

2.2.2 Fluorescence Response to Potential Changes

The voltage response of the dyes was established in whole-cell patched voltage-clamped HEK cells. Bath application of 200 nM VF dyes for 15 minutes at 37 °C resulted in cellular staining localized to the plasma membrane in Figure 2.2a and Figure 2.3a. All images depict cells without any voltage manipulation, where V_m is close to -60 mV. Importantly, loading conducted at 37 °C did not result in significant internalization of the dye molecule. Furthermore, throughout the course of evaluation in HEK cells (45 to 60 minutes), we observe negligible dye internalization or loss of voltage sensitivity, as measured by the change in voltage sensitivity recorded from cells patched at the beginning of a trial (approximately 5-15 min post-loading) and at the end of a trial (approximately 30-60 min post-loading).

The deviation in sensitivity is low (<5%), and this is reflected in the small error bars in Figure 2.3b. This suggests that, under these conditions, the initial orientation of the dye within the membrane is established early during loading and very little inversion of the VoltageFluor occurs. We corroborated this finding by examining the cellular staining of VF dyes as a function of dye incubation time and found little change in the localization after loading VF2.1(OMe).H for either 10 minutes or 85 minutes in Figure 2.8. Uniform orientation of the dyes is critical for obtaining voltage sensitivity, because an equal distribution of “chromophore in” and “chromophore out” orientations would result in net zero voltage sensitivity.

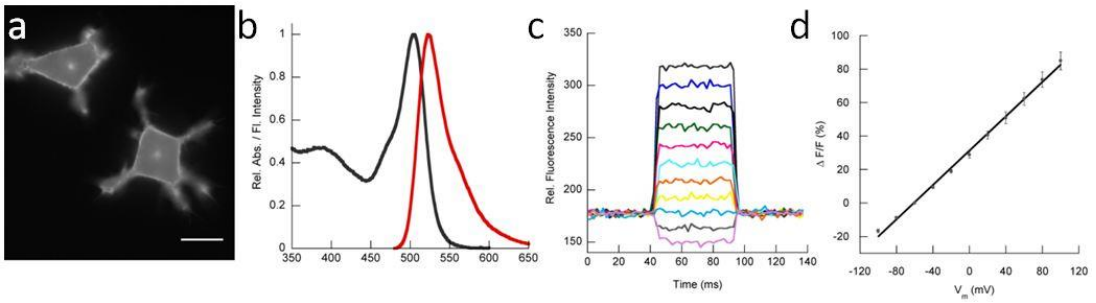

Figure 2.2 Characterization of VoltageFluor 2.1(OMe).H in HEK cells. a) HEK cells stained with 200 nM VF2.1(OMe).H for 15 minutes at 37 °C. Scale bar is 20 μm. b) Absorbance and emission profile of VF2.1(OMe).H at pH 9, 0.01% Triton X-100. c) Fluorescence response of VF2.1(OMe).H in voltage-clamped cells from a), plotted against time, during 50 ms steps from -60 mV to +100 mV followed by steps decreasing in potential by 20 mV increments to -100 mV. d) Linearity of VF2.1(OMe).H response (ΔF/F) vs. final membrane potential in the physiologically relevant range (±100 mV). Each data point represents three separate measurements. Error bars are ±SEM for ≥ 3 separate experiments.

In an effort to determine the sensitivity of our VF Dyes to changes in membrane potential, whole-cell, voltage-clamped HEK cells were held at -60 mV and then stepped to hyper- and depolarizing potentials 20 mV steps ranging from -100 mV to +100 mV in Figure 2.2c and d. After background subtraction, voltage sensitivities ranging from 4% to 49% ΔF/F per 100 mV were measured for the VF dyes, with VF2.1.Me least and VF2.1OMe.Cl most sensitive, with VF2.1OMe.H registering 48% ΔF/F per 100 mV.

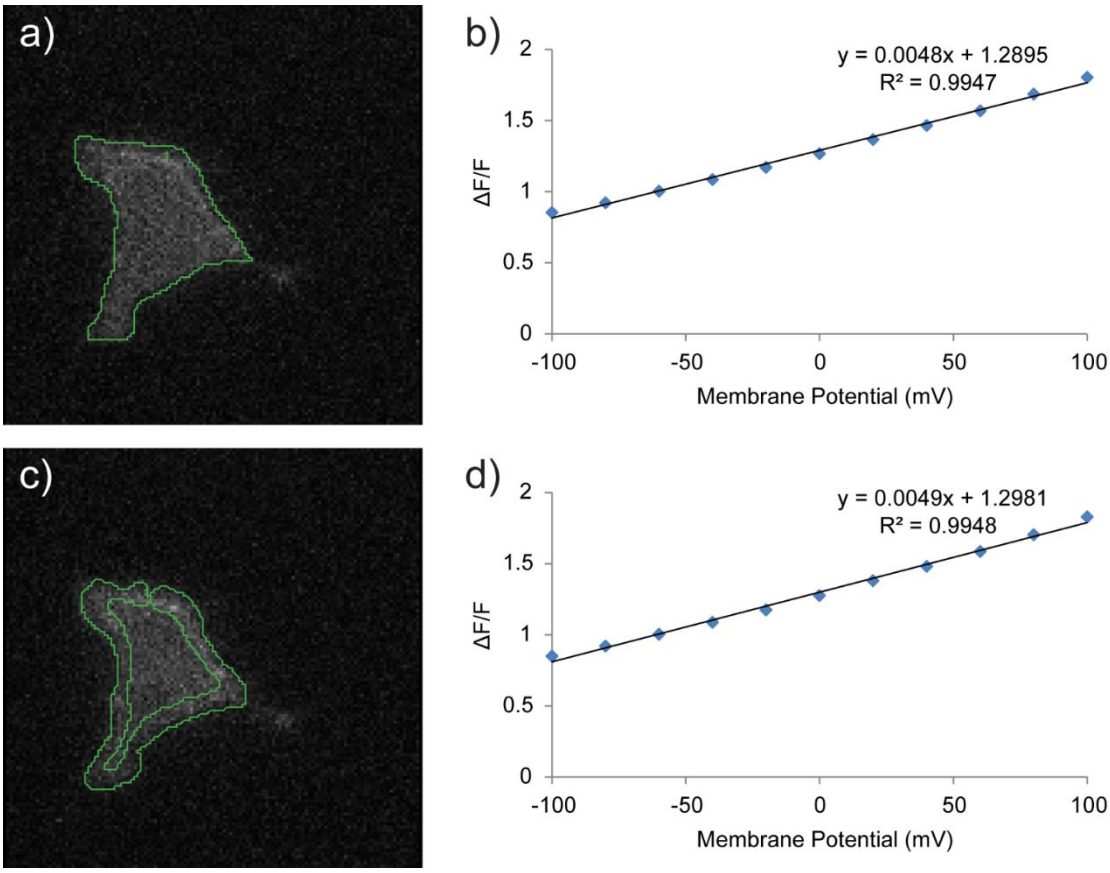

Figure 2.9 indicates an example of region of interest (ROI) selection for determining voltage sensitivity. Importantly, control compound VF2.0.Cl, which lacks an electron-rich aniline donor, shows no voltage sensitivity in Figure 2.10.

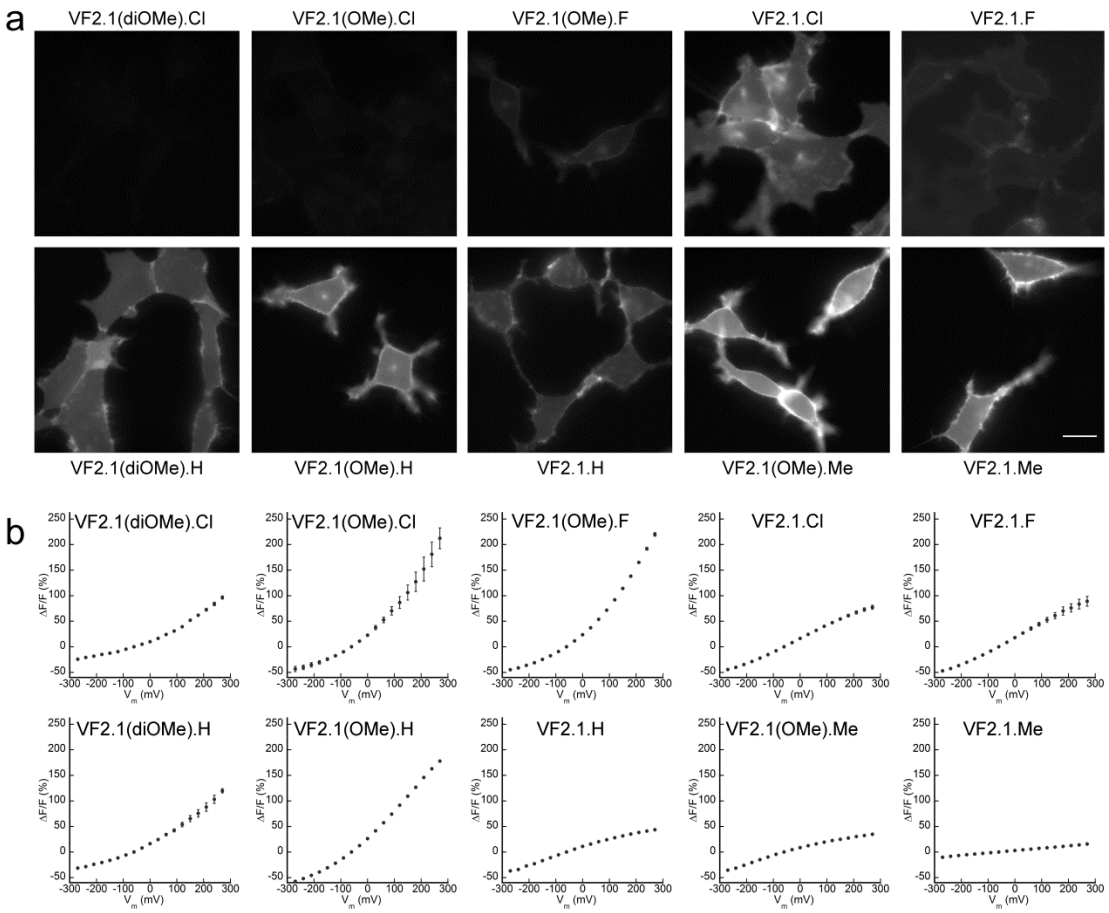

Figure 2.3 Staining and voltage sensitivity of VoltageFluor dyes in HEK cells. a) Epifluorescence images of HEK cells incubated in HBSS buffer containing 200 nM of the indicated VoltageFluor dyes for 15 min at 37°C. All acquisition and analysis parameters are identical, to enable an estimation of the relative brightness of the dyes in a cellular context. Scale bar is 20 μm. Cells are not under voltage-clamp conditions. b) Fluorescence response of representative VoltageFluor dyes vs. membrane potential. Voltage-clamped HEK cells were held at -60 mV and then stepped to the indicated potential. The relative change in fluorescence (ΔF/F) is plotted against the final membrane potential for VoltageFluor dyes loaded in HEK cells at a concentration of 200 nM. Error bars are ±SEM for $n \geq 3$ for each dye.

To further explore the linearity of the VF series we applied a more extreme hyper- and de-polarizing stepping paradigm to HEK cells loaded with VF dyes, assaying a range spanning ±300 mV. Still larger steps proved too much of a strain on the cells and could not be reliably measured. At extremely hyperpolarizing potentials (large negative potential inside the cell), we hypothesized PeT would be maximally activated and the VF dye would be at its dimmest state. Conversely, at larger depolarizing potentials (large positive potential inside), PeT quenching

would be entirely relieved, and the dye would be at its maximal brightness. Fluorescence responses were measured as before, and steps were provided in 30 mV increments to cover the range from ±300 mV. The first generation dye VF2.1.Cl, as well as VF2.1diOMe.H, VF2.1OMe.H and VF2.1.F, fit within a range that encompassed, or nearly encompassed, the minimum and maximum, meaning that the 600 mV range of potentials spanned the energetics required to switch PeT completely on or off in Figure 2.3b. VF dyes bearing more electron rich aniline donors (OMe, diOMe) and/or electron-poor fluorophores, such as VF2.1diOMe.Cl, VF2.1OMe.Cl, and VF2.1OMe.F, showed fluorescence responses

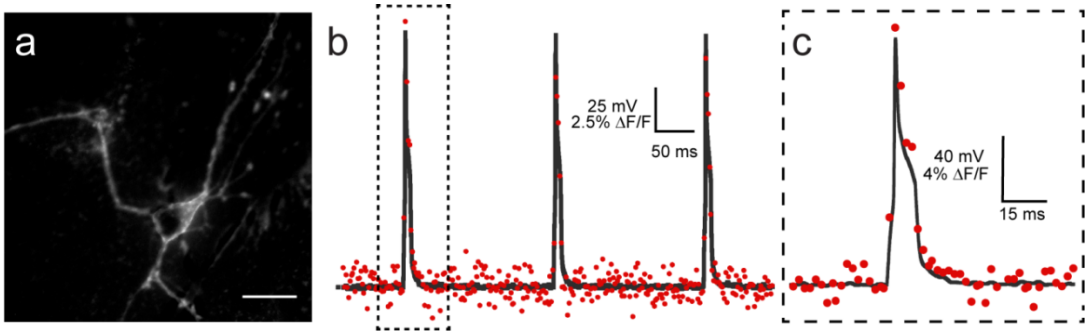

Figure 2.4 Application of VF2.1(OMe).H to sensing action potentials in cultured neurons. a) Epifluorescence image of cultured rat hippocampal/cortical neurons stained with 200 nM VF2.1(OMe).H for 15 minutes at 37 °C. Scale bar is 20 μm. b) Dual optical and electrophysiological recordings of evoked action potentials in cultured neurons. c) Expanded time scale of the first stimulation in (b).

that generally comprised the lower bound of the sigmoidal curve at hyperpolarizing potentials, indicating that PeT processes dominate in this regime. Only at extremely depolarizing potentials (>100 mV) did significant voltage sensitivity manifest. A final grouping of dyes, including VF2.1.H, VF2.1OMe.Me, and VF2.1.Me, displayed fluorescence responses confined to the asymptote achieved at extreme depolarizing potentials. In this regime, radiative pathways predominate, giving bright signals that can only be quenched upon extreme hyperpolarization of the cell membrane.

2.2.3 Estimation of (ΔG_{PeT} + w)

To gain a more quantitative understanding of the factors that contribute to voltage sensitivity, we measured the redox potentials of both the donors and acceptors within the VF framework. The oxidation and reduction potentials of dimethyl anilines and substituted sulfofluoresceins were measured via cyclic voltammetry. As expected, Cl-substituted sulfofluorescein was most readily reduced (E^o (A/A^-) -2.02 V vs ferrocene, Fc), followed by F-substituted sulfofluorescein (-2.10 V vs Fc). Unsubstituted sulfofluorescein was 130 mV more difficult to reduce (-2.24 V vs Fc), and Me-substituted sulfofluorescein was the most difficult to reduce (-2.32 V vs Fc) in Figure 2.11**.** Measuring oxidation potentials of the donors proved more challenging, as the resulting radical cations undergo further oxidation and reaction to form benzidine species, limiting our ability to report oxidation potentials of the pure dimethylaniline species.[7] We instead measured the oxidation potential of synthetic intermediates **4**, which, on account of substitution *para-* to the dimethylamino group, restricted formation of confounding dimeric species. Oxidation of the phenylenevinylene dimethylanilines were still fairly reactive, giving irreversible voltammograms, but provided more reliable initial oxidation measurements in Figure 2.11. The unsubstituted donor measured at the initial oxidation peak was the least readily oxidized (E^o (D/D^+) +0.129 V vs Fc). A single methoxy substitution *ortho-* to the dimethylamino group gave an oxidation potential of 0.090 V vs Fc, while 2,5-dimethoxy aniline was the most readily oxidized at 0.033 V vs Fc. With these values in hand, we could estimate the driving force for PeT through the use of the Rehm-Weller equation,[32] $\Delta G_{PeT} = \Delta E^{\circ}_{ox} - \Delta E^{\circ}_{red} - \Delta E_{0,0} - w$, where ΔE°_{ox} is the oxidation potential of the donor, ΔE°_{red} is the reduction potential of the acceptor/fluorophore, $\Delta E_{0,0}$ is the energy required to excite the chromophore into relevant window of ±100 mV in Figure 2.3b and Figure 2.6. However, the response was not linear, and significant quenching is observed at hyperpolarizing/neutral potentials. Only upon achieving more extreme depolarizing

potentials do these dyes unquench to give significant fluorescence responses to changing membrane potentials in Figure 2.3b. Conversely, for the three VF dyes with ($\Delta G_{PeT} + w$) greater than -0.08 eV, sufficient driving force is not available to quench fluorescence, and so radiative pathways dominate VF2.1.H, VF2.1OMe.Me, and VF2.1.Me in Figure 2.3b

This results in low voltage sensitivity (5-16% ΔF/F per 100 mV) in the physiological range that becomes larger only upon increased hyperpolarization. Finally, the four VF dyes with intermediate (ΔG_{PeT} + w) values, ranging from -0.13 to -0.22 eV show the most linear responses to membrane potential changes within the physiologically relevant range of ±100 mV in Figure 2.3b, with moderate (27%) to high (48%) voltage sensitivity Figure 2.6. These dyes include VF2.1.Cl, VF2.1.F, VF2.1diOMe.H, and VF2.1OMe.H. These data suggest a threshold of (ΔG_{PeT} + w) values less than -0.08 eV, but no lower than -0.27 eV, are required to achieve voltage sensitivity greater than 20% ΔF/F per 100 mV. Two dyes that meet this criteria, VF2.1OMe.Cl and VF2.1OMe.H show high voltage sensitivity, at 49 and 48% ΔF/F per 100 mV, a >80% improvement over the initial VF2.1.Cl compound. Although the absolute sensitivity of VF2.1OMe.Cl is marginally greater than VF2.1OMe.H, the more negative (ΔG_{PeT} + w), which results in more quenching at physiological membrane potential, makes VF2.1OMe.H more suitable for investigations of membrane potential fluctuations at or near -60 mV (nominal resting membrane potential for many neurons). Additionally, the brighter staining of HEK cell the first electronically excited state, and *w* is a work term representing the energy required to separate two charges. Due to the minor structural differences between the VF compounds, *w* remains relatively constant across the VF series, though its absolute magnitude remains difficult to estimate with precision. The ($\Delta G_{PeT} + w$) values are summarized in Figure 2.6.

VF dyes bearing electron-withdrawing groups (Cl, F) on the fluorophore and electron-donating groups (OMe, diOMe) on the donor had the most negative ($\Delta G_{PeT} + w$) values, while

VF dyes with electron-donating (H, Me) fluorophores and unsubstituted dimethylanilines had the highest ($\Delta G_{PeT} + w$) values. The experimentally estimated ($\Delta G_{PeT} + w$) values correlates well with the fluorescence response of the VF dyes at extreme potentials. For the three dyes with ($\Delta G_{PeT} + w$) values lower than -0.23 eV, VF2.1diOMe.Cl, VF2.1OMe.Cl, and VF2.1OMe.F, voltage sensitivity was moderate to high (20% to 49%ΔF/F per 100 mV) in the physiologically with VF2.1OMe.H over VF2.1OMe.Cl, made it the optimal probe for subsequent biological applications.

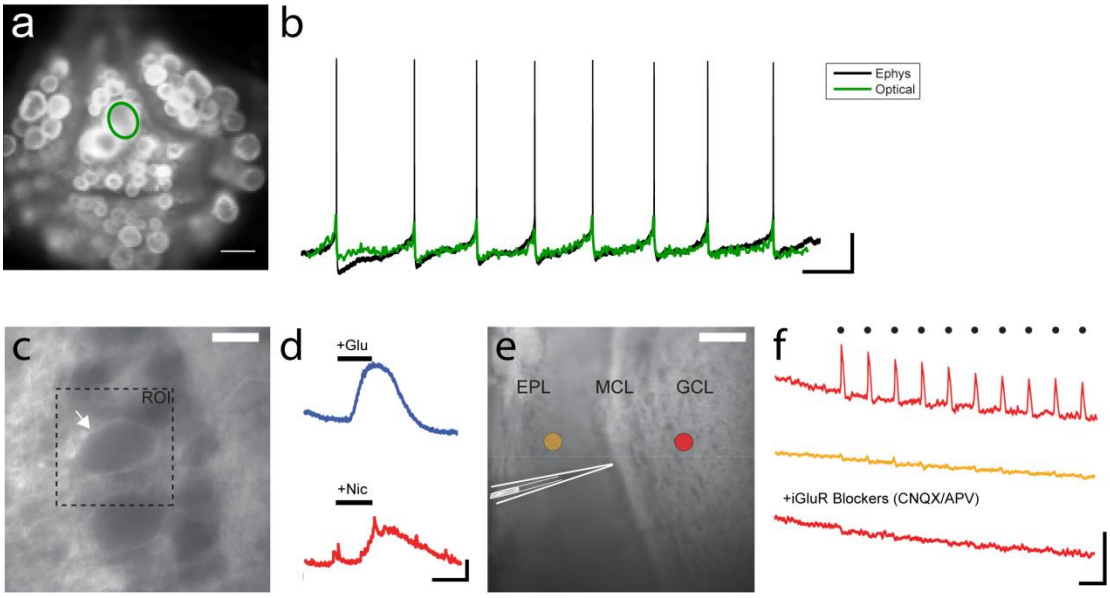

Figure 2.5 Applications of VF2.1OMe.H a) Epifluorescence image of *H. medicinalis* mid-body ganglia stained with VF2.1OMe.H. Scale bar is 50 µm. b) Optical (green) and electrophysiological (black) recording of spontaneous activity in the leech ganglia from ROI indicated in a). The calibration bar is 0.3% ΔF/F, 4 mV, and 1 s. c) Epifluorescence image of a sagittal mouse olfactory bulb (OB) slice loaded with VF2.1OMe.H (500 nM). The dotted square represents the ROI used for quantification. The white arrow points to the plasma membrane of a mitral cell (MC) loaded with VF dye. The scale bar is 10 µm. d) Optical recordings (0.5 Hz acquisition) showing the fluorescence response of VF2.1OMe.H in the cell from (c) to glutamate (blue trace, +Glu, 100 µM, 1.5 min.) and nicotine (red trace, +Nic, 30 µM, 1.5 min.). The calibration bar is 2% ΔF/F and 2 min. e) Epifluorescence wide field view of another olfactory bulb slice loaded with VF2.1OMe.H. A patch electrode was used to electrically stimulate in the vicinity of the mitral cell layer (MCL). The top calibration bar is 50 µm. Orange and red circles indicate regions of interest used for analysis in f). f) Optical recordings (200 Hz acquisition) in the external plexiform layer (EPL, orange) or granule cell layer (GCL, red). The timing of the stimulus pulse is indicated by black dots (10 ms, 10 Hz). The stimulus produces a voltage change in the granule cell layer (GCL, upper red trace) but not in the external plexiform layer (EPL, middle orange trace). The responses in the GCL are abolished in the presence of ionotropic glutamate receptors (iGluR) blockers (APV, 100µM; CNQX, 10µM; bottom red trace). The calibration bar is 2% ΔF/F and 100 ms.

2.2.4 Characterization of VF2.1OMe.H in Neurons

With a more sensitive dye in hand we sought to test its utility in a number of neurologically interesting preparations. First, we applied VF2.1OMe.H to cultured cortical neurons in Figure 2.4. Bath application of the dye extensively stained neuronal cell membranes, as determined by epifluorescence microscopy in Figure 2.4a. Confocal imaging of

VF2.1OMe.H-stained neurons established localization to the cellular membrane with very little visible internalization in Figure 2.12

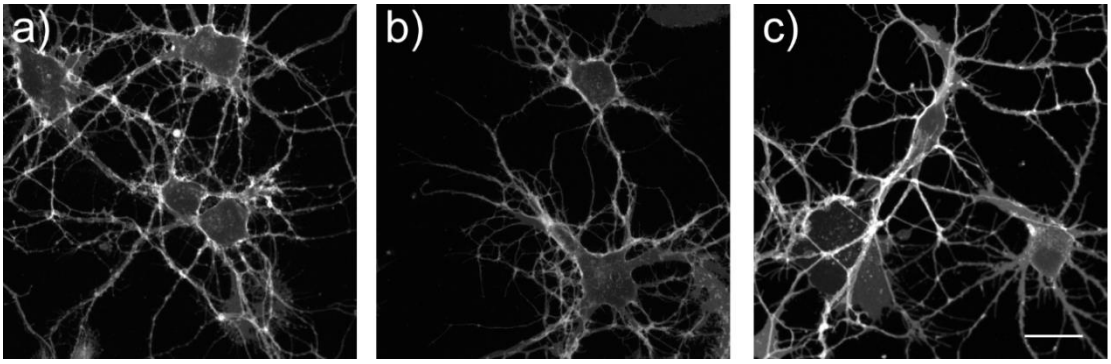

Figure 2.12. These experiments also show little internalization even with an extended loading time of 2 hours Figure 2.12. VF2.OMe.H readily detected action potentials in single trials with a signal to noise ratio of 28:1, near two-fold improvement over VF2.1.Cl. The inherently fast nature by which VF dyes sense changes in membrane potential ($\tau_{on/off} < 150$ μs) offers superior fidelity in reproducing electrical signals compared to protein based sensors with longer response times, for example ArcLight Q239 ($\tau_{on/off}$ = 10-50 ms).[8,9] Beyond culture, one of the promises of voltage imaging is the ability to spatially reconstruct patterns of activity within a functional network.

For this purpose, the medicinal leech has proven to be an important model system for understanding circuit dynamics, because it not only contains several hundred functionally connected neurons, but also provides ready access to both electrophysiological and voltage-sensitive optical recording. Small molecule indicators have a distinct advantage over protein-based indicators because of the difficulty of transfecting adult leech neurons.[10] We prepared desheathed mid-body ganglia from *H. medicinalis* stained with VF2.1OMe.H (200 nM, 20 min.). Following treatment with VF2.1OMe.H, cellular membranes in the ganglia showed strong fluorescence characteristic of VF dyes in Figure 2.5a. Using paired electrode recording (20-40 MΩ) in conjunction with fluorescence imaging, we monitored fluorescence as a

function of membrane potential. Spontaneously firing action potentials from the Retzius cell were clearly distinguished optically Figure 2.5b, and the time course matched that of the intracellular electrode in the black trace of Figure 2.5b. VF2.1OMe.H detects not only supra-threshold spikes, but also slower depolarization and re polarizations following action potential. These repolarizations were not observed in the rat optical or electrophysiological traces due to a stimulus artifact that bled slightly into the repolarization phase of the action potential. In both cases (rat and leech), the optical trace clearly follows the electrophysiology, establishing the fidelity of the VF dyes for tracking real membrane potential changes. The action potentials in the leech optical recording appear truncated due to undersampling in the fluorescence channel (acquisition speed is 50 Hz). The fractional change in fluorescence is approximately 3x larger than with VF2.1.Cl, consistent with the improvement (approximately 2x) observed in HEK cells.

Compound	R_1=	R_2=	R_3=	R_4=	$E°(D^+/D)$ (V)[a]	$E°(A/A^-)$ (V)[a]	λabs (nm)[b]	λem (nm)[b]	ΔG_{00} (eV)	$\Delta G°_{PeT}$ + w (eV)	ΔF/F[c]	Φ_{Fl}[b]
VF2.1diOMe.Cl	$N(Me)_2$	OMe	OMe	Cl	0.033	-2.02	521	535	2.38	-0.325	20	0.26
VF2.1OMe.Cl	$N(Me)_2$	OMe	H	Cl	0.090	-2.02	522	536	2.38	-0.263	49	0.13
VF2.1OMe.F	$N(Me)_2$	OMe	H	F	0.090	-2.11	509	528	2.44	-0.243	44	0.05
VF2.1.Cl	$N(Me)_2$	H	H	Cl	0.129	-2.02	522	536	2.38	-0.224	27	0.05
VF2.1.F	$N(Me)_2$	H	H	F	0.129	-2.11	508	524	2.44	-0.209	30	0.10
VF2.1diOMe.H	$N(Me)_2$	OMe	OMe	H	0.033	-2.24	504	522	2.46	-0.186	30	0.24
VF2.1OMe.H	**$N(Me)_2$**	**OMe**	**H**	**H**	**0.090**	**-2.24**	**504**	**524**	**2.46**	**-0.130**	**48**	**0.04**
VF2.1.H	$N(Me)_2$	H	H	H	0.129	-2.24	507	528	2.45	-0.076	16	0.11
VF2.1OMe.Me	$N(Me)_2$	OMe	H	Me	0.090	-2.32	515	536	2.41	0.003	13	0.04
VF2.1.Me	$N(Me)_2$	H	H	Me	0.129	-2.32	513	532	2.42	0.033	5	0.38
VF2.0.Cl	H	H	H	Cl	1.080[d]	-2.02	521	538	2.38	0.722	0	0.50

[a] vs. Ferrocene (Fc). [b] 0.01% Triton X-100, 5 mM sodium phosphate, pH 9. [c] %ΔF/F Me per 100 mV asured in voltage-clamped HEK cells. [d] Oxidation potential of stilbene taken from Ref 33.

Figure 2.6 Properties of VF Dyes

Next, we assessed the ability of the dye to detect voltage changes in brain slice—a more challenging endeavor considering the complexity, scale, and diversity of the preparation.

Efforts to visualize voltage changes in slice are hampered by small fractional changes in fluorescence. State of the art indicators all have significant shortcomings in this context. For example, the low brightness of QuasAr requires intense laser power to achieve sensing, limiting the observable field to ~ 200 μm^2 before tissue heating becomes a concern.[11] Small molecule voltage-sensitive dyes have inherent limitations as well, particularly with indiscriminate staining of all plasma membranes. Increasing the voltage sensitivity of indicators can partially ameliorate this obstacle, and so we were hopeful that the improved sensitivity of VF2.1OMe.H would allow us to measure membrane potential changes optically in a brain slice.

We turned to the olfactory bulb (OB) of mice because it contains a well-characterized synaptic connectivity which has largely been explored through traditional electrophysiological means or by optical imaging through absorbance techniques.[12,13] Within the OB, sensory input excites principal neurons—the mitral and tufted cells (MCs). Activation of MCs excites, via ionotropic glutamate receptors, surrounding local inhibitory neurons, or granule cells (GCs).[14] Staining of OB slice with VF2.1OMe.H (500 nM, 20 min incubation), resulted in strong fluorescence signals from the cell membranes of OB neurons, in particular the large MCs in Figure 2.5c. Activation of MCs by bath application of glutamate gives a large increase in fluorescence intensity, lasting several minutes (optical recording rate = 0.5 Hz) and consistent with activation of the MCs in Figure 2.5d ("G", 100 μM, 2 min; 4.13 ± 0.40%, n=6 $p<0.01$). Additionally, in agreement with previous findings,[35] application of the acetylcholine receptor agonist, nicotine in Figure 2.5d ("N", 30 μM, 2 min), also depolarized MCs ($\Delta F/F$, 3.02 ± 0.27%, n=6 $p<0.01$). Next, we conducted electrical stimulations (10 ms pulses, 10 Hz) in the vicinity of the MC layer (MCL), to synaptically activate granule cells while optically recording (200 Hz frame rate) from this cell layer (GCL). Focal electrical stimulation revealed a fast, robust increase in fluorescence in the GCL in Figure 2.5e, f, red circle and red upper trace, $\Delta F/F$ 1.91 ± 0.23%, n=5, $p<0.01$), owing to activation of granule cells by glutamate released

from MCs. Importantly, this excitation did not elicit a response in the external plexiform layer (EPL) in Figure 2.5e and f orange circle and red trace demonstrating that VF2.1OMe.H can track synaptic transmission from the MCL to the GCL. Additionally, this transmission was sensitive to ionotropic glutamate receptor (iGluR) blockade by APV and CNQX in Figure 2.5f, in the red lower trace (100 and 10 μM; ΔF/F, 0.07 ± 0.15%, n=5, $p<0.01$). When the same experiments were conducted with VF2.1.Cl in order to compare its performance vs. VF2.1OMe.H, the optical response to identical stimulation was substantially larger for VF2.1OMe.H, consistent with results in HEK cells, rat neurons, and leech ganglia. The response from VF2.1OMe.H was 2x larger than VF2.1.Cl for electrical stimulation and 3x to 4x larger under stimulation with glutamate or nicotine, respectively in Figure 2.13. ($p < 0.0015$ in all cases, T-test, n = 6). These experiments and direct comparisons demonstrate the utility of the VF dyes—and especially VF2.1OMe.H—for conducting both fast and slow *in vitro* slice network physiology.

2.2.5 Supporting Figures

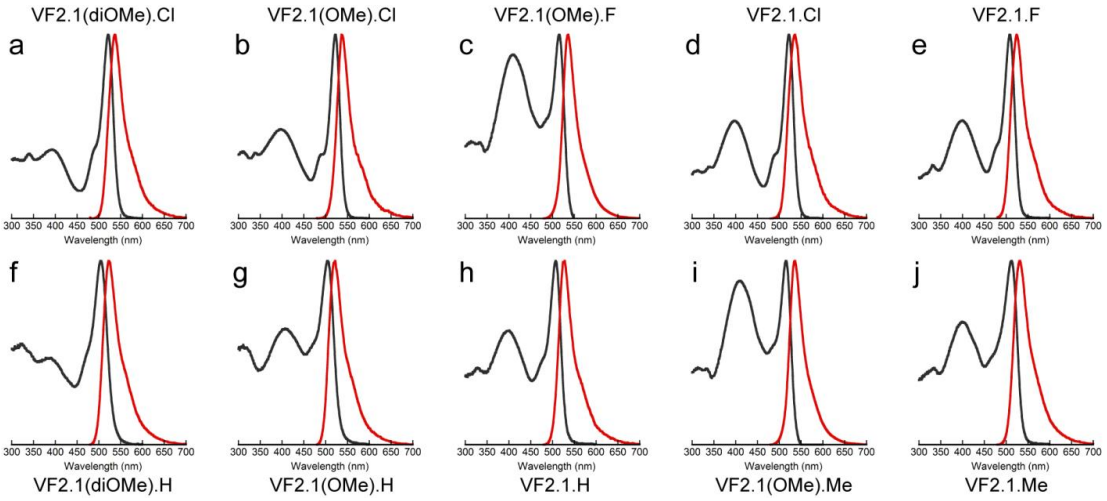

Figure 2.7 Absorbance and emission profiles of VF dyes at pH 9, 0.01% Triton X-100.

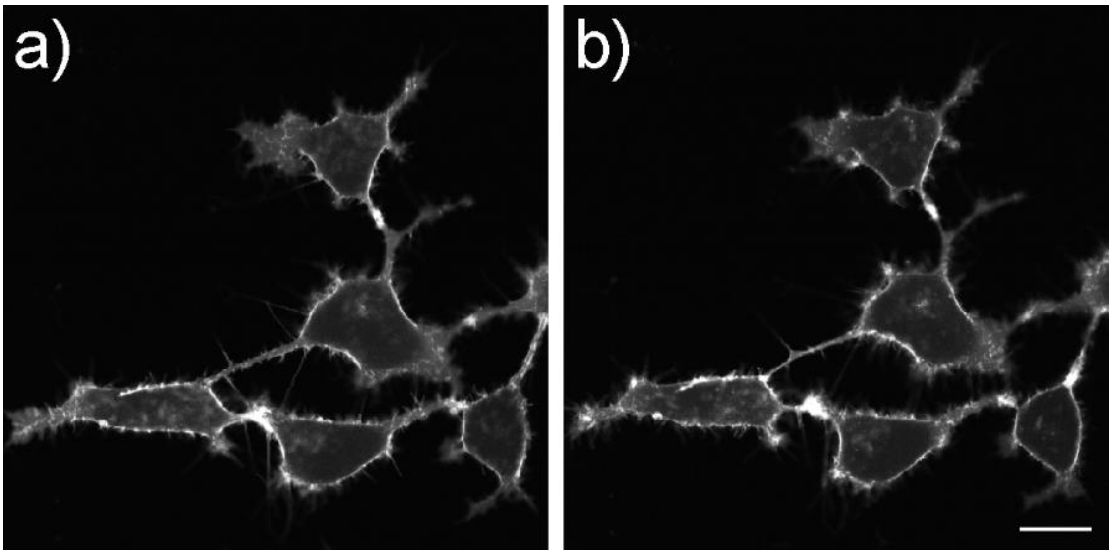

Figure 2.8 Long term staining of HEK cells with VF2.1(OMe).H. Confocal fluorescence microscopy images of HEK cells incubated in HBSS containing 200 nM VF2.1(OMe).H at 37 °C for 15 min. a) Image captured 10 minutes after incubation b) Subsequent visualization of the same field of cells 75 minutes later indicates minimal dye internalization. Scale bar is 20 μm.

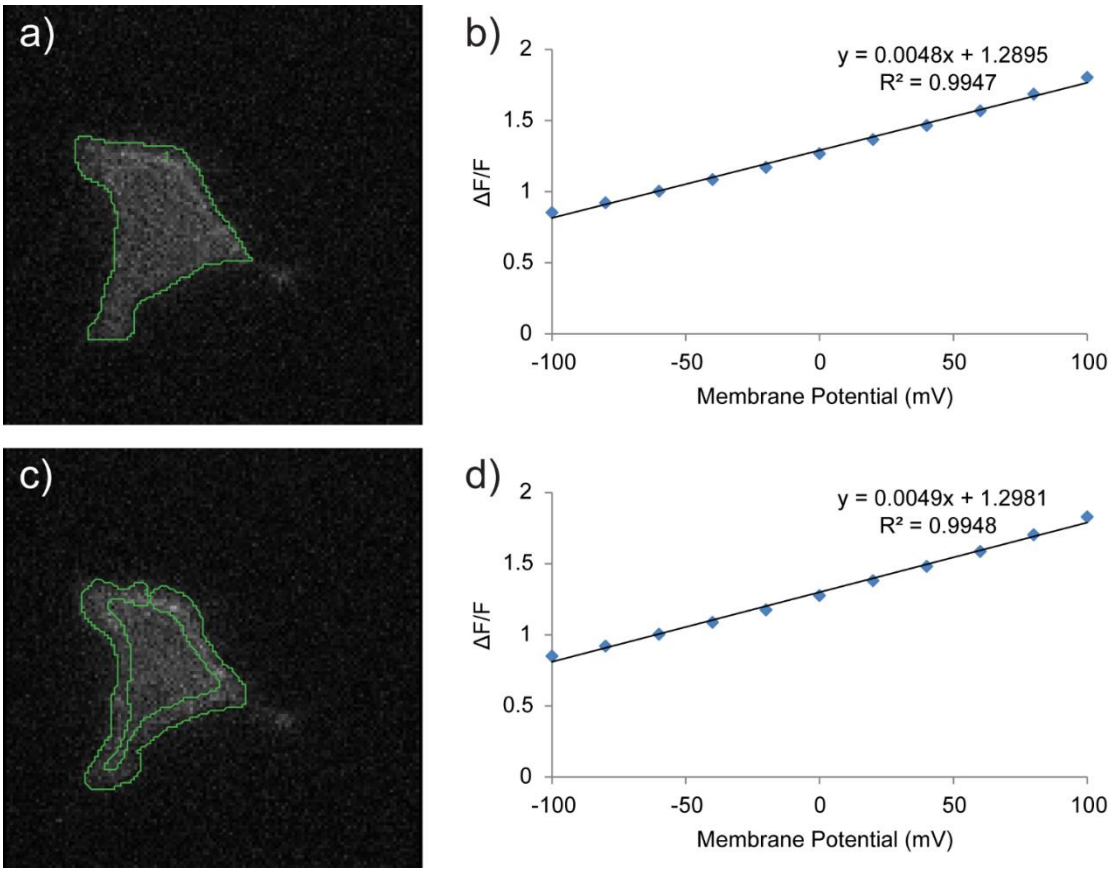

Figure 2.9 Comparison of region of interest (ROI) shape on measured voltage sensitivity in HEK cells. HEK cells were stained with VF2.1(OMe).H and subjected to whole-cell patch-clamp electrophysiology and fluorescence imaging, as in Figure 2 in the main text. All data in this figure was acquired once, the difference is in the analysis. a/c) ROI used to determine the change in fluorescence upon depolarizing and hyperpolarizing voltage steps. b/d) ΔF/F vs. final membrane potential. In both cases (full ROI (a) or membrane-only ROI (c)), the voltage sensitivity is within experimental error, 48% vs 49% per 100 mV.

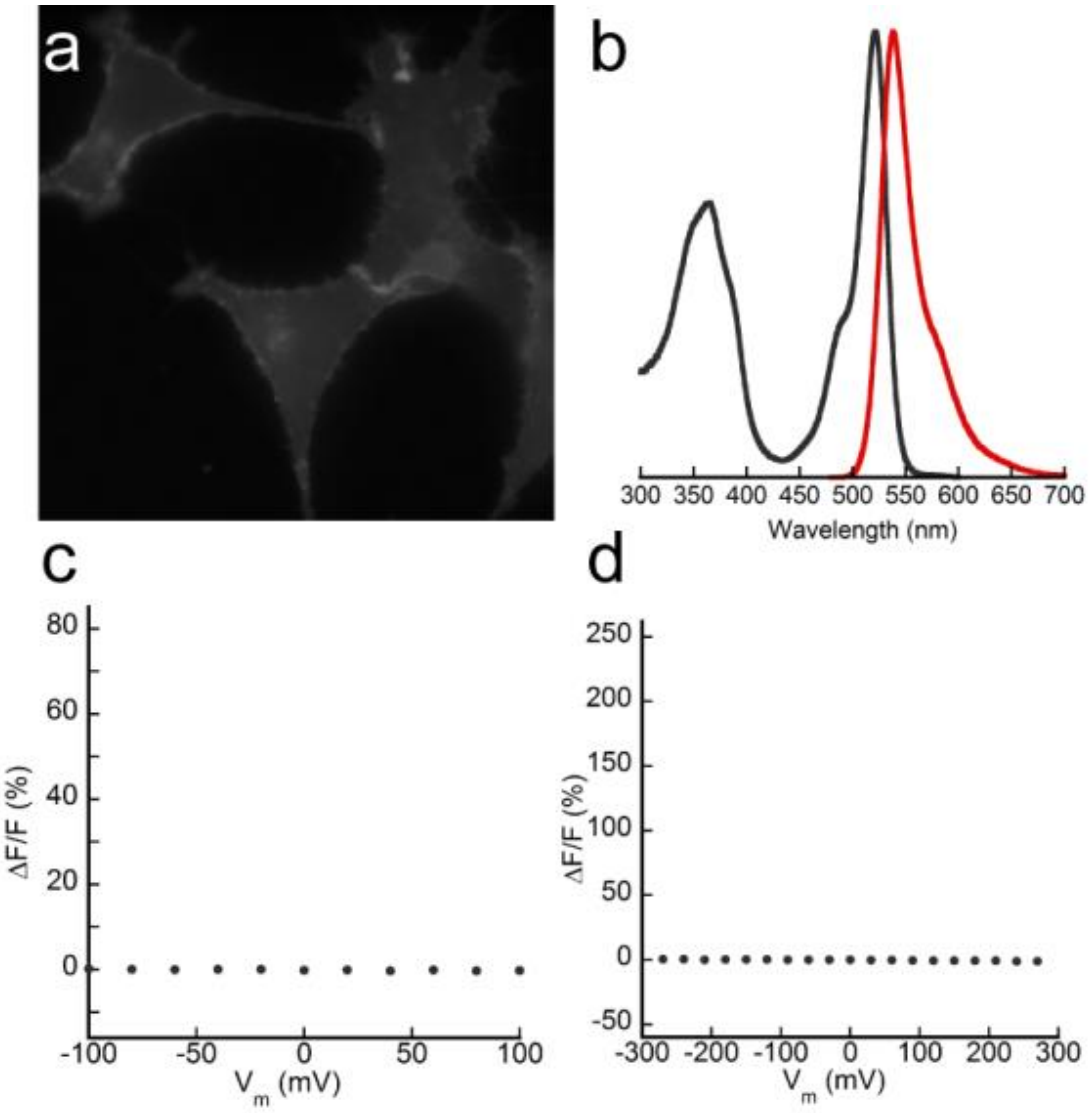

Figure 2.10 Characterization of VoltageFluor 2.0.Cl in HEK cells. a) HEK cells stained with 200 nM VF2.0.Cl for 15 minutes at 37 °C. b) Absorbance and emission profile of VF2.0.Cl at pH 9, 0.01% Triton X-100. c) Fractional change in VF2.0.Cl fluorescence in voltage-clamped cells from a), stepped from a holding potential of -60 mV to the indicated final potential (± 100 mV). d) Fluorescence response at extreme potentials (± 300 mV). Each data point represents three separate measurements. Error bars are ±SEM for ≥ 3 separate experiments.

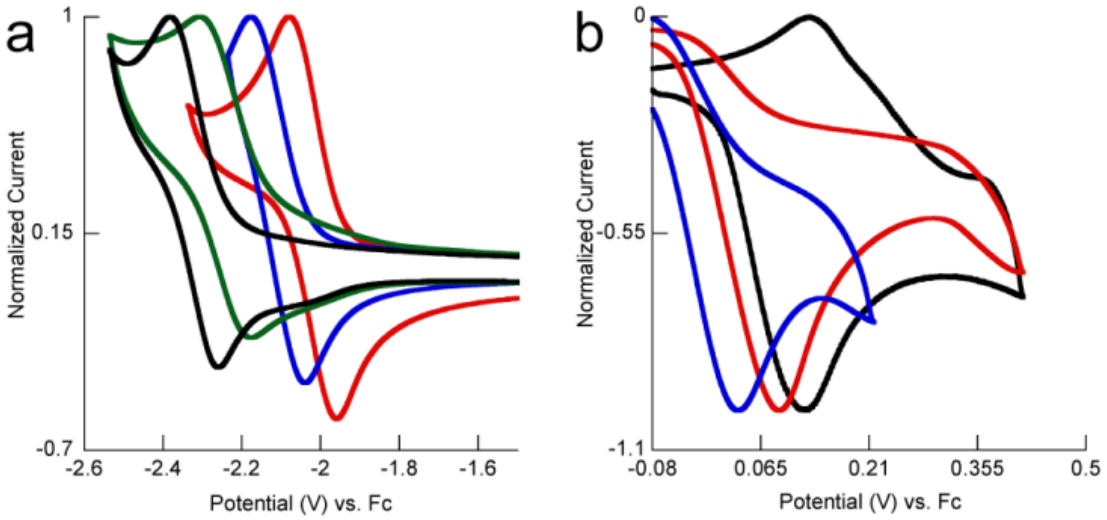

Figure 2.11 Electrochemical characterization of VoltageFluor components. a) Cyclic voltammogram of 2,7- di-chloro (red), di-fluoro (blue), di-hydro (green) or di-methyl (black) substituted sulforfluoresceins (5). b) Cyclic voltagmmogram of substituted dimethylamino-para-vinylstilbenes (4), R2=R3=H (black), R2=OMe, R3=H, (red), R2=R3=OMe (blue). All scans were performed in DMF, at a scan rate of 200 mV/s, with a 3 mm glassy carbon working electrode, a Pt counter electrode, and a Ag/AgNO3 reference. All potentials are reported against an internal Fc+/Fc couple.

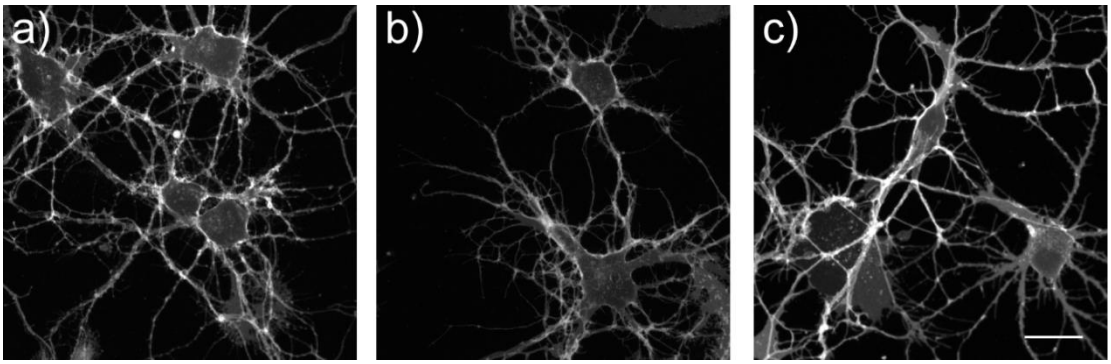

Figure 2.12 VF2.1OMe.H stains neuronal membranes. a-c) Three separate neurons stained with VF2.1(OMe).H (200 nM, up to 2 hours, 25 °C) by bath application. The neurons were washed once, then imaged using confocal microscopy. Clear membrane staining is observed in all cases. Scale bar is 20 μm.

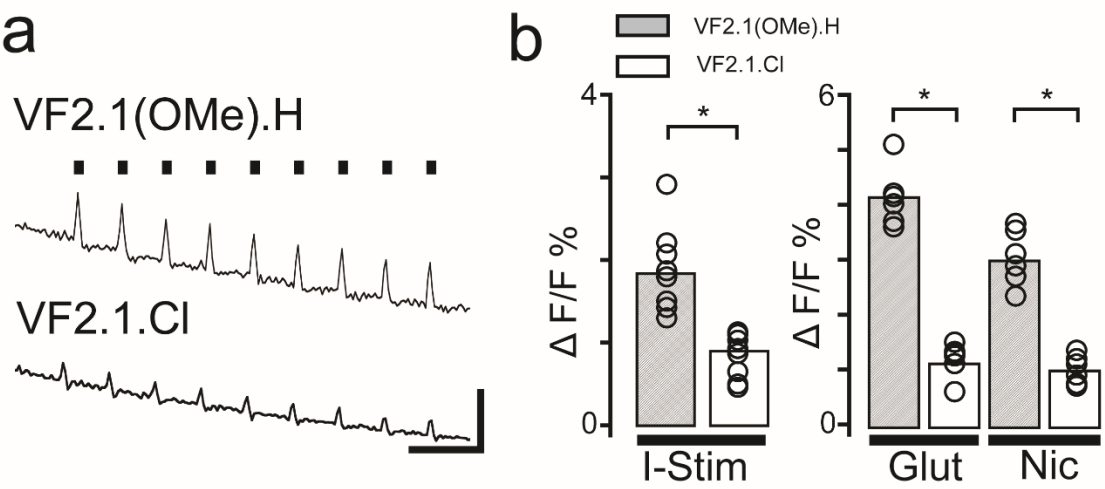

Figure 2.13 Comparison of VoltageFluor dye performance in olfactory bulb slice. Olfactory bulb slices were prepared and loaded with VF dyes as in Figure 5c-f, in the main text. Freshly prepared olfactory bulb preparations were loaded with either VF2.1(OMe).H, as in the main text, or with VF2.1.Cl. Experimental stimuli and imaging conditions were identical to the conditions in Fig5c-f. a) Comparison of optical response (ΔF/F) of VF2.1(OMe).H (*upper trace*) and VF2.1.Cl (*lower trace*) in the granule cell layer (GCL) vs. time upon electrical stimulation in the mitral cell layer (MCL). Traces are uncorrected for bleaching of the dye. Scale bar is 150 ms and 2% ΔF/F. b) Summary of responses obtained with VF2.1(OMe).H and VF2.1.Cl to electrical simulation (I-Stim; experiments performed as in Figure 5c/d) and pharmacologically evoked activity (Glut = glutamate, 100 μM, Nic = nicotine, 30 μM; experiments performed as in Figure 5c/d). For electrical stimulation, VF2.1(OMe).H (grey bars) displays about 2-fold greater sensitivity vs. VF2.1.Cl (white bars), while for pharmacological stimulation, VF2.1(OMe).H is approximately 4x- and 3x- more sensitive for glutamate and nicotine, respectively. * $p < 0.0015$, Student's T-test, n =6.

2.3 Methods

2.3.1 General Synthetic and Analytical Measurements

$Pd(OAc)_2$ was from Strem Chemicals. All other chemicals were purchased from Sigma-Aldrich and used as received unless otherwise noted. 2',7'-dichloro-5-iodosulfofluorescein and 2',7'-dichloro-5-iodosulfofluorescein were synthesized according to literature procedure.[15] N,N-dimethyl-4-vinylaniline, (E)-4-(4-(dimethylamino)styryl)benzaldehyde, (E)-N,N-dimethyl-4-(4-vinylstyryl)aniline, 4-nitro-2-sulfobenzoic acid, 4-amino-2-sulfobenzoic acid, and 4-iodo-

2-sulfobenzoic acid were synthesized according to literature procedure.[2] Anhydrous solvents and reagents (THF, DMF,NEt_3) were obtained as SureSeal bottles from Sigma-Aldrich. Thin-layer chromatography and flash chromatography were performed using EMD pre-coated silica gel 60 F-254 plates and silica gel 60 (230-400 mesh). Alumina was activity 1, 70-230 mesh. UV-Vis absorbance and fluorescence spectra were recorded on a UV 2700 (Shimadzu) and Fluorolog 2 (Spex) fluorimeter, respectively. Analytical, semi-preparative, and preparative HPLCs were performed on Agilent HPLCs, with Luna C_{18}(2) columns (Phenomenex) using water (solvent A) and acetonitrile (solvent B) with 0.05% TFA as an additive or 0.1 M triethylammonium acetate, pH 7 (solvent A) and acetonitrile (solvent B). Low resolution ESI mass spectrometry was performed on an Agilent LC/MSD Trap XCT coupled to an Agilent HPLC. High resolution mass spectra were acquired on a ThermoFisher Orbitrap XL hybrid mass spectrometer. ^{1}H NMR spectra were collected in $CDCl_3$ or d_6-DMSO (Cambridge Isotope Laboratories, Cambridge, MA) at 25 ºC on a 400 Varian Mercury Plus or Jeol ECA 500 spectrometer at the Department of Chemistry and Biochemistry NMR Facility at the University of California, San Diego. All chemical shifts are reported in the standard δ notation of parts per million using the peak of residual proton or carbon signals of $CDCl_3$ or $(CD_3)_2SO$ as an internal reference.

2.3.2 Electrochemistry

All electrochemical experiments were performed using a BASi Epsilon potentiostat and single compartment electrochemical cell. Glassy carbon (BASi 3 mm diameter) was used as the working electrode, a Pt wire was used as the counter, and an Ag wire in 0.1M $AgNO_3$ acetonitrile separated from the solution by a Vycor tip was purchased as a kit from BASi (MF-2062) and used as a pseudo reference. All electrochemical experiments were performed in dimethyl formamide with 0.1 M tetrabutylammonium hexafluorophosphate as the supporting

electrolyte, and were purged with nitrogen before cyclic voltammograms (CVs) were taken. All experiments were performed at a 200 mV/s scan rate. Ferrocen was used as an internal standard. All oxidation potentials were taken at the peak of the initial oxidation curve. All reduction potentials were taken as the average of the reduction peak and subsequent oxidation peak of the reduced species.

2.3.3 Patch Clamping neurons and HEK Cells

HEK293 cells were cultured in DMEM (CellGrow) supplemented with 10% FBS, 1% penicillin/streptomycin (Invitrogen) and plated on glass bottom culture dishes (35 mm dish, 14 mm microwell with No. 0 coverglass) (MatTek Corporation). Hippocampal neurons were dissected from postnatal day 0 or 1 rat pups and plated on poly-D-lysine-coated glass bottom culture dishes. Neuronal recordings were made 14-28 days in culture.

Electrophysiological recordings of HEK293 cells and cultured neurons were performed with an Axopatch 200A or 200B amplifier (Molecular Devices) at room temperature. The extracellular solution consisted of (in mM) 145 NaCl, 20 glucose, 10 HEPES, 3 KCl, 2 CaCl2, 1 MgCl2 (pH 7.35, 310 mOsm). The intracellular solution contained (in mM) 115 potassium gluconate, 10 BAPTA tetrapotassium salt, 10 HEPES, 5 NaCl, 10 KCl, 2 ATP disodium salt, 0.3 GTP trisodium salt (pH 7.25, 290 mOsm).

For fluorescence microscopy studies in HEK 293A cells and hippocampal neurons, light was provided by a xenon arc lamp powered by an Optiquip Power supply (Optiquip) with a mechanical shutter controlled by a Lambda 10-2 controller (Sutter). Light from the xenon arc lamp was filtered through a 10% neutral density filter, a 480 nm filter (30 nm bandpass, Chroma), a 510 nm dichroic (Semrock), a 540 nm emission filter (50 nm bandpass, Semrock), and focused through a 40x/1.4 oil objective.

Epifluorescence images were acquired with a Cascade II 512, CoolSNAP cf2 or Evolve 128 (Photometrics) controlled with Slidebook software (Intelligent Imaging Innovations).

2.3.4 Confocal Imaging

Confocal images of HEK cells and cultured cortical rat neurons were acquired with a Nikon A1 microscope, standard eGFP filter set, and a 25x 1.10 oil objective. HEK cells and neurons were bath incubated with 200 nM of VF2.1(OMe).H for 15 minutes followed by a wash. Cells were imaged 10 to 120 minutes after the wash in the extracellular solution described above. Images were analyzed with Nikon Imaging System Elements software.

2.3.5 Leech Studies

Isolated midbody ganglia (ganglia 8-16) were dissected from *Hirudo medicinalis* and the ventral side was desheathed using standard procedures. The voltage sensitive dye was combined with HEPES saline down to the desired concentration (100-300 nM), and 1.5 μL of a 20% (w/v) solution of Pluronic F-127 in DMSO. The dye was then continuously pumped over the ganglion to help with penetration into the cell membranes for 20-30 minutes. Electrophysiological measurements were made with paired electrode recordings with resistances in the range of 20-40 MΩ. Electrode 1 acted as the recording electrode, which constantly monitored membrane potential, and electrode 2 acted as the current injecting electrode. Spontaneous Retzius cell activity was measured with a single electrode. Imaging was done with a Cascade 128+ EMCCD camera (Photometrics). The filter set was standard for FITC. The fluorescence illumination was from an LED that has its peak excitation wavelength in the excitation range for FITC. Image acquisition rates for the spontaneous imaging were made at 50Hz at 128x128 pixel resolution under a 20x, 0.5NA objective (Fig 5). Acquisition and analysis were run with custom-made software. The data is stored in Matlab-readable files.

2.3.6 Acute Olfactory Bulb Slice

Animals

All animal procedures were carried out in accordance with the guidelines of the institutional animal care and use committee of the University of Maryland. Electrophysiological and imaging experiments were performed on brain slices obtained from C57/BL6 mice (1-3 weeks old, Jackson Laboratories, ME).

Slice Preparation

Experiments were performed in olfactory bulb (OB) slices using methods previously described.[16] Briefly, mice were anesthetized with isoflurane and decapitated, and the brain was quickly removed and placed in oxygenated ice-cold artificial cerebrospinal fluid (ACSF) containing low Ca^{2+} (1 mM) and high Mg^{2+} (3 mM). Sagittal and horizontal sections (250 μm) of the OB were sliced using a Leica vibrating microslicer (Redding, CA). Slices were then transferred to an incubation chamber containing normal ACSF (see below) and left to recuperate first at 35°C for 30 min, and at room temperature thereafter. In all experiments, unless otherwise stated, the extracellular solution is ACSF of the following composition (in mM): 125 NaCl, 25 $NaHCO_3$, 1.25 NaH_2PO_4, 3 KCl, 2 $CaCl_2$, 1 $MgCl_2$, 3 myo-inositol, 0.3 ascorbic acid, 2 Na-pyruvate, and 15 glucose, continuously oxygenated (95% O_2-5% CO_2) to give a pH 7.4 and an osmolarity of ~305 mOsm. Experiments were performed at room temperature.

2.3.7 Dye Application

20 minutes prior to optical recordings experiments, slices were transferred to a 30 mm Millicell culture dish insert (Millipore Corp, Billerica, Ma) with 3 mL of normal oxygenated ACSF. For OB slices, we found that local delivery of the dye provided better staining than bath application. An Eppendorf pipette was used to evenly "paint" 0.2-1.5 μL of 2 mM (prepared in DMSO)

VF2.1OMe.H onto the slices. The Eppendorf pipette was positioned approximately 8 mm from the slice and the dye was carefully ejected into solution above the slice over several seconds. Labeled slices were incubated for 20 minutes in the culture dish and then transferred to a submerged recording chamber mounted on the stage of an Olympus BX51 microscope.

2.3.8 Data Acquisition and Analysis

Labeled slices were observed using fluorescence illumination and 10X and 40X water immersion objectives. Illumination was achieved using an OPTOLED green LED (exciter 488 nm center wave length, Chroma, Bellow Falls, VT ; Cairn Research LTD, UK) and the emitted light was collected by an ORCA-Flash4.0 V2 sCMOS camera (Hamamatsu, Japan) and images recorded using the HCimage software (Hamamatsu, Japan). Imaging recordings, as well as, electrical stimulations were commanded using the PatchMaster software (HEKA USA, Bellmore, NY). Imaging analysis was performed offline using ImageJ processing and IgorPro software (Wavemetrics, OR). Data are shown as the mean ± SEM and statistical significance was determined using the Student *t* test. (*S*)-1-Aminopropane-1,3-dicarboxylic acid(Glutamate, G), 6-cyano-7-nitroquinoxaline-2,3-dione disodium (CNQX), DL-2-Amino-5-phosphonopentanoic acid (APV), (−)-nicotine ditartrate (N), were prepared from stocks and added to the bathing solution. The speed of perfusion allowed for full solution exchange in <1 min. All drugs were purchased from Tocris Cookson (UK). To stimulate MCs, we used a patch electrode pipette filled with ACSF. Square current pulses were delivered using a stimulus isolator unit (A.M.P.I., Jerusalem, Israel). The stimulus intensity (0.5–3 mA, 10 ms) was adjusted to evoke responses in the granule cell layer (GCL). The optical traces in Figure 5d and 5f are uncorrected for bleaching.

2.3.9 Data Analysis

For voltage sensitivity measurements, regions of interest (ROIs) were drawn around clamped cells and the mean fluorescence measured in Slidebook (Intelligent Imaging Innovations) or ImageJ (NIH). For HEK cells, background fluorescence was subtracted by measuring the fluorescence where no cells grew. For HEK cells, there was no difference in voltage sensitivity calculation when the ROI included the cytosol or if the ROI was a "doughnut" that included mainly the cell membrane as in Figure 2.9. For experiments in neurons, the background fluorescence was not subtracted. In all cases, ΔF/F was calculated by dividing the fluorescence signal by the average fluorescence for a baseline of 10-20 frames prior to, and after stimulation.

2.3.10 Supporting Information

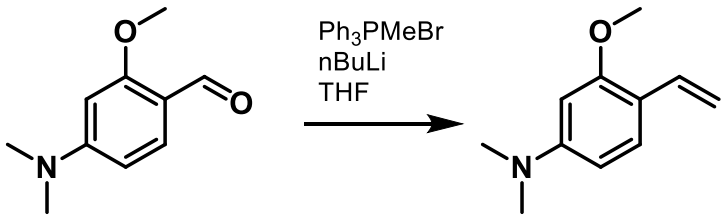

Synthesis of 2-methoxy-4-N,N-dimethylaminostyrene.

An oven-dried round bottom flask was charged with methyltriphenylphosphonium bromide (4.3 g, 12 mmol, 1.8 equiv.) and 50 mL anhydrous THF and stirred under N_2. A 1.6 M solution of *n*-butyllithium in hexanes was added via syringe (6.7 mL, 10.7 mmol, 1.6 equiv.) at room temperature. After stirring for 30 min, 4-N,N-dimethyl-2-methoxybenzaldehyde (1.12 g, 6.69 mmol, 1.0 equiv.) was added. After stirring overnight, the reaction was poured into 100 mL of hexanes. The suspension was filtered through Celite and concentrated under reduced pressure. The residue was taken up in EtOAc and filtered through a thin pad (1-2 cm) of silica. Removal of solvents under reduced pressure provided 1.18g of a yellow oil (99%). ^{1}H NMR ($CDCl_3$, 300 MHz): δ 7.28 (2H, d, *J* = 8.6 Hz); 6.60 (3H, m); 5.50 (1H, d, *J* = 17.8 Hz); 4.98 (1H, d, *J*

= 10.3 Hz); 3.27 (4H, m); 1.57 (4H, q, *J* = 7.4 Hz); 1.35 (4H, sextet, *J* = 7.4 Hz); 0.96 (6H, t, *J* = 7.4 Hz).

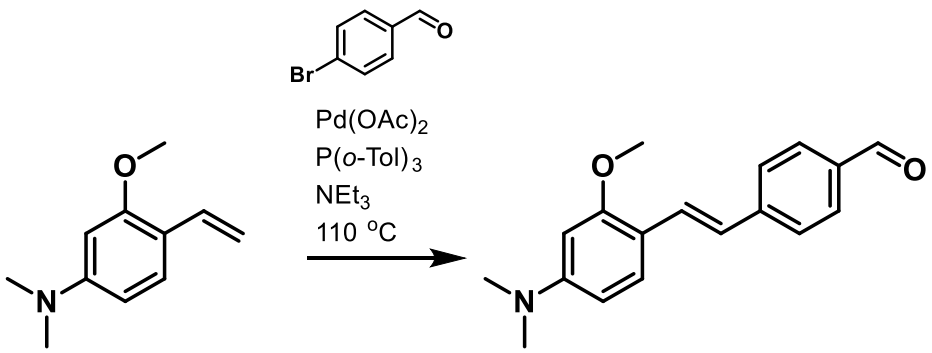

Synthesis of (E)-4-(4-(dimethylamino)-2-methoxystyryl)benzaldehyde.

An oven-dried round bottom flask was equipped with a stir bar and charged with 2-methoxy-4-N,N-dimethylaminostyrene (868 mg, 4.9 mmol, 1.25 equiv.), $Pd(OAc)_2$ (10 mg, 0.049 mmol, 0.01 equiv.), tri-*o*-tolylphosphine (30 mg, 0.10 mmol, 0.02 equiv.), and bromobenzaldehyde (723 mg, 3.9 mmol, 1.00 equiv.). The flask was evacuated and backfilled three times with N_2. Triethylamine (2.5 mL) was added, the round bottom sealed, and heated at 110°C. After stirring 20 hours, the reaction vessel was cooled to room temperature, dissolved in EtOAc and washed with saturated ammonium chloride twice. The organic portions were then collected and washed with saturated NaCl. The organic portions were dried over Na_2SO_4, filtered, and concentrated under reduced pressure. The orange solid was minimally redissolved in methylene chloride and triturated with hexanes to give the title compound as an orange powder, 728 mg (53%). ^{1}H NMR ($CDCl_3$, 300 MHz): δ 9.95 (s, 1H), 7.81 (2H, d, *J* = 8.3 Hz), 7.66 – 7.40 (4H, m), 6.98 (1H, d, *J* = 16.4 Hz), 6.35 (1H, dd, *J* = 8.6, 2.4 Hz), 6.21 (1H, d, *J* = 2.3 Hz), 3.91 (3H, s), 3.03 (6H, s).

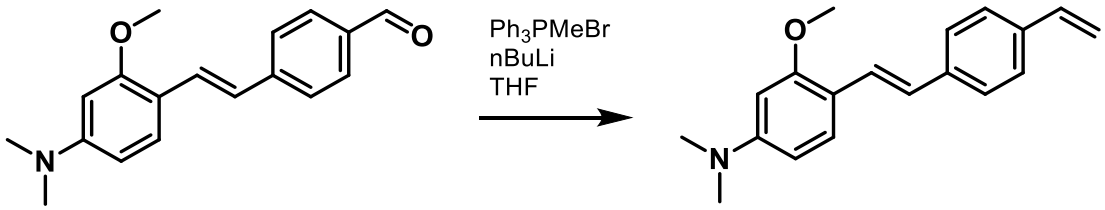

Synthesis of (E)-2-methoxy-N,N-dimethyl-4-(4-vinylstyryl)aniline.

An oven-dried round bottom flask was charged with methyltriphenylphosphonium bromide (1.27 g, 3.57 mmol, 1.8 equiv.) and 50 mL anhydrous THF and stirred under N_2. A 1.6 M solution of *n*-butyllithium in hexanes was added via syringe (1.98 mL, 3.17 mmol, 1.6 equiv.) at room temperature. After stirring for 30 min, (E)-4-(4-(dimethylamino)-2-methoxystyryl)benzaldehyde (558 mg, 1.98 mmol, 1.0 equiv.) was added. After stirring overnight, the reaction was poured into 100 mL of methylene chloride. The suspension was filtered through alumina and concentrated under reduced pressure. The residue was taken up in minimal hexanes and triturated in ethanol. The suspension was filtered and washed with ethanol to give 553 mg of a yellow solid (53%). ^{1}H NMR (300 MHz, $CDCl_3$): δ 7.57 – 7.41 (4H, m), 7.41 – 7.34 (3H, m), 6.98 (1H, d, *J* = 16.4 Hz), 6.71 (1H, dd, *J* = 17.6, 10.9 Hz), 6.54 (1H, bs) 5.74 (1H, d, *J* = 17.6 Hz), 5.22 (1H, d, *J* = 10.9 Hz), 3.91 (3H, s), 3.04 (6H, s).

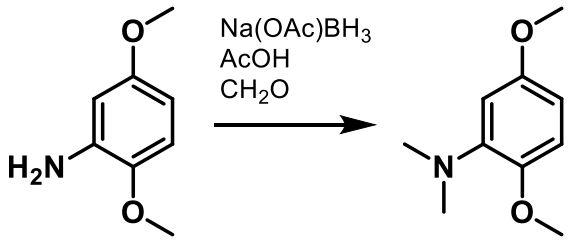

Synthesis of 2,5-dimethoxy-N,N-dimethylaniline.

An oven-dried round bottom flask was charged with 2,5-dimethoxy-aniline (4 g, 26.1 mmol, 1 equiv.), paraformaldehyde (8g, 266 mmol, 10 equiv.), and glacial acetic acid (160 mL) and stirred under N_2. After stirring for 2 hours sodium cyanoborohydride (8 g, 127 mmol, 4.87

equiv.) was added. After stirring overnight the solution was added to 25% sodium hydroxide (200 mL) on ice. The aqueous layer was extracted three times with methylene chloride. The organic layers were collected and filtered through a thin pad (1-2 cm) of silica. Removal of solvents under reduced pressure provided 2.29 g of a yellow liquid (48%). ^{1}H NMR (400 MHz, $CDCl_3$): δ 6.75 (1H, d, *J* = 8.7 Hz), 6.55 (1H, d, *J* = 2.9 Hz), 6.45 (1H, dd, *J* = 8.7, 3.0 Hz), 3.83 (3H, s), 3.76 (3H, s), 2.78 (6H. s).

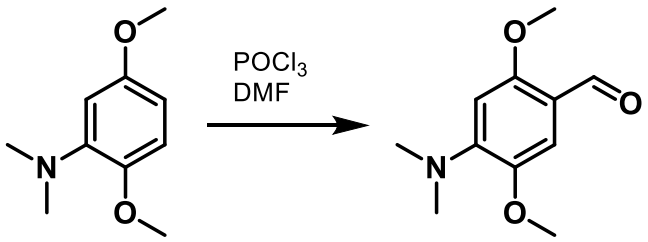

Synthesis of 2,5-dimethoxy-4-N,N-dimethylaminobenzaldehyde.

An oven-dried round bottom flask was charged with 2,5-dimethoxy-N,N-dimethylaniline (2 g, 11 mmol, 1 equiv.) and DMF (1.70 mL, 22 mmol, 2 equiv.) under N_2. The solution was cooled to 0°C and phosphorous oxychloride (1.21 mL, 13 mmol, 1.2 equiv.) was added dropwise. The solution was heated to 65°C. After stirring overnight water (20 mL), followed by 1 M sodium hydroxide solution (20 mL), was added yielding a cloudy yellow solution that was extracted three times with methylene chloride. The organic portions were washed with saturated sodium chloride and dried with anhydrous sodium sulfate. Removal of solvents under reduced pressure provided a brown liquid (1.8g, 78%). ^{1}H NMR (400 MHz, $CDCl_3$): δ 10.24 (1H, s), 7.26 (1H, s), 6.33 (1H, s), 3.88 (3H, s), 3.84 (3H, s), 2.95 (6H, s).

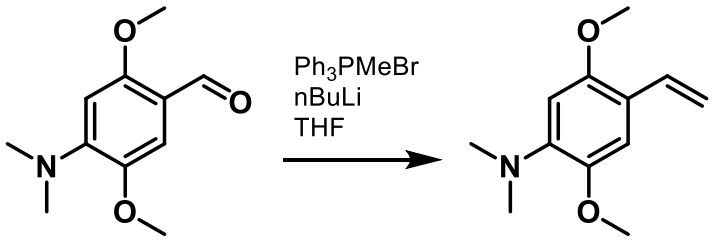

Synthesis of 2,5-dimethoxy-4-N,N-dimethylaminostyrene.

An oven-dried round bottom flask was charged with methyltriphenylphosphonium bromide (4.61 g, 12.9 mmol, 1.8 equiv.) and 50 mL anhydrous THF and stirred under N_2. A 1.6 M solution of *n*-butyllithium in hexanes was added via syringe (7.17 mL, 11.5 mmol, 1.6 equiv.) at room temperature. After stirring for 30 min, 2,5-dimethoxy-4-N,N-dimethylaminobenzaldehyde (1.5 g, 7.17 mmol, 1.0 equiv.) was added. After stirring overnight, the reaction was poured into 100 mL of hexanes. The suspension was filtered through Celite and concentrated under reduced pressure. The residue was taken up in EtOAc and filtered through a thin pad (1-2 cm) of silica. Removal of solvents under reduced pressure provided 1.11g of a yellow oil (74%). (400 MHz, $CDCl_3$): δ 6.99 (1H, dd, *J*=18.0, 7.2 Hz), 6.97 (1H, s), 6.50 (1H, s), 5.60 (1H, d, *J*=20 Hz), 5.16 (1H, d, *J*=12.0 Hz), 3.87 (4H, s), 3.82 (2H, s), 2.81 (6H, s).

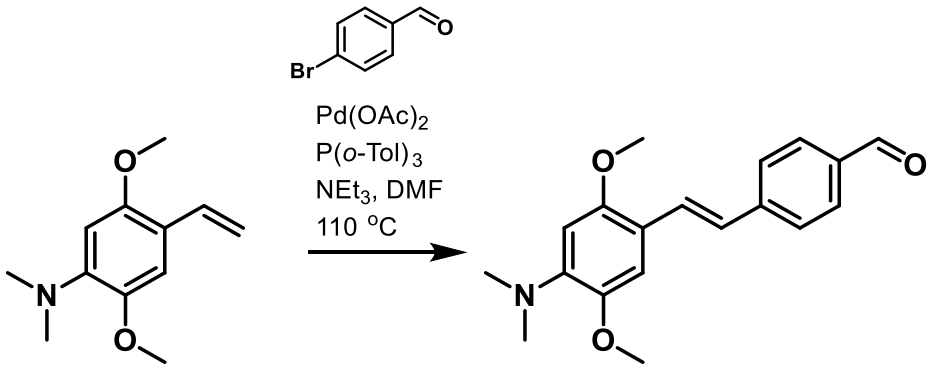

Synthesis of (E)-4-(4-(dimethylamino)-2,5-dimethoxystyryl)benzaldehyde.

An oven-dried round bottom flask was equipped with a stir bar and charged with 2,5-dimethoxy-4-N,N-dimethylaminostyrene (1 g, 4.8 mmol, 1.00 equiv.), $Pd(OAc)_2$ (11 mg, 0.048 mmol, 0.01 equiv.), tri-*o*-tolylphosphine (44 mg, 0.144 mmol, 0.03 equiv.), and bromobenzaldehyde (888 mg g, 4.8 mmol, 1.00 equiv.). The flask was evacuated and backfilled three times with N_2. Triethylamine (1.67 mL) was added, the round bottom sealed and heated at 110°C. After stirring 20 hours, the reaction vessel was cooled to room temperature, dissolved in methylene chloride and washed with saturated ammonium chloride twice. The organic portions were then collected and washed with saturated NaCl. The organic portions were then dried over Na_2SO_4, filtered, and concentrated under reduced pressure. The orange solid was minimally redissolved in methylene chloride and triturated with hexanes. The precipitate was then purified via flash chromatography in a hexanes and ethyl acetate solvent to give the title compound as an orange powder, 800 mg (54%). ^{1}H NMR (400 MHz, CDCl3): δ 9.96 (1H, s), 7.83 (2H, d, J = 8 Hz), 7.63 (2H, d J = 12 Hz), 7.58 (1H, s), 7.07 (1H, s), 7.00 (1H, d, J = 16.4 Hz), 6.50 (1H, s), 3.91 (3H, s), 3.87 (3H, s), 2.86 (6H, s).

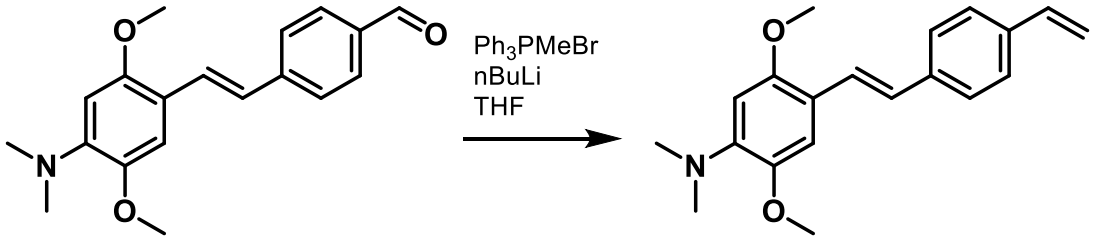

Synthesis of (E)-2,5-dimethoxy-N,N-dimethyl-4-(4-vinylstyryl)aniline.

An oven-dried round bottom flask was charged with methyltriphenylphosphonium bromide (1.65 g, 4.63 mmol, 1.8 equiv.) and 50 mL anhydrous THF and stirred under N_2. A 1.6 M solution of *n*-butyllithium in hexanes was added via syringe (2.6 mL, 4.12 mmol, 1.6 equiv.) at -78°C. After stirring for 30 min at room temperature, (E)-4-(4-(dimethylamino)-2,5-dimethoxystyryl)benzaldehyde (800 mg, 2.58 mmol, 1.0 equiv.) was added. After stirring

overnight, the reaction was poured into 100 mL of hexanes. The suspension was filtered through Celite and concentrated under reduced pressure. The residue was taken up in minimal hexanes and triturated in ethanol. The suspension was filtered to give 496 mg of a yellow solid (62%). ^{1}H NMR (400 MHz, $CDCl_3$): δ 7.49 (2H, d, *J* = 8.3 Hz), 7.44 (1H, d, *J* = 16.5 Hz), 7.39 (2H, d, *J* = 8.3 Hz), 7.08 (1H, s), 6.97 (1H, d, *J* = 16.4 Hz), 6.71 (1H, dd, *J* = 17.6, 10.9 Hz), 6.53 (1H, s), 5.75 (1H, d, *J* = 17.6 Hz), 5.23 (1H, d, *J* = 10.9 Hz), 3.92 (3H, s), 3.87 (3H, s), 2.85 (6H, s).

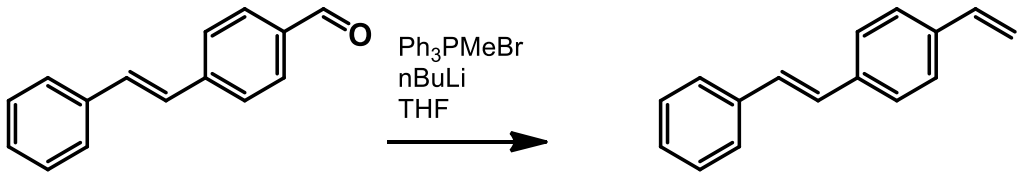

Synthesis of (E)- 1-ethenyl-4-(2-phenylethenyl)-benzene.

An oven-dried round bottom flask was charged with methyltriphenylphosphonium bromide (3.08g, 8.6 mmol, 1.8 equiv.) and 10 mL anhydrous THF and stirred under N_2. A 1.6 M solution of *n*-butyllithium in hexanes was added via syringe (2.2 mL, 3.5 mmol, 1.6 equiv.) at -78ºC. After stirring for 1 hour at room temperature, 4-(2-phenylethenyl)-benzaldehyde (1.0 g, 4.8 mmol, 1.0 equiv.) was added. After stirring overnight, the reaction was poured into 50 mL of hexanes. The suspension was filtered through Celite and concentrated under reduced pressure. The light yellow solid was taken up in hexanes and purified by flash chromatography on silica gel using hexanes as an eluent. Removal of solvents under reduced pressure provided 0.23 g (23%) of a white powder. ($CDCl_3$, 400 MHz): δ 7.52 (2H, m); 7.45 (3H, d, *J* = 14.9 Hz); 7.34 (3H, m); 7.11 (2H, s); 6.73 (1H, dd, *J* = 17.6, 11.0 Hz); 5.77 (1H, d, *J* = 16.8 Hz); 5.26 (1H, d, *J* = 9.9 Hz).

.

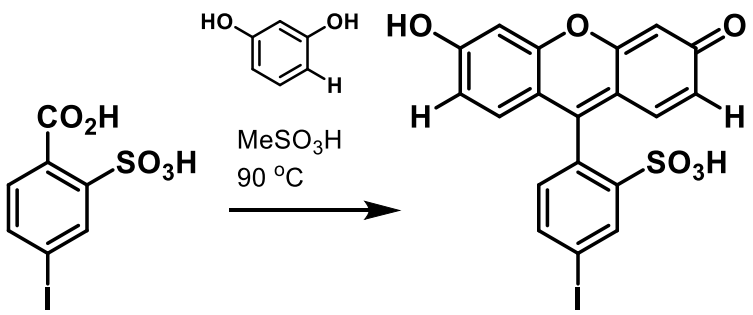

Synthesis of 2-(6-hydroxy-3-oxo-3H-xanthen-9-yl)-5-iodobenzenesulfonic acid.

A mixture of 4-iodo-2-sulfobenzoic acid (50 mg, 0.15 mmol, 1.0 equiv.) and resorcinol (41 mg, 0.37 mmol, 2.5 equiv.) were mixed together in a 4 mL vial equipped with a stirbar. Approximately 250 μL of neat methanesulfonic acid was added, and the reaction was stirred in an oil bath pre-heated to 90 °C for 18 hours. The reaction was cooled on ice and precipitation of a green solid was induced by addition of approximately 2 mL H_2O. The solid was filtered on a Büchner funnel, and the remaining solid was transferred and washed with approximately 3 mL H_2O. After drying, the dark green solid was dissolved in 2-3 mL 10% NaOH and an additional 1 mL H_2O. This solution was cooled on ice and acidified with approximately 5 mL of ice-cold concentrated HCl. The yellow mixture was filtered to give 2-(6-hydroxy-3-oxo-3H-xanthen-9-yl)-5-iodobenzenesulfonic as a brown solid (61 mg, 88% yield). ^{1}H NMR ($(CD_3)_2SO$, 400 MHz): δ 8.28 (1H, d, J = 1.7 Hz), 7.98 (1H, dd, J = 8.0, 1.8 Hz), 7.40 (2H, d, J = 9.2 Hz), 7.28 (2H, d, J = 2.2 Hz), 7.14 (2H, dd, J = 9.2, 2.2 Hz), 7.10 (1H, d, J = 8.0 Hz). ESI-MS+: calculated for MH^+, 494.9, found 494.9.

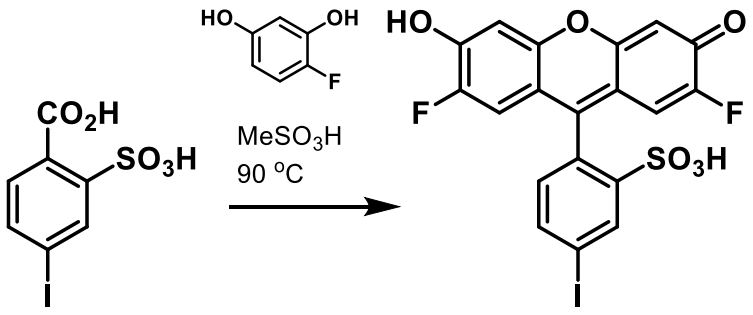

Synthesis of 2-(2,7-difluoro-6-hydroxy-3-oxo-3H-xanthen-9-yl)-5-iodobenzenesulfonic acid.

A mixture of 4-iodo-2-sulfobenzoic acid (50 mg, 0.15 mmol, 1.0 equiv.) and 2-fluororesorcinol (39 mg, 0.30 mmol, 2.0 equiv.) were mixed together in a 4 mL vial equipped with a stirbar. Approximately 250 μL of neat methanesulfonic acid was added, and the reaction was stirred in an oil bath pre-heated to 90 °C for 18 hours. The reaction was cooled on ice and precipitation of a yellow solid was induced by addition of 2 mL of ice-cold H_2O. This precipitate was filtered and dried on a Büchner funnel. The dried solid was dissolved in 1 mL 10% NaOH and 0.5 mL H_2O and subsequently acidified with 2 mL of ice-cold concentrated HCl, giving a bright yellow precipitate that gave, upon filtration on Büchner funnel and drying, 31 mg (39% yield) of 2-(2,7-difluoro-6-hydroxy-3-oxo-3H-xanthen-9-yl)-5-iodobenzenesulfonic acid as an orange/brown solid. ^{1}H NMR ($(CD_3)_2SO$, 400 MHz): δ 8.27 (1H, d, J = 1.8 Hz), 7.91 (1H, dd, J = 8.0, 1.9 Hz), 7.03 (1H, d, J = 8.0 Hz), 6.81 (2H, d, J = 7.2 Hz), 6.61 (2H, d, J = 11.4). ^{19}F NMR ($(CD_3)_2SO$, 470 MHz). δ -132.8. ESI-MS+: calculated for MH^+, 530.9, found 530.9.

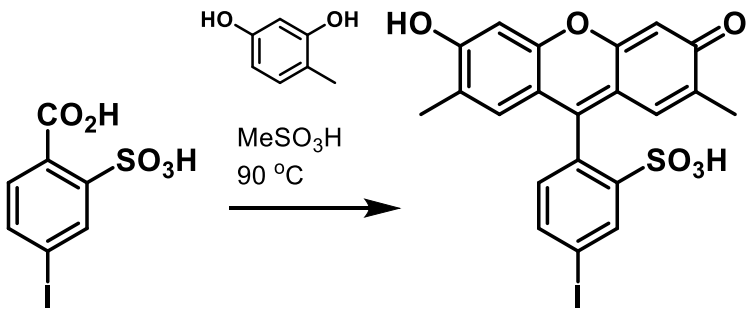

Synthesis of 2-(2,7-dimethyl-6-hydroxy-3-oxo-3H-xanthen-9-yl)-5 iodobenzenesulfonic acid.

A mixture of 4-iodo-2-sulfobenzoic sodium salt (50 mg, 0.15 mmol, 1.0 equiv.) and 2-methylresorcinol (35 mg, 0.28 mmol, 2.0 equiv.) were mixed together in a 4 mL vial equipped with a stirbar. Approximately 250 μL of neat methanesulfonic acid was added, and the reaction was stirred in an oil bath pre-heated to 90 °C for 18 hours. The reaction was cooled on ice and precipitation of a yellow solid was induced by addition of 2 mL of ice-cold H_2O. The orange-

yellow precipitate was filtered and dried on a Büchner funnel. The dried solid was dissolved in 3 mL cold 10% NaOH. Added 2 mL H_2O was added and the solution subsequently acidified with 3 mL of ice-cold concentrated HCl. The suspension was spun at 2500 rpm for 10 minutes, giving a bright yellow precipitate/pellet. The supernatant was decanted, the pellet triturated with diethyl ether, and the resulting suspension was filtered and dried on a Büchner funnel to give 48 mg of 2-(2,7-dimethyl-6-hydroxy-3-oxo-3H-xanthen-9-yl)-5-iodobenzenesulfonic acid as yellow solid (66% yield). ^{1}H NMR ($(CD_3)_2SO$, 400 MHz): δ 8.31 (1H, d, J = 1.7 Hz), 7.99 (1H, dd, J = 8.0, 1.8 Hz), 7.24 (2H, s), 7.19 (2H, s), 7.08 (1H, d, J = 8.0 Hz), 2.14 (6H, s). ESI-MS+: calculated for MH^+, 523.0, found 523.0.

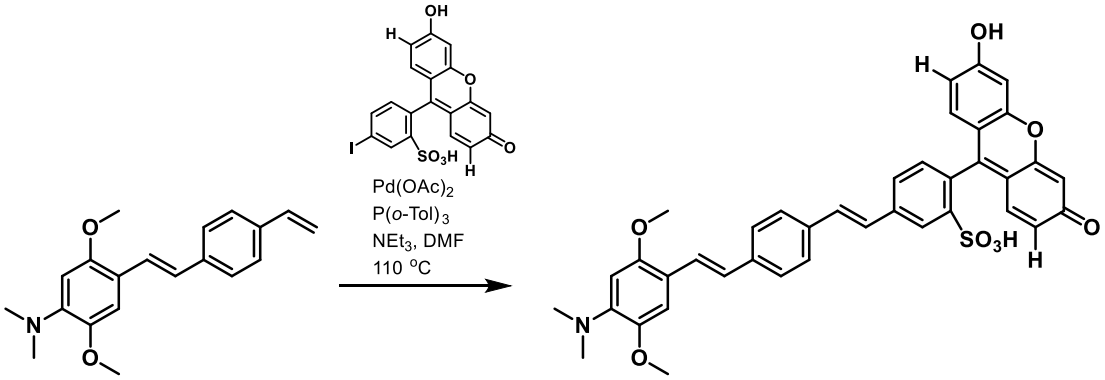

Synthesis of 5-((E)-4-((E)-4-(dimethylamino)-2,5-dimethoxystyryl)styryl)-2-(6-hydroxy-3-oxo-3H-xanthen-9-yl)benzenesulfonic acid. (VF2.1(diOMe).H)

In a 5 mL round bottom flask equipped with a stir bar, (E)-2,5-dimethoxy-N,N-dimethyl-4-(4-vinylstyryl)aniline (10 mg, 0.032 mmol, 1.0 equiv.), 2-(6-hydroxy-3-oxo-3H-xanthen-9-yl)-5-iodobenzenesulfonic acid (16 mg, 0.032 mmol, 1.0 equiv.), $Pd(OAc)_2$ (1 mg, 0.0045 mmol, 0.14 equiv.), and P(o-Tol)$_3$ (3 mg, 0.01 mmol, 0.31 equiv.) were added. The round bottom was sealed with a rubber septum and evacuated and backfilled with N_2 three times. Anhydrous DMF (1 mL) and NEt_3 (0.10 mL) were added via syringe and the reaction stirred at 110 °C for 18 hours. The reaction was cooled and concentrated to dryness. The solid was taken up in minimal

DMF and was purified by preparative HPLC on a Luna C_{18} column with a gradient of 10% MeCN in H_2O with 0.05% TFA ramping to 90% MeCN in 20 minutes. The resulting material was concentrated to dryness to give approximately 1 mg of a dark brown solid. ^{1}H NMR ($(CD_3)_2SO$, 500 MHz): δ 8.17 (1H, s), 7.76 (2H d, *J* = 5 Hz), 7.69 (2H, d, *J* =10 Hz), 7.57 (2H, d, *J* = 5 Hz), 7.47-7.42 (2H, m), 7.39 (1H, s), 7.31 (1H, d, *J* = 5 Hz), 7.28-7.23 (1H, m), 7.19 (1H, d, *J*= 10 Hz), 7.16 (1H, s), 7.06 (1H, s), 6.95 (2H, d, *J*= 10 Hz) 6.74-6.53 (2H, m), 3.84 (3H, s), 3.84 (3H, s), 2.81 (6H, s). HR-ESI-MS: calculated for MH^+ 676.2006, found 676.2013.

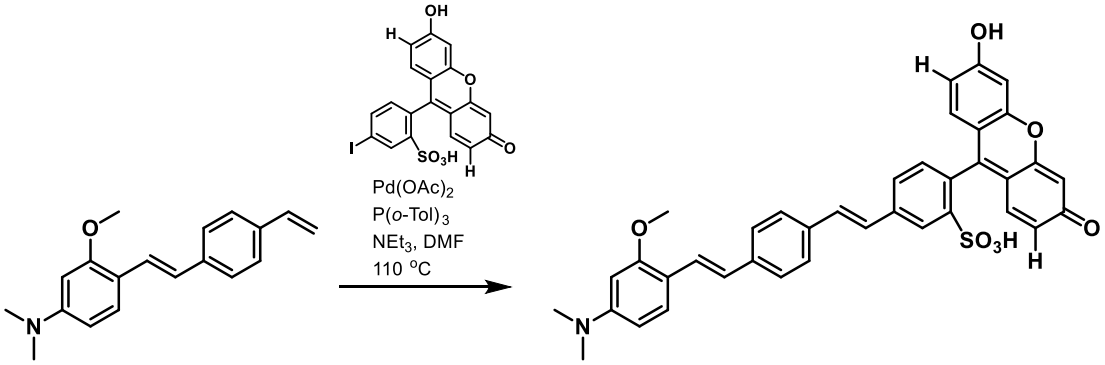

Synthesis of 5-((E)-4-((E)-4-(dimethylamino)-2-methoxystyryl)styryl)-2-(6-hydroxy-3-oxo-3H-xanthen-9-yl)benzenesulfonic acid. (VF2.1(OMe).H)

In a 10 mL round bottom flask equipped with a stir bar, (E)-2-methoxy-N,N-dimethyl-4-(4-vinylstyryl)aniline (100 mg, 35.8 mmol, 1.0 equiv.), 2-(6-hydroxy-3-oxo-3H-xanthen-9-yl)-5-iodobenzenesulfonic acid (177 mg, 35.8 mmol, 1.0 equiv.), $Pd(OAc)_2$ (0.8 mg, 0.0036 mmol, 0.01 equiv.), and P(*o*-Tol)$_3$ (3.3mg, 0.011 mmol, 0.03 equiv.) were added. The round bottom was sealed with a rubber septum and evacuated and backfilled with N_2 three times, anhydrous DMF (2 mL) and NEt_3 (0.125 mL) were added via syringe. The reaction stirred at 110 °C for 14 hours. The reaction was cooled and concentrated to dryness. The solid was taken up in minimal methylene chloride and MeOH solution and filtered through Celite. The solution was then triturated with hexanes and filtered. The brown solid was purified by preparative HPLC on a Luna C_{18} column with a gradient of 10% MeCN in H_2O with 0.05% TFA ramping to 90%

MeCN in 20 minutes. The resulting material was concentrated to dryness to give 22 mg of a dark brown solid. ^{1}H NMR ($(CD_3)_2SO$, 500 MHz): δ 8.18 (1H, s), 7.95 (1H s), 7.83 (1H, d, *J* =8.0 Hz), 7.67 (2H, d, *J* = 8.6 Hz), 7.52 (2H, d, *J*=8.6 Hz), 7.50 (1H, d, *J*=9.2 Hz), 7.44 (1H, d, *J* = 7.4 Hz), 7.41-7.37 (2H, m), 7.36 (1H, s), 7.27 (1H, d, *J*=8.0 Hz), 7.18 (2H, s), 7.07 (2H, d, *J*=9.2 Hz) 7.02 (1H, d, *J*=16 Hz), 6.37 (1H, d, *J*=6.9 Hz), 6.31 (1H, s), 3.87 (3H, s), 2.98 (6H, s) ^{13}C NMR ($(CD_3)_2SO$, 500 Hz), δ 170.68, 167.45, 162.02, 158.28, 157.61, 150.73, 147.08, 138.99, 138.14, 134.73, 134.46, 129.40, 127.15, 126.14, 125.88, 125.18, 123.54, 119.49, 119.24, 117.17, 116.90, 114.21, 105.53, 105.17, 101.79, 101.56, 93.07, 95.78, 55.55, 55.16, 36.00, 30.98. HR-ESI-MS: calculated for MH^+ 646.1900, found 616.1794.

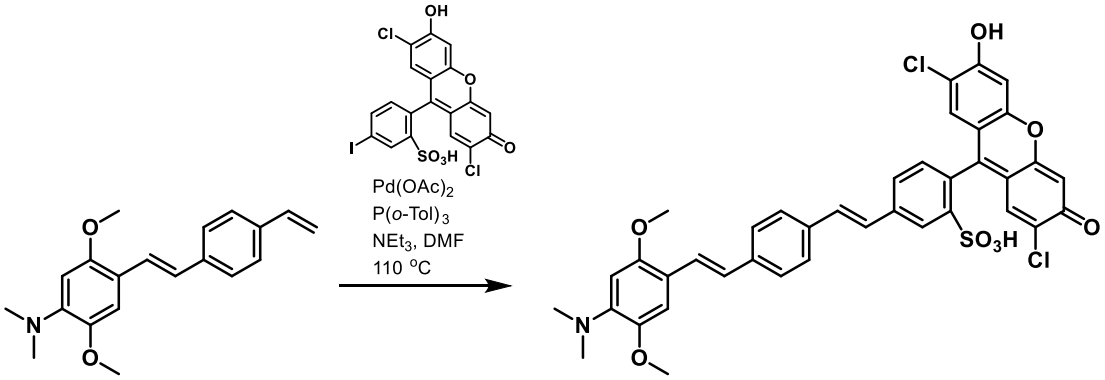

Synthesis of 2-(2,7-dichloro-6-hydroxy-3-oxo-3H-xanthen-9-yl)-5-((E)-4-((E)-4-(dimethylamino)-2,5-dimethoxystyryl)styryl)benzenesulfonic acid. (VF2.1(diOMe).Cl)

In a 5 mL round bottom flask equipped with a stir bar, (E)-2,5-dimethoxy-N,N-dimethyl-4-(4-vinylstyryl)aniline (10 mg, 0.032 mmol, 1.0 equiv.), 2-(2,7-dichloro-6-hydroxy-3-oxo-3H-xanthen-9-yl)-5-iodobenzenesulfonic acid (18 mg, 0.032 mmol, 1.0 equiv.), $Pd(OAc)_2$ (1 mg, 0.0045 mmol, 0.14 equiv.), and P(*o*-Tol)$_3$ (3 mg, 0.01 mmol, 0.31 equiv.) were added. The round bottom was sealed with a rubber septum, evacuated, and backfilled with N_2 three times. Anhydrous DMF (2 mL) and NEt_3 (0.125 mL) were added via syringe and the reaction stirred at 110 °C for 16 hours. The reaction was cooled and concentrated to dryness. The dark brown

solid was taken up in minimal DMF and purified by preparative HPLC on a Luna C_{18} column with a gradient of 10% MeCN in H_2O with 0.05% TFA ramping to 90% MeCN in 20 minutes. The resulting material was concentrated to dryness to give approximately 1 mg of a dark brown solid. ^{1}H NMR ($(CD_3)_2SO$, 500 MHz): δ 8.15 (1H, s), 7.77 (1H, d, *J* =5 Hz), 7.66 (2H, d, *J* = 10 Hz), 7.53 (2H, d, *J* = 10 Hz), 7.42-7.39 (2H, m), 7.37 (1H, d, *J* =15 Hz), 7.27 (1H, d, *J* =10 Hz), 7.22 (1H, d, 10 Hz), 7.19 (1H, s), 7.16 (1H, s), 7.12 (1H, d, *J* =10 Hz) 7.06 (1H, s) 6.95 (1H, s), 6.47 (1H, s), 3.80 (3H, s), 3.78 (3H, s), 2.74 (6H, s). HR-ESI-MS: calculated for MH^+ 744.1226, found 744.1237.

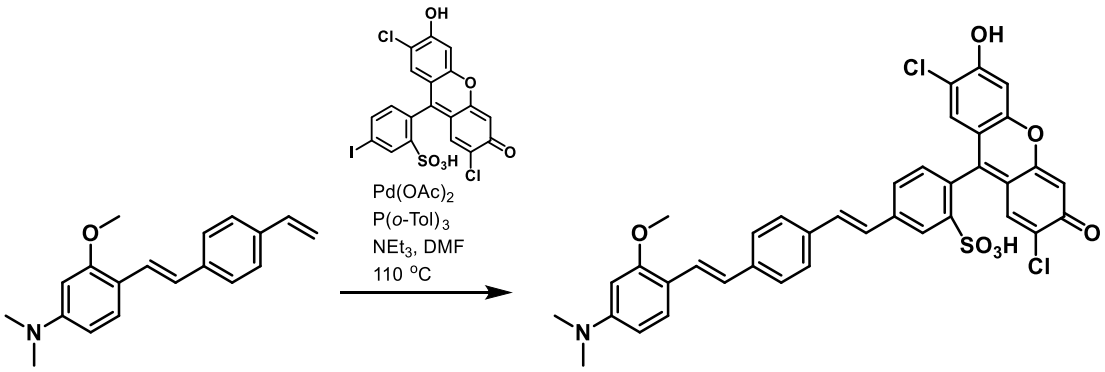

Synthesis of 2-(2,7-dichloro-6-hydroxy-3-oxo-3H-xanthen-9-yl)-5-((E)-4-((E)-4-(dimethylamino)-2-methoxystyryl)styryl)benzenesulfonic acid. (VF.2.1(OMe).Cl)

In a 5 mL round bottom flask equipped with a stir bar, (E)-2-methoxy-N,N-dimethyl-4-(4-vinylstyryl)aniline (8 mg, 0.0286 mmol, 1.1 equiv.), 2-(2,7-dichloro-6-hydroxy-3-oxo-3H-xanthen-9-yl)-5-iodobenzenesulfonic acid (11.7 mg, 0.0261 mmol, 1.0 equiv.), $Pd(OAc)_2$ (1.87 mg, 0.0083 mmol, 0.32 equiv.), and P(*o*-Tol)$_3$ (5.53 mg, 0.0182 mmol, 0.7 equiv.) were added. The round bottom was sealed with a rubber septum, evacuated, and backfilled with N_2 three times. Anhydrous DMF (1 mL) and NEt_3 (0.09 mL) were added via syringe and the reaction stirred at 110 °C for 16 hours. The reaction was cooled and concentrated to dryness. The dark brown solid was taken up in minimal DMF and was purified by preparative HPLC on a Luna C_{18} column with a gradient of 10% MeCN in H_2O with 0.05% TFA ramping to 90% MeCN in

20 minutes. The resulting material was concentrated to dryness to give approximately 1 mg of a dark brown solid. ^{1}H NMR ($(CD_3)_2SO$, 500 MHz): δ 8.17 (1H, s), 7.80 (1H, d, *J*=10 Hz), 7.67 (2H, d, *J* =10Hz), 7.64-7.61 (1H, m), 7.57-7.54 (1H, m), 7.52 (2H, d, *J*=10), 7.49 (1H, s), 7.47-7.40 (2H, m), 7.37 (1H, d, 15 Hz), 7.30-7.16 (1H, m), 7.06 (1H, d, *J*=20 Hz), 6.98 (1H, s) 6.37 (1H, d, *J*=10 Hz) 6.30 (1H, s), 3.87 (3H, s), 2.97 (6H, s). HR-ESI-MS: calculated for MH^+ 714.1120, found 714.1124.

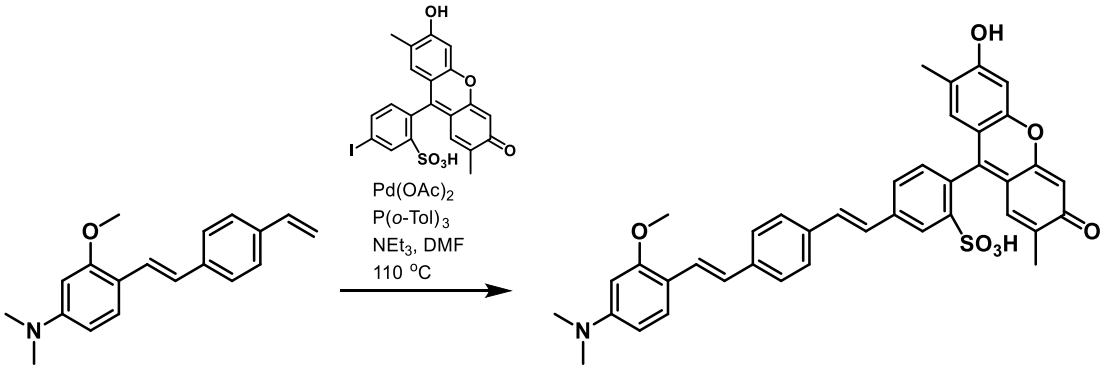

Synthesis of 5-((E)-4-((E)-4-(dimethylamino)-2-methoxystyryl)styryl)-2-(6-hydroxy-2,7-dimethyl-3-oxo-3H-xanthen-9-yl)benzenesulfonic acid. (VF.2.1(OMe).Me)

In a 5 mL round bottom flask equipped with a stir bar, (E)-2-methoxy-N,N-dimethyl-4-(4-vinylstyryl)aniline (5 mg, 0.019 mmol, 1.0 equiv.), 2-(2,7-dimethyl-6-hydroxy-3-oxo-3H-xanthen-9-yl)-5-iodobenzenesulfonic acid (10 mg, 0.019 mmol, 1.0 equiv.), $Pd(OAc)_2$ (1.0 mg, 0.0045 mmol, 0.24 equiv.), and P(*o*-Tol)$_3$ (4 mg, 0.0132 mmol, 0.69 equiv.) were added. The round bottom was sealed with a rubber septum, evacuated, and backfilled with N_2 three times. Anhydrous DMF (1 mL) and NEt_3 (0.50 mL) were added via syringe and the reaction stirred at 110 °C for 10 hours. The reaction was cooled and concentrated to dryness. The dark brown solid was taken up in minimal DMF and purified by preparative HPLC on a Luna C_{18} column with a gradient of 10% MeCN in 1 M triethylammonium acetate pH 7.0 with ramping to 90% MeCN in 20 minutes and holding at 100% MeCN for 10 minutes. The resulting material was concentrated to dryness to give approximately 1 mg of a dark brown solid. ^{1}H NMR ($(CD_3)_2SO$,

500 MHz): δ 8.16 (1H, s), 7.74 (1H, d, *J* = 6.9 Hz), 7.66 (1H, d, *J* = 7.4 Hz), 7.57-7.51 (3H, m), 7.47-7.40 (2H, m), 7.35 (1H, s), 7.31-7.23 (2H, m), 7.13 (1H, d, *J* = 8 Hz), 7.02 (1H, s) 7.01-6.93 (2H, m) 6.71 (1H, s), 6.36 (1H, d, *J*=8.6), 6.30 (1H, s), 3.87 (3H, s), 2.97 (6H,s), 1.91 (6H,s). HR-ESI-MS: calculated for MH^+ 674.2213, found 674.2223.

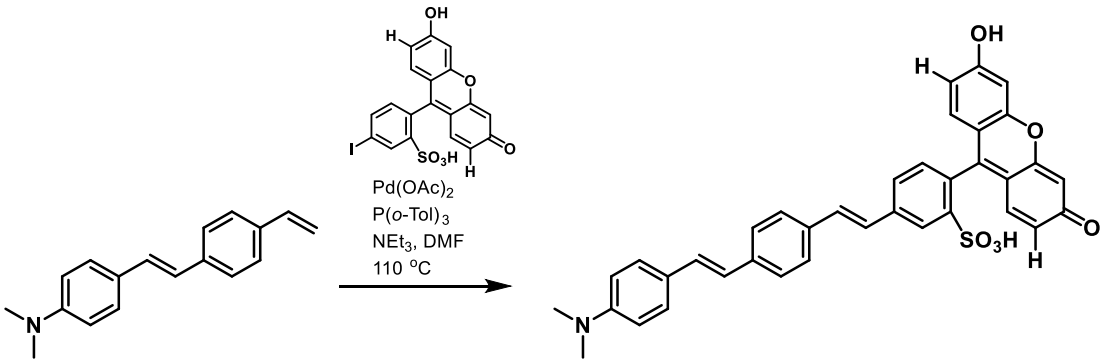

Synthesis of 5-((E)-4-((E)-4-(dimethylamino)styryl)styryl)-2-(6-hydroxy-3-oxo-3H-xanthen-9-yl)benzenesulfonic acid. (VF2.1.H)

In a long-neck vial equipped with a stir bar and a Teflon septum, (E)-N,N-dimethyl-4-(4-vinylstyryl)aniline (5 mg, 0.02 mmol, 1.0 equiv.), 2-(6-hydroxy-3-oxo-3H-xanthen-9-yl)-5-iodobenzenesulfonic acid (10 mg, 0.02 mmol, 1.0 equiv.), $Pd(OAc)_2$ (1 mg, 0.0045 mmol, 0.32 equiv.), and P(*o*-Tol)$_3$ (3 mg, 0.01 mmol, 0.74 equiv.) were added. The vial was evacuated and backfilled with N_2 three times, anhydrous DMF (0.5mL) and NEt_3 (0.07 mL) were added via syringe, the septum was replaced, and the reaction stirred at 110 °C for 12 hours. The dark red reaction was cooled, diluted with CH_2Cl_2 and MeOH, filtered through Celite, and acidified with AcOH. The reaction was concentrated to dryness, triturated with CH_2Cl_2, diluted with 10-fold excess hexanes and filtered. A small amount was purified by preparative HPLC on a Luna C_{18} column with a gradient of 10% MeCN in H_2O with 0.05% TFA ramping to 90% MeCN in 20 minutes. The resulting material was lyophilized overnight to give 0.8 mg of an orange solid. ^{1}H NMR ($(CD_3)_2SO$, 500 MHz): δ 8.16 (1H, s), 7.73 (2H, d, *J* = 9.2 Hz), 7.67 (2H, d, *J* = 8.0

Hz), 7.57 (2H, d, *J* = 8.0 Hz), 7.46 (2H, d, *J* = 8.6 Hz), 7.41 (1H, s), 7.37 (1H, s), 7.20 (2H, d, *J* = 16.6 Hz), 7.18 (1H, s), 7.07 (1H, s), 7.01 (1H, d, *J* = 16.6 Hz), 6.97 (1H, s), 6.89 (2H, br. d, *J* = 8.6 Hz), 6.74 (2H, d, *J* = 9.2 Hz), 2.95 (6H, s). HR-ESI-MS: calculated for MH^+ 616.1794, found 616.1790.

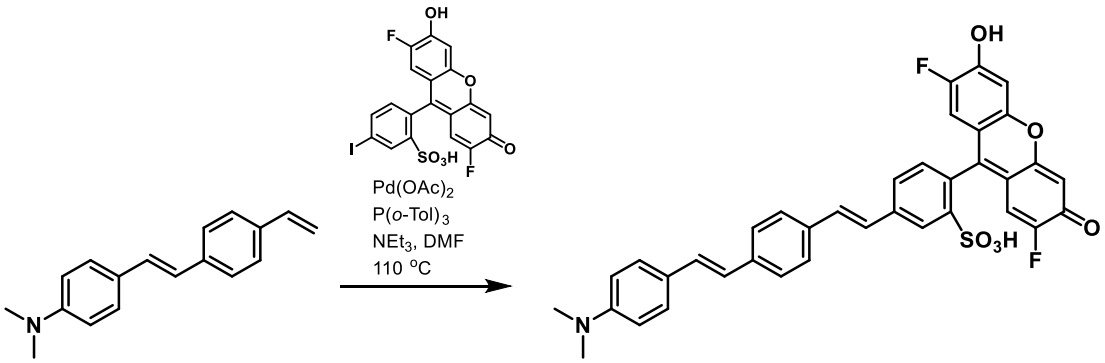

Synthesis of 2-(2,7-difluoro-6-hydroxy-3-oxo-3H-xanthen-9-yl)-5-((E)-4-((E)-4-(dimethylamino)styryl)styryl)benzenesulfonic acid. (VF2.1.F)

In a long-neck vial equipped with a stir bar and a Teflon septum, (E)-N,N-dimethyl-4-(4-vinylstyryl)aniline (9 mg, 0.038 mmol, 1.0 equiv.), 2-(2,7-difluoro-6-hydroxy-3-oxo-3H-xanthen-9-yl)-5-iodobenzenesulfonic acid (20 mg, 0.028 mmol, 1.0 equiv.), $Pd(OAc)_2$ (1 mg, 0.0045 mmol, 0.12 equiv.), and P(*o*-Tol)$_3$ (3 mg, 0.01 mmol, 0.26 equiv.) were added. The vial was evacuated and backfilled with N_2 three times, anhydrous DMF (0.8 mL) and NEt_3 (0.13 mL) were added via syringe, the septum was replaced, and the reaction stirred at 110 °C for 18 hours. The reaction was cooled, diluted with CH_2Cl_2 and MeOH, filtered through Celite, and acidified with AcOH. The reaction was concentrated to dryness, triturated with CH_2Cl_2, diluted with 10-fold excess hexanes and filtered. A small amount was purified by preparative HPLC on a Luna C_{18} column with a gradient of 10% MeCN in H_2O with 0.05% TFA ramping to 80% MeCN in 20 minutes. The resulting material was lyophilized overnight to give 3 mg of an orange solid. ^{1}H NMR ($(CD_3)_2SO$, 400 MHz): δ 8.15 (1H, d, *J* = 1.7 Hz), 7.75 (1H dd, *J* = 8.1,

1.8 Hz), 7.65 (2H, d, *J* = 8.4 Hz), 7.56 (2H, d, *J* = 8.3 Hz), 7.48 (3H, m), 7.39 (2H, d, *J* = 16.0 Hz), 7.25-7.13 (3H, m), 6.76 (3H, m), 6.60 (2H, d, *J* = 11.5 Hz), 2.96 (6H, s). ^{19}F NMR (d_6-DMSO, 470 MHz). δ -133.4. HR-ESI-MS: calculated for MH^+ 652.1605, found 652.1605.

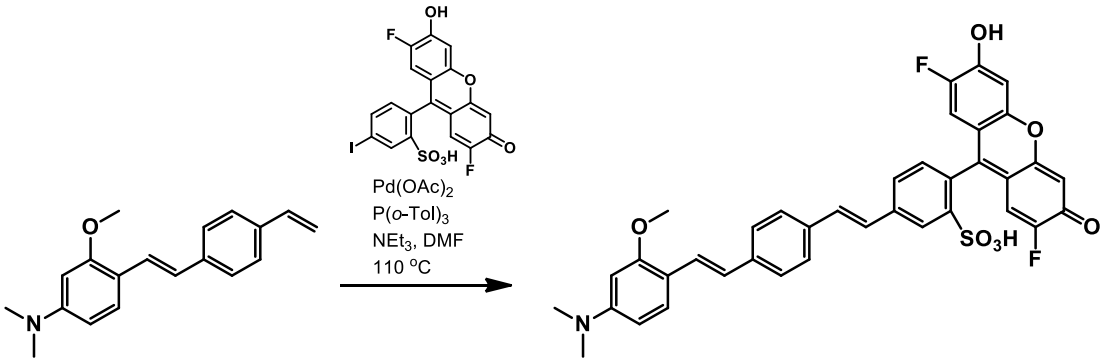

Synthesis of 2-(2,7-difluoro-6-hydroxy-3-oxo-3H-xanthen-9-yl)-5-((E)-4-((E)-4-(dimethylamino)-2-methoxy-styryl)styryl)benzenesulfonic acid. (VF2.1(OMe).F)

In a 5 mL round bottom flask equipped with a stir bar, (E)-2-methoxy-N,N-dimethyl-4-(4-vinylstyryl)aniline (5 mg, 0.0179 mmol, 1 equiv.), 2-(2,7-difluoro-6-hydroxy-3-oxo-3H-xanthen-9-yl)-5-iodobenzenesulfonic acid (10 mg, 0.0179 mmol, 1.0 equiv.), $Pd(OAc)_2$ (1 mg, 0.0045 mmol, 0.25 equiv.), and P(*o*-Tol)$_3$ (4 mg, 0.0132 mmol, 0.74 equiv.) were added. The round bottom was sealed with a rubber septum, evacuated, and backfilled with N_2 three times. Anhydrous DMF (1 mL) and NEt_3 (0.5 mL) were added via syringe and the reaction stirred at 110 °C for 16 hours. The reaction was cooled and concentrated to dryness. The dark brown solid was taken up in minimal DMF and was purified by preparative HPLC on a Luna C_{18} column with a gradient of 10% MeCN in H_2O with 0.05% TFA ramping to 90% MeCN in 20 minutes. The resulting material was concentrated to dryness to give approximately 1 mg of a dark brown solid. ^{1}H NMR ($(CD_3)_2SO$, 500 MHz): δ 8.17 (1H, s), 7.78 (2H, d, *J*=8 Hz), 7.66 (2H, d, *J* =8 Hz), 7.51 (3H, d, *J*=8), 7.47-7.33 (2H, m), 7.21 (2H, d, *J*=8), 7.00 (2H, d, *J*=16.6), 6.62 (2H, bs), 6.36 (1H, d, 8.6 Hz), 6.29 (1H, s), 3.87 (3H, s), 2.97 (6H, s). HR-ESI-MS: calculated for MH^+ 682.17113, found 682.1721.

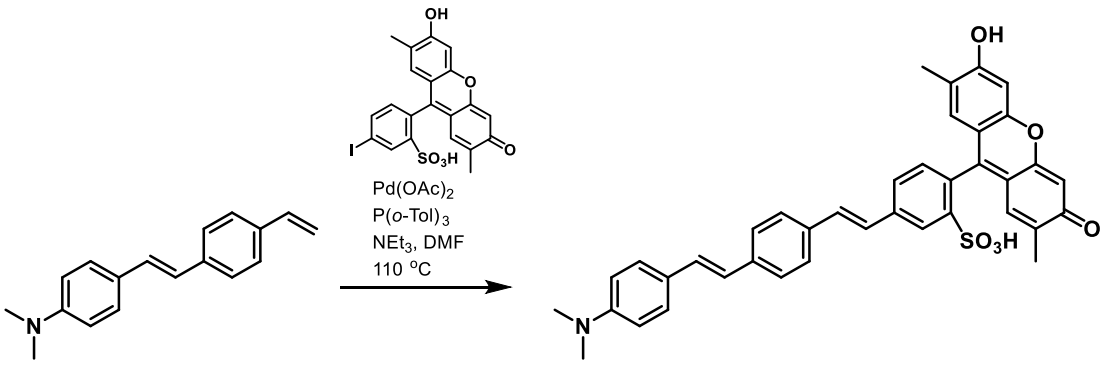

Synthesis of 5-((E)-4-((E)-4-(dimethylamino)styryl)styryl)-2-(6-hydroxy-2,7-dimethyl-3-oxo-3H-xanthen-9-yl)benzenesulfonic acid. (VF2.1.Me)

In a long-neck vial equipped with a stir bar and a Teflon septum, (E)-N,N-dimethyl-4-(4-vinylstyryl)aniline (5 mg, 0.019 mmol, 1.0 equiv.), 2-(2,7-dimethyl-6-hydroxy-3-oxo-3H-xanthen-9-yl)-5-iodobenzenesulfonic acid (10 mg, 0.019 mmol, 1.0 equiv.), $Pd(OAc)_2$ (1 mg, 0.0045 mmol, 0.23 equiv.), and P(*o*-Tol)$_3$ (3 mg, 0.01 mmol, 0.53 equiv.) were added. The vial was evacuated and backfilled with N_2 three times, anhydrous DMF (0.5 mL) and NEt_3 (0.07 mL) were added via syringe, the septum was replaced, and the reaction stirred at 110 °C for 18 hours. The reaction was cooled, diluted with CH_2Cl_2 and MeOH, filtered through Celite, and acidified with AcOH. The reaction was concentrated to dryness, triturated with CH_2Cl_2, diluted with 10-fold excess hexanes and filtered. A small amount was purified by preparative HPLC on a Luna C_{18} column with a gradient of 10% MeCN in H_2O with 0.05% TFA ramping to 80% MeCN in 20 minutes. The resulting material was lyophilized to give 1 mg of an orange solid. ^{1}H NMR ($(CD_3)_2SO$, 400 MHz): δ 8.16 (1H, d, *J* = 1.7 Hz), 7.78 (1H, dd, *J* = 8.1, 1.7 Hz), 7.65 (2H, d, *J* = 8.1 Hz), 7.55 (2H, d, *J* = 8.1 Hz), 7.46-7.39 (4H, m), 7.21-7.09 (5H, m), 7.0-6.92 (2H, m), 6.73 (2H, d, *J* = 8.7), 2.92 (6H, s), 2.08 (6H, s). HR-ESI-MS: calculated for MH^+ 644.2107, found 644.2108.

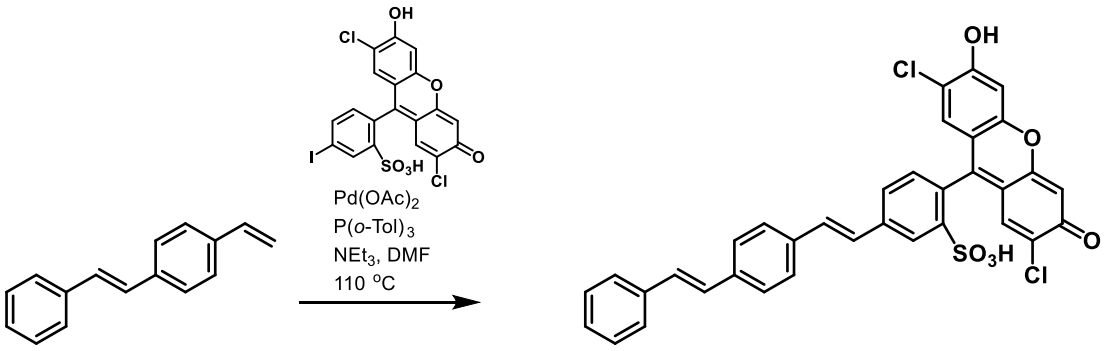

Synthesis of 2-(2,7-dichloro-6-hydroxy-3-oxo-3H-xanthen-9-yl)-5-((E)-4-((E)-styryl)styryl)benzenesulfonic acid. (VF2.0.Cl)

In a 5 mL round bottom flask equipped with a stir bar (E)- 1-ethenyl-4-(2-phenylethenyl)-benzene (8 mg, 0.038 mmol, 1.0 equiv.), 2-(2,7-dimethyl-6-hydroxy-3-oxo-3H-xanthen-9-yl)-5-iodobenzenesulfonic acid (22 mg, 0.038 mmol, 1.0 equiv.), $Pd(OAc)_2$ (1.0 mg, 0.0045 mmol, 0.12 equiv.), and P(*o*-Tol)$_3$ (3 mg, 0.0099 mmol, 0.38 equiv.) were added. The round bottom was sealed with a rubber septum, evacuated, and backfilled with N_2 three times. Anhydrous DMF (0.5 mL) and NEt_3 (0.050 mL) were added via syringe and the reaction stirred at 110 °C for 10 hours. The reaction was cooled and concentrated to dryness. The resulting solid was taken up in dichloromethane (2 mL) and methanol (0.5 mL) and acidified with acetic acid (0.05 mL). The partially dissolved suspension was filtered through celite to give a brown solution that was concentrated to dryness. The solid was taken up in minimal dichloromethane and triturated with hexanes to give an orange solid. ^{1}H NMR ($(CD_3)_2SO$, 500 MHz): δ 8.15 (1H, s), 7.77 (2H, d, *J* = 10 Hz), 7.69 (3H, d, *J* = 10 Hz), 7.64 (2H, s), 7.61 (3H, t, *J* = 10 Hz), 7.43 (2H, s), 7.37 (2H, d, *J* = 5 Hz), 7.34 (1H, s), 7.28 (2H, d, *J* = 10 Hz), 7.26-7.22 (2H, m). HR-ESI-MS: calculated for MH^+ 641.0593, found 641.0598.

2.4 Discussion

Voltage imaging with small molecules has been limited to staining of single cells in a brain slice or to measurement of optical "field potentials" that report population changes and require spike-timed averaging.[17,18] One problem has been the lack of fast, sensitive, non-disruptive probes to report on membrane potential changes. To address this concern, we here now reported the design, synthesis, and application of a new family of voltage-sensitive dyes—VoltageFluors (VFs)—that make use of photoinduced electron transfer from an electron-rich aniline through a conjugated phenylenevinylene molecular wire to a xanthene chromophore for fast, sensitive voltage sensing in a variety of neuronal contexts. The VF family of dyes displays visible excitation and emission profiles that enable optical voltage recording at peak excitation and emission wavelengths, large linear responses to changes in membrane potential, negligible capacitance loading of membranes, and fast, turn-on optical responses capable of resolving action potentials and sub-threshold membrane potential dynamics in neurons.

As a chemical platform, the VF dyes offer a tunable approach to voltage sensing, in which alteration of the electron affinities results in modulation of the voltage sensitivity of the dye. This study demonstrates, for the first time, that modulation of ΔG_{PeT} alters the voltage-sensitivity of VF dyes and establishes unequivocally the requirement of an electron-rich donor for voltage sensing, as indicated by the lack of voltage response from VF2.0.Cl. Analysis of the relative driving force for electron transfer derived from experimentally determined oxidation/reduction potentials suggests that the range of -0.08 V to -0.27 V yields sensors with high voltage sensitivity and linearity within a physiologically relevant window of ±100 mV. The most sensitive of the VF dyes—VF2.1OMe.Cl and VF2.1OMe.H—have voltage sensitivities of 49 and 48% ΔF/F per 100 mV, respectively, and compare favorably to other "fast" voltage dyes that function via an electrochromic sensing mechanism and have typical

voltage sensitivities ranging from 10 to 28% ΔF/F per 100 mV.[17,19] Although high voltage sensitivities can be achieved with electrochromic dyes by excitation at the far red edge of the excitation spectrum and collection with a similarly narrow emission filter, this requires off-peak excitation, the use of potentially phototoxic high-intensity illumination, and sampling of only a small fraction of emitted, voltage-sensitive photons. For voltage imaging, which is inherently photon-limited due to the fast sampling nature (0.5-2 kHz range) of the experiment, sacrificing a majority of excitation and emission photons can be problematic, making approaches like VF dyes that use all excitation and emission photons for sensing ideally suited for voltage imaging. Due to its improved linear response to membrane potential change, we used VF2.1OMe.H to monitor action potentials in cultured neurons with enhanced SNR over previous VF dyes (28:1 vs 16:1). We also demonstrated the enhanced utility of VF2.1OMe.H in leech ganglia for monitoring spontaneous activity with a 3-fold improvement of SNR compared to VF2.1.Cl. Finally, applications in brain slices show that VF2.1OMe.H can report on both slow and fast network physiology in a complex neuronal environment. The performance of VF2.1OMe.H in these preparations are summarized in

The optimal voltage probe remains elusive. The best voltage-sensitive proteins, QuasAr1, ASAP1, and ArcLight Q239 have issues with brightness, sensitivity, and speed respectively.[9,11,20] In addition, improved derivatives like Ace2-mNeon have a turn-off response to depolarization which lead to a lower signal to noise ratio.[21] These issues have been addressed by VF dyes. Current VF dyes represent a significant advance in sensitivity over previous VF dye incarnations, although much work remains. First, because VF dyes have no genetically encoded component yet, non-specific staining in heterogeneous samples severely decreases the apparent voltage sensitivity. Genetic targeting of VF dyes in a two-component system would enable analysis of genetically defined cells and improve signal-to-noise. Second, VF2.1OMe.H, described here shows a greater than 100% ΔF/F per 100 mV at extremely

depolarized potentials, indicating greater sensitivities can be reasonably achieved. Third, longer wavelengths would be beneficial for thick samples, lower autofluorescence, and multiplex imaging with currently available probes. The generality of the VoltageFluor PeT platform predicts the chemical tractability of these efforts, which are ongoing in our labs.

Sample	ΔF/F	SNR
HEK cells	48%[a]	38:1
Rat Neurons	10%[a]	28:1
Leech Neurons	2-4%[a,b]	17:1
Olfactory Bulb Slice	2%[c]	17:1

[a] per 100 mV change, calibrated by simultaneous electrophysiological measurement. [b] No background subtraction. Images sampled at 50 Hz. [c] Uncalibrated; no background subtraction.

Figure 2.14 VF2.1OMe.H Performance in Biological Samples

2.5 Acknowledgements

Chapter 2, in part, is a reprint of the work as it appears in Journal of the American Chemical Society, published January 2015. The dissertation author was the primary author of this material and contributed to experimental design, execution of experiments, interpretation of data, generation of figures and editing of manuscript. Clifford R. Woodford, E. Paxon Frady, Richard S. Smith, Benjamin Morey, Gabriele Canzi, Sakina F. Palida, Ricardo C. Araneda, William B. KristanJr., Clifford P. Kubiak, Evan W. Miller, and Roger Y. Tsien Improved PeT Molecules for Optically Sensing Voltage in Neurons. Journal of the American Chemical Society **137**(5): 1817-1824 (2015).

2.6 Bibliography

1. Peterka, D. S., Takahashi, H. & Yuste, R. Imaging voltage in neurons. *Neuron* **69,** 9–21 (2011).

2. Tanner, G. A., Sandoval, R. M. & Dunn, K. W. Two-photon in vivo microscopy of sulfonefluorescein secretion in normal and cystic rat kidneys. *Am. J. Physiol. Renal Physiol.* **286,** F152–60 (2004).

3. Minta, A., Kao, J. P. Y. & Tsien, R. Y. Fluorescent indicators for cytosolic calcium based on rhodamine and fluorescein chromophores. *J. Biol. Chem.* **264,** 8171–8178 (1989).

4. Kojima, H., Nakatsubo, N., Kikuchi, K., Kawahara, S., Kirino, Y., Nagoshi, H., Hirata, Y. & Nagano, T. Detection and imaging of nitric oxide with novel fluorescent indicators: diaminofluoresceins. *Anal. Chem.* **70,** 2446–2453 (1998).

5. He, Q., Miller, E. W., Wong, A. P. & Chang, C. J. A selective fluorescent sensor for detecting lead in living cells. *J. Am. Chem. Soc.* **128,** 9316–9317 (2006).

6. Zheng, S., Lynch, P. L. M., Rice, T. E., Moody, T. S., Gunaratne, H. Q. N. & de Silva, a. P. Structural effects on the pH-dependent fluorescence of naphthalenic derivatives and consequences for sensing/switching. *Photochem. Photobiol. Sci.* **11,** 1675 (2012).

7. Larumbe, D., Gallardo, I. & Andrieux, C. P. Anodic oxidation of some tertiary amines. *J. Electroanal. Chem. Interfacial Electrochem.* **304,** 241–247 (1991).

8. Miller, E. W., Lin, J. Y., Frady, E. P., Steinbach, P. A., Kristan, W. B. & Tsien, R. Y. Optically monitoring voltage in neurons by photo- induced electron transfer through molecular wires. *Proc. Natl. Acad. Sci.* **109,** 2114–2119 (2011).

9. Jin, L., Han, Z., Platisa, J., Wooltorton, J. R. A., Cohen, L. B. & Pieribone, V. A. Single Action Potentials and Subthreshold Electrical Events Imaged in Neurons with a Fluorescent Protein Voltage Probe. *Neuron* **75,** 779–785 (2012).

10. Baker, M. W. & Macagno, E. R. Characterizations of Hirudo medicinalis DNA promoters for targeted gene expression. *J. Neurosci. Methods* **156,** 145–153 (2006).

11. Hochbaum, D. R., Zhao, Y., Farhi, S. L., Klapoetke, N., Werley, C. A., Kapoor, V., Zou, P., Kralj, J. M., Maclaurin, D., Smedemark-Margulies, N., Saulnier, J. L., Boulting, G. L., Straub, C., Cho, Y. K., Melkonian, M., Wong, G. K.-S., Harrison, D. J., Murthy, V. N., Sabatini, B. L., Boyden, E. S., Campbell, R. E. & Cohen, A. E. All-optical electrophysiology in mammalian neurons using engineered microbial rhodopsins. *Nat. Methods* **11,** 825–33 (2014).

12. Smith, R. S. & Araneda, R. C. Cholinergic Modulation of Neuronal Excitability in the Accessory Olfactory Bulb. *J Neurophysiol* 2963–2974 (2010). doi:10.1152/jn.00446.2010.The

13. Keller, A., Yagodin, S., Aroniadou-anderjaska, V., Zimmer, L. A., Ennis, M., Jr, N. F. S. & Shipley, M. T. Functional Organization of Rat Olfactory Bulb Glomeruli Revealed by Optical Imaging. **18,** 2602–2612 (1998).

14. Shipley, M. T. & Ennis, M. Functional Organization of Olfactory System. *J. Neurobiol.* **30,** 123–176 (1996).

15. Jiao, G.-S., Han, J. W. & Burgess, K. Syntheses of regioisomerically pure 5- or 6-halogenated fluoresceins. *J. Org. Chem.* **68,** 8264–7 (2003).

16. Smith, R. S., Weitz, C. J. & Araneda, R. C. Excitatory Actions of Noradrenaline and Metabotropic Glutamate Receptor Activation in Granule Cells of the Accessory Olfactory Bulb. *Journal of Neurophysiology* **102,** 1103–1114 (2009).

17. Yan, P., Acker, C. D., Zhou, W.-L., Lee, P., Bollensdorff, C., Negrean, A., Lotti, J., Sacconi, L., Antic, S. D., Kohl, P., Mansvelder, H. D., Pavone, F. S. & Loew, L. M. Palette of fluorinated voltage-sensitive hemicyanine dyes. *Proc. Natl. Acad. Sci.* **109,** 20443–20448 (2012).

18. Refojo, D., Schweizer, M., Kuehne, C., Ehrenberg, S., Thoeringer, C., Vogl, a. M., Dedic, N., Schumacher, M., von Wolff, G., Avrabos, C., Touma, C., Engblom, D., Schutz, G., Nave, K. -a., Eder, M., Wotjak, C. T., Sillaber, I., Holsboer, F., Wurst, W. & Deussing, J. M. Glutamatergic and Dopaminergic Neurons Mediate Anxiogenic and Anxiolytic Effects of CRHR1. *Science (80-.).* **333,** 1903–1907 (2011).

19. Kuhn, B. & Fromherz, P. Anellated Hemicyanine Dyes in a Neuron Membrane: Molecular Stark Effect and Optical Voltage Recording. *J. Phys. Chem. B* **107,** 7903–7913 (2003).

20. St-Pierre, F., Marshall, J. D., Yang, Y., Gong, Y., Schnitzer, M. J. & Lin, M. Z. High-fidelity optical reporting of neuronal electrical activity with an ultrafast fluorescent voltage sensor. *Nat. Neurosci.* **17,** 884–9 (2014).

21. Gong, Y., Huang, C., Li, J. Z., Grewe, B. F., Zhang, Y., Eismann, S. & Schnitzer, M. J. High-speed recording of neural spikes in awake mice and flies with a fluorescent voltage sensor. *Science (80-.).* **350,** 1–11 (2015).

Chapter 3 Improved Molecular Bridges for Effective Electron Transfer in VF Dyes

3.1 Introduction

Electron transfer from the donor to acceptor of VF dyes is an essential component of realizing an effective sensor. Understanding and utilizing effective approaches for manipulating electron transfer from first principles offers a unique opportunity for developing an optimal VF dye. Electron transfer can be categorized as either inner sphere (within a single molecules), as seen in VF dyes, or outer sphere (between two molecules). Both types have provided valuable insight toward understanding electron transfer and have guided VF dye development. Early outer sphere experimental results help form the Nobel Prize winning Marcus Theory of electron transfer. The work of Rudy Marcus showed that these reactions largely depended on the oxidation and reduction potentials of the respective electron donors and acceptors together with a reorganization energy that took into account bond lengths, solvent orientation, and molecular distances among other variables.[1,2]

Importantly, inner sphere electron transfer, predominant in VF dyes, has also provided principles for VF dye design. First observed in inorganic complexes, inner sphere electron transfer requires a bridge to act as a conduit through which an electron must pass from the donor to the acceptor.[3] These inner sphere systems eventually expanded to organic molecules to be studied as molecular electronic devices.[4] Organic molecules have the advantage of almost limitless chemical modification capable of tuning their electronic characteristics to great effect. Beyond molecular devices, conjugated organic polymers applied as bulk materials in electronics have enjoyed immense success as effective semiconductors.[5] Optimized bridges for electron transfer is a widely

studied area with regard to electronics and solar cell applications. However, precious little work has been done to optimize bridges in VF dyes towards improved voltage sensors.

3.1.1 Alternatives to Phenylene Vinylene Electron Transfer Bridges

Early compounds such as phenylene vinylene polymers doped with either electron donors or acceptors proved to be promising materials with unique conductivities to be exploited.[6] Phenylene vinylene bridges were also shown to have some of the shortest attenuation factors in molecular electronics, which translates to efficient electron transfer.[7,8] The first generation of VF Dyes used a phenylene vinylene bridge to great effect, but just as other bridges proved to be more conductive electronic materials, it was hypothesized other bridges may be more effective in VF dyes as improved conductors.

Thiophene and furan aromatic moieties are natural substitutions to their phenyl counterparts. Both species have lower delocalization energies than benzene which would allow for more efficient electron transfer.[9,10] In this work, VF dyes with furan and thiophene substitutions were synthesized and characterized in patch clamp HEK cells to determine the effects of altered bridges on voltage sensitivity. Fluorescent response curves with respect to changes in membrane potential showed definitively that thiophene vinylene bridges act as better conductors than phenylene vinylene bridges.

3.1.2 Promoting Longer Electron Transfer Distances

In addition to efficient electron transfer, promoting a longer distance of electron transfer from the aniline donor to the fluorescein bridge represents one of the most fundamentally beneficial approaches for improving the voltage sensitivity of VF dyes. Intuitively, if the donated electron must pass through a larger portion of the electric field to quench fluorescence, then the electric field should have a relatively larger effect on the extent of fluorescence quenching. This truth should make longer VF dyes more sensitive to voltage.

One potential avenue to achieve longer distances of effective electron transfer is by removing electron density in the bridge, and promoting electron transfer more exclusively from the distal aniline moiety. An electron poor bridge may be achieved by adding electron-withdrawing groups capable of siphoning electron density from the phenylene vinylene system. A VF dye with a fluorine substituted on the bridge offered a promising first pass to test this theory.

Achieving electron transfer in longer dyes is possible by lengthening the bridge as well. Unfortunately, electron transfer becomes increasingly more challenging with distance.[11] Electron transfer is thought to occur via either a tunneling or hopping mechanism determined largely by the distance traveled by the electron. Tunneling is the predominant method of electron transfer at shorter distances, and experimentally, tunneling has been seen in distances up to 2.5 nm.[12] Electron transfer in VF dyes is thought to fall within this distance regime. Beyond 2.5 nm, a hopping mechanism must be employed. Graduating to longer electron transfer distances through hopping requires some additional considerations. Numerous studies have shown that a hoping mechanism is facilitated by energy matching of the aniline donor, bridge, and fluorescein acceptor.[13,14] Faster rates and more probable electron transfer have been experimentally observed in longer oligomers of phenylene vinylene with donors and acceptors of similar energies as measured by cyclic voltammetry.[15] This breakthrough has prompted work towards increasing the length of the phenylene vinylene bridge of VF dyes in a similar manner. The energy levels of the bridge was tuned through substitution of phenyl rings and through replacement with thiophene rings for improved electron hopping at longer distances.

Dyes with very large driving forces for electron transfer were also developed as well in hopes that this would promote electron transfer over longer distances. Finally, VF dyes with an entirely new structure where the bridge connects to the acceptor were developed toward improving more efficient electron transfer.

None of the efforts to increase the length of electron transfer resulted in any meaningful improvements to sensitivity as hoped. It appeared all of the efforts suffered from a combination of poor membrane staining and low voltage sensitivity.

3.2 Results

3.2.1 Furan Bridges

The first dye with a new bridge synthesized and shown in Figure 3.1a contains the same donor and bridge as VF2.1.Cl, but the central phenyl ring of the bridge has been replaced with a furan. This substitution did not significantly alter the synthetic approach in developing the new probe named VF2fur.1.Cl. Alternating Heck coupling and Wittig reactions proved to be viable with the new bridge. Upon purification, VF2fur.1.Cl was added to HEK cells showing localization to plasma membrane. Labeled cells were then patch-clamped and interrogated over a range of potentials varying from -100 mV to +100 mV holding at -60 mV.

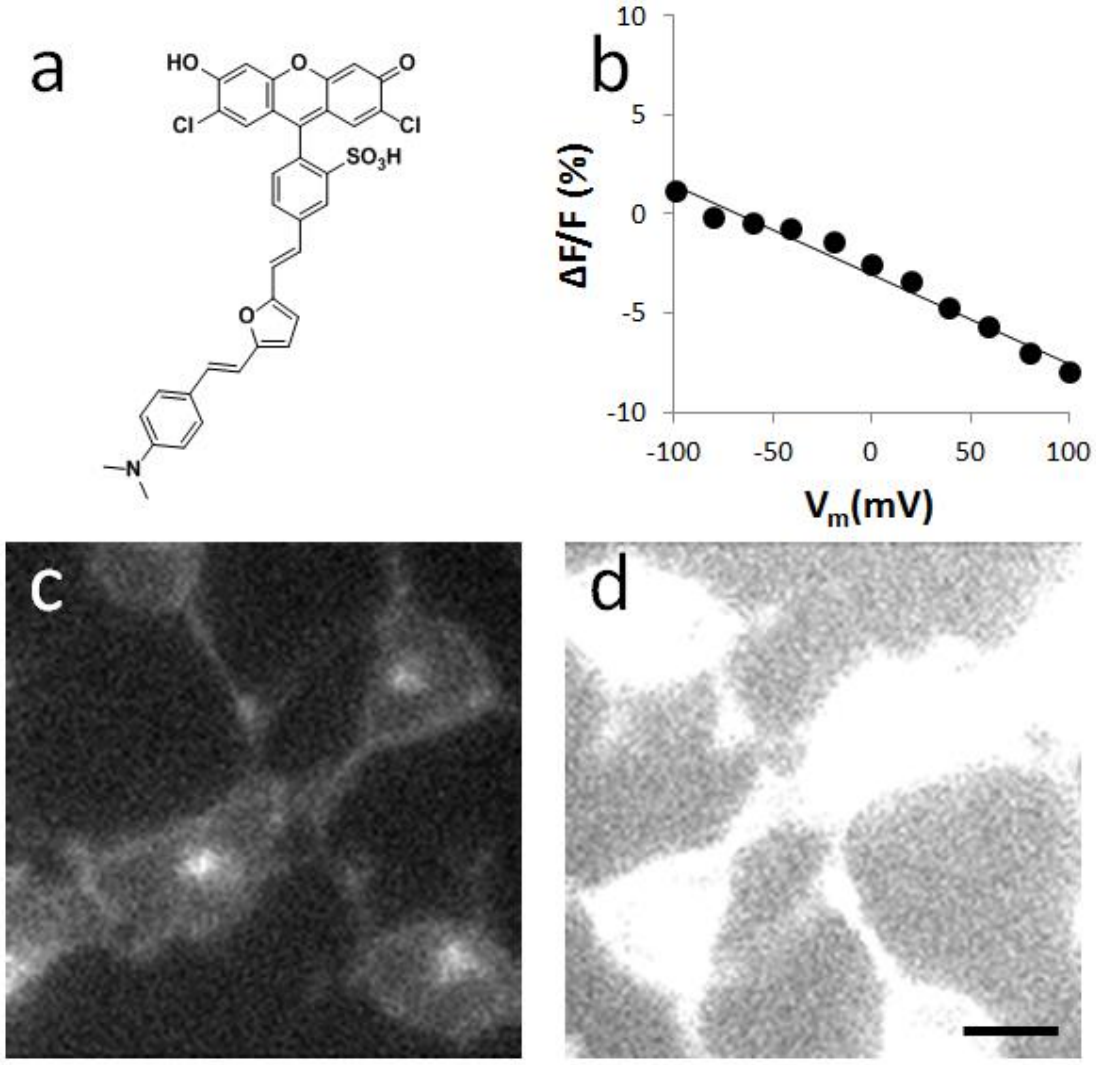

Figure 3.1. Structure and Characterization of VF2fur.1.Cl in HEK cells. (a) Structure of VF2fur.1.Cl where the central phenyl ring is replaced with a furan ring. (b) VF2fur.1.Cl response % ΔF/F vs. final membrane potential. (c) High speed camera image of initial frame captured during imaging in (b). (d) Image of same dish of cells after voltage sensitivity experiment in (b). Scale bar is 20 μm.

Interestingly, VF2fur.1.Cl was the first dye to show a brightening in more depolarized potentials and a dimming in more hyperpolarized potentials as seen by the negative slope in Figure 3.1b. Based on this HEK cell data, VF2fur.1.Cl only shows a -5% ΔF/F per 100 mV which is far lower than earlier iterations. Beyond this, VF2fur.1.Cl curiously becomes significantly brighter upon illumination with 480 nm light as seen in Figure 3.1c and Figure 3.1d. Typically, VF dyes

show a small degree of dimming presumably due to photo-bleaching. This is the first instance where a VF dye was shown to become brighter upon illumination.

The negative slope seen in Figure 3.1b could indicate a potential reverse electron transfer where an electron is transferred from the fluorescein fluorophore to the furan bridge or aniline. This type of electronic movement, opposite form that seen in other VF dyes, would give this same type of negative slope.

However, any explanation is little more than speculation given the lack of investigation into this probe due to its low voltage sensitivity. However, one possibility is that brightening is observed do to a photochemical reaction of the furan destroying the bridge and drastically reducing the level of PeT seen in VF2fur.1.Cl. This would result in the drastic increase in brightness observed. Regardless of the mechanism, based on the strange brightening phenomenon coupled with the low voltage sensitivity, investigation into VF dyes with furan bridges was discontinued.

3.2.2 Thiophene Bridges

In addition to furan-substituted bridges, thiophenes were also explored. A similar synthetic methodology of alternating Heck couplings and wittig reactions was also employed to reach the desired VF dye as seen in Figure 3.2. Thiophene bridges were combined with a range of donors and acceptors to give a series of dyes with varying driving forces for electron transfer. Unsubstituted aniline electron donors and methoxy donors were readily coupled to the suitable thiophene aldehyde. Both compounds were then bound to fluorescein acceptors with chloro-substitution and unsubstituted versions. All of these donor and acceptor combinations were previously used in concert with phenyl bridges in chapter 2 with great success.

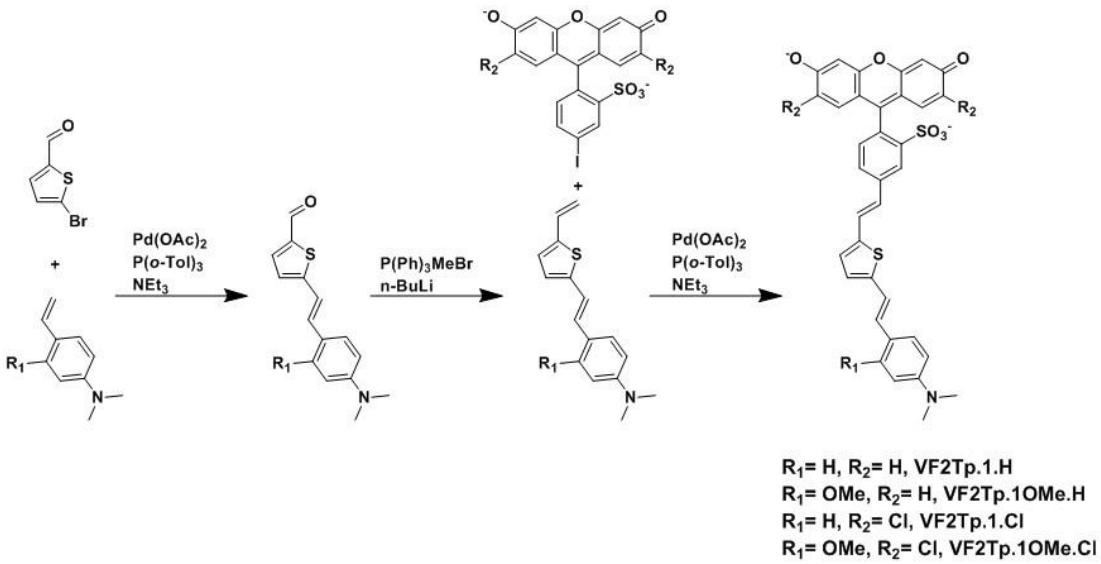

Figure 3.2 Synthetic Scheme of Thiophene Bridges

Thiophene bridges offered much greater promise than furan substitutions when tested for voltage sensitivity in HEK cells. The entire range of four thiophene substituted VF dyes all appeared to stain HEK cell membranes specifically with minimal internalization or aggregation as seen in Figure 3.3a-d. In all cases, fluorescence was relatively dim compared to VF dyes with phenyl substituted bridges. Thiophene is more polar than benzene which could have potentially limited the lipophilicity of the thiophene substituted dyes and lead to lower membrane staining. Thiophene substituted dyes may also simply be dimmer due to a lower quantum yield. Thiophene bridges are expected to be improved conductors promoting PeT to a greater extent than phenyl bridges and leading to more fluorescence quenching. This may be the reason for dim cell staining as well.

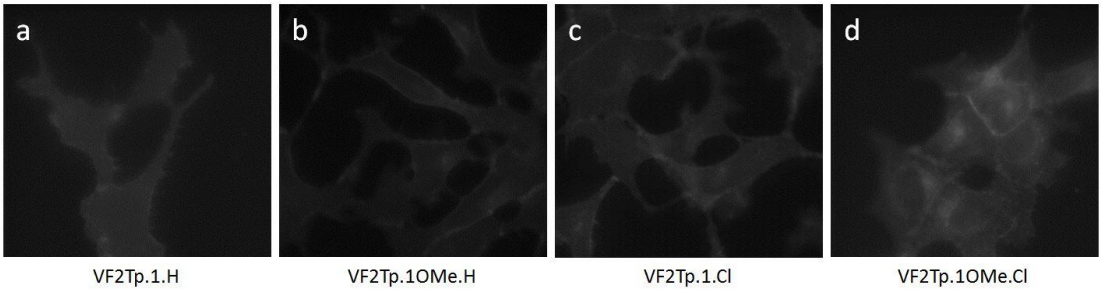

Figure 3.3 HEK cell staining of VF dyes with Thiophene Bridges

Upon staining, HEK cells were then patch clamped and stepped to a range of membrane potentials to measure fluorescence sensitivity to changes in voltage. VF2Tp.1.H gave a 37% ΔF/F per 100 mV, a value more than double the 15% ΔF/F per 100 mV measured in VF2.1.H as seen in Figure 3.4b. In addition, VF2Tp.1.Cl was measured to give a 37% ΔF/F per 100 mV compared to 26% ΔF/F per 100 mV for VF2.1.Cl. Here again the thiophene derivative offered markedly improved voltage sensitivity. However, both VF2Tp.1OMe.Cl with a 14% ΔF/F per 100 mV and VF2Tp.1OMe.H with a 13% ΔF/F per 100 mV were both less sensitive than their phenyl substituted counterparts with 48% and 46% ΔF/F per 100 mV sensitivities respectively. Thiophene bridges did not represent an across the board improvement to voltage sensitivity values in HEK cells, but did show improvements in some donor bridge combinations.

Thiophene bridges do appear to improve the probability of photoinduced electron transfer relative to fluorescence based on the shape of the voltage sensitivity curves in Figure 3.4b. As discussed in chapter 2, when interrogating the fluorescence response to voltage at more extreme potentials ranging from -300 mV to +300 mV definitive curve shapes arise. With regard to thiophene bridges, the VF dye with the weakest driving force, VF2Tp.1.H, appears to have a small slope throughout the negative potentials interrogated. Upon reaching positive membrane potentials however the dye does appear to experience a relatively high sensitivity to voltage based on the steeper slope, before slightly leveling off again. All three other thiophene-based dyes have small slopes throughout the range of potentials and have increasingly larger slopes at more positive

potentials. No appreciable decrease in slope at even the most positive potentials is realized, indicating fluorescence is never the dominant mechanism for these dyes. In contrast, both VF.2.1.Cl and VF2.1OMe.H appear to have decreasing slopes at the most positive potentials indicating fluorescence is beginning to dominate over PeT. With regard to VF2.1.H, fluorescence appears to be predominant throughout and only at the most negative potentials does PeT begin to quench the high level of fluorescence as shown by the increasingly steeper slope seen in Figure 3.4b. Based on the different shapes of the fluorescence response curve to changes in voltage, thiophene dyes show a much higher probability to undergo PeT and thus appear to be better electron conductors capable of facilitating PeT more effectively than their phenyl counterparts.

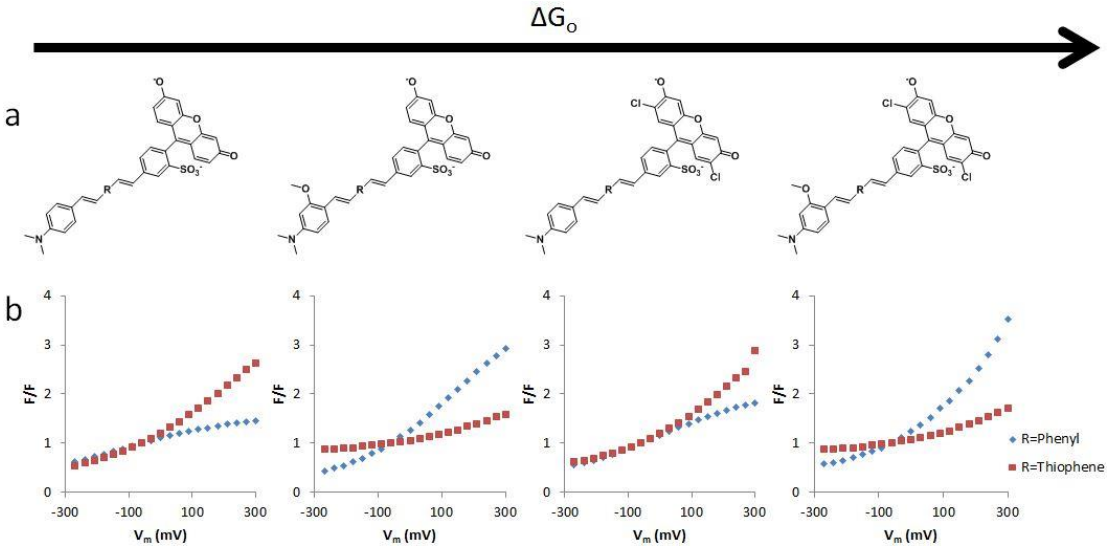

Figure 3.4 Voltage sensitivity of VF dyes with thiophene bridges compared to phenyl bridges. (a) Structure of VF dye where R is either a thiophene or phenyl group. Dyes are arranged from left to right in order of increasing driving force for electron transfer (ΔG_o). (b) Fluorescence response of VoltageFluor dyes with phenyl bridges (blue diamond) and thiophene bridges (red square) vs. membrane potential. Voltage-clamped HEK cells were held at -60 mV and then stepped to the indicated potential. The relative fluorescence (F/F) is plotted against the final membrane potential for VoltageFluor dyes loaded in HEK cells at a concentration of 200 nM

3.2.3 Electron Poor Bridges

The initial attempt to force longer electron transfer distances required the development of electron poor bridges. Fluorine substitution on the phenyl ring offered an excellent first pass given

its relatively similar properties to hydrogen atoms while remaining quite electron withdrawing. Synthesis of the new dye named VF2F.1.Cl was just as in dyes developed in chapter 2, however, a 2-fluoro substituted benzaldehyde was used instead. As expected, fluorine substitution had little effect on membrane staining of HEK cells and appeared highly localized to the plasma membrane as seen in Figure 3.5b. Labeled cells were then patch-clamped and interrogated as outlined above over ±100 mV potentials. VF2F.1.Cl showed a 4% ΔF/F per 100 mV in Figure 3.5d. This value was far below VF2.1.Cl, the same dye without a bridge fluorine substitution, which showed a 27% ΔF/F per 100 mV.

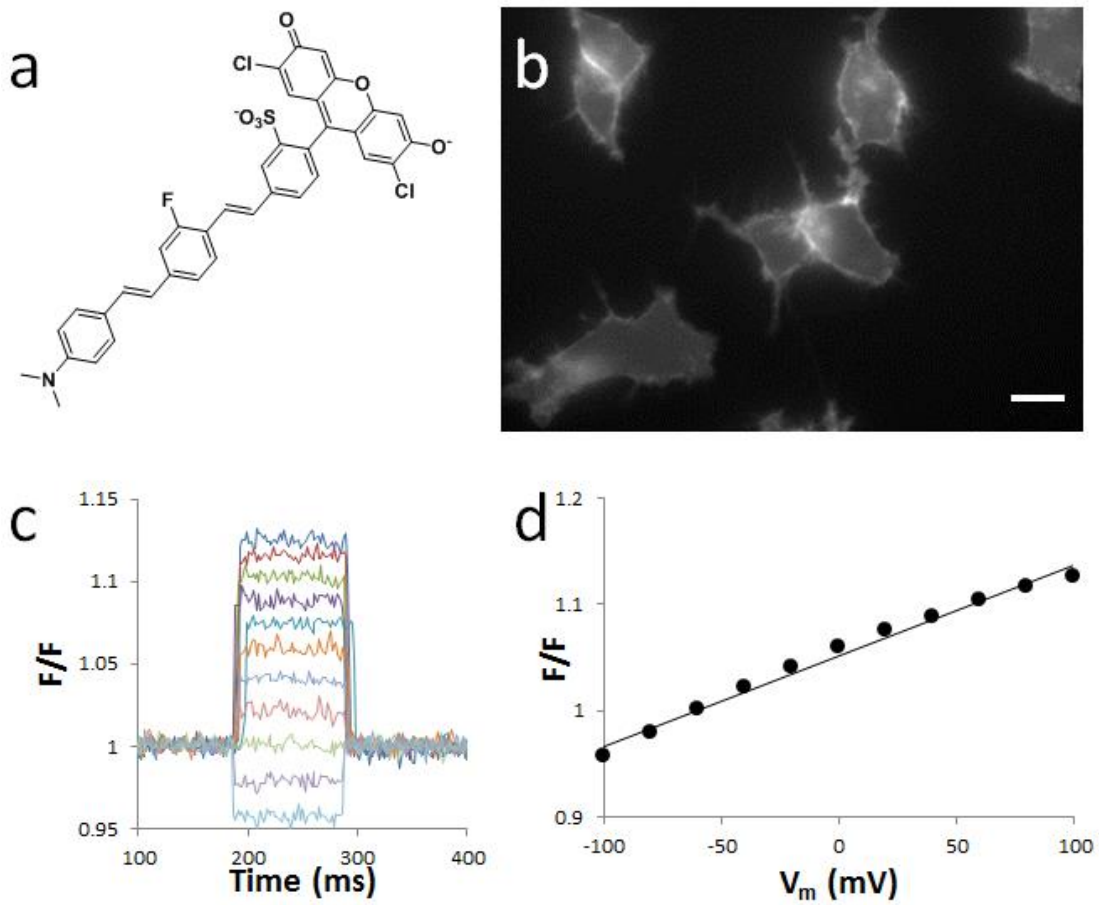

Figure 3.5 Structure and Characterization of VF2F.1.Cl in HEK cells. (a) Structure of VF2F.1.Cl. (b) Epifluorescence image of HEK cells stained with 2 μM dye for 15 min. at 37°C in culture. Scale bar is 20 μm. (c) Fluorescence response of VF2F.1.Cl in voltage-clamped cells from (b), plotted against time during 100 ms steps from -60 mV to +100 mV followed by steps decreasing in potential by 20mv increments to -100 mV. (d) Single trial response of VF2F.1.Cl (F/F) vs. final membrane potential of data collected in (c).

3.2.4 Longer Bridges

Given the propensity for phenylene vinylene bridges to be extended into the longer distance electron hoping regime and their previous success in VF dyes outlined in chapter 2, these bridges provided an excellent starting point towards lengthening VF dyes. Initially, a single additional phenylene vinylene unit was added to give VF3.1.H as shown in Figure 3.6a. To further interrogate the potential of longer VF dyes, however, another phenylene vinylene unit was installed to give the longest VF dye synthesiszed to date, VF4.1.H as seen in Figure 3.6d. The addition of another

phenylene vinylene unit in VF4.1.Cl further reduced the highest energy levels of the bridge molecular orbitals in hopes of better matching the donor and acceptor.

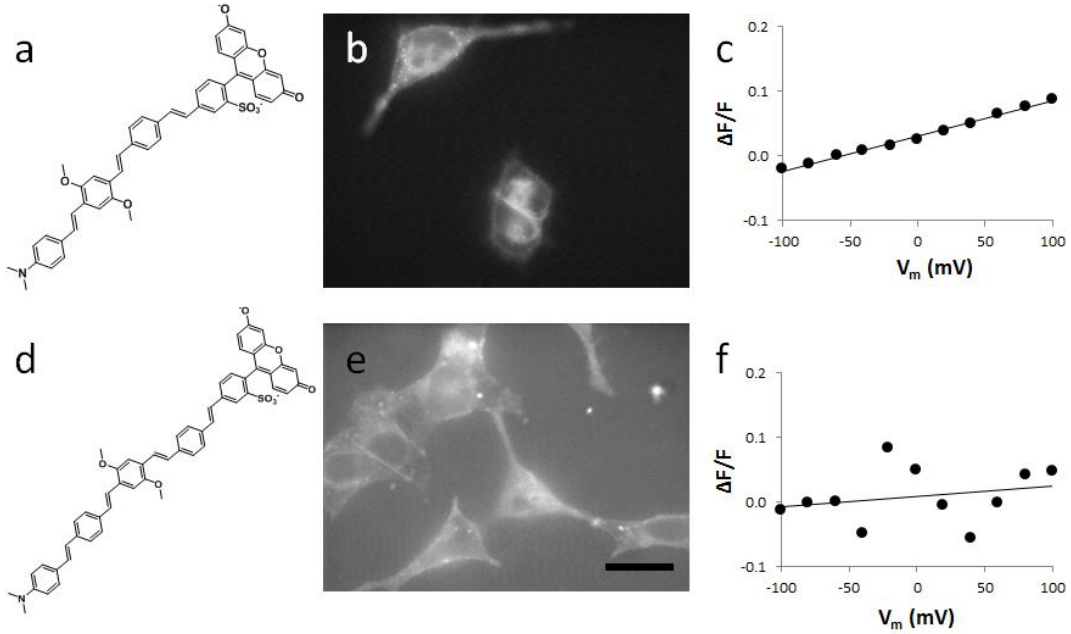

Figure 3.6 Voltage Sensitivity of VF Dyes with Longer Bridges in HEK Cells. (a) Structure of VF3.1.H. (b) Epifluorescence image of HEK cells stained with 2 μM dye for 15 min. at 37ºC in culture. (c) Single trial response of VF3.1.H (ΔF/F) vs. final membrane potential. Fluorescence response of VF3.1.H was measured in voltage-clamped cells from (b) during 100 ms steps from -60 mV to +100 mV followed by steps decreasing in potential by 20mv increments to -100 mV. (d) Structure of VF4.1.H. (e) Epifluorescence image of HEK cells stained with 600 nM dye added in a 50% pluronic mixture for 15 min. at 37ºC in culture. Scale bar is 20 μm. (f) Single trial response of VF4.1.H (ΔF/F) vs. final membrane potential measured as in (c).

Synthesis of VF dyes with longer bridges was approached with the same tried and true alternating Heck and Wittig coupling reactions. However, these longer dyes necessarily generated longer hydrophobic regions that created unique solubility problems. It was found dichloromethane provided the best solubility, but was often not appropriate for the reaction required for synthesis. This added challenge of minimal solubility reduced yields, but did not preclude total synthesis. Sufficient dye was isolated for staining cultured HEK cells and interrogated for voltage sensitivity via patch clamped cells and epifluorescent imaging.

As seen in both Figure 3.6b and e, cell staining was not as optimal as shorter dyes. Staining appears much more diffuse throughout the cell, and even somewhat punctate in Figure 3.6e. Additionally, the VF4.1.H did not appear to enjoy much uptake by cells at all given the low levels of fluorescence seen.

Both VF3.1.H and VF4.1.H did not show any improvements in voltage sensitivity with 5% and 1% ΔF/F per 100 mV respectively as seen in Figure 3.6c and f. VF4.1.H also showed a relatively non-linear response to changes in voltage compared to VF3.1.H, which should be attributed to the dim fluorescence recorded.

With such poor voltage sensitivities observed in longer phenylene vinylene bridges, a shift to thiophene vinylene bridges was made to realize improved VF dyes with longer bridges. VF3Tp.1.Cl as shown in Figure 3.7 replaced the two phenyl moieties seen in VF3.1.H with thiophenes given their demonstrated improved conductivity. The improved sensitivity seen in VF2Tp.1.Cl did not translate to VF3Tp.1.Cl. This longer dye showed negligible voltage sensitivity with a 1% ΔF/F per 100 mV shown in Figure 3.7b.

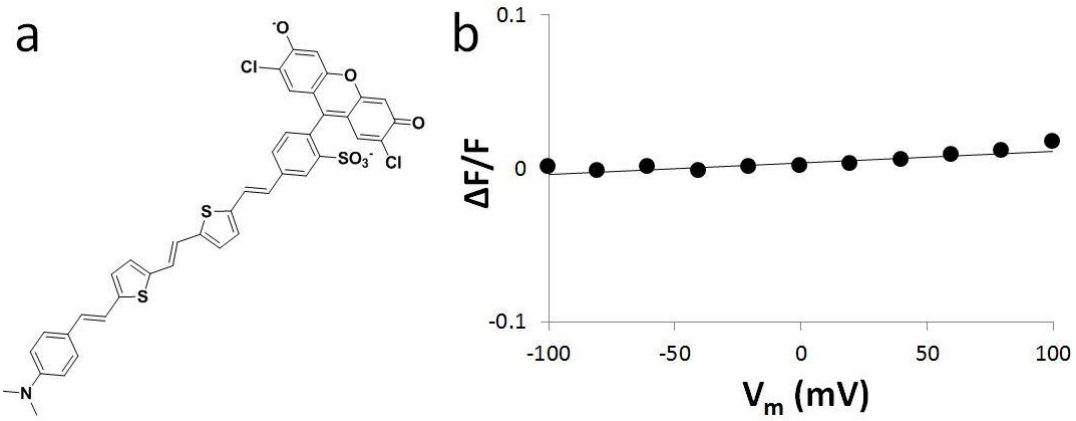

Figure 3.7 Structure and Voltage Sensitivity of a longer VF dye with a thiophene bridge. (a) Structure of VF3Tp.1.Cl. (b) Single trial response of VF3Tp.1.Cl (ΔF/F) vs. final membrane potential. Fluorescence response of VF3Tp.1.Cl was measured in voltage-clamped cells during 100 ms steps from -60 mV to +100 mV followed by steps decreasing in potential by 20mv increments to -100 mV.

3.2.5 Longer Bridges Couple with a Strong Driving Force for Electron Transfer

Improved bridges are an essential component toward facilitating electron transfer over longer distances. Additional improvements to the electron donor and acceptor may facilitate longer range electron transfer as well. Increasing the driving force for electron transfer is known to increase the rate of electron transfer by decreasing the required activation energy.[11] The VF dye with the highest driving force for electron transfer made to this point was VF2.1diOMe.Cl with a ΔG_o+w value of -0.03 eV. Substituting the chloro groups for stronger electron withdrawing groups should still further increase the driving force value calculated through the Rehm-Weller Equation discussed in chapter 2. Trifluoromethyl is a much stronger withdrawing group and could be easily substituted onto a fluorescein derivative with new radical trifluoromethylating reagents.[16] NMR spectroscopy confirmed synthesis of an asymmetrical trifluoromethylated fluorescein for HEK coupling to a range of donors and bridges in Figure 3.8.

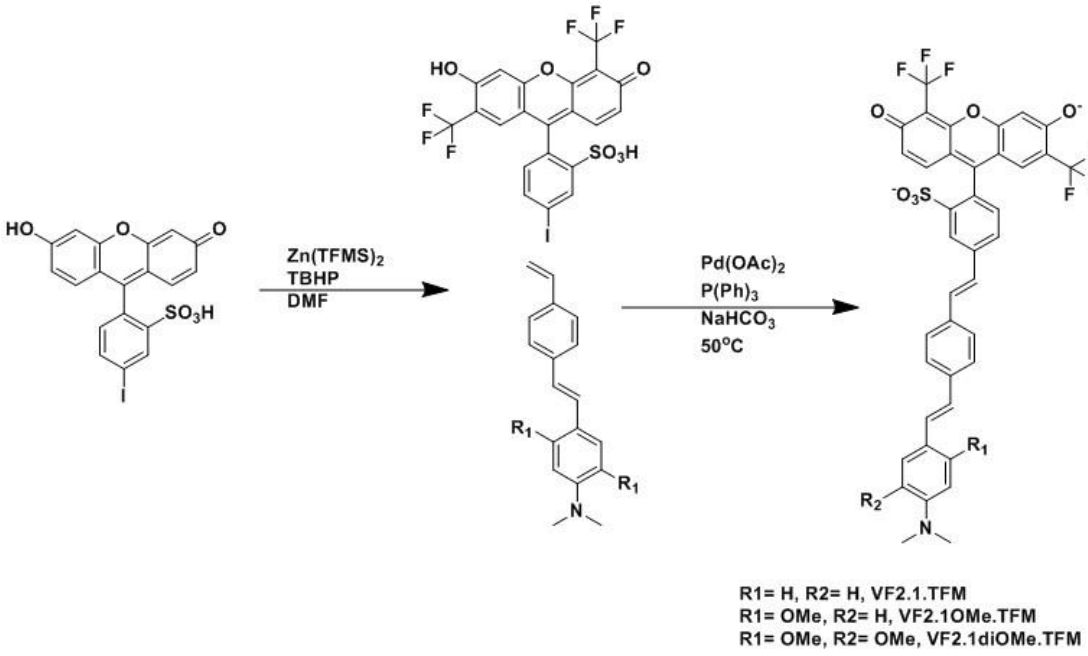

Figure 3.8 Trifluoromethylated VF Dye Synthetic Scheme

The effect of trifluoromethylation on the reduction potential of the fluorescein VF dye acceptor was determined by cyclic voltammetry in Figure 3.9. Trifluoromethylsulfonfluorescein had a reduction potential ($E(A/A^-)$) of -1.44 V vs. Fc compared to -2.02 V vs. Fc for dichlorosulfonfluorescein, the next most readily reduced VF acceptor. Accordingly, trifluoromethylated VF dyes appear to have dramatically increased driving forces for electron transfer compared to other substitutions as calculated by the Rehm-Weller equation and shown in Figure 3.11.

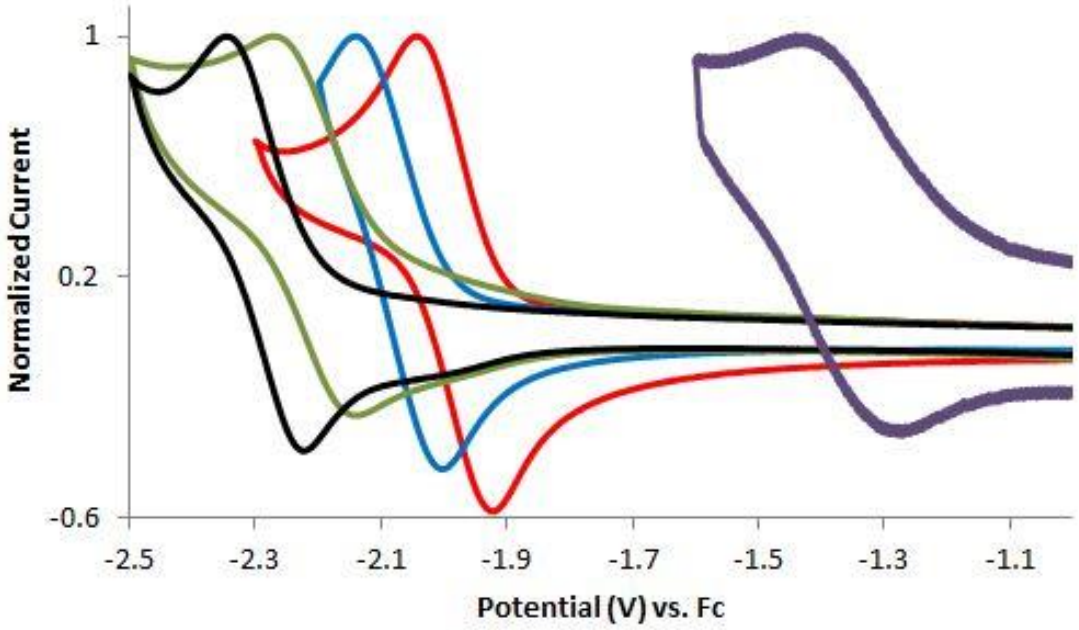

Figure 3.9 Cyclic voltammetry oftrifluoromethylated VF acceptor in relation to other VF acceptors.

Three second generation VF dyes with the trifluoromethylated acceptor were synthesized as shown in Figure 3.8. All three were applied to HEK cells and were patch clamped to measure voltage sensitivity in Figure 3.10. In data not shown, all three dyes appeared quite dim when staining HEK cells. Fluorine is known to have unique solubility properties and such a high concentration of fluorine atoms on these VF dyes may have impeded membrane staining. In

addition, the very strong driving force for electron transfer may have greatly reduced the quantum yield of these dyes giving very little fluorescence, similar to the effect thiophene bridges may have had in Figure 3.3. When tested for sensitivity, VF2.1.TFM had the highest voltage sensitivity ever recorded in HEK cells with a 50% ΔF/F per 100 mV in the physiologically relevant ± 100 mV range. VF2.1OMe.TFM was not far behind with a 37% ΔF/F per 100 mV in this range. VF2.1diOMe.TFM was the least sensitive with a 12% ΔF/F per 100 mV in HEK cells. For all three dyes, standard error of the mean (SEM) values were higher than typically seen. This may be due the low photon count recorded given how dim all three dyes were. This may also have been due to disruption of the membrane and poor electronic control of an unstable HEK cell. Overall, SEM values were still quite low over the three trials shown in Figure 3.10.

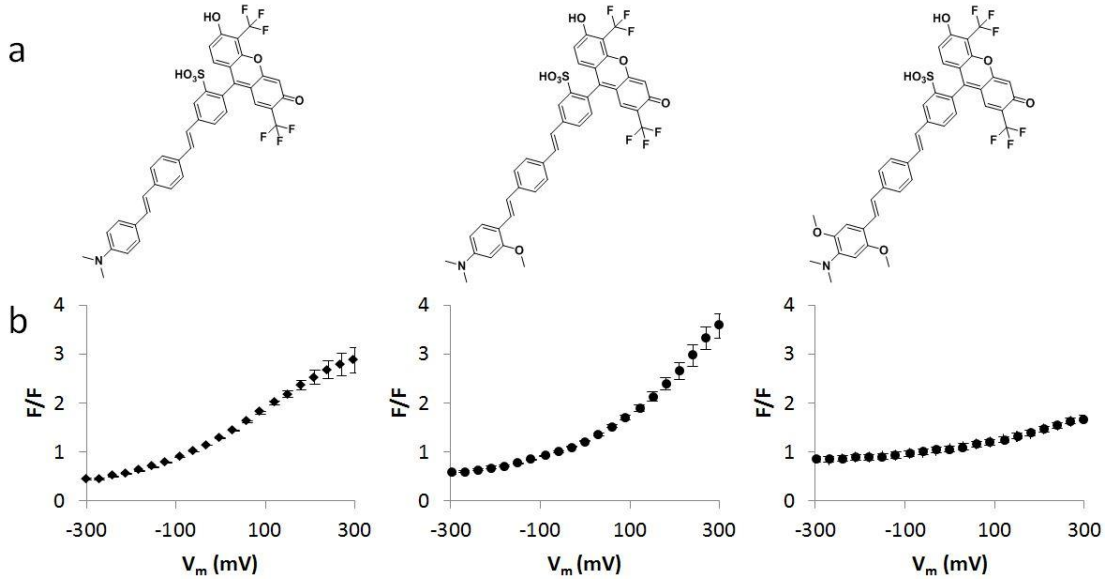

Figure 3.10 Structure and voltage sensitivity of trifluoromethylated VF dyes. (a) Structure from left to right of VF2.1.TFM, VF2.1OMe.TFM, and VF2.1diOMe.TFM. (b) Fluorescence response of representative VoltageFluor dyes vs. membrane potential. Voltage-clamped HEK cells were held at -60 mV and then stepped to the indicated potential. The relative fluorescence (F/F) is plotted against the final membrane potential for VoltageFluor dyes loaded in HEK cells at a concentration of 200 nM. Error bars are ±SEM for $n \geq 3$ for each dye.

PeT appeared to dominate for both VF2.1diOMe.TFM and VF2.1OMe.TFM given the shapes of both curves. Throughout the entire ± 300 mV range both dyes had steadily increasing slopes with no sign of any flattening. This indicates PeT is still relatively favored over fluorescence. VF2.1.TFM does not have this shape, but the SEM clearly increases quite a bit at the most positive potentials. This could indicated the patch clamp seal was beginning to weaken and the membrane potential was not as high as indicated in reality. Accordingly, it is difficult to infer what the shape of the curve indicates with regard to the extent of PeT or fluorescent mechanisms of relaxation in play. Undoubtedly, the trifluoromethylated acceptor represents a potentially valuable new VF dye.

VoltageFluor	ΔG_o+w (eV)	% ΔF/F per 100 mV
VF2.1diOMe.TFM	-0.64	12
VF2.1OMe.TFM	-0.47	37
VF2.1.TFM	-0.45	50
VF2.1diOMe.Cl	-0.03	29
VF2.1diOMe.H	0.13	34
VF2.1OMe.Cl	0.14	49
VF2.1.Cl	0.15	26
VF2.1.F	0.17	28
VF2.1OMe.H	0.30	56
VF2.1.H	0.31	16
VF2.1OMe.Me	0.42	12
VF2.1.Me	0.43	4

Figure 3.11 Driving Force and voltage sensitivity of TFM substituted acceptor with other VF dyes

Trifluoromethylation appears to dramatically increase the driving force for electron transfer as shown in Figure 3.11. It has also proven to be a capable acceptor for second-generation VF dyes leading to some of the most sensitive dyes to date, albeit with brightness issues. A trifluoromethylated acceptor with a dimethoxy donor was an attractive combination for longer VF dyes. Toward this end, VF3.1diOMe.TFM was synthesized as shown in Figure 3.12a. VF3.1diOMe.TFM was then applied to HEK cells to test voltage sensitivity. Very little

fluorescence was seen upon bath application of the dye. Longer dyes are inherently greasier and large aggregates may have formed that were washed away during loading. Cells appeared healthy via bright field imaging in Figure 3.12b. Poor membrane staining is a likely culprit for the negligible sensitivity to voltage seen in Figure 3.12d. Addition of solubilizing agents such as pluronic could improve membrane staining and voltage sensitivity. Even with these efforts, overall, VF3.1diOMe.TFM does not appear to be a promising voltage sensor.

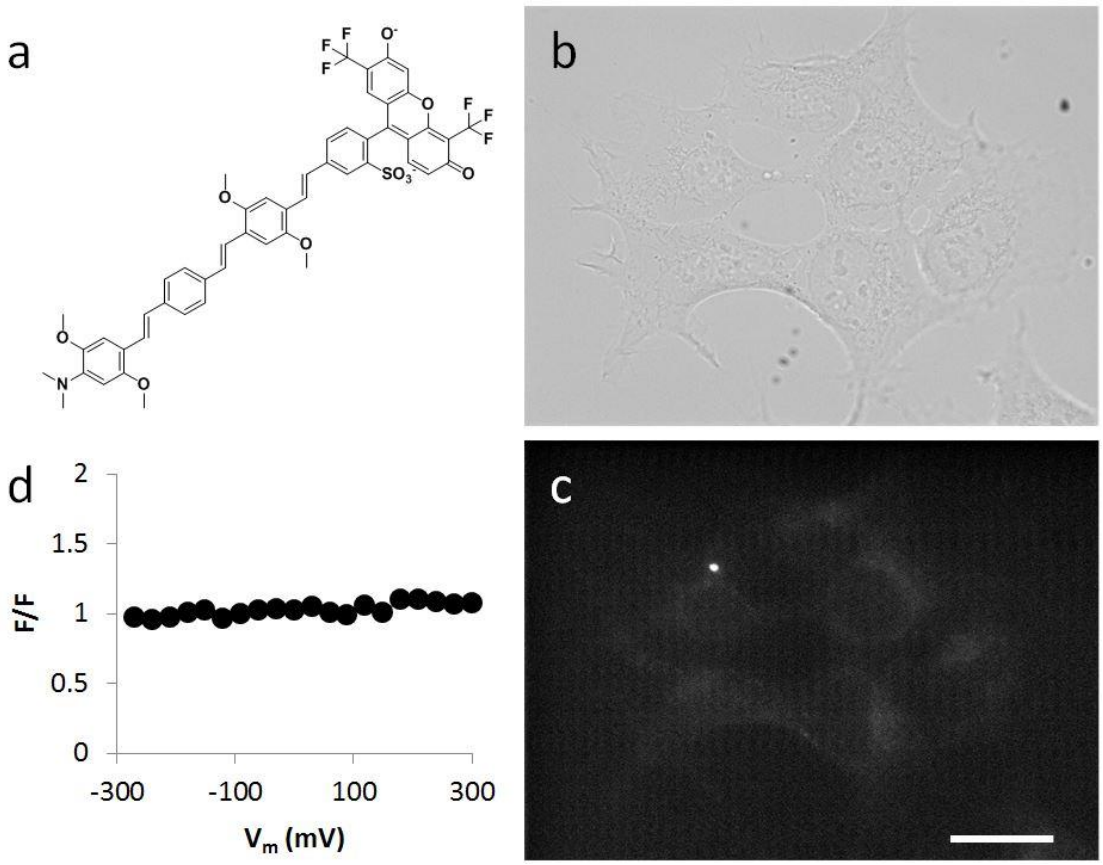

Figure 3.12 Structure and characterization of VF3.1diOMe.TFM. (a) Structure of VF3.1diOMe.TFM. (b) Bright field image of HEK cells stained with (a) in HBSS buffer containing 200 nM of the indicated VoltageFluor dyes for 15 min at 37°C. (c) Epifluorescent image of cells from (b). Scale bar is 20 μm. (d) Fluorescence response of VF3.1diOMe.TFM vs. membrane potential. Voltage-clamped HEK cells were held at -60 mV and then stepped to the indicated potential. The relative fluorescence (F/F) is plotted against the final membrane potential for VF3.1diOMe.TFM loaded in HEK cells at a concentration of 200 nM.

3.2.6 Alternative Bridge and Acceptor Attachment

Electron donors, bridges, and acceptors are all essential components to VF dyes. The orientation of each component has been consistent thusfar. All previous dyes coupled the alkene of the bridge to the halogenated phenylsulfonate of the fluorescein-like acceptor. In an effort to explore the effect coupling of the bridge and acceptor may have a second orientation was explored where the alkene was connected directly to the xanthene moiety as shown in Figure 3.13a. This orientation has the potential benefit of the bridge and acceptor lying on the same plane for improved electron transfer. Unfortunately, upon staining HEK cells, this new dye did not appear to be fluorescent at all in Figure 3.13c. There was no voltage sensitivity since no fluorescent signal was observable. It is possible this connection disrupted the fluorescence of the fluorescein-like molecule and was not amenable for voltage imaging.

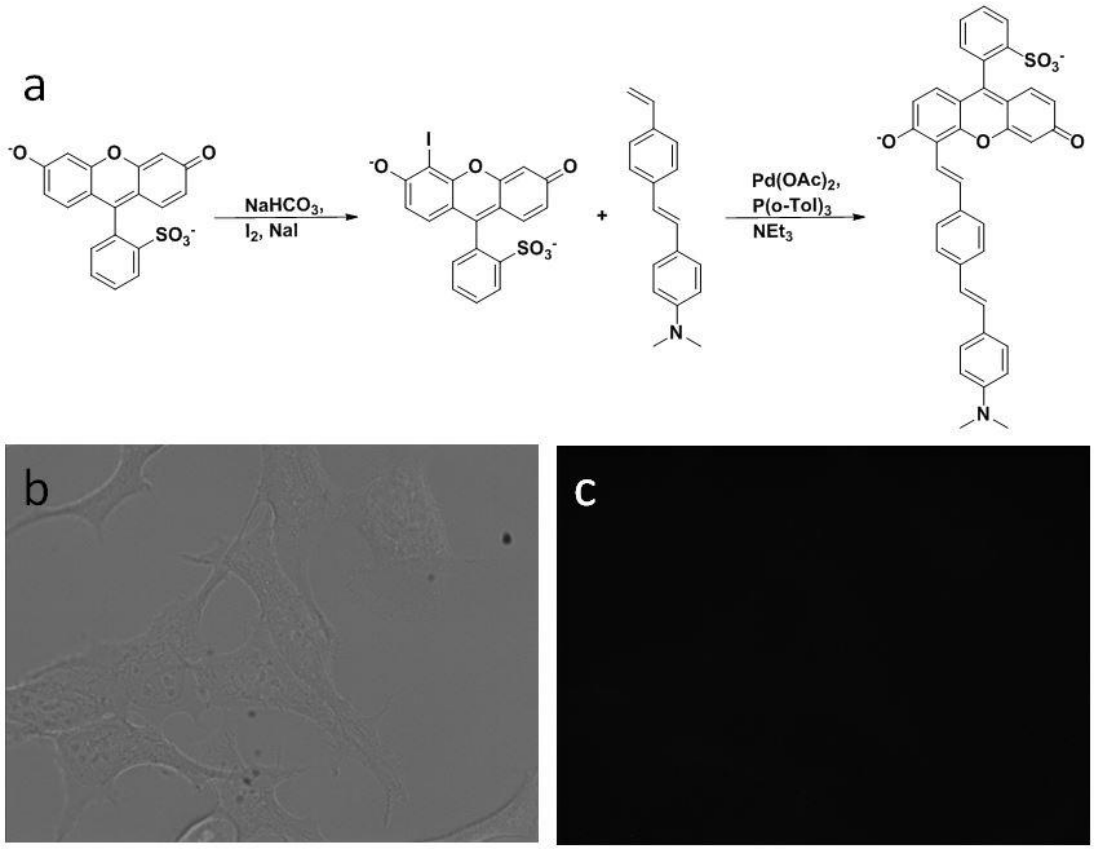

Figure 3.13 Synthesis and characterization in HEK cells of a VF dye with an inverted fluorescein acceptor. (a) Synthetic scheme. (b) Bright field image of HEK cells stained. (c) Epifluorescent image of HEK cells from (b) stained with 200 nM VF dye for 15 min. at 37°C.

3.3 Methods

3.3.1 General Synthetic and Analytical Measurements

As described in Chapter 2

3.3.2 Data Analysis

As described in Chapter 2

3.3.3 Patch Clamping Neurons and HEK Cells

As described in Chapter 2

3.3.4 Supporting Information

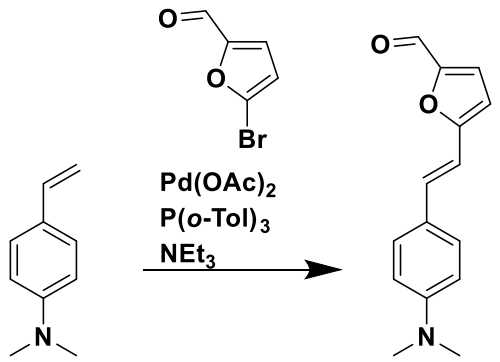

Synthesis of (E)-5-(4-(dimethylamino)styryl)furan-2-carbaldehyde

An oven-dried round bottom flask was equipped with a stir bar and charged with 4-N,N-dimethylaminostyrene (440 mg, 3 mmol, 1.25 equiv.), $Pd(OAc)_2$ (5.4 mg, 0.024 mmol, 0.01 equiv.), tri-*o*-tolylphosphine (15 mg, 0.02 mmol, 0.02 equiv.), and 5-bromofuran-2-carbaldehyde (420 mg, 2.4 mmol, 1.00 equiv.). The flask was evacuated and backfilled three times with N_2. Triethylamine (0.86 mL) was added, the round bottom sealed, and heated at 110°C. After stirring 20 hours, the reaction vessel was cooled to room temperature, dissolved in EtOAc and washed with saturated ammonium chloride twice. The organic portions were then collected and washed with saturated NaCl. The organic portions were dried over Na_2SO_4, filtered, and concentrated under reduced pressure. The orange solid was minimally redissolved in methylene chloride and triturated with hexanes to give the title compound as an orange powder, 130 mg (22%). ^{1}H NMR (400 MHz, CHLOROFORM-*d*) δ ppm 3.02 (s, 6 H) 6.44 (d, *J*=3.67 Hz, 1 H) 6.70 (d, *J*=7.33 Hz, 1H) 6.74 (d, *J*=14.66 Hz, 1 H) 7.25 (d, *J*=3.67 Hz, 1 H) 7.26 - 7.27 (m, 1 H) 7.35 (d, *J*=16.13 Hz, 1 H) 7.42 (d, *J*=8.80 Hz, 1 H) 9.54 (s, 1 H)

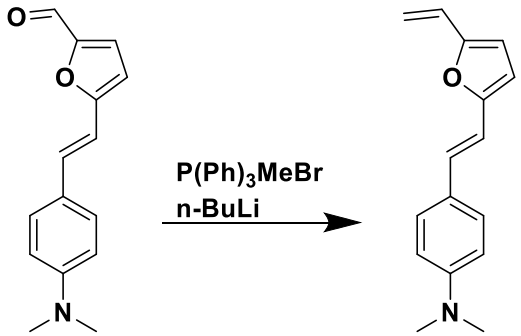

Synthesis of (E)-N,N-dimethyl-4-(2-(5-vinylfuran-2-yl)vinyl)aniline.

An oven-dried 10mL round bottom flask was charged with methyltriphenylphosphonium bromide (0.346 g, 0.97 mmol, 1.8 equiv.) and 10 mL anhydrous THF and stirred under N_2. A 1.6 M solution of *n*-butyllithium in hexanes was added via syringe (0.54 mL, 0.86 mmol, 1.6 equiv.) at room temperature to give an orange solution. After stirring for 30 min, (E)-5-(4-(dimethylamino)styryl)furan-2-carbaldehyde (130 mg, 0.538 mmol, 1.0 equiv.) was added. After stirring overnight, the reaction was poured into 50 mL of hexane. The suspension was filtered through celite and concentrated under reduced pressure. The residue was taken up in minimal hexanes and triturated in methylene chloride. The suspension was filtered to give 36 mg of a yellow solid

^{1}H NMR (400 MHz, CHLOROFORM-*d*) δ ppm 2.99 (s, 6 H) 5.16 (d, *J*=11.36 Hz, 2 H) 5.74 (d, *J*=17.60 Hz, 2 H) 6.26 (d, *J*=15.03 Hz, 1 H) 6.26 (d, *J*=8.43 Hz, 2 H) 6.50 (dd, *J*=17.41, 11.18 Hz, 2 H) 6.70 - 6.74 (m, 4 H) 7.04 (d, *J*=16.13 Hz, 2 H) 7.39 (d, *J*=8.80 Hz, 3 H) 7.49 (d, *J*=7.70 Hz, 3 H) 7.55 (d, *J*=6.60 Hz, 1 H) 7.69 (dd, *J*=11.91, 8.25 Hz, 3 H)

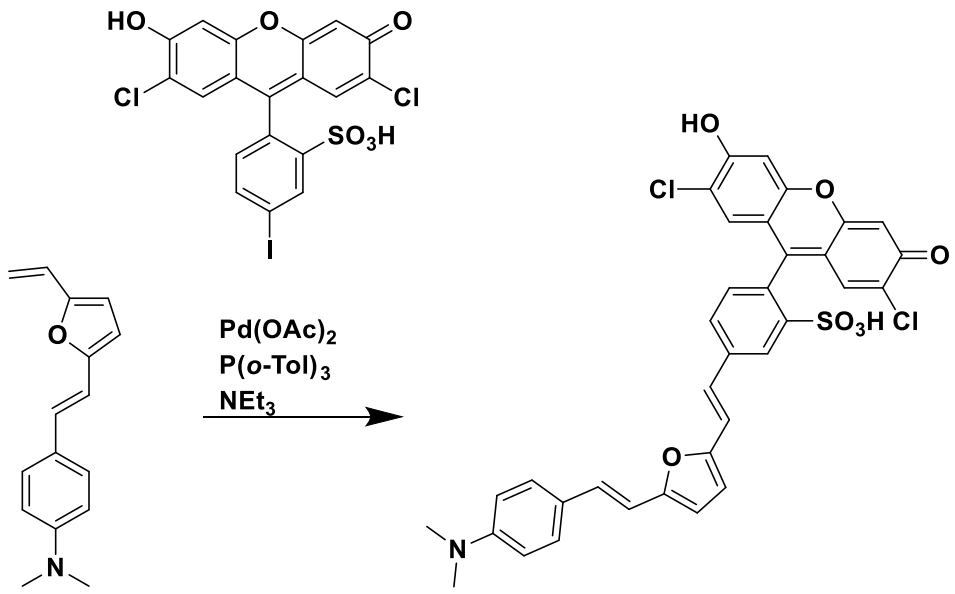

Synthesis of VF2Fur.1.Cl

An oven-dried 5 mL round bottom flask was equipped with a stir bar and charged with (E)-N,N-dimethyl-4-(2-(5-vinylfuran-2-yl)vinyl)aniline (36 mg, 0.15 mmol, 1.1 equiv.), $Pd(OAc)_2$ (1 mg, 4.4 μmol, 0.32 equiv.), tri-*o*-tolylphosphine (2 mg, 5.6 μmol, 0.7 equiv.), and 2-(2,7-dichloro-6-hydroxy-3-oxo-3H-xanthen-9-yl)-5-iodobenzenesulfonic acid (76 mg, 0.136 mmol, 1.00 equiv.). The flask was evacuated and backfilled three times with N_2. Triethylamine (1 mL) was added, the round bottom sealed, and heated at 110°C. After stirring 20 hours, the reaction appeared compete by TLC and the vessel was cooled to room temperature, dissolved in 1:1 hexanes:methylene chloride and acidified with conc. HCl on ice to give a dark brown solution that was filtered and collected. The brown solid was redissolved in DMF for purification by preparative HPLC on a Luna C_{18} column with a gradient of 10% MeCN I H_2O with 0.05% TFA ramping to 90% MeCN in 20 minutes. The resulting material was concentrated to dryness to give approximately 1 mg of a dark brown solid. HPLC-MS found $[M^+] = 674.4$

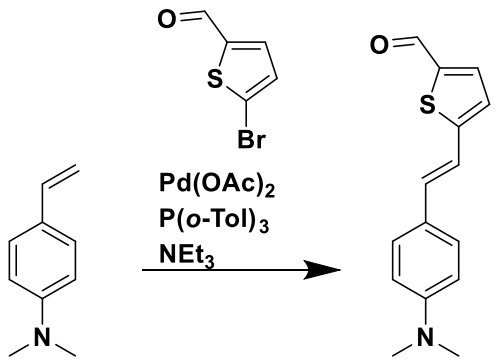

Synthesis of (E)-5-(4-(dimethylamino)styryl)thiophene-2-carbaldehyde

An oven-dried 10 mL round bottom flask was equipped with a stir bar and charged with 4-N,N-dimethylaminostyrene (318 mg, 2.16 mmol, 1.25 equiv.), $Pd(OAc)_2$ 3.6 mg, 0.0173 mmol, 0.01 equiv.), tri-*o*-tolylphosphine (10 mg, 0.0345 mmol, 0.02 equiv.), and 5-bromothiophene-2-carbaldehyde (330 mg, 1.73 mmol, 1.00 equiv.). The flask was evacuated and backfilled three times with N_2. Triethylamine (1.25 mL) was added, the round bottom sealed, and heated at 110°C. After stirring 20 hours, the reaction vessel was cooled to room temperature, dissolved in methylene chloride and washed with saturated ammonium chloride twice. The organic portions were then collected and washed with saturated NaCl. The organic portions were dried over Na_2SO_4, filtered, and concentrated under reduced pressure. The orange solid was minimally redissolved in methylene chloride and triturated with hexanes to give the title compound as an orange powder, 30 mg. ^{1}H NMR (400 MHz, CHLOROFORM-*d*) δ ppm 2.97 (s, 6 H) 6.65 (d, *J*=8.80 Hz, 1 H) 6.92 - 7.09 (m, 5 H) 7.36 (d, *J*=8.80 Hz, 1 H) 7.60 (d, *J*=3.67 Hz, 1 H) 9.77 (s, 1 H)

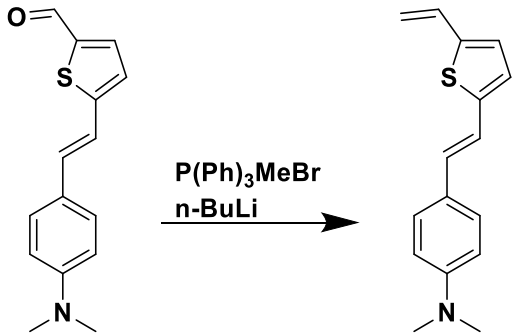

Synthesis of (E)-N,N-dimethyl-4-(2-(5-vinylthiophen-2-yl)vinyl)aniline.

An oven-dried round bottom flask was charged with methyltriphenylphosphonium bromide (0.075 g, 0.210 mmol, 1.8 equiv.) and 10 mL anhydrous THF and stirred under N_2. A 1.6 M solution of *n*-butyllithium in hexanes was added via syringe (0.3 mL, 0.187 mmol, 1.6 equiv.) at room temperature to give an orange solution. After stirring for 30 min, (E)-5-(4-(dimethylamino)styryl)thiophene-2-carbaldehyde (30 mg, 0.117 mmol, 1.0 equiv.) was added. After stirring overnight, the reaction was poured into 20 mL of hexane. The suspension was filtered through celite and concentrated under reduced pressure. The residue was taken up in ethyl acetate and filtered through alumina and concentrated under reduced pressure to give 30 mg of a yellow solid. (99%) ^{1}H NMR (300 MHz, CHLOROFORM-*d*) δ ppm 3.00 (s, 6 H) 5.13 (d, *J*=11.00 Hz, 1 H) 5.54 (d, *J*=17.33 Hz, 1 H) 6.71 (d, *J*=9.08 Hz, 1 H) 6.71 (d, *J*=8.50 Hz, 1 H) 6.78 (d, *J*=6.60 Hz, 1 H) 6.82 - 7.03 (m, 4 H) 7.38 (d, *J*=8.80 Hz, 1 H) 7.37 (d, *J*=7.00 Hz, 1 H)

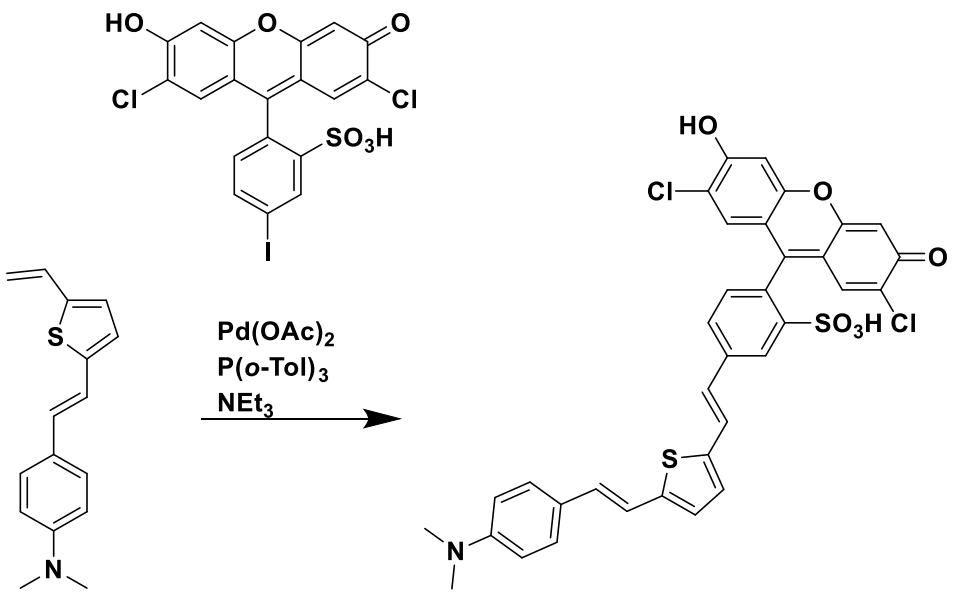

Synthesis of VF2Tp.1.Cl

An oven-dried 5 mL round bottom flask was equipped with a stir bar and charged with (E)-N,N-dimethyl-4-(2-(5-vinylthiophen-2-yl)vinyl)aniline (8 mg, 31 μmol, 1 equiv.), $Pd(OAc)_2$ (1 mg, 4.4 μmol.), tri-*o*-tolylphosphine (3 mg, 8.4 μmol.), and 2-(2,7-dichloro-6-hydroxy-3-oxo-3H-xanthen-9-yl)-5-iodobenzenesulfonic acid (18 mg, 31 μmol, 1.00 equiv.). The flask was evacuated and backfilled three times with N_2. Triethylamine (83 μL) was added, the round bottom sealed, and heated at 110°C. After stirring 20 hours the vessel was cooled to room temperature, dissolved in 1:1 hexanes:methylene chloride and concentrated to dryness. The brown solid was then taken up in 1M NaOH and carefully acidified with conc. HCl on ice to give a dark brown solid that was filtered and collected. The brown solid was redissolved in DMF for purification by preparative HPLC on a Luna C_{18} column with a gradient of 10% MeCN I H_2O with 0.05% TFA ramping to 90% MeCN in 20 minutes. The resulting material was concentrated to dryness to give approximately 1 mg of a dark brown solid. HPLC-MS found $[M^+] = 690.2$

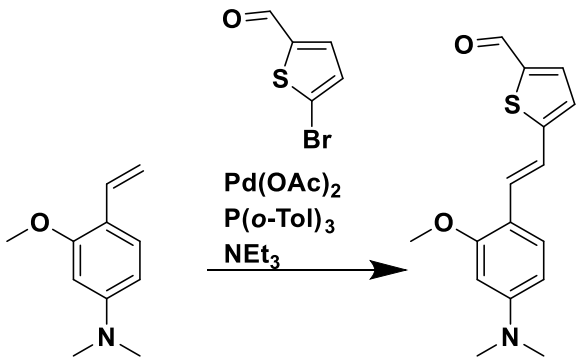

Synthesis of (E)-5-(4-(dimethylamino)-2-methoxystyryl)thiophene-2-carbaldehyde

An oven-dried round bottom flask was equipped with a stir bar and charged 3-methoxy-N,N-dimethyl-4-vinylaniline (177 mg, 1 mmol, 1 equiv.), $Pd(OAc)_2$ 2.24 mg, 0.01 mmol, 0.01 equiv.), tri-*o*-tolylphosphine (6.1 mg, 0.02 mmol, 0.02 equiv.), and 5-bromothiophene-2-carbaldehyde (1.119 mL, 1 mmol, 1.00 equiv.). The flask was evacuated and backfilled three times with N_2. Triethylamine (0.35 mL) was added, the round bottom sealed, and heated at 110°C. After stirring 20 hours, the reaction vessel was cooled to room temperature, dissolved in methylene chloride and washed with saturated ammonium chloride twice. The organic portions were then collected and washed with saturated NaCl. The organic portions were dried over Na_2SO_4, filtered, and concentrated under reduced pressure to give the title compound as a dark red sticky solid. ^{1}H NMR (400 MHz, CHLOROFORM-*d*) δ ppm 3.04 (s, 6 H) 3.92 (s, 3 H) 6.33 (d, *J*=6.97 Hz, 1 H) 7.06 (d, *J*=3.67 Hz, 1 H) 7.11 (d, *J*=16.13 Hz, 1 H) 7.38 - 7.48 (m, 2 H) 7.63 (d, *J*=4.03 Hz, 1 H) 7.73 (d, *J*=3.67 Hz, 1 H) 9.81 (s, 1 H)

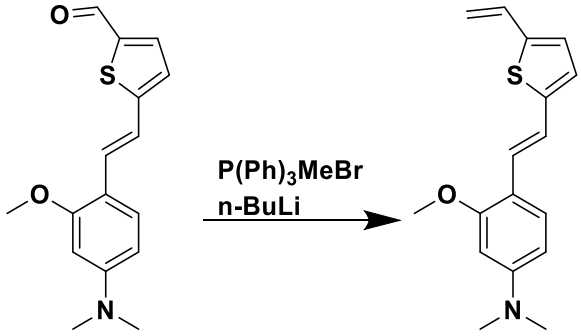

Synthesis of (E)-3-methoxy-N,N-dimethyl-4-(2-(5-vinylthiophen-2-yl)vinyl)aniline

An oven-dried round bottom flask was charged with methyltriphenylphosphonium bromide (0.237 g, 0.66 mmol, 1.8 equiv.) and 10 mL anhydrous THF and stirred under N_2. A 1.6 M solution of *n*-butyllithium in hexanes was added via syringe (0.368 mL, 0.59 mmol, 1.6 equiv.) at room temperature to give an orange solution. After stirring for 30 min, (E)-5-(4-(dimethylamino)-2-methoxystyryl)thiophene-2-carbaldehyde (106 mg, 0.37 mmol, 1.0 equiv.) was added. After stirring overnight, the reaction was poured into 50 mL of hexane. The solution was concentrated under reduced pressure to give an impure oil by TLC. The compound was purified by flash chromatography in 5% ethyl acetate in hexanes to give 8 mg of product. (7.6%) ^{1}H NMR (400 MHz, CHLOROFORM-*d*) δ ppm 3.01 (s, 6 H) 3.90 (s, 3 H) 5.10 (d, *J*=11.00 Hz, 1 H) 5.51 (d, *J*=17.23 Hz, 1 H) 6.22 (d, *J*=2.20 Hz, 1 H) 6.34 (dd, *J*=8.80, 2.20 Hz, 1 H) 6.76 (dd, *J*=17.60, 10.26 Hz, 1 H) 6.82 (s, 1 H) 7.01 - 7.19 (m, 3 H) 7.39 (d, *J*=8.80 Hz, 1 H)

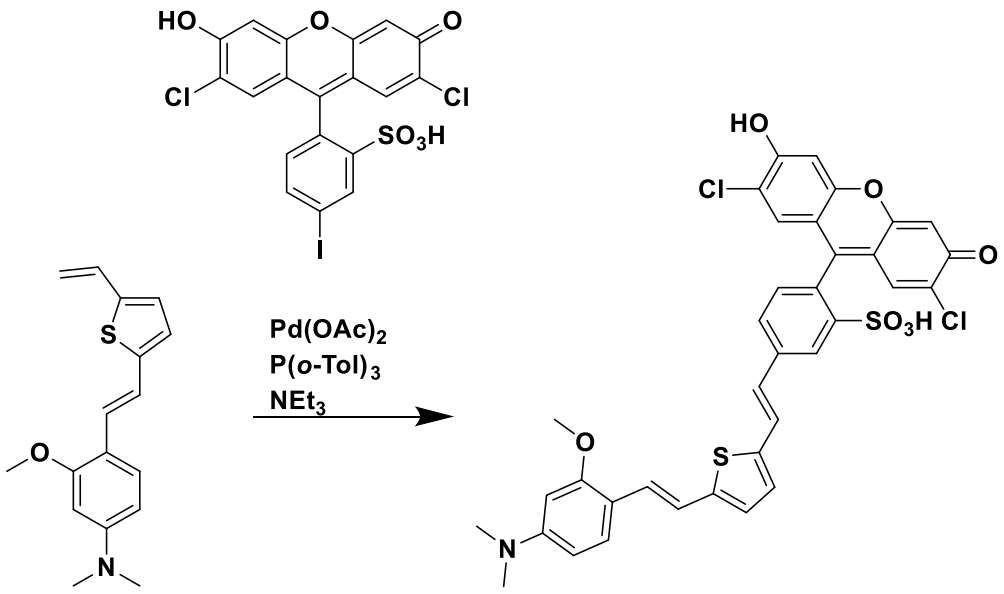

Synthesis of VF2Tp.1OMe.Cl

An oven-dried 10 mL round bottom flask was equipped with a stir bar and charged with (E)-3-methoxy-N,N-dimethyl-4-(2-(5-vinylthiophen-2-yl)vinyl)aniline (8 mg, 28 μmol, 1 equiv.),

$Pd(OAc)_2$ (1 mg, 4.4 μmol. 0.16 eq.), tri-*o*-tolylphosphine (3 mg, 8.4 μmol., 0.35 eq.), and 2-(2,7-dichloro-6-hydroxy-3-oxo-3H-xanthen-9-yl)-5-iodobenzenesulfonic acid (16 mg, 28 μmol, 1.00 equiv.). The flask was evacuated and backfilled three times with N_2. Triethylamine (50 μL) was added, the round bottom sealed, and heated at 110°C. After stirring 20 hours the vessel was cooled to room temperature, and concentrated to dryness. The brown solid was then taken up in DMF and minimal acetic acid for purification by preparative HPLC on a Luna C_{18} column with a gradient of 10% MeCN I H_2O with 0.05% TFA ramping to 90% MeCN in 20 minutes. The resulting material was concentrated to dryness to give approximately 1 mg of a dark brown solid. HPLC-MS found $[M^+]$ = 720.3

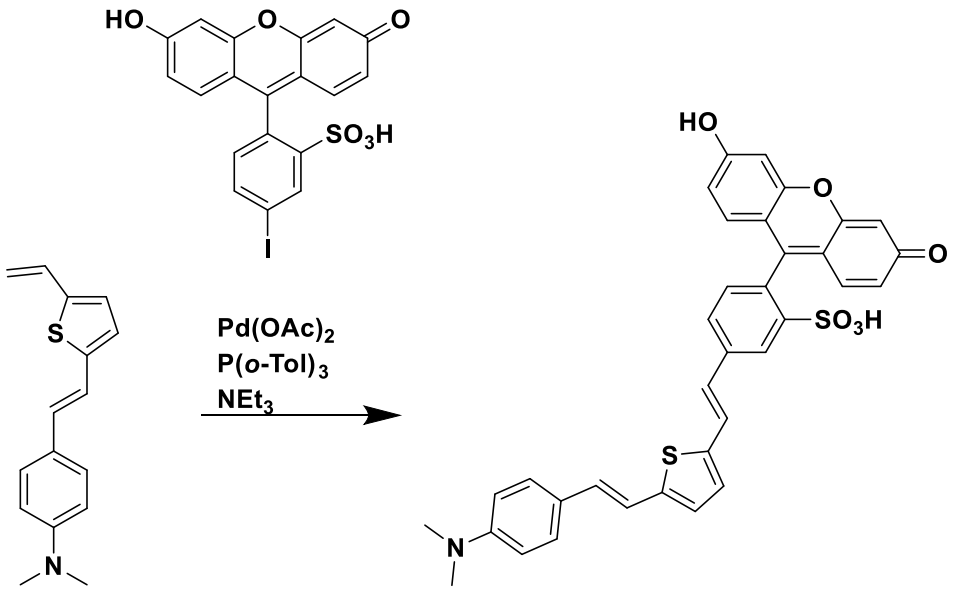

Synthesis of VF2Tp.1.H

An oven-dried 10 mL round bottom flask was equipped with a stir bar and charged with (E)-N,N-dimethyl-4-(2-(5-vinylthiophen-2-yl)vinyl)aniline (4 mg, 16 μmol, 1 equiv.), $Pd(OAc)_2$ (1 mg, 4.4 μmol.), tri-*o*-tolylphosphine (3 mg, 8.4 μmol.), and 2-(6-hydroxy-3-oxo-3H-xanthen-9-yl)-5-iodobenzenesulfonic acid (7.7 mg, 16 μmol, 1.00 equiv.). The flask was evacuated and backfilled three times with N_2. Triethylamine (100 μL) was added, the round bottom sealed, and heated at

110°C. After stirring 20 hours the vessel was cooled to room temperature, and concentrated to dryness. The brown solid was then taken up in DMF and minimal acetic acid for purification by preparative HPLC on a Luna C_{18} column with a gradient of 10% MeCN I H_2O with 0.05% TFA ramping to 90% MeCN in 20 minutes. The resulting material was concentrated to dryness to give approximately 1 mg of a dark brown solid. HPLC-MS found [M^+] = 622.3

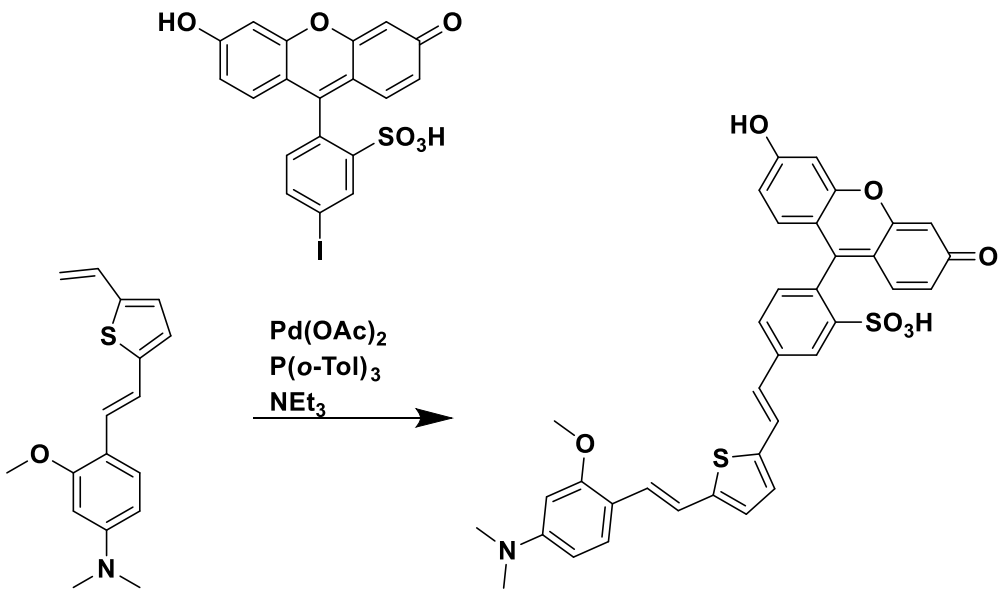

Synthesis of VF2Tp.1OMe.H

An oven-dried round bottom flask was equipped with a stir bar and charged with (E)-3-methoxy-N,N-dimethyl-4-(2-(5-vinylthiophen-2-yl)vinyl)aniline (5 mg, 18 μmol, 1 equiv.), $Pd(OAc)_2$ (1 mg, 4.4 μmol.), tri-*o*-tolylphosphine (3 mg, 8.4 μmol.), and 2-(6-hydroxy-3-oxo-3H-xanthen-9-yl)-5-iodobenzenesulfonic acid (8.7 mg, 18 μmol, 1.00 equiv.). The flask was evacuated and backfilled three times with N_2. Triethylamine (7 μL) was added, the round bottom sealed, and heated at 110°C. After stirring 20 hours the vessel was cooled to room temperature, and concentrated to dryness. The brown solid was then taken up in DMF and minimal acetic acid for purification by preparative HPLC on a Luna C_{18} column with a gradient of 10% MeCN I H_2O with 0.05% TFA ramping to

90% MeCN in 20 minutes. The resulting material was concentrated to dryness to give approximately 1 mg of a dark brown solid. HPLC-MS found [M^+] = 652.3

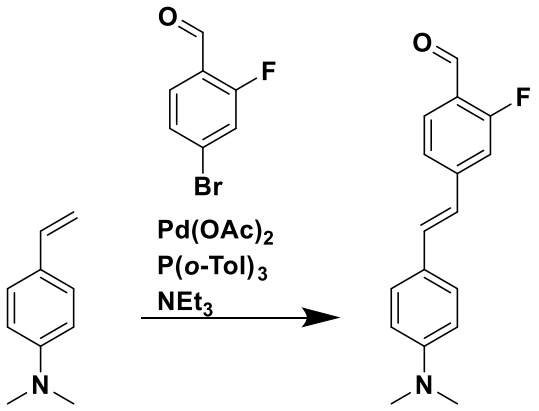

Synthesis of (E)-4-(4-(dimethylamino)styryl)-2-fluorobenzaldehyde

An oven-dried round bottom flask was equipped with a stir bar and charged N,N-dimethyl-4-vinylaniline (300 mg, 2 mmol, 1.25 equiv.), $Pd(OAc)_2$ 120 mg, 0.016 mmol, 0.01 equiv.), tri-*o*-tolylphosphine (10 mg, 0.032 mmol, 0.02 equiv.), and 4-bromo-2-fluoro-benzaldehyde (331 mg, 1.6 mmol, 1.00 equiv.). The flask was evacuated and backfilled three times with N_2. Triethylamine (0.35 mL) was added, the round bottom sealed, and heated at 110°C. After stirring 20 hours, the reaction vessel was cooled to room temperature, dissolved in methylene chloride and hexanes washed with saturated ammonium chloride twice. The organic portions were then collected and washed with saturated NaCl. The organic portions were dried over Na_2SO_4, filtered, and concentrated under reduced pressure. The orange solid was then purified by flash chromatography using a mixture of hexanes and ethyl acetate. ^{1}H NMR (400 MHz, CHLOROFORM-*d*) δ ppm 3.03 (s, 6 H) 6.59 (d, *J*=8.43 Hz, 1 H) 6.67 (d, *J*=12.46 Hz, 1 H) 6.72 (d, *J*=8.80 Hz, 1 H) 6.88 (d, *J*=16.13 Hz, 1 H) 7.11 - 7.25 (m, 1 H) 7.34 (d, *J*=8.07 Hz, 1 H) 7.45 (d, *J*=8.43 Hz, 1 H) 7.73 (t, *J*=7.70 Hz, 1 H) 7.82 (t, *J*=7.70 Hz, 1 H) 10.30 (s, 1 H)

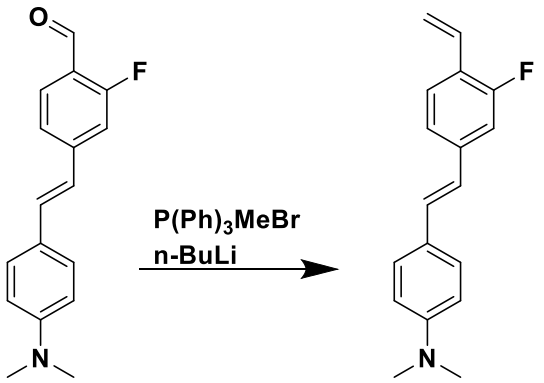

Synthesis of (E)-4-(3-fluoro-4-vinylstyryl)-N,N-dimethylaniline

An oven-dried round bottom flask was charged with methyltriphenylphosphonium bromide (0.131 g, 0.94 mmol, 1.8 equiv.) and 3 mL anhydrous THF and stirred under N_2. A 1.6 M solution of *n*-butyllithium in hexanes was added via syringe (0.52 mL, 0.832 mmol, 1.6 equiv.) at room temperature to give an orange solution. After stirring for 30 min, (E)-4-(4-(dimethylamino)styryl)-2-fluorobenzaldehyde (140 mg, 0.52 mmol, 1.0 equiv.) was added. After stirring overnight, the reaction was poured into 10 mL of hexane. The suspension was filtered by celite to give a yellow solution concentrated under vacuum to dryness. The resulting yellow solid was collected and judged to be a pure 140 mg of product. (43%) ^{1}H NMR (300 MHz, CHLOROFORM-*d*) δ ppm 3.00 (s, 6 H) 5.34 (d, *J*=11.00 Hz, 1 H) 5.81 (d, *J*=17.88 Hz, 1 H) 6.72 (d, *J*=8.53 Hz, 1 H) 6.80 - 6.92 (m, 2 H) 7.00 - 7.23 (m, 4 H) 7.33 (d, *J*=8.25 Hz, 1 H) 7.38 - 7.47 (m, 2 H)

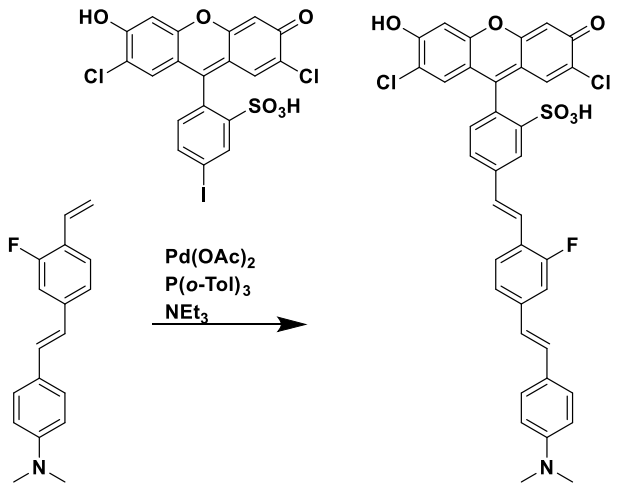

Synthesis of VF2.1F.Cl

An oven-dried 10 mL round bottom flask was equipped with a stir bar and charged with (E)-4-(3-fluoro-4-vinylstyryl)-N,N-dimethylaniline (13 mg, 50 μmol, 1.1 equiv.), $Pd(OAc)_2$ (2 mg, 3 μmol.), tri-*o*-tolylphosphine (6 mg, 18 μmol.), and 2-(2,7-dichloro-6-hydroxy-3-oxo-3H-xanthen-9-yl)-5-iodobenzenesulfonic acid (16 mg, 30 μmol,). The flask was evacuated and backfilled three times with N_2. Triethylamine (100 μL) was added, the round bottom sealed, and heated at 110°C. After stirring 20 hours the vessel was cooled to room temperature, and concentrated to dryness. The brown solid was then taken up in DMF and minimal acetic acid for purification by preparative HPLC on a Luna C_{18} column with a gradient of 10% MeCN I H_2O with 0.05% TFA ramping to 90% MeCN in 20 minutes. The resulting material was concentrated to dryness to give approximately 1 mg of a dark brown solid. HPLC-MS found $[M^+]$ = 702.3

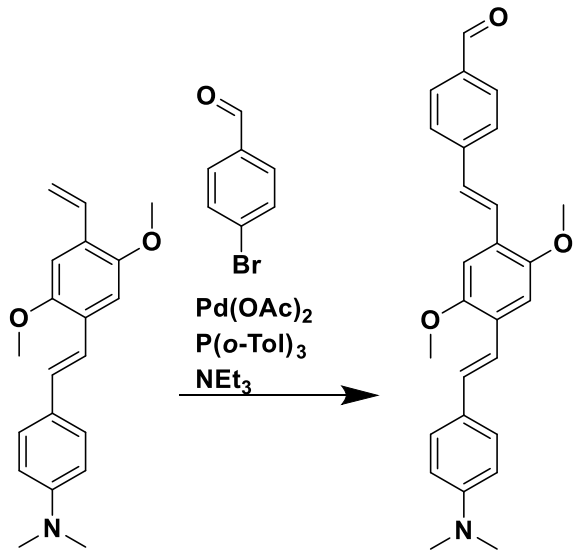

Synthesis of 4-((E)-4-((E)-4-(dimethylamino)styryl)-2,5-dimethoxystyryl)benzaldehyde

An oven-dried 10 mL round bottom flask was equipped with a stir bar and charged (E)-4-(2,5-dimethoxy-4-vinylstyryl)-N,N-dimethylaniline (100 mg, 323 mmol, 1.0 equiv.), $Pd(OAc)_2$ 0.7 mg, 0.0032 mmol, 0.01 equiv.), tri-*o*-tolylphosphine (2 mg, 0.0065 mmol, 0.02 equiv.), and 4-bromo-benzaldehyde (60 mg, 0.323 mmol, 1.00 equiv.). The flask was evacuated and backfilled three times with N_2. Triethylamine (0.25 mL) was added, the round bottom sealed, and heated at 110°C. After stirring 20 hours, the reaction vessel was full of bright orange solid and was cooled to room temperature. The solid was dissolved in methylene chloride and washed with saturated ammonium chloride twice. The organic portions were then collected and washed with saturated NaCl. The organic portions were dried over Na_2SO_4, filtered, and concentrated under reduced pressure. The orange solid was judged pure giving 111mg (83%). ^{1}H NMR (400 MHz, CHLOROFORM-*d*) δ ppm 3.01 (s, 6 H) 3.94 (s, 3 H) 3.96 (s, 3 H) 6.73 (d, *J*=7.33 Hz, 1 H) 7.07 - 7.18 (m, 5 H) 7.27 (s, 1 H) 7.28 (br. s., 1 H) 7.32 (s, 1 H) 7.48 (d, *J*=7.33 Hz, 1 H) 7.65 (s, 1 H) 7.70 (d, *J*=6.60 Hz, 1 H) 7.87 (d, *J*=6.97 Hz, 1 H) 10.00 (s, 1 H)

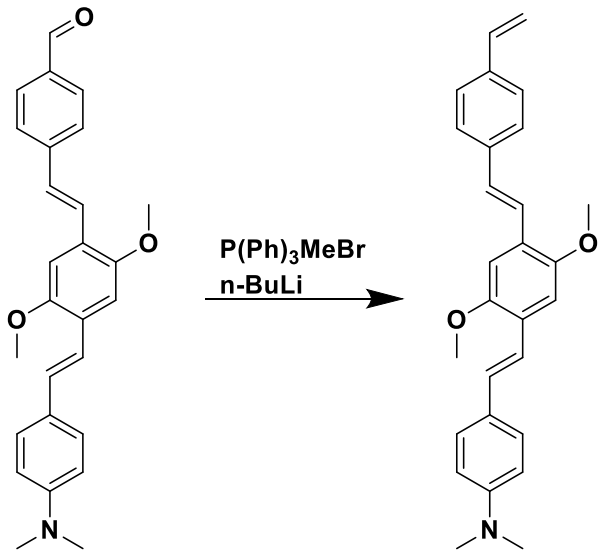

Synthesis of 4-((E)-2,5-dimethoxy-4-((E)-4-vinylstyryl)styryl)-N,N-dimethylaniline

An oven-dried round bottom flask was charged with methyltriphenylphosphonium bromide (0.155 g, 0.435 mmol, 1.8 equiv.) and 6 mL anhydrous THF and stirred under N_2. A 1.6 M solution of *n*-butyllithium in hexanes was added via syringe (0.24 mL, 0.378 mmol, 1.6 equiv.) at room temperature to give an orange solution. After stirring for 30 min, 4-((E)-4-((E)-4-(dimethylamino)styryl)-2,5-dimethoxystyryl)benzaldehyde (100 mg, 0.242 mmol, 1.0 equiv.) was added. After stirring overnight, the reaction was poured into 20 mL of hexane. The suspension was filtered by celite to give a yellow solution concentrated under vacuum to dryness. The resulting yellow solid was collected and carried forward without further purification. ^{1}H NMR (400 MHz, CHLOROFORM-*d*) δ ppm 3.00 (s, 6 H) 3.93 (br. s., 3 H) 3.93 (br. s., 3 H) 5.25 (d, *J*=12.46 Hz, 1 H) 5.78 (d, *J*=17.23 Hz, 1 H) 6.68 - 6.77 (m, 1 H) 6.73 (d, *J*=6.97 Hz, 1 H) 7.04 - 7.15 (m, 4 H) 7.30 (d, *J*=14.30 Hz, 1 H) 7.39 - 7.54 (m, 8 H)

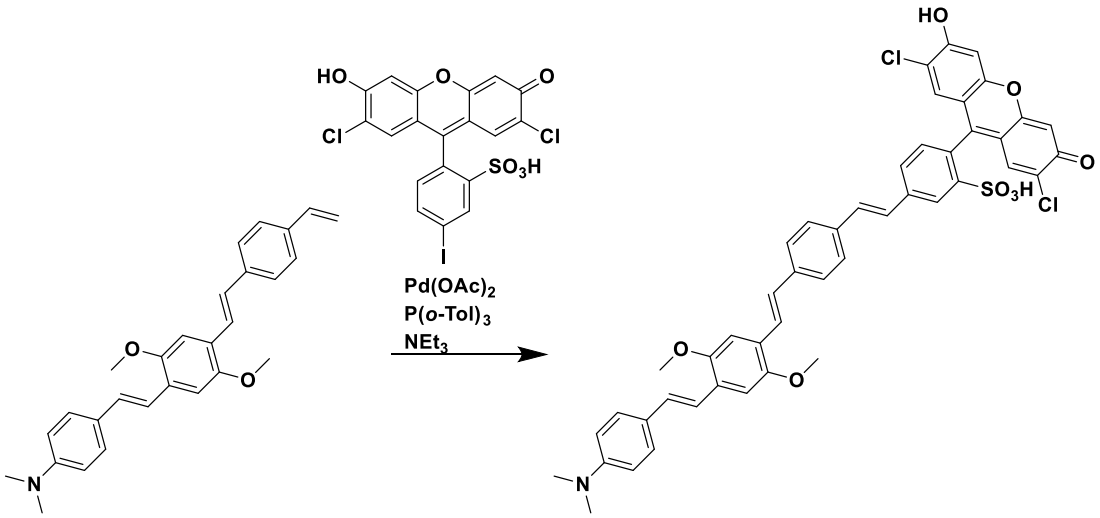

Synthesis of VF3.1.Cl

An oven-dried 10 mL round bottom flask was equipped with a stir bar and charged with 4-((E)-2,5-dimethoxy-4-((E)-4-vinylstyryl)styryl)-N,N-dimethylaniline (8 mg, 19 μmol, 1 equiv.), $Pd(OAc)_2$ (1 mg, 4.4 μmol.), tri-*o*-tolylphosphine (3 mg, 10 μmol.), and 2-(2,7-dichloro-6-hydroxy-3-oxo-3H-xanthen-9-yl)-5-iodobenzenesulfonic acid (11 mg, 19 μmol, 1 eq.). The flask was evacuated and backfilled three times with N_2. Triethylamine (51 μL) was added, the round bottom sealed, and heated at 110°C. After stirring 20 hours the vessel was cooled to room temperature, and concentrated to dryness. The brown solid was then taken up in DMF and minimal acetic acid for purification by preparative HPLC on a Luna C_{18} column with a gradient of 10% MeCN I H_2O with 0.05% TFA ramping to 90% MeCN in 20 minutes. The resulting material was concentrated to dryness to give approximately 1 mg of a dark brown solid. HPLC-MS found $[M^+] = 846.3$

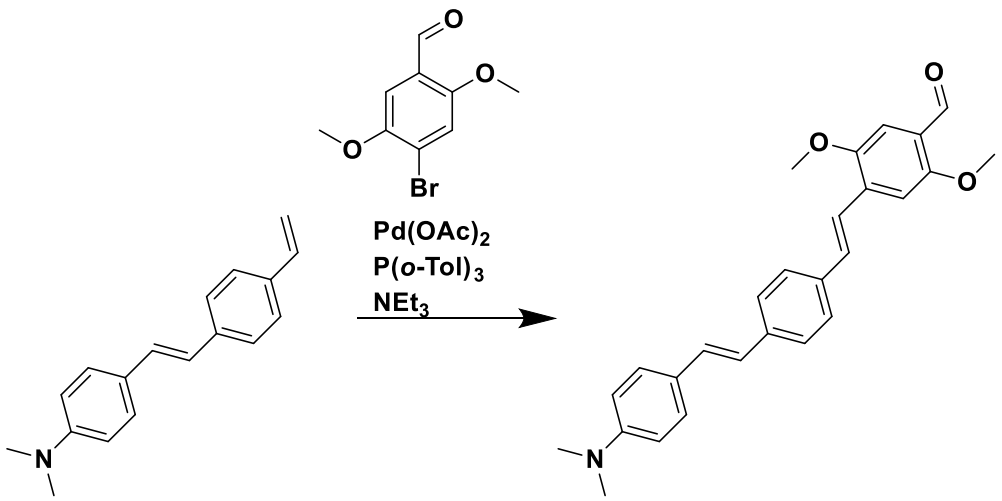

Synthesis of 4-((E)-4-((E)-4-(dimethylamino)styryl)styryl)-2,5-dimethoxybenzaldehyde

An oven-dried 10 mL round bottom flask was equipped with a stir bar and charged (E)-N,N-dimethyl-4-(4-vinylstyryl)aniline (100 mg, 0.4 mmol, 1.0 equiv.), $Pd(OAc)_2$ (3 mg, 0.0013 mmol, 0.01 equiv.), tri-*o*-tolylphosphine (9 mg, 0.003 mmol, 0.03 equiv.), and 4-bromo-2,5-dimethoxybenzaldehyde (100 mg, 0.4 mmol, 1.00 equiv.). The flask was evacuated and backfilled three times with N_2. Triethylamine (0.5 mL) and DMF (0.5 mL) were added and the round bottom was sealed and heated at 110°C. After stirring 20 hours, the reaction vessel was full of bright orange solid and was cooled to room temperature. The solid was dissolved in a large amount of methylene chloride and washed with saturated ammonium chloride twice. The organic portions were then collected and washed with saturated NaCl. The organic portions were dried over Na_2SO_4, filtered, and concentrated under reduced pressure. The orange solid was not purified any further. ^{1}H NMR (400 MHz, CHLOROFORM-*d*) δ ppm 3.01 (s, 6 H) 3.91 (s, 3 H) 3.99 (s, 3 H) 6.73 (d, *J*=8.80 Hz, 3 H) 7.02 (d, *J*=86.52 Hz, 4 H) 7.08 (d, *J*=54.62 Hz, 3 H) 7.21 (s, 2 H) 7.25 (s, 1 H) 7.35 (s, 1 H) 7.44 (d, *J*=8.80 Hz, 3 H) 7.47 (d, *J*=6.23 Hz, 2 H) 7.50 - 7.56 (m, 6 H) 10.44 (s, 1 H)

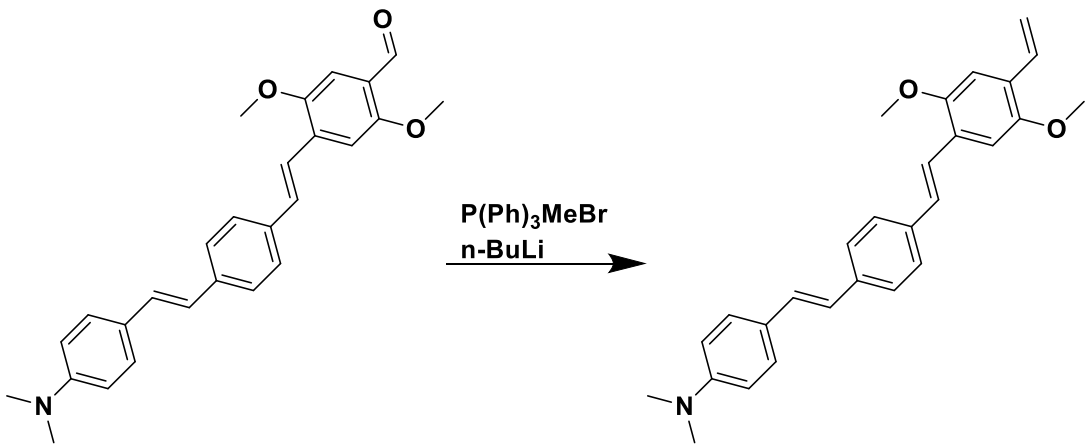

Synthesis of 4-((E)-4-((E)-2,5-dimethoxy-4-vinylstyryl)styryl)-N,N-dimethylaniline

An oven-dried round bottom flask was charged with methyltriphenylphosphonium bromide (0.132 g, 0.37 mmol, 1.8 equiv.) and 10 mL anhydrous THF and stirred under N_2. A 1.6 M solution of *n*-butyllithium in hexanes was added via syringe (0.24 mL, 0.378 mmol, 1.6 equiv.) at -78°C to give a yellow solution. After stirring for 30 min, 4-((E)-4-((E)-4-(dimethylamino)styryl)styryl)-2,5-dimethoxybenzaldehyde (85 mg, 0.2 mmol, 1.0 equiv.) in 5 mL methylene chloride was added. After stirring overnight, the reaction was added to 20 mL of hexanes. The suspension was filtered through celite to give a yellow solution concentrated under vacuum to dryness. The resulting 24 mg of yellow solid was collected and carried forward without further purification. ^{1}H NMR (400 MHz, CHLOROFORM-*d*) δ ppm 3.00 (s, 6 H) 3.90 (s, 6 H) 5.30 (d, *J*=11.36 Hz, 1 H) 5.77 (d, *J*=18.70 Hz, 1 H) 6.73 (d, *J*=8.80 Hz, 2 H) 6.93 (d, *J*=16.50 Hz, 1 H) 7.02 - 7.14 (m, 5 H) 7.41 - 7.54 (m, 7 H)

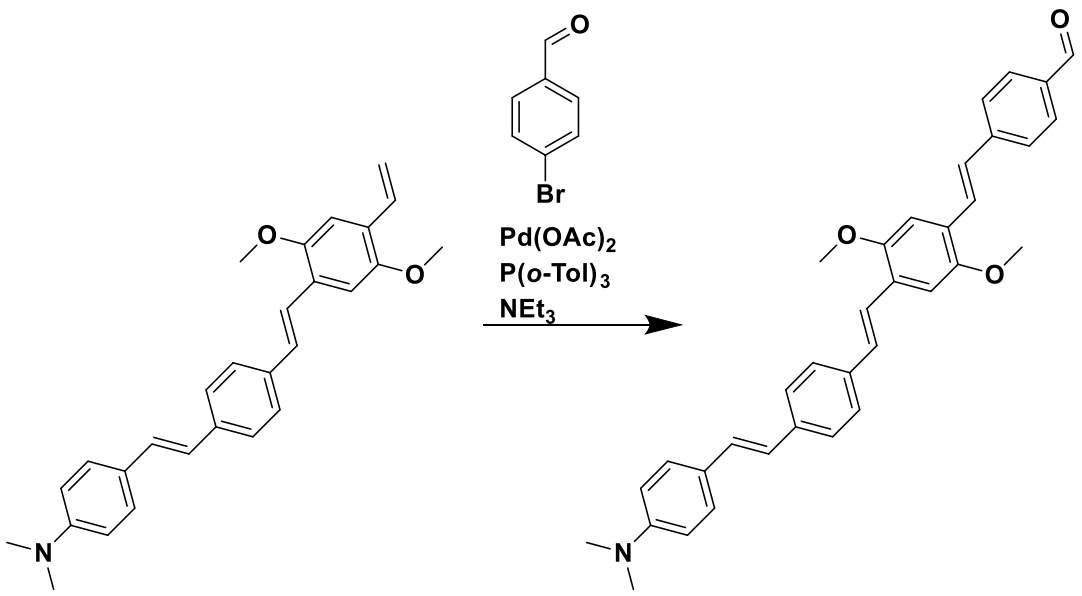

Synthesis of 4-((E)-4-((E)-4-((E)-4-(dimethylamino)styryl)styryl)-2,5-dimethoxystyryl)benzaldehyde

An oven-dried 10 mL round bottom flask was equipped with a stir bar and charged 4-((E)-4-((E)-2,5-dimethoxy-4-vinylstyryl)styryl)-N,N-dimethylaniline (20 mg, 0.05 mmol, 1.0 equiv.), $Pd(OAc)_2$ (1 mg, 0.0045 mmol,), tri-*o*-tolylphosphine (3 mg, 0.01 mmol,), and 4-bromo-benzaldehyde (9 mg, 0.045 mmol, 1.00 equiv.). The flask was evacuated and backfilled three times with N_2. Triethylamine (0.200 mL) and DMF (0.5 mL) were added and the round bottom was sealed and heated at 110°C. After stirring 20 hours, the reaction vessel was full of bright orange solid and was cooled to room temperature. The solid was dissolved in a large amount of methylene chloride and washed with saturated ammonium chloride twice. The organic portions were then collected and washed with saturated NaCl. The organic portions were dried over Na_2SO_4, filtered, and concentrated under reduced pressure. The orange solid was taken up in methylene chloride and precipitated by addition of hexanes. The resulting solid was filtered and dried. ^{1}H NMR (300 MHz, CHLOROFORM-*d*) δ ppm 3.00 (s, 6 H) 3.90 (s, 6 H) 5.29 (d, *J*=10.73 Hz, 1 H) 5.76 (d, *J*=16.23

Hz, 1 H) 6.73 (d, *J*=8.53 Hz, 2 H) 6.92 (d, *J*=15.95 Hz, 1 H) 7.01 - 7.21 (m, 6 H) 7.40 - 7.56 (m, 9 H) 7.71 (d, *J*=6.05 Hz, 1 H) 7.88 (d, *J*=8.25 Hz, 1 H) 10.00 (s, 1 H)

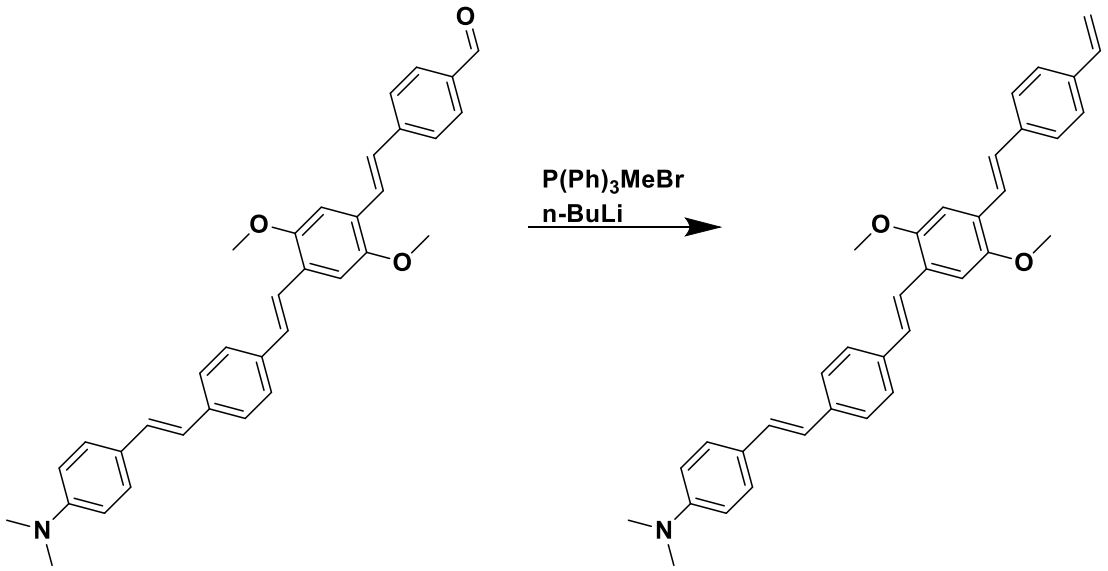

Synthesis of 4-((E)-4-((E)-2,5-dimethoxy-4-((E)-4-vinylstyryl)styryl)styryl)-N,N-dimethylaniline

An oven-dried 25 mL round bottom flask was charged with methyltriphenylphosphonium bromide (0.063 g, 0.175 mmol, 1.8 equiv.) and 10 mL anhydrous THF and stirred under N_2. A 1.6 M solution of *n*-butyllithium in hexanes was added via syringe (0.1 mL, 0.16 mmol, 1.6 equiv.) at -78°C to give a yellow solution. After warming to room temperature and stirring for 2 hr, 4-((E)-4-((E)-4-((E)-4-(dimethylamino)styryl)styryl)-2,5-dimethoxystyryl)benzaldehyde (50 mg, 0.097 mmol, 1.0 equiv.) in 20 mL methylene chloride was added. After stirring overnight, the reaction was added to 20 mL of hexanes. The suspension was filtered through celite to give a yellow solution concentrated under vacuum to dryness. The resulting solid was taken up in methylene chloride and purified by flash chromatography in methylene chloride. The resulting solid was further purified by semi-preparative HPLC on a Luna C_{18} column with a gradient of 10% MeCN I H_2O with 0.05% TFA ramping to 100% MeCN in 20 minutes and holding at 100% MeCN for 10 miutes. ^{1}H NMR (400 MHz, CHLOROFORM-*d*) δ ppm 3.00 (s, 6 H) 3.91 (s, 6 H) 5.31 (d, *J*=11.36 Hz, 1 H) 5.78 (d,

J=17.96 Hz, 1 H) 6.74 (d, *J*=8.80 Hz, 2 H) 6.93 (d, *J*=16.13 Hz, 1 H) 7.04 - 7.14 (m, 7 H) 7.41 - 7.55 (m, 11 H)

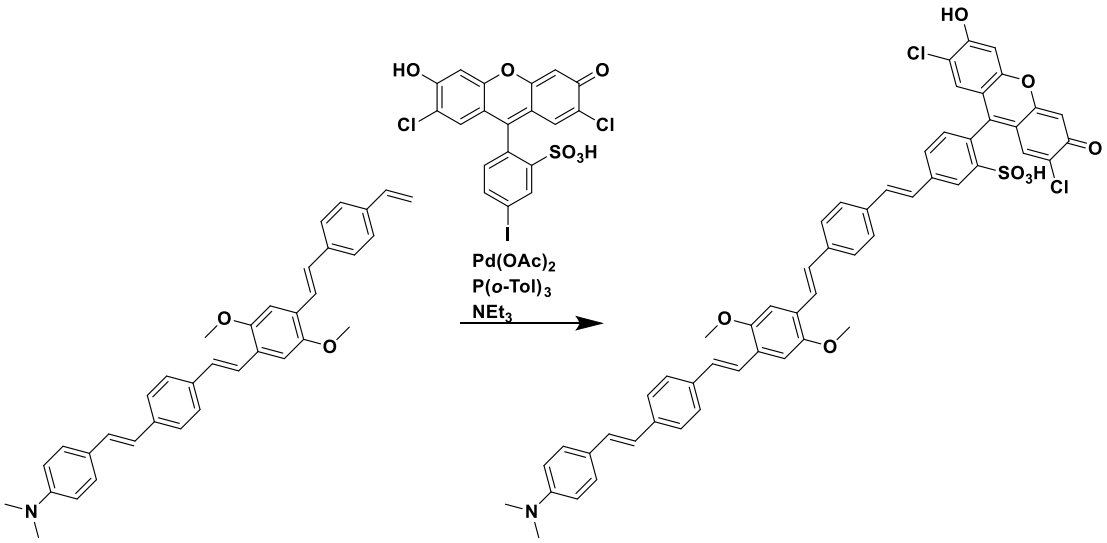

Synthesis of VF4.1.Cl

An oven-dried 10 mL round bottom flask was equipped with a stir bar and charged with 4-((E)-4-((E)-2,5-dimethoxy-4-((E)-4-vinylstyryl)styryl)styryl)-N,N-dimethylaniline (5 mg, 10 μmol, 1 equiv.), $Pd(OAc)_2$ (1 mg, 4.4 μmol.), tri-*o*-tolylphosphine (3 mg, 10 μmol.), and 2-(2,7-dichloro-6-hydroxy-3-oxo-3H-xanthen-9-yl)-5-iodobenzenesulfonic acid (5.5 mg, 10 μmol, 1 eq.). The flask was evacuated and backfilled three times with N_2. Triethylamine (20 μL) and DMF (200 μL) was added, the round bottom sealed, and heated at 110°C. After stirring 20 hours the vessel was cooled to room temperature, and concentrated to dryness. The brown solid was then taken up in DMF and minimal acetic acid for purification by preparative HPLC on a Luna C_{18} column with a gradient of 10% MeCN I H_2O with 0.05% TFA ramping to 90% MeCN in 20 minutes. The resulting material was concentrated to dryness to give approximately 1 mg of a dark brown solid. HPLC-MS found $[M^+]$ = 948.0

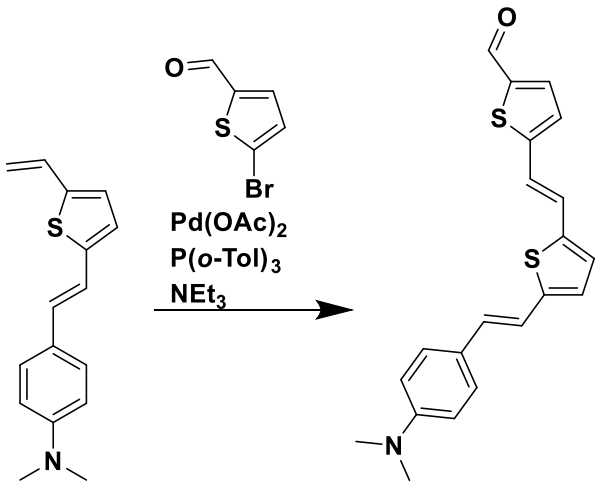

Synthesis of 5-((E)-2-(5-((E)-4-(dimethylamino)styryl)thiophen-2-yl)vinyl)thiophene-2-carbaldehyde

An oven-dried 10 mL round bottom flask was equipped with a stir bar and charged 5-((E)-2-(5-((E)-4-(dimethylamino)styryl)thiophen-2-yl)vinyl)thiophene-2-carbaldehyde (70 mg, 0.275 mmol, 1.0 equiv.), $Pd(OAc)_2$ (6.4 mg, 0.028 mmol,), tri-*o*-tolylphosphine (17 mg, 0.055 mmol,), and 5-bromothiophene-2-carbaldehyde (0.33 mL, 27.5 mmol, 1.00 equiv.). The flask was evacuated and backfilled three times with N_2. Triethylamine (1.0 mL) was added and the round bottom was sealed and heated at 110°C. After stirring 20 hours, the reaction vessel was full of bright orange solid and was cooled to room temperature. The solid was dissolved in methylene chloride and washed with saturated ammonium chloride twice. The organic portions were then collected and washed with saturated NaCl. The organic portions were dried over Na_2SO_4, filtered, and concentrated under reduced pressure. The orange solid was taken up in methylene chloride and precipitated by addition of hexanes. The resulting solid was filtered and dried to give 0.1g (~100%). ^{1}H NMR (400 MHz, CHLOROFORM-*d*) δ ppm 3.00 (s, 6 H) 6.71 (d, *J*=8.80 Hz, 2 H) 6.86 - 6.93 (m, 4 H) 6.97 (d, *J*=4.03 Hz, 1 H) 7.02 (d, *J*=3.30 Hz, 1 H) 7.10 (d, *J*=4.03 Hz, 1 H) 7.37 (d, *J*=8.80 Hz, 2 H) 7.65 (d, *J*=4.03 Hz, 1 H) 9.84 (s, 1 H)

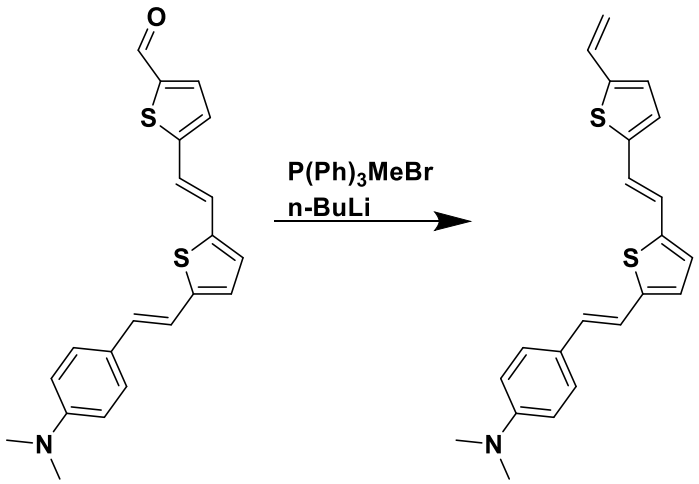

Synthesis of 4-((E)-4-((E)-2,5-dimethoxy-4-((E)-4-vinylstyryl)styryl)styryl)-N,N-dimethylaniline An oven-dried 25 mL round bottom flask was charged with methyltriphenylphosphonium bromide (0.175 g, 0.5 mmol, 1.8 equiv.) and 5 mL anhydrous THF and stirred under N_2. A 1.6 M solution of *n*-butyllithium in hexanes was added via syringe (0.27 mL, 0.44 mmol, 1.6 equiv.) at -78°C to give a yellow solution. After warming to room temperature and stirring for 1 hr., 5-((E)-2-(5-((E)-4-(dimethylamino)styryl)thiophen-2-yl)vinyl)thiophene-2-carbaldehyde (100 mg, 0.274 mmol, 1.0 equiv.) was added. After stirring overnight, the reaction was added to 30 mL of hexanes. The suspension was filtered through celite to give a yellow solution concentrated under vacuum to dryness. The resulting orange powder was judged pure yielding 30 mg (30%) ^{1}H NMR (400 MHz, CHLOROFORM-*d*) δ ppm 3.00 (s, 6 H) 5.15 (d, *J*=11.00 Hz, 1 H) 5.54 (d, *J*=17.23 Hz, 1 H) 6.68 - 6.98 (m, 5 H) 7.37 (d, *J*=8.80 Hz, 2 H) 7.45 - 7.50 (m, 2 H) 7.53 - 7.59 (m, 2 H) 7.65 - 7.71 (m, 2 H)

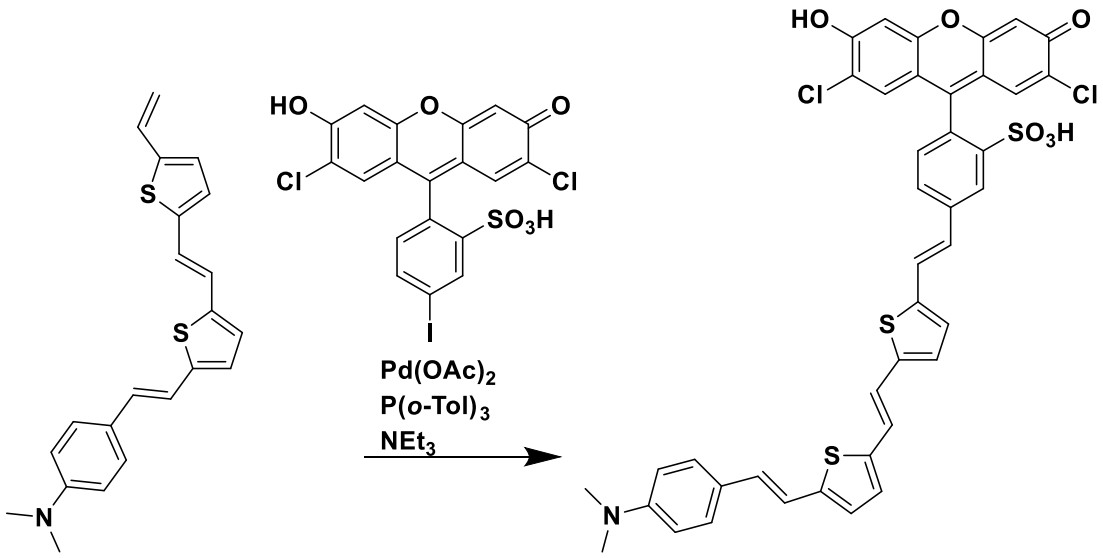

Synthesis of VF3Tp.1.Cl

An oven-dried 10 mL round bottom flask was equipped with a stir bar and charged with 4-((E)-4-((E)-2,5-dimethoxy-4-((E)-4-vinylstyryl)styryl)styryl)-N,N-dimethylaniline (8 mg, 22 μmol, 1 equiv.), $Pd(OAc)_2$ (1 mg, 4.4 μmol.), tri-*o*-tolylphosphine (3 mg, 10 μmol.), and 2-(2,7-dichloro-6-hydroxy-3-oxo-3H-xanthen-9-yl)-5-iodobenzenesulfonic acid (12 mg, 22 μmol, 1 eq.). The flask was evacuated and backfilled three times with N_2. Triethylamine (500 μL) and DMF (1 mL) was added, the round bottom sealed, and heated at 110°C. After stirring 20 hours the vessel was cooled to room temperature, and concentrated to dryness. The brown solid was then taken up in methylene chloride (2 mL), methanol (0.5 mL), and acetic acid (0.05 mL) and filtered through celite. The solution was then concentrated to dryness under vacuum and taken up in minimal methylene chloride. This solution was precipitated upon addition of hexanes and filtered through celite again. After concentrating to dryness under vacuum the red solid was taken up in 1:1 dimethysulfoxide and acetic acid for purification by preparative HPLC on a Luna C_{18} column with a gradient of 50% MeCN in H_2O with 0.05% TFA ramping to 100% MeCN in 20 minutes. The resulting material

was concentrated to dryness to give approximately 1 mg of a dark brown solid. HPLC-MS found $[M^+]$ = 798.0 $[M^{2+}]$ = 400.5

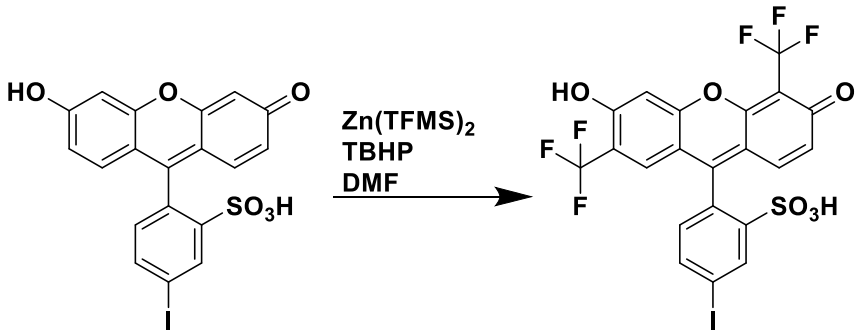

Synthesis of 2-(6-hydroxy-3-oxo-4,7-bis(trifluoromethyl)-3H-xanthen-9-yl)-5-iodobenzenesulfonic acid

An oven dried 25 mL round bottom flask was charged with 2-(6-hydroxy-3-oxo-3H-xanthen-9-yl)-5-iodobenzenesulfonic acid (10 mg, 0.022 mmol, 1 eq.) , dimethyl formamide (1 mL), and Zinc Trifluoromethyl Sulfinate (22 mg, 0.067 mmol, 3 eq.). The flask was cooled to 0°C and tert-butyl hydrogen peroxide was added (15 μL mg, 0.112 mmol, 5 eq. The reaction mixture was warmed to 50°C and stirred overnight. After filtering and concentrating to dryness under vacuum the brown solid was taken up in 1:1 DMF and acetic acid for purification by preparative HPLC on a Luna C_{18} column with a gradient of 10% MeCN in H_2O with 0.05% TFA ramping to 90% MeCN in 20 minutes. The resulting material was concentrated to dryness. ^{1}H NMR (400 MHz, DMSO-d_6) δ ppm 6.89 (d, *J*=8.80 Hz, 1 H) 6.96 (d, *J*=5.13 Hz, 1 H) 6.99 (s, 1 H) 7.26 (d, *J*=7.70 Hz, 1 H) 7.27 (s, 1 H) 7.56 (d, *J*=7.33 Hz, 1 H) 7.96 (s, 1 H)

^{19}F NMR (376 MHz, DMSO-d_6) δ ppm -67.26 (s, 3 F) -59.12 (s, 3 F)

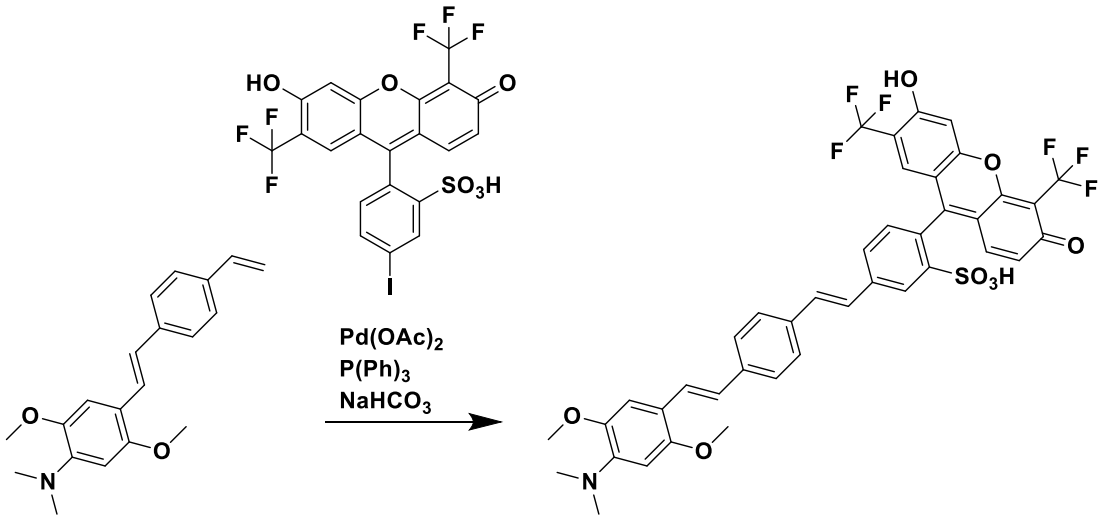

Synthesis of VF2.1diOMe.TFM

An oven dried 5 mL round bottom flask was charged with 2-(6-hydroxy-3-oxo-4,7-bis(trifluoromethyl)-3H-xanthen-9-yl)-5-iodobenzenesulfonic acid (1.26mg, 0.002 mmol, 1 eq.), (E)-2,5-dimethoxy-N,N-dimethyl-4-(4-vinylstyryl)aniline (0.62 mg.0.002 mmol, 1 eq.), palladium acetate (0.5 mg, 0.002 mmol, 1 eq.), triphenylphosphine (1.75 mg, 0.006 mmol, 3.3 eq.), and sodium bicarbonate (o.5 mg, 0.006 mmol, 3 eq.). The reaction vessel was sealed and put under nitrogen with dimethyl formamide (0.5 mL). It was then heated to 50^{o}C and stirred for 2 hours. The reaction was cooled to room temperature and concentrated under vacuum. The solid was then taken up as a slurry methylene chloride and centrifuged. The supernatant was discarded and the pellet was redissolved in water as a slurry again and centrifuged. The supernatant was again discarded and the pellet was judged to be pure product. HPLC-MS found [M^{+}] = 812.5

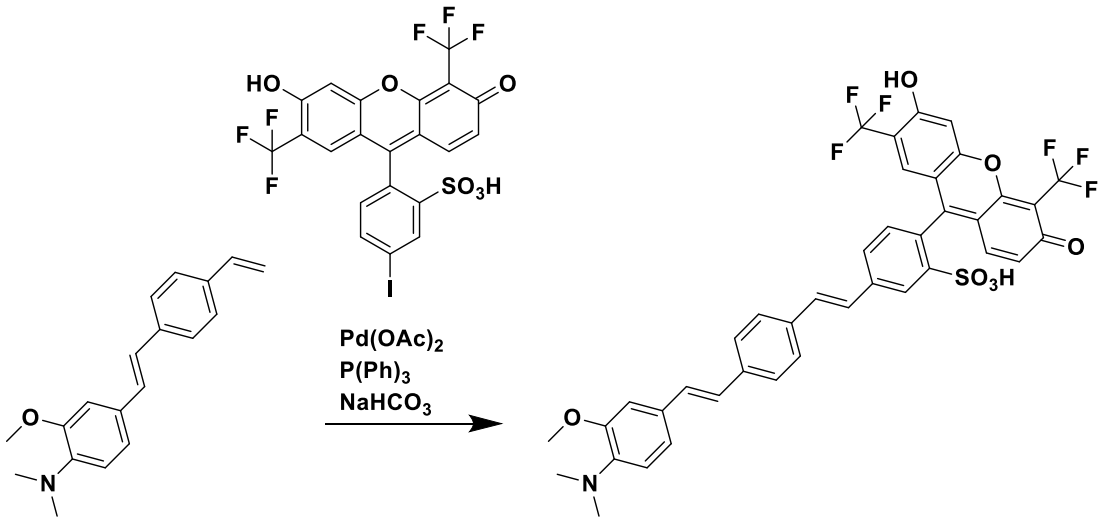

Synthesis of VF2.1OMe.TFM

An oven dried 5 mL round bottom flask was charged with 2-(6-hydroxy-3-oxo-4,7-bis(trifluoromethyl)-3H-xanthen-9-yl)-5-iodobenzenesulfonic acid (2.3 mg, 0.0036 mmol, 1 eq.), (E)-2-methoxy-N,N-dimethyl-4-(4-vinylstyryl)aniline (1 mg.0.0036 mmol, 1 eq.), palladium acetate (0.8 mg, 0.0035 mmol, 1.1 eq.), triphenylphosphine (3 mg, 0.012 mmol, 3.3 eq.), and sodium bicarbonate (0.9 mg, 0.011 mmol, 3 eq.). The reaction vessel was sealed and put under nitrogen with dimethyl formamide (1 mL). It was then heated to 50^{o}C and stirred overnight. The reaction was cooled to room temperature and concentrated under vacuum. The solid was then taken up as a slurry methylene chloride and centrifuged. The supernatant was discarded and the pellet was redissolved in water as a slurry again and centrifuged. The supernatant was again discarded and the pellet was taken up in dimethyl sulfoxide for purification bysemi- preparative HPLC on a Luna C_{18} column with a gradient of 60% MeCN in H_2O with 0.05% TFA ramping to 100% MeCN in 20 minutes. The resulting material was concentrated to dryness. HPLC-MS found [M^+] = 782.6

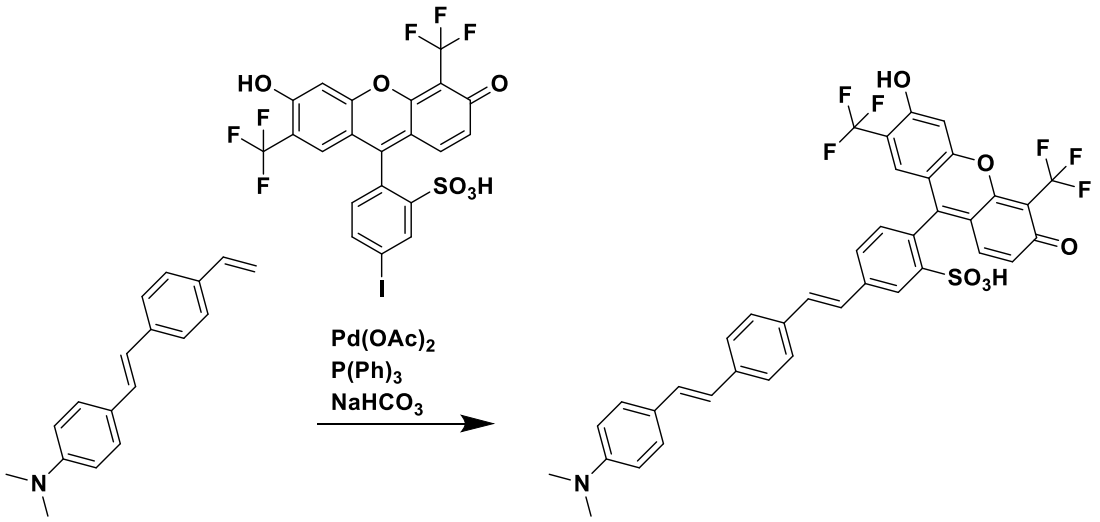

Synthesis of VF2.1.TFM

An oven dried 5 mL round bottom flask was charged with 2-(6-hydroxy-3-oxo-4,7-bis(trifluoromethyl)-3H-xanthen-9-yl)-5-iodobenzenesulfonic acid (2.5 mg, 0.004 mmol, 1 eq.), (E)-N,N-dimethyl-4-(4-vinylstyryl)aniline (1 mg.0.004 mmol, 1 eq.), palladium acetate (1 mg, 0.004 mmol, 1 eq.), triphenylphosphine (3.5 mg, 0.013 mmol, 3.3 eq.), and sodium bicarbonate (1 mg, 0.012 mmol, 3 eq.). The reaction vessel was sealed and put under nitrogen with dimethyl formamide (1 mL). It was then heated to 50^{o}C and stirred overnight. The reaction was cooled to room temperature and concentrated under vacuum. The solid was then taken up as a slurry methylene chloride and centrifuged. The supernatant was discarded and the pellet was redissolved in water as a slurry again and centrifuged. The supernatant was again discarded and the pellet was taken up in dimethyl sulfoxide for purification by semi- preparative HPLC on a Luna C_{18} column with a gradient of 60% MeCN in H_2O with 0.05% TFA ramping to 100% MeCN in 20 minutes. The resulting material was concentrated to dryness. HPLC-MS found [M^+] = 752.3

It was then taken up in dimethyl formamide and acetic acid for purification by preparative HPLC on a Luna C_{18} column with a gradient of pH 7, 10% 1M triethylammonium acetate in H_2O ramping to 90% MeCN in 20 minutes.

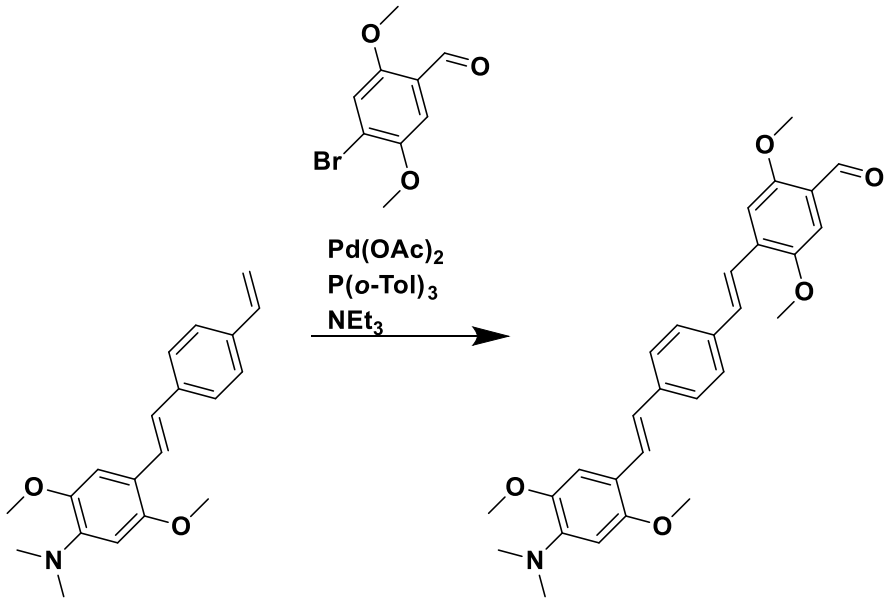

Synthesis of 4-((E)-4-((E)-4-(dimethylamino)-2,5-dimethoxystyryl)styryl)-2,5-dimethoxybenzaldehyde

An oven-dried 10 mL round bottom flask was equipped with a stir bar and charged (E)-2,5-dimethoxy-N,N-dimethyl-4-(4-vinylstyryl)aniline (100 mg, 0.324 mmol, 1.0 equiv.), palladium acetate (1 mg, 0.0044 mmol,), tri-*o*-tolylphosphine (4 mg, 0.013 mmol,), and 4-bromo-2,5-dimethoxybenzaldehyde (80 mg, 0.324 mmol, 1.00 equiv.). The flask was evacuated and backfilled three times with N_2. Triethylamine (0.25 mL) was added and the round bottom was sealed and heated at 110°C. After stirring 20 hours, the reaction vessel was full of bright orange solid and was cooled to room temperature. The solid was dissolved in methylene chloride and washed with saturated ammonium chloride twice. The organic portions were then collected and washed with saturated NaCl. The organic portions were dried over Na_2SO_4, filtered, and concentrated under reduced pressure. The orange solid was taken up in methylene chloride and precipitated by addition

of hexanes. The resulting solid was filtered and dried. ^{1}H NMR (400 MHz, CHLOROFORM-*d*) δ ppm 2.89 (br. s., 6 H) 3.90 (br. s., 3 H) 3.95 (br. s., 3 H) 7.02 (d, *J*=15.40 Hz, 1 H) 7.16 (d, *J*=17.23 Hz, 2 H) 7.44 - 7.59 (m, 5 H) 7.67 (d, *J*=7.70 Hz, 2 H) 7.88 (d, *J*=7.70 Hz, 2 H) 10.00 (s, 1 H)

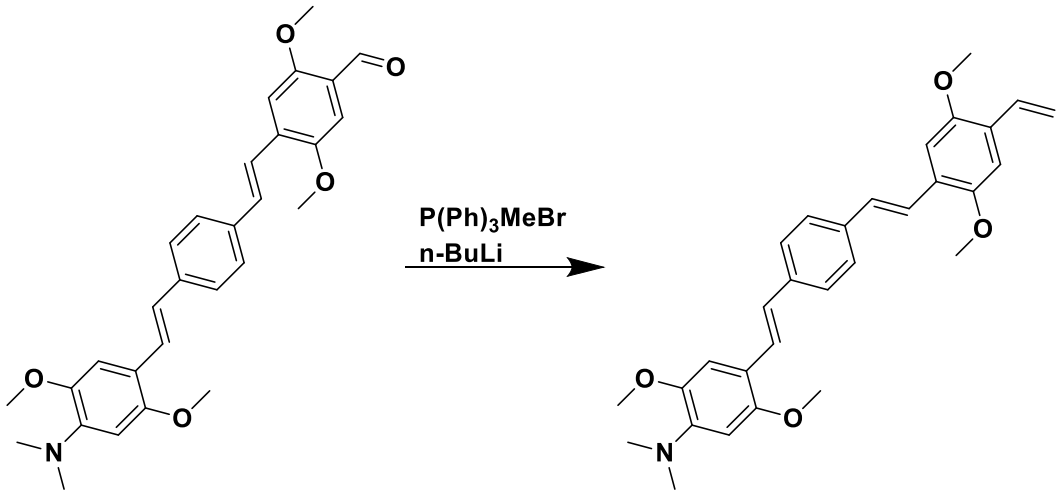

Synthesis of 4-((E)-4-((E)-2,5-dimethoxy-4-vinylstyryl)styryl)-2,5-dimethoxy-N,N-dimethylaniline

An oven-dried 105 mL round bottom flask was charged with methyltriphenylphosphonium bromide (0.065 g, 0.13 mmol, 1.8 equiv.) and25 mL anhydrous THF and stirred under N_2. A 1.6 M solution of *n*-butyllithium in hexanes was added via syringe (0.1 mL, 0.115 mmol, 1.6 equiv.) at -78^{o}C to give a yellow solution. After warming to room temperature and stirring for 1 hr., 4-((E)-4-((E)-4-(dimethylamino)-2,5-dimethoxystyryl)styryl)-2,5-dimethoxybenzaldehyde (34 mg, 0.072 mmol, 1.0 equiv.) was added. After stirring overnight, the reaction was added to 10 mL of hexanes. The suspension was filtered through celite to give a yellow solution concentrated under vacuum to dryness. The resulting product was not further purified. ^{1}H NMR (400 MHz, CHLOROFORM-*d*) δ ppm 2.88 (s, 6 H) 3.90 (s, 3 H) 3.94 (s, 3 H) 3.98 (s, 1 H) 5.29 (d, *J*=10.63 Hz, 1 H) 5.76 (d, *J*=17.60 Hz, 1 H) 6.95 - 7.16 (m, 3 H) 7.21 (s, 1 H) 7.35 (s, 1 H) 7.42 - 7.60 (m, 5 H) 7.63 - 7.78 (m, 3 H)

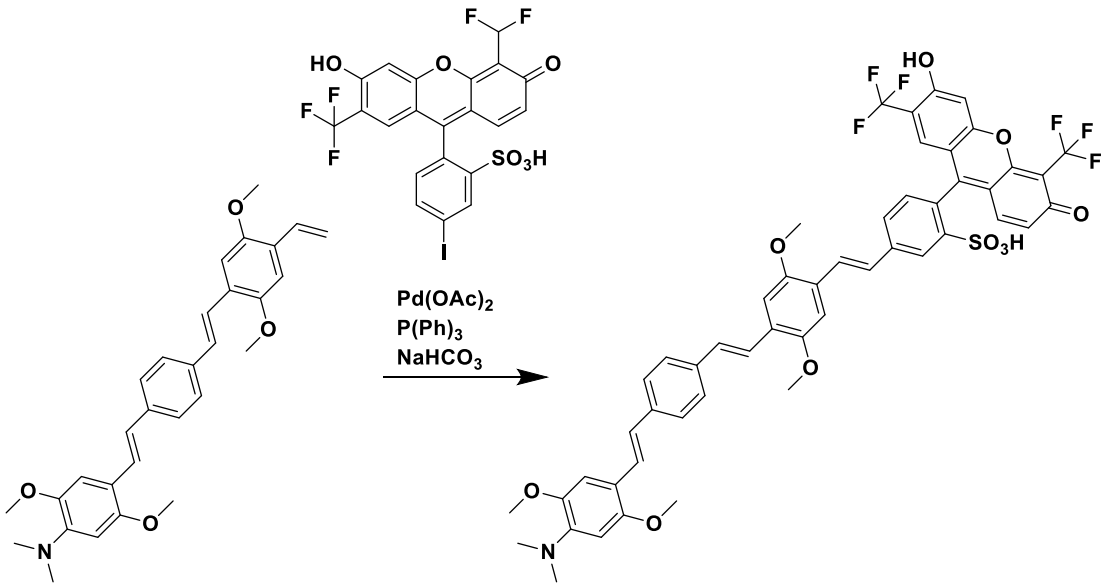

Synthesis of VF3.1diOMe.TFM

An oven dried 5 mL round bottom flask was charged with 2-(6-hydroxy-3-oxo-4,7-bis(trifluoromethyl)-3H-xanthen-9-yl)-5-iodobenzenesulfonic acid (6.3 mg, 0.01 mmol, 1 eq.), 4-((E)-4-((E)-2,5-dimethoxy-4-vinylstyryl)styryl)-2,5-dimethoxy-N,N-dimethylaniline (5 mg.0.01 mmol, 1 eq.), palladium acetate (1 mg, 0.004 mmol), triphenylphosphine (4 mg, 0.015 mmol.), and sodium bicarbonate (1 mg, 0.012 mmol.). The reaction vessel was sealed and put under nitrogen with dimethyl formamide (1 mL). It was then heated to 50^{o}C and stirred overnight. The reaction was cooled to room temperature and concentrated under vacuum. The solid was then taken up as a slurry methylene chloride and centrifuged. The supernatant was discarded and the pellet was redissolved in water as a slurry again and centrifuged. The supernatant was again discarded and the pellet was taken up in dimethyl sulfoxide for purification bysemi- preparative HPLC on a Luna C_{18} column with a gradient of 60% MeCN in H_2O with 0.05% TFA ramping to 100% MeCN in 20 minutes. The resulting material was concentrated to dryness. HPLC-MS found [M^+] = 975.6

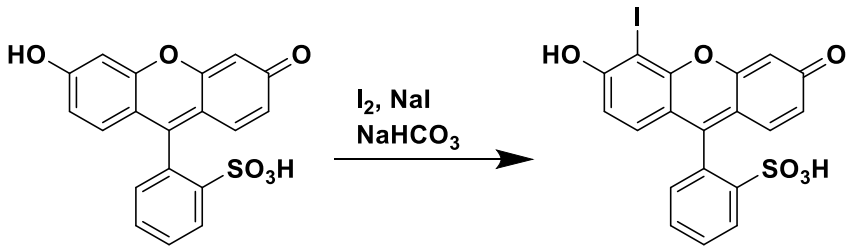

Synthesis of 2-(6-hydroxy-5-iodo-3-oxo-3H-xanthen-9-yl)-5-iodobenzenesulfonic acid

An oven dried round bottom flask was charged with sulfonfluorescein (200 mg, 0.543 mmol, 1 eq.), iodine (138 mg, 0.543 mmol, 1 eq.), and sodium iodide (136 mg, 0.91 mmol, 1.67 eq.) and stirred at room temperature overnight giving a range of iodine substituted products by HPLC-MS. Product was purified by preparative HPLC on a Luna C_{18} column with a gradient of 10% MeCN in H_2O with 0.05% TFA ramping to 90% MeCN in 20 minutes. The resulting material was concentrated to dryness. ^{1}H NMR (300 MHz, DMSO-d_6) δ ppm 5.43 (d, *J*=5.23 Hz, 1 H) 6.54 (d, *J*=9.63 Hz, 1 H) 6.77 - 7.01 (m, 3 H) 7.19 (d, *J*=6.33 Hz, 1 H) 7.45 - 7.63 (m, 2 H) 7.95 (d, *J*=8.80 Hz, 1 H)

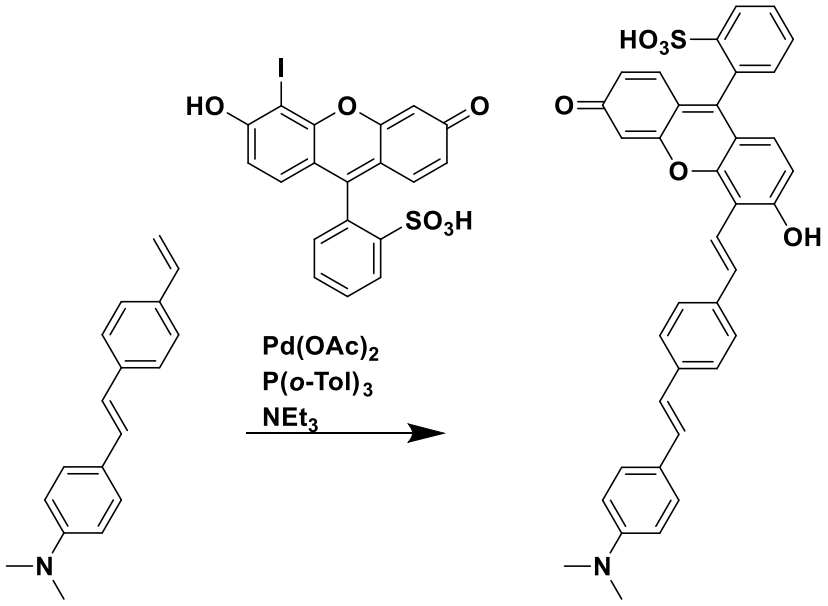

Synthesis of 2-(5-((E)-4-((E)-4-(dimethylamino)styryl)styryl)-6-hydroxy-3-oxo-3H-xanthen-9-yl)benzenesulfonic acid

An oven-dried 10 mL round bottom flask was equipped with a stir bar and charged (E)-N,N-dimethyl-4-(4-vinylstyryl)aniline (1 mg, 0.004 mmol, 1.0 equiv.), palladium acetate (1 mg, 0.0044 mmol,), tri-*o*-tolylphosphine (3 mg, 0.01 mmol,), and 2-(6-hydroxy-5-iodo-3-oxo-3H-xanthen-9-yl)-5-iodobenzenesulfonic acid (2 mg, 0.004 mmol, 1.00 equiv.). The flask was evacuated and backfilled three times with N_2. Triethylamine (0.005 mL)and DMF (0.5 mL) was added and the round bottom was sealed and heated at 110°C. After stirring 20 hours, the reaction vessel was cooled to room temperature and concentrated to dryness under vacuum. The solid was dissolved in methylene chloride with 5% methanol and purified by preparative HPLC on a Luna C_{18} column with a gradient of 10% MeCN in H_2O with 0.05% TFA ramping to 90% MeCN in 20 minutes. The resulting material was concentrated to dryness. HPLC-MS found $[M^-] = 614.2$

3.4 Discussion

Improving electron transfer through new types of molecular bridges, longer distance electron transfer, increased driving force, and novel orientations were met with varying degrees of success. Thiophene dyes in particular appeared to offer improved levels of electron transfer that lead to more sensitive dyes, but none above VF2.1OMe.H from chapter 2. The unique electron transfer characteristics of thiophene bridges could certainly prove useful for future iterations of VF dyes. This work also represents the successful application of optoelectronic principles toward improved VF dye synthesis. Beyond the successful implementation of thiophene bridges in VF dyes, one obvious improvement not yet explored are rigidized thiophene bridges. Limiting the degrees of freedom locks molecular bridges in favorable conformations for electron transfer that could further enhance efficient electron transfer.[17] Thiophenes are also 5-membered rings rather than the 6-membered benzene rings employed in earlier iterations. Unlike phenyl bridges, thiophene bridges are not bilaterally symmetrical, which puts a kink in the thiophene bridge that limits the amount of the electric field electron transfer passes through. It also puts electron transfer

at an angle rather than directly parallel to the electric field which should reduce sensitivity. Rigidization of thiophene bridges should alleviate both of these potential issues as well.

Development of longer bridges in VF dyes has thus far been far less fruitful. Given the voltage sensing mechanism, longer dyes represent one of the most promising approaches toward more sensitive dyes. However, this is in direct opposition to the challenge of facilitating electron transfer over longer distances via an electron hopping mechanism. Effective membrane staining of HEK cells is another added challenge given the large hydrophobic bridge found in longer dyes that may promote aggregation. It appears the current efforts to lengthen bridges by changing to a thiophene-based system or increasing the driving force for electron transfer with very electron poor acceptors is not a viable option given the current attempts. Practically speaking, longer dyes add significant synthetic challenges as well that make generating larger libraries of compounds challenging. One potential move forward is in silico design of dyes with desirable electronic characteristics to further guide rational design.

It is clear the bridge acts as much more than a lipophilic spacer given the results observed in this chapter. Physical, chemical, and biological considerations ranging from electronic structure to reactivity and cellular compatibility all appear to play a role in developing an ideal bridge for voltage sensing. A huge variety of moieties may be interrogated toward improved VF dyes and a combination of borrowing innovations from other fields such as optoelectronics, experimental efforts, and computational studies should all push development further. The improved sensitivity promised by longer bridges is too tempting a goal to abandon.

3.5 Bibliography

1. Marcus, R. A. On the Theory of Oxidation-Reduction Reactions Involving Electron Transfer. I. *J. Chem. Phys.* **24,** 966 (1956).

2. Marcus, R. A. Electrostatic Free Energy and Other Properties of States Having Nonequilibrium Polarization. I. *J. Chem. Phys.* **24,** 979 (1956).

3. Taube, H., Myers, H. & Rich, R. L. OBSERVATIONS ON THE MECHANISM OF ELECTRON TRANSFER IN SOLUTION 1. *J. Am. Chem. Soc.* **75,** 4118–4119 (1953).

4. Aviram, A. & Ratner, M. A. Molecular rectifiers. *Chem. Phys. Lett.* **29,** 277–283 (1974).

5. MacDiarmid, A. G. 'Synthetic metals': A novel role for organic polymers (Nobel lecture). *Angew. Chemie - Int. Ed.* **40,** 2581–2590 (2001).

6. Blom, P. W. M., de Jong, M. J. M. & Vleggaar, J. J. M. Electron and hole transport in poly(p-phenylene vinylene) devices. *Appl. Phys. Lett.* **68,** 3308 (1996).

7. Sikes, H. D., Smalley, J. F., Dudek, S. P., Cook, A. R., Newton, M. D., Chidsey, C. E. D. & Feldberg, S. W. Rapid Electron Tunneling Through Oligophenylenevinylene Bridges. *Science (80-.).* **291,** 1519–1523 (2001).

8. Pourtois, G., Beljonne, D., Cornil, J., Ratner, M. a & Brédas, J. L. Photoinduced electron-transfer processes along molecular wires based on phenylenevinylene oligomers: a quantum-chemical insight. *J. Am. Chem. Soc.* **124,** 4436–47 (2002).

9. Jen, A. K.-Y., Rao, V. P., Wong, K. Y. & Drost, K. J. Functionalized thiophenes: second-order nonlinear optical materials. *J. Chem. Soc. Chem. Commun.* 90–92 (1993). doi:10.1039/C39930000090

10. Elandaloussi, E. H., Benahmed-gasmi, A., Riou, A., Gorgues, A. & Roncali, J. Oligo (furan-2,5-diylvinylene)s as pi-conjugating spacers in linearly extended hybrid tetrat hiafulvalene analogues. *J. Mater. Chem.* **6,** 1859–1863 (1996).

11. Boxer, S. G. Mechanisms of long-distance electron transfer in proteins: lessons from photosynthetic reaction centers. *Annu. Rev. Biophys. Biophys. Chem.* **19,** 267–99 (1990).

12. Gray, H. Long-Range Electron Tunneling. *J. Am. Chem. Soc.* (2014).

13. Giacalone, F., Segura, J. L., Martín, N. & Guldi, D. M. Exceptionally small attenuation factors in molecular wires. *J. Am. Chem. Soc.* **126,** 5340–1 (2004).

14. Marcus, R. A. & Sutin, N. Electron transfer in biology and chemistry_Marcus_Biochem Biophys Acta_1985.pdf. *Biochim. Biophys. Acta* **811,** 265–322 (1985).

15. Davis, W. B., Svec, W. A., Ratner, M. A. & Wasielewski, M. R. Molecular-wire behaviour in p-phenylenevinylene oligomers. *Nature* **396,** 60–63 (1998).

16. Fujiwara, Y., Dixon, J. a, O'Hara, F., Funder, E. D., Dixon, D. D., Rodriguez, R. a, Baxter, R. D., Herlé, B., Sach, N., Collins, M. R., Ishihara, Y. & Baran, P. S. Practical and innate carbon-hydrogen functionalization of heterocycles. *Nature* **492,** 95–9 (2012).

17. Roncali, J., Thobie-gautier, C., Elandaloussi, E. H. & Frke, P. Control of the Bandgap of Conducting Polymers by Rigidification of the Pi-Conjugated System. *J. Chem. Soc., Chem. Commun.* 2249–2250 (1994).

Chapter 4 Far Red Fluorescent VF Dyes

Toward Complex Biological Application

4.1 Introduction

Far field fluorescent imaging of probes within biological systems faces inherent challenges from the confounding optical characteristics of these systems. The absorbance, fluorescence, and scattering properties of molecules ubiquitous in nature interact with stimulating light to subtract, add, and blur recorded signal.[1] Given how precious every photon is to voltage imaging as discussed in chapter 1, overcoming the added background noise generated by biological system is paramount to an ideal voltage sensor applied to more complex preparations.

One potential option is to simply remove as much of the unnecessary biological milieu as possible without appreciably affecting the activity to be recorded. This presents a challenge of defining what affects the defined activity and what does not, which may not be a practical option in many instances. A significant amount of work towards this end has been done in the neurobiological community however. Tissue clearing methods like CLARITY, which removed highly scattering lipids from brain tissue while keeping the remaining structure intact, are an exciting approach toward higher resolution imaging of neuronal structure.[2] This particular approach is untenable in voltage imaging experiments for a number of reasons, especially the complete destruction of the membrane involved. Currently, no optical clearing approaches compatible with voltage imaging experiments are available, and this does not appear to be an active area of research - perhaps rightly so.

A second, far more studied approach toward reducing biological background noise is to develop a fluorescent probe that interacts with light orthogonally to the biological preparation. The absorbance and scattering of light is highly dependent on the wavelength of light used in fluorescence imaging. There is a notable "window" in the biological absorbance and scattering spectrum from 650 nm to 900 nm where light is less perturbed.[3] Developing a VF dye that absorbs and emits in this region represents a significant improvement, especially in the more complex preparations where voltage dyes hold the most promise.

Beyond simply representing a higher resolution approach for voltage imaging, far red fluorescent VF dyes can be coupled with other optical tools that utilize bluer portions of the visual spectrum for a broader range of experimental approaches. Two of the most promising compliments to voltage sensors are calcium sensors and optogenetic electrical activity manipulators like channelrhodopsin.[4,5] While red fluorescent calcium indicators have been developed, probes active in the blue region retain the most favorable characteristics in terms of kinetics and brightness.[6] Ideally, a red voltage sensor together with the best blue calcium sensor could report on activity of both signals in concurrent spatial and temporal regimes. However, given that serviceable red calcium sensors and blue voltage sensors exist, this would merely enhance the signal acquisition quality for some applications and open the opportunity for application in merely the most complicated preparations.

In contrast, a number of red optogenetic activators have been developed, but all of them retain activity throughout the visible spectrum into the blue, preventing the concurrent use of a blue voltage sensor.[7,8] There are however, optogenetic activators that retain activity solely in the blue region of the spectrum leaving open the opportunity for use of a red voltage sensor simultaneously.[9] This combination creates the possibility for all optical electrophysiology where light can be used to both stimulate and record activity, which obviates the need for any direct contact to the biological preparation with any electrodes. By using light

instead of electrodes, broad areas can be stimulated and recorded from across a field of view. All optical electrophysiology also provides greater spatial resolution by stimulating and recording specific regions inaccessible to electrodes while also opening up the ability to specifically probe subtypes of cells, specific regions, or cell types with a desired type of activity previously inaccessible.[10] These advantages have the potential to revolutionize electrophysiology, providing access to experimental questions previously unanswerable. Realizing this revolution however, requires a red voltage sensor capable of recording in these settings.

Voltage sensors that use a photoinduced electron transfer (PeT) mechanism to sense changes in membrane potential represent a promising approach toward developing a probe with far red fluorescence. PeT is a fundamental physical phenomenon that can be engineered in conjunction with any fluorophore, in principle.[11] While fluorescein represented an excellent starting point for VF dyes given their wide use as PeT based sensors of a multitude of other signals, recent work has focused on VF dyes with a Cy5 fluorophore towards far red fluorescent voltage sensing as seen in Figure 4.1.[12–15]

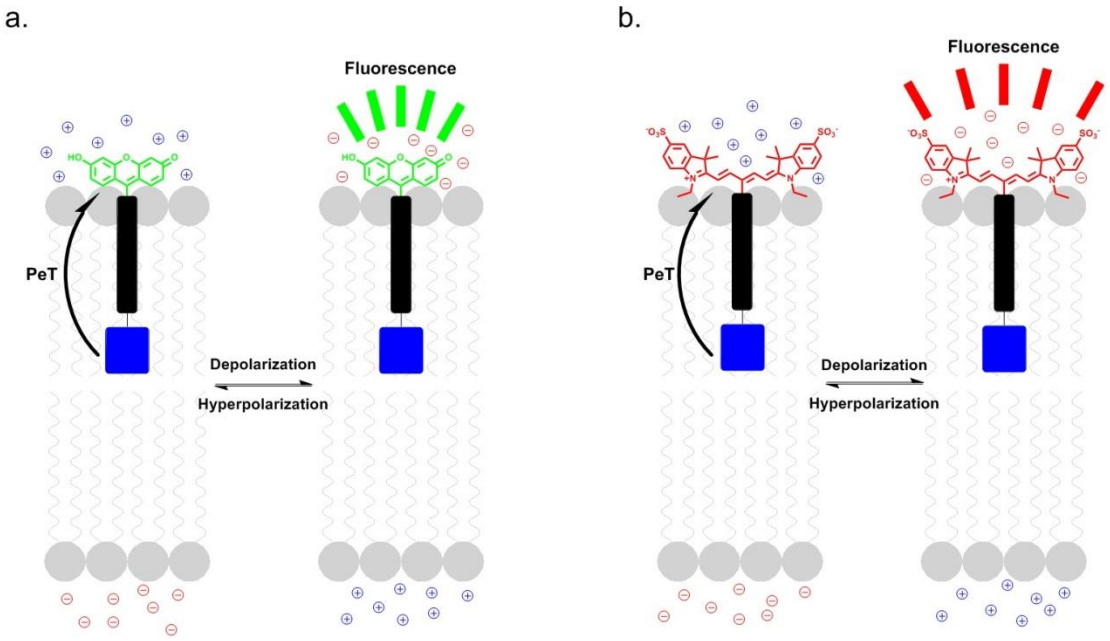

Figure 4.1 Expanded color palette of VF dyes containing a canonical electron donor in blue, electron bridge in black, and electron acceptor as either a fluorescein (a) or Cy5 (b). At hyperpolarized potentials both dyes realize an increased probability for PeT, while at depolarized potentials are more likely to fluoresce, either in the green (a) or red (b) portion of the spectrum.

Optimization of both bridges and donors increased voltage sensitivity in HEK cells from 1% to 25% ΔF/F per 100 mV in the best dye, termed VF Red. This new far red dye was then applied to cultured neurons toward imaging action potentials in single trials. Finally, all optical electrophysiology applications only possible with far red sensors such as VF Red were performed.

4.2 Results

The aniline electron donor and phenylene vinylene bridge have been shown to be capable moieties toward achieving sensitive VF dyes. These offered an excellent starting point in development of a far-red probe utilizing a Cy5 electron acceptor. There are a number of approaches that could potentially be used in coupling the phenylene vinylene bridge to the Cy5

fluorophore. As shown in Figure 3.13, the point at which the bridge is connected to the fluorophore can be quite important. Cy5 is an often used fluorescent handle with connection points off the indolium nitrogen and phenyl ring being the most popular. In contrast, the central polymethine groups are traditionally unaltered. For the purposed of a VF dye though, it was proposed that synthesizing a symmetrical molecule by attachment of the bridge to the central methane would be the best approach. The free energy for electron transfer in VF dyes is highly dependent upon the orientation of the dye in the membrane electric field, $\vec{E}$ as described by the equation $\Delta G = \Delta G_o - \Delta\vec{\mu} \cdot \vec{E}$ where ΔG represents the free energy for electron transfer. The charge transferred, given by $\Delta\vec{\mu}$, is a vector highly sensitive to the orientation of charge transfer relative to the membrane electric field. Aligning the dye parallel to the electric field increases the strength of this term essential for improving voltage sensitivity.

Synthesizing a symmetrical VF dye requires attachment of the phenylene vinylene bridge to the central methine of the Cy5 as seen in Figure 4.2. Synthesis of Cy5 was carried out using the traditional Fischer indole synthesis to generate **4.2**. Quaternzation via a SN2 reaction gave **4.3.** The final condensation reaction to generate the Cy5 derivative **4.4**, was performed with bromo-phenyl malondialdehyde rather than the typical unsubstituted dialdehyde to generate a suitable Heck coupling partner capable of coupling to a range of donor and bridges combinatorially.

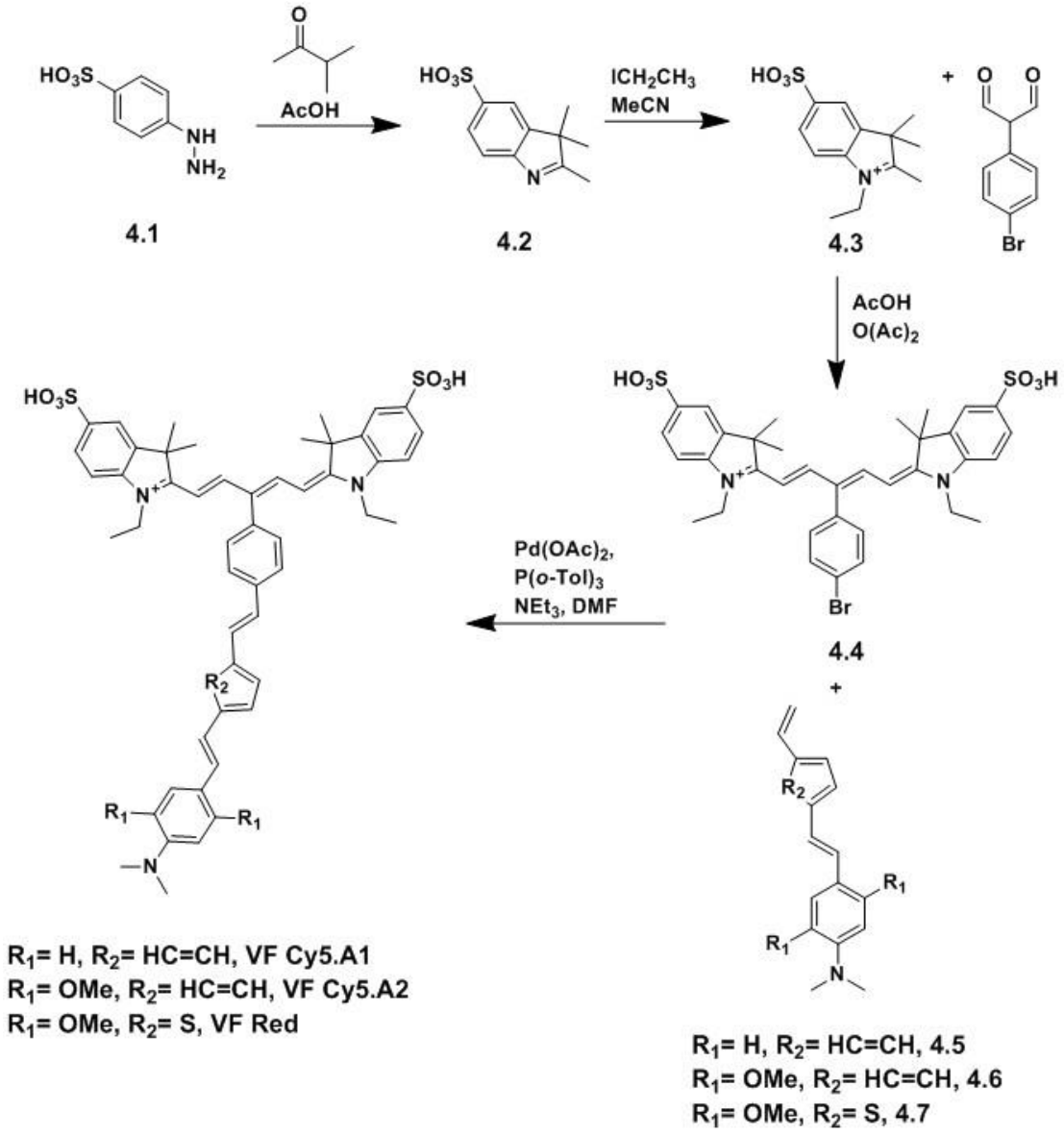

Figure 4.2 Synthetic scheme for Cy5-based VF dyes.

Upon synthesis and purification of VF dyes by HPLC, the first generation dyes did indeed retain the far red fluorescent characteristics of typical Cy5 dyes with absorbance and emission maxima at 649 nm and 670 nm respectively as seen in Figure 4.3a.[16] All three dyes were then incubated with HEK cells, washed, and imaged through wide field fluorescence microscopy. VFCy5.A1 appeared mainly localized to cell membranes evenly throughout the cell.

VFCy5.A2 appeared to be more punctate with some localization to endosomes or foci on the membrane. VF Red appeared similar to VFCy5.A2 showing some degree internalization and localization while retaining diffuse membrane staining to some extent as well. All three probes showed limited toxicity as HEK cells retained normal morphology and no indications of cell death upon visual inspection up to two hours after staining.

Voltage sensitivity in HEK cells was determined upon patch clamping cells stained as in Figure 4.3b. All three dyes showed varying degrees of voltage sensitivity. VFCy5.A1 showed minimal sensitivity with a 1% ΔF/F per 100 mV. Additionally, after recording voltage sensitivity over the wider ±300 mV, the trace appeared to be consistently slightly concave indicating that PeT was relatively weak and only began to have appreciable effects at the most negative potentials as discussed in chapter 2 more thoroughly. Upon this result, VFCy5.A2 was synthesized and tested. The larger driving force for PeT attributed to the electron rich dimethoxy substituted aniline donor resulted in a 10% ΔF/F per 100 mV, an order of magnitude more sensitive than VFCy5.A1. While VFCy5.A2 did show more appreciable sensitivity at physiologically relevant potentials, it still retained a concave shape indicating the inherent probability for PeT of the molecule was too low. Work discussed in chapter 3 described improved bridges with thiophenes instead of phenyl groups for greater conductivity. In an effort to improve PeT and thus, sensitivity, the central phenyl ring of VFCy5.A2 was replaced with a thiophene to give VF Red. This new dye with a still further increased probability to undergo PeT was tested for voltage sensitivity in HEK cells as shown in Figure 4.3c. VF Red showed a 25% ΔF/F per 100 mV, 2.5 times better than VFCy5.A2 and similar to VF2.1.Cl. The trace of VF Red had a distinct s-shape where the steepest, most sensitive portion was centered over the physiologically relevant range of ±100 mV, ideal for biological studies.

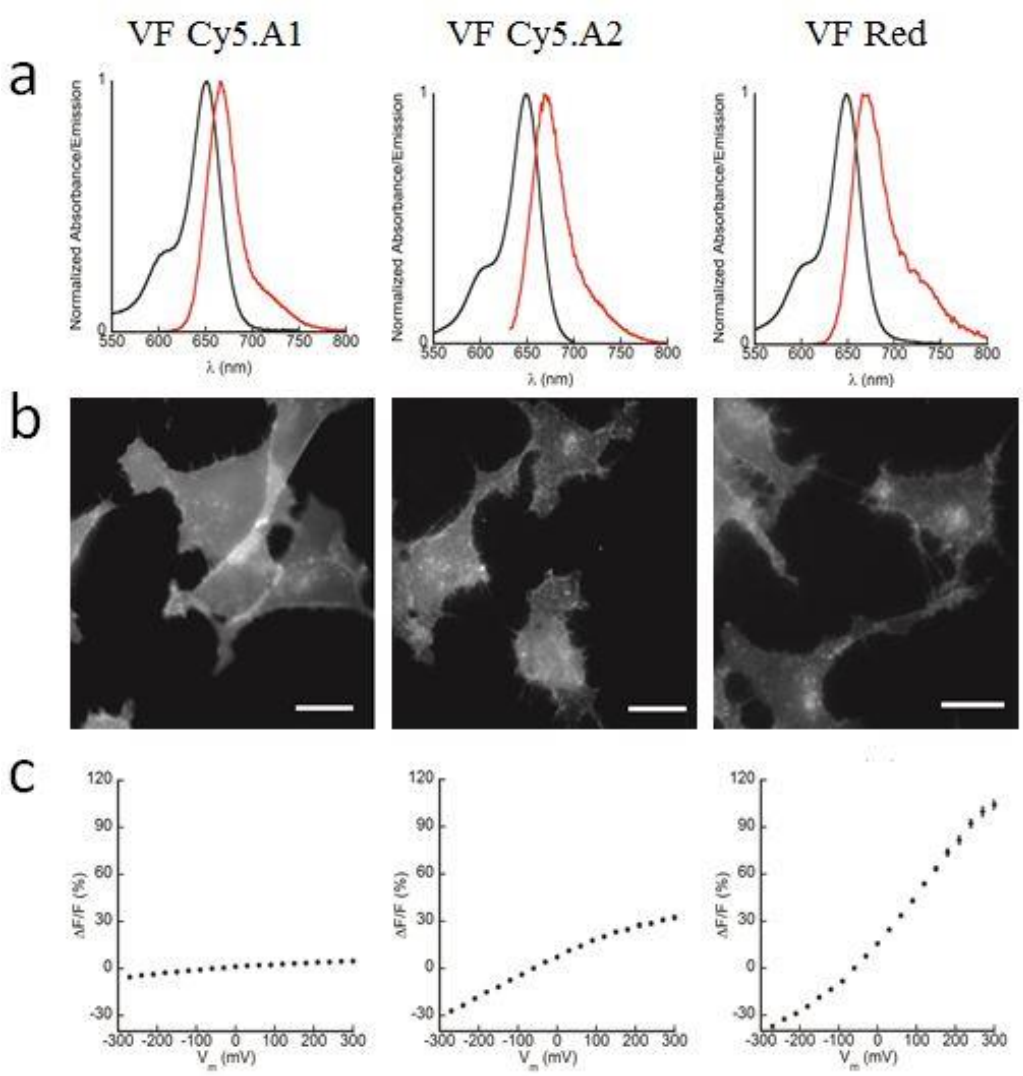

Figure 4.3 Characterization of rationally designed far-red VF dyes with improved donors and bridges. VF2.1.Cy5 is described in the first column, VF2.1diOMe.Cy5 in the middle column, and VF Red in the final colum. (a) The absorbance and emission profiles in MeOH. (b) HEK cells stained with 200 nM dye for 15 min. at 37ºC. Scale bars are 20 μm. (c) Fluorescence response of dyes vs. membrane potential. Voltage clamped HEK cells were held at -60 mV and then stepped to the indicated potential. The relative change in fluorescence (ΔF/F) is plotted agaist the final membrane potential for VoltageFluor dyes loaded in HEK cells as in (b). Error bars are ±SEM for $n \geq 3$ for each dye.

In addition to optimization of the donor and bridge for far-red fluorescent voltage sensing, Cy5 itself is quite amenable to modification toward still further improvements. A range of Cy5 derivatives with varying substituents on the indolium nitrogen, alpha carbon, and

phenyl ring toward improved solubility, cell localization, and optimal electron density were then developed.

Substitution of the sulfonate of VF Red to a more electron withdrawing sulfonamide group created a more electron poor acceptor that could further promote PeT and potentially, a more sensitive dye. Addition of the sulfonamide group also created a valuable molecular handle for attaching cell-targeting groups to potentially be explored. The potassium salt of the indole used in earlier Cy5 synthesis was used as a starting material to generate the sulfonamide substituted species through an acid halide intermediate. Quaternization via an SN-2 reaction and condensation to the Cy5 dye gave the desired Cy5 species suitable for Heck coupling to generate a range of sulfonamide substituted VF dyes as seen in Figure 4.4.

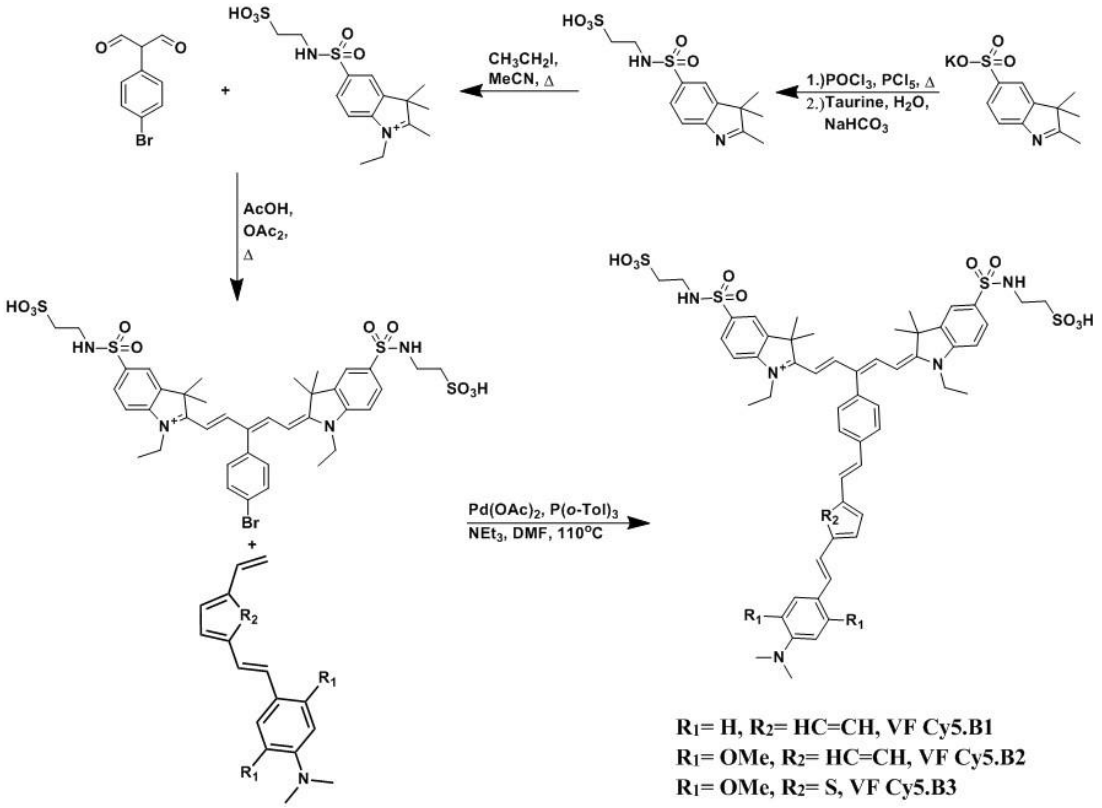

Figure 4.4 Synthetic Scheme for the Synthesis of Sulfonamide Substituted Cy5-based VF dyes

The same spectrum of donors and bridges with varying propensities for electron transfer used in Figure 4.2 were applied to the sulfonamide substituted acceptor as well to generate a suite of dyes with varying driving forces for electron to be tested in HEK cells. All three dyes were bath applied as previously discussed and shown to be fluorescent in the far red as seen in Figure 4.5a.

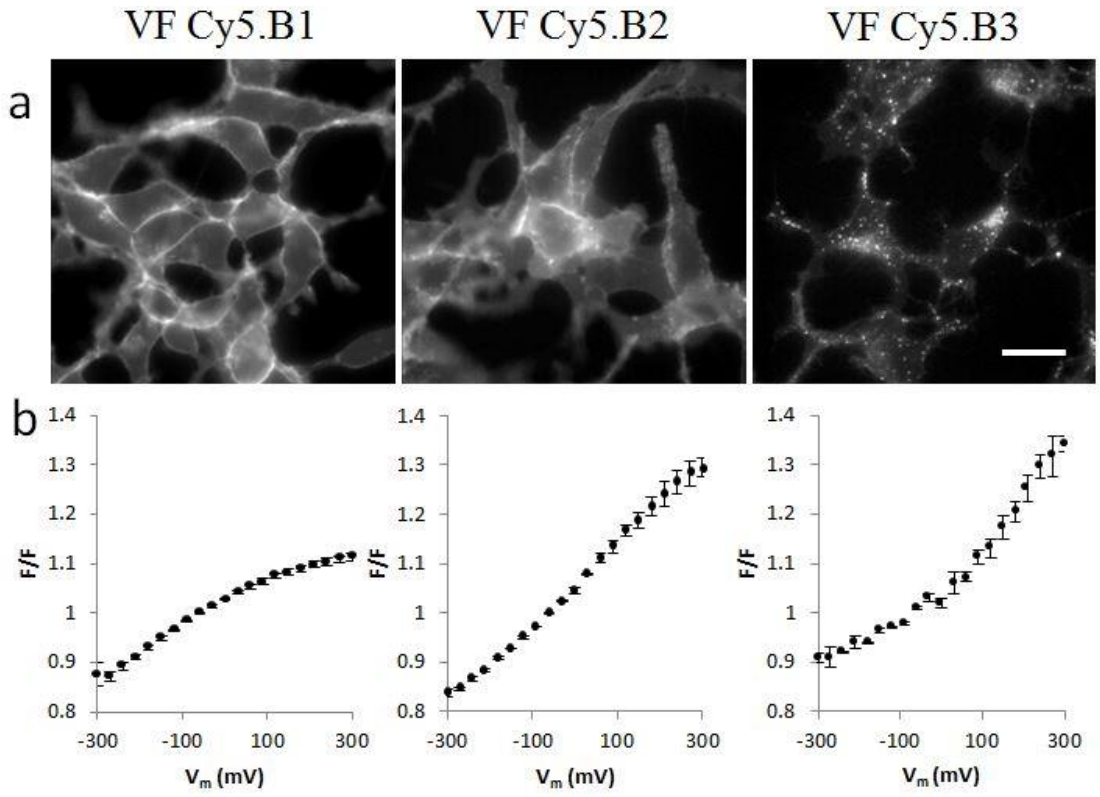

Figure 4.5 Characterization of Sulfonamide substituted VF Cy5 dyes in HEK cells. (a) Epifluorescent imaging of HEK cells stained with 200 nM dye for 15 min. at 37ºC. Scale bar is 20 μm. (b) Fluorescence response of dyes vs. membrane potential. Voltage clamped HEK cells were held at -60 mV and then stepped to the indicated potential. The relative fluorescence (F/F) is plotted against the final membrane potential for VoltageFluor dyes loaded in HEK cells as in (a). Error bars are ±SEM for $n \geq 3$ for each dye.

Membrane staining of VF Cy5.B1 appeared diffuse and largely localized to membranes as seen through epifluorescence. Interestingly, these characteristics did not appear to translate as well to VF Cy5.B2 and B3. VF Cy5.B3 was almost entirely localized to puncta on the membrane and internalized to endosomes with very little dye seen at the membrane. VF

Cy5.B2 appeared to be in between these two extremes with some membrane staining and some localization to internal puncta, though the majority appeared to be localized to the plasma membrane.

Patch clamping of stained HEK cells to test for voltage sensitivity gave relatively insensitive results across all dyes with a sulfonamide substituted Cy5 acceptor. VF Cy5.B1 showed a 4% ΔF/F per 100 mV, well below the 25% seen with VF Red. Notably though, the 4% ΔF/F per 100 mV of VF Cy5.B1 was better than the 1% seen in VF Cy5.A1, a dye with the same donor and bridge. Similar to the Cy5.A series of dyes, VF Cy5B.1 also had a concave shape indicating stronger probabilities for PeT should increase voltage sensitivities. Addition of dimethoxy groups to the aniline in VF Cy5.B2 did indeed offer such an improvement exhibiting an 8% ΔF/F per 100 mV, a similar value to VF Cy5.A2. While VF Cy5.A2 still retained a concave shape, VF Cy5.B2 appeared to have an s-shape that more closely resembled VF Red. VF Cy5.B3 proved as much showing no improvement to voltage sensitivity with a 7% ΔF/F per 100 mV. In addition, the concave shape of the trace indicated that PeT dominated throughout the range of potentials observed in Figure 4.5b. Overall, while it appeared the sulfonamide may have improved the driving force for PeT by providing a more electron poor acceptor, there was no improvement in membrane sensitivity compared to VF Red.

In an effort to continue to improve voltage sensitivity, additional electron withdrawing substitutions were made, where a methyl amide group replaced the ethyl group attached to the indolium nitrogen. This was achieved through the same nucleophilic substitution reaction performed with 2-chloro-acetamide rather than iodoethane in Figure 4.6. The rest of the dye was synthesized as above.

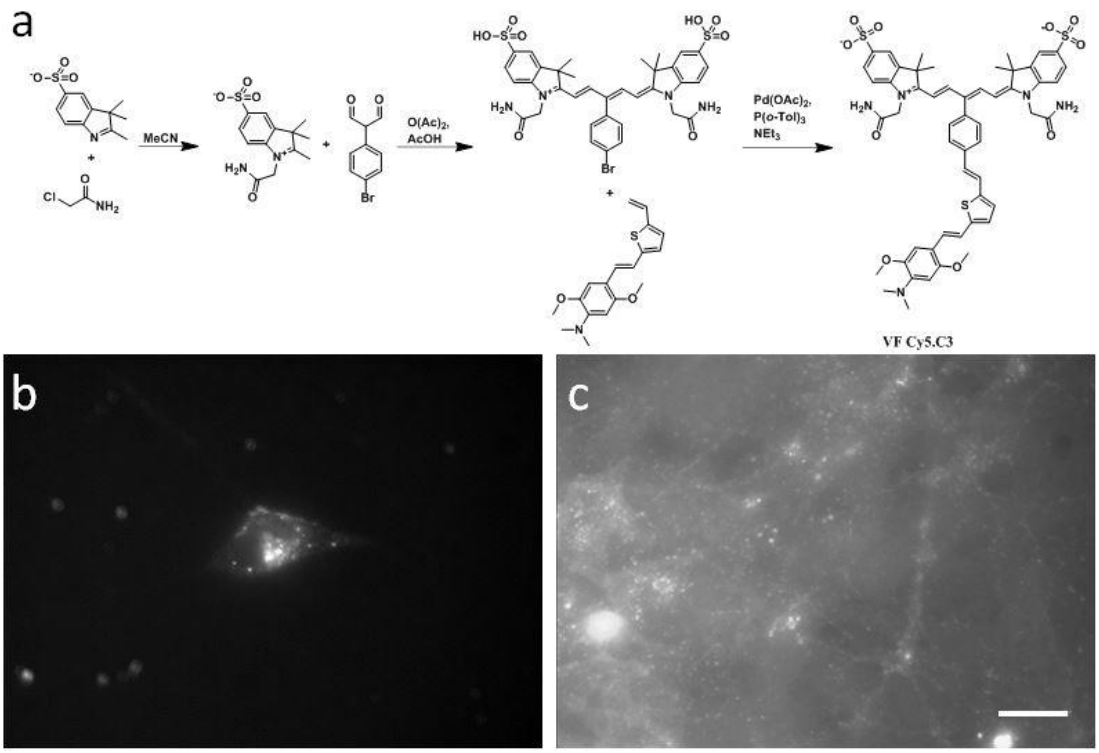

Figure 4.6 (a) Synthetic Scheme of VF Cy5.C3. (b) Epifluorescent imaging of HEK cells stained with 200 nM dye for 15 min. at 37ºC. (c) Epifluorescent imaging of cultured cortical rat neurons applied as in (b). Scale bar is 20 μm.

VF Cy5.C3 appeared to aggregate within cells upon staining of HEK cells with dye. Significant hot spots within cells were observed as well as smaller puncta. Little of the dye appeared to stain membranes. Attempts to deliver the dye with pluronic, at low temperature, and at differing concentrations in data not shown did not improve membrane staining.

HEK cells provide a suitable model system for testing voltage sensitivities of VF dyes due to their robust growth, low maintenance, and accessibility for patch clamping. However, their morphology is not the same as systems neurobiologists hope to study. It was important to verify that the poor membrane staining seen in HEK cells translated to neurons. Accordingly, VF Cy5.C3 was applied to cultured cortical neurons as well. Just as in HEK cells, very little membrane staining was observed. Rather than internalize however, there was almost

no fluorescence at all. What fluorescence there was did appear to be localized to puncta within cells though.

Previous work had shown that replacing the thiophene group in the bridge with a phenyl group could improve membrane staining. The improved driving force for PeT generated by the electron poor amide-substituted Cy5 acceptor was potentially enough to optimize the driving force with a phenyl bridge while improve membrane staining. Toward this end, VF Cy5.3B was synthesized and applied to HEK cells in Figure 4.7b.

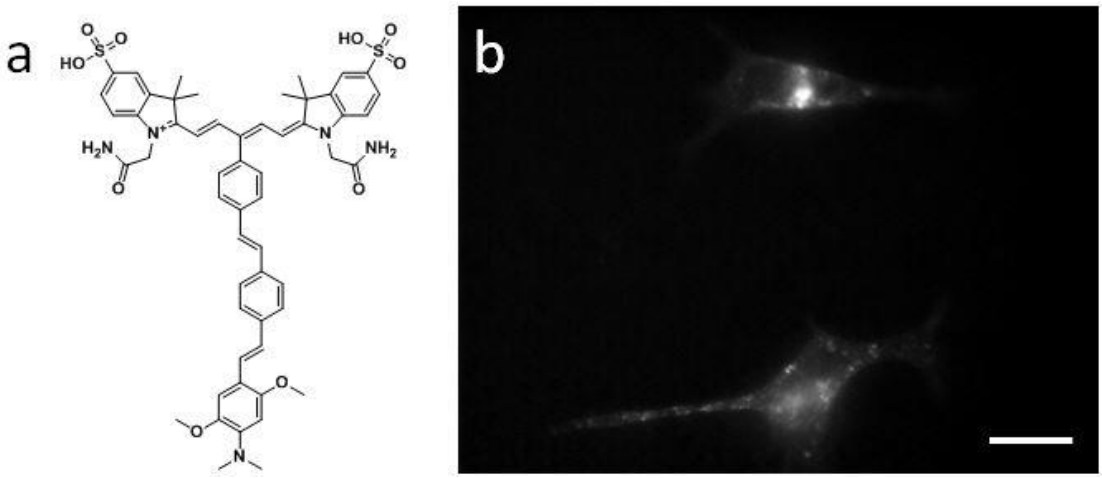

Figure 4.7 Characterization of VF Cy5.C2 (a) Structure and (b)Fluorescence Imaging of dye in HEK cells. Epifluorescent imaging of HEK cells stained with 200 nM dye for 15 min. at 37ºC. Scale bar is 20 μm.

VF Cy5.C2 did not appear to localize to the extracellular membrane. Similar to VF Cy5.C3, this dye with the phenyl bridge also appeared to aggregate within the cell localizing to small punctate areas. The poor membrane localization and dim fluorescence in both HEK cells and neurons gave no incentive to further characterize the dye.

Unlike the fluorescein-base probes, VF dyes with Cy5 acceptors have shown far less membrane localization thus far. One potential reason for this is poor lipophilicity. The extent of membrane staining may be improved by changing where the polar sulfonate groups are placed on the molecule. Beyond sulfonation on the phenyl ring, the dimethyl groups at the 3

position of the indolium ring represent a potential site for addition of sulfonate groups as shown by the synthesis of VF Cy5.D in Figure 4.8a. This new dye was developed first by generating the butyl sulfonate substituted ketone necessary for fischer indole synthesis and canonical cy5 synthesis. The new ketone was made by nucleophilic ring opening of butyl sultone by the enolate generated from sodium hydride followed by an acid hydrolysis of the ester.

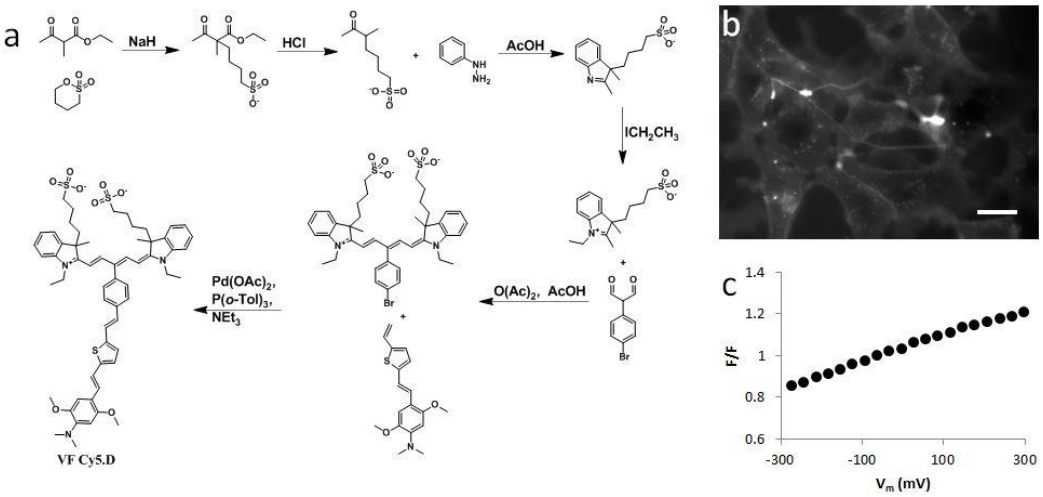

Figure 4.8 Synthesis and Characterization of VF Cy5.D. (a) Synthetic Scheme. (b)Fluorescence imaging of dye in HEK cells. Epifluorescent imaging of HEK cells stained with 200 nM dye for 15 min. at 37ºC. Scale bar is 20 μm. (c) Fluorescence response of dye vs. membrane potential. Voltage clamped HEK cells were held at -60 mV and then stepped to the indicated potential. The relative fluorescence (F/F) is plotted against the final membrane potential for VoltageFluor dyes loaded in HEK cells as in (b)

This new VF dye could potentially embed itself further into the membrane compared to previous iterations. The butyl sulfonate groups may potentially act as snorkels allowing the hydrophobic cy5 fluorophore to embed farther into the hydrophobic membrane interior where the electric field is the strongest, to more effectively sense changes in voltage.[17] VF Cy5.D did appear to stain HEK cell membranes more effectively as seen in Figure 4.8b. Dye appeared diffuse throughout the cell membrane with a few bright spots where hydrophobic aggregates were seen. Overall, staining was on par with other successful probes indicating this new design

could provide a viable voltage sensor. However, upon patch clamping of stained HEK cells and stepping to a range of membrane potentials, it was found VF Cy5.D only showed a 6% ΔF/F per 100 mV, a value 4x lower than VF Red which contained the same donor and bridge.

VF Cy5.D moved the hydrophilic sulfonate groups much farther from the electron acceptor than seen in VF Red. This change may have improved cell staining, but also moved electron withrdrawing sulfonate groups much farther from the chromophore, potentially reducing the driving force for PeT. Combining the favorable staining of VF Cy5.D attributable to the sulfonate location with the sensitivity of VF Red generated by the electron withdrawing groups on the acceptor could potentially result in an even more effective voltage sensor. Fluorine represents and ideal substitution toward this goal by being both highly electron withdrawing and relatively hydrophobic. VF Cy5.E was synthesized with perfluorinated phenyl rings on the indolium species toward this end. Starting from the tetrafluoro aniline, a diazonium intermediate was generated and reduced to the phenylhydrazine. Fischer indole synthesis was then utilized with the butyl-sulfonate ketone utilized in VF Cy5.D synthesis followed by a Heck coupling to the the full dye in Figure 4.9a.

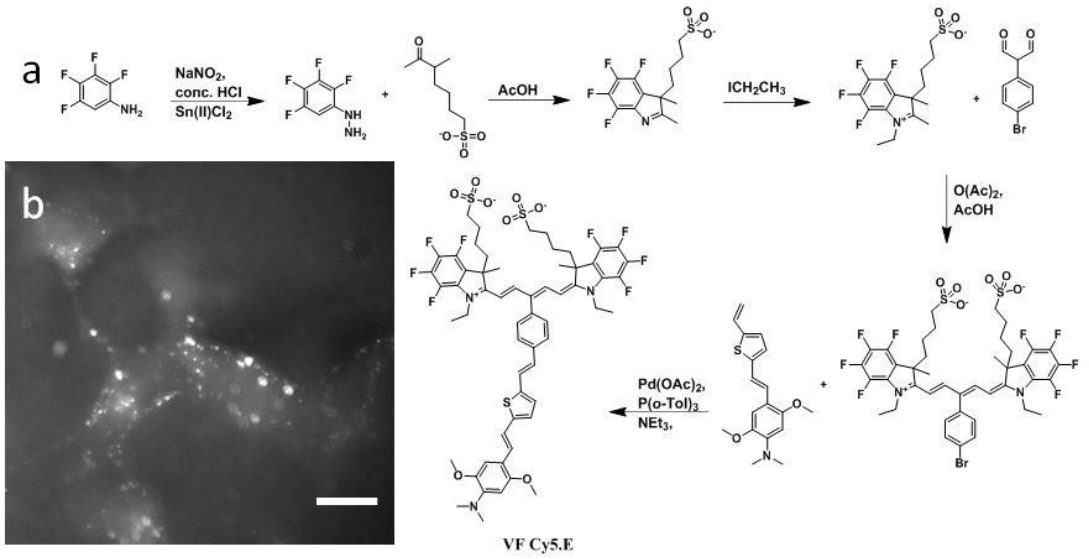

Figure 4.9 Synthesis and Characterization of VF Cy5.E. (a) Synthetic Scheme. (b)Fluorescence imaging of dye in HEK cells. Epifluorescent imaging of HEK cells stained with 200 nM dye for 15 min. at 37ºC. Scale bar is 20 μm.

VF Cy5.E was then applied to HEK cells toward testing for voltage sensitivity. Cells stained with VF Cy5.E appeared to aggregate on cells when viewed through fluorescence microscopy. Aggregates typically larger than endosomes or other vesicles found in cells were found throughout imaged cells indicating VF Cy5.E may have self-aggregated to give this type of staining. Voltage sensitivity was not determined, but given the poor membrane staining compared to the best VF dyes, VF Cy5.E did not appear to offer any improvement.

A final attempt toward synthesizing a novel Cy5 acceptor was made through a hybrid of the VF Red acceptor utilizing a sulfonated phenyl group together with electron withdrawing fluorine groups. A sulfonate was initially installed on the aniline precursor through an electrophilic aromatic substitution followed by previously discussed synthetic techniques toward generating VF Cy5.F in Figure 4.10a. VF Cy5.F appeared to aggregate to a large extent when applied to HEK cells similarly to VF Cy5.E. Very little fluorescence was seen at the plasma membrane and large globules of fluorescence dominated the landscape. Both VF Cy5.E and VF Cy5.F contained fluorine substitutions, which may have contributed to the aggregation

seen by fluorescence. However, this type of staining was never seen with VF2.1.F in Figure 2.3. As expected given the poor membrane staining, VF Cy5.F did not appear to be very sensitive to voltage with a 5% ΔF/F per 100 mV. The trace in Figure 4.10c appeared to have a convex shape as well which would indicate that PeT was the dominant mechanism of relaxation to the ground state throughout the range of potentials. The high probability of PeT is not surprising given the strong driving force for electron transfer generated by substitution with highly electronegative fluorine atoms and electron withdrawing sulfonate groups.

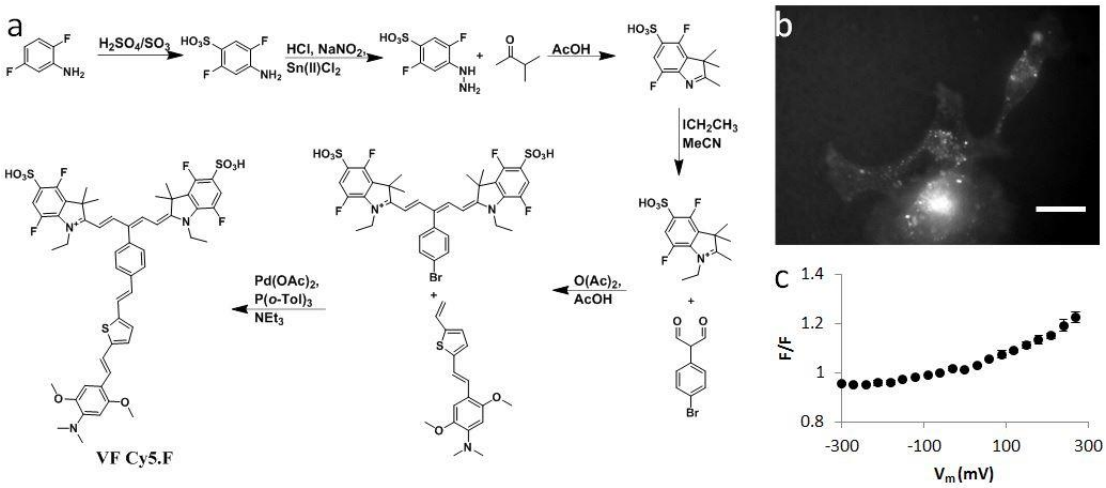

Figure 4.10 Synthesis and Characterization of VF Cy5.F. (a) Synthetic Scheme. (b)Fluorescence imaging of dye in HEK cells. Epifluorescent imaging of HEK cells stained with 200 nM dye for 15 min. at 37ºC. Scale bar is 20 μm. (c) Fluorescence response of dye vs. membrane potential. Voltage clamped HEK cells were held at -60 mV and then stepped to the indicated potential. The relative fluorescence (F/F) is plotted against the final membrane potential for VoltageFluor dyes loaded in HEK cells as in (b)

A wide range of Cy5 acceptors were developed and combined with proven donors and bridges to develop more sensitive far red fluorescent VF dyes. Many of the combinations did not stain membrane sufficiently and showed voltage sensitivities under a 10% ΔF/F per 100 mV. Fortunately, VF Red was shown to have a strong voltage sensitivity in HEK cells and offered the best option for far-red fluorescent voltage sensing with VF dyes. Given the strong membrane staining and high sensitivity, VF Red was then applied to neuronal cell culture

toward imaging action potentials. VF Red appeared highly localized to the plasma membrane of neurons with minimal internalization. As expected, additional staining of surrounding glia cells and neuropil contributed to the fluorescent signal as well seen in Figure 4.11a.

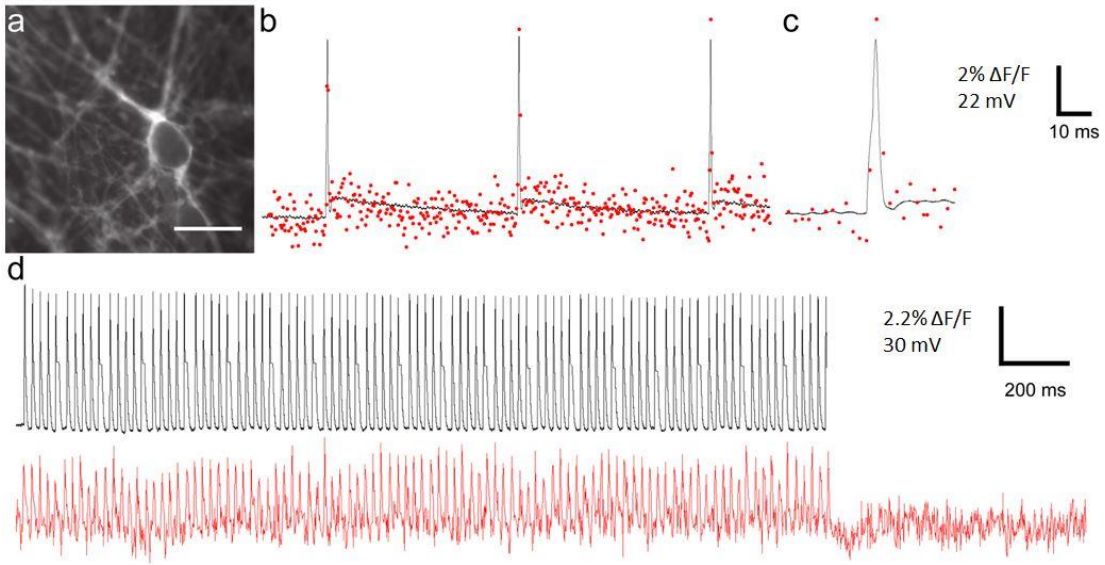

Figure 4.11 VF Red in Cultured Cortical Rat Neurons. (a) Epifluorescent imaging of cortical rat neurons stained with 200 nM dye for 15 min. at 37ºC. Scale bar is 20 μm. (b) VF Red fluorescence recording in a single trial of evoked action potentials in red together with electrophysiology measurements in black. Red points indicate change in fluorescence from baseline in single frames captured at 500 Hz. (c) Expansion of the third action potential recording from (b). (d) Train of action potentials evoked at a rate of 50 Hz. Trace of the change in fluorescence from baseline fluorescence shown in red and electrophysiology measurement is shown in black.

To assess the ability of VF Red to sense evoked electrical activity in cultured neurons, cells were patch clamped and injected with sufficient depolarizing current to generate action potentials. VF Red was able to detect all three action potentials in a single trial imaging with an EMCCD camera imaging at 500 Hz as shown in Figure 4.11b. Imaging at this low of a frequency makes capturing more than a small portion of the action potential impossible, but was still fast enough to definitively capture each spike with a 10% ΔF/F per 100 mV. More importantly, VF Red gave a signal to noise ratio of 9:1, a value high enough to reliably record neuronal activity in a single trial. VF Red was also shown to be a robust probe capable of

reliably capturing long rapid trains of electrical spikes in Figure 4.11d. The fluorescent signals of the final spikes were just as clear as the initial spikes with no sign of signal deterioration.

One of the great promises of far-red voltage sensors is coupling with light sensitive electrical activators like channel rhodopsin in an effort to develop all optical, electrode free, electrophysiological methods. Neurons expressing ChIEF, a light sensitive cation channel capable of depolarizing neurons when stimulated with blue light were stained with VF Red as well. VF Red may be optimally excited with 650 nm light, much farther red than is capable of activating ChIEF, which was stimulated with 470 nm light. Filtering out the stimulating blue light and only observing the red changes in fluorescence allowed for neurons to be both excited by blue light, and recorded independently in the far red as seen in Figure 4.12c. 50 ms pulses of blue light were sufficient to evoke action potentials in ChIEF expressing neurons identified by co-expression with eGFP. The spikes were clearly seen with high fidelity by fluorescence imaging and verified by patch clamp recordings. There was no indication the red light used to monitor activity had any depolarizing effect on ChIEF. Additionally, no blue light used to stimulate bled through to the red channel.

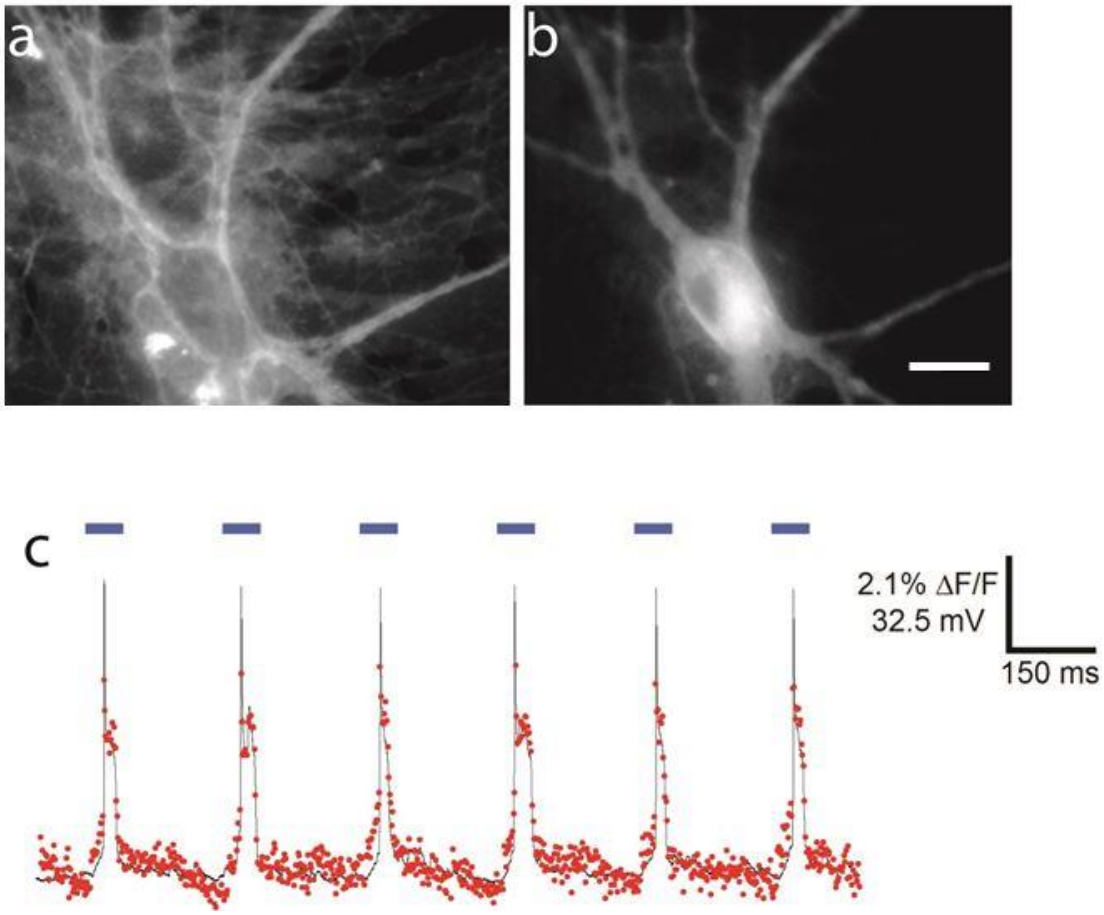

Figure 4.12 All Optical Electrophysiology of VF Red with ChIEF. (a) Epifluorescent imaging of cortical rat neurons stained with 200 nM dye for 15 min. at 37°C. (b) Epifluorescent image of ChIEF-EGFP expressing cultured neurons. Scale bar is 20 μm. (c) Pulses of 470 nm light used to evoke electrical activity in neurons are shown in blue. The 500 Hz EMCCD recording of VF Red changes in fluorescence intensity from baseline is shown in red. Electrode recording of membrane potential is shown in black.

4.3 Methods

4.3.1 General Synthetic and Analytical Measurements

As described in Chapter 2

4.3.2 Data Analysis

As described in Chapter 2

4.3.3 Patch Clamping Neurons and HEK Cells

As described in Chapter 2 with changes to the light filtered. A 10% neutral density filter, a 609 nm filter (54 nm bandpass, Semrock), a 649 nm dichroic (Semrock), and a 685 nm emission filter (40 nm bandpass, Semrock) were used.

4.3.4 All Optical electrophysiology

ChIEF-eGFPLentivirus Production

Viral vectors were generated as described initially in previous work and reproduced herein.[7] The gene encoding *oChIEF-EGFP* was subcloned into a generation 2 lentiviral construct with the hSyn promoter. The lentivirus was made according to the protocols at http://vectorcore.salk.edu/protocols.php with minor modifications. In brief, 293A cells (Life Technologies, Carlsbad, CA) were grown to 85 % confluency and transfer vectors containing ChR-FP, psPAX2 and pMD2.G (gifts from Professor Didier Trono) were transfected with calcium phosphate (Clontech, Mountainview, CA). Virus particles were harvested from serum-free medium and concentrated with 20 % sucrose cushion with ultracentrifugation. The titre of lentivirus was estimated with Lentivirus Rapid Quantitation Kit (Cell Biolabs Inc. San Diego CA, USA) in parallel just before each infection. The lentiviral vector was a gift from Dr. Ed Boyden (MIT).

Optical Stimulation of *ChIEF-EGFP* Transfected Neurons

The light source was a Melles Griot 100 mW 488 nm ion laser fitted with a fiber optic cable placed directly above the neurons of interest. Filtering of incident 488 nm light was achieved by addition of a second 685 nm emission filter (40 nm bandpass, Semrock).

4.3.5 Synthetic methods

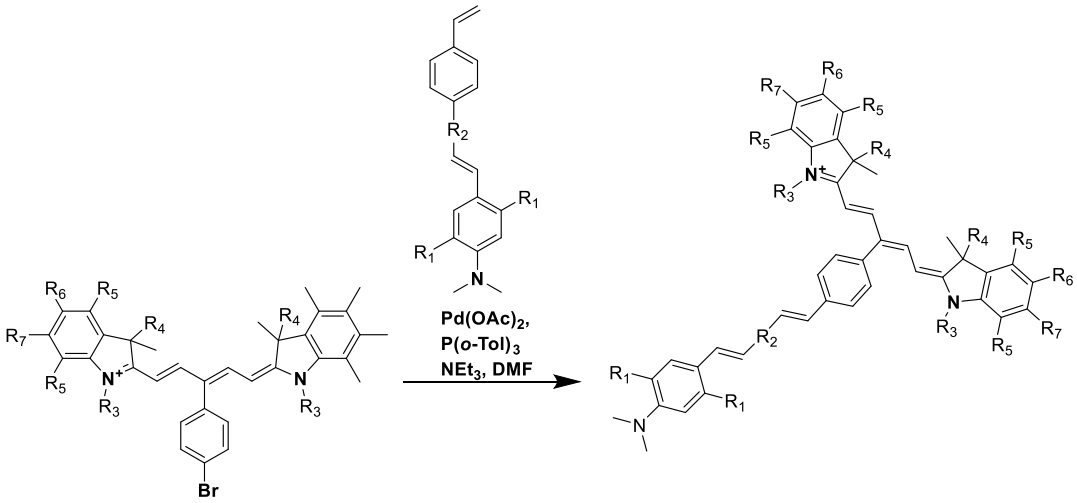

Synthesis of VF Cy5 dyes

In a 5 mL round bottom flask equipped with a stir bar, the viny aromatic aniline (1 eq.), cy5-like fluorophore (1.0 eq.), $Pd(OAc)_2$ (1 mg, 0.0045 mmol), and P(*o*-Tol)$_3$ (3 mg, 0.01 mmol) were added. The round bottom was sealed with a rubber septum, evacuated, and backfilled with N_2 three times. Triethylamine (10 µL, ~2.5 eq.) and DMF (0.1 mL) were added via syringe and the reaction stirred at 110 °C for 16 hours. The reaction was cooled and concentrated to dryness. The dark green solid was taken up in minimal DMF and acetic acid and purified by preparative HPLC on a Luna C_{18} column with a gradient of 10% MeCN in 1M triethylammonium acetate pH7 in H_2O ramping to 90% MeCN in 20 minutes. The resulting material was concentrated to dryness to give approximately 1 mg of a dark blue solid. All identifications and purifications performed by HPLC and ESI-MS.

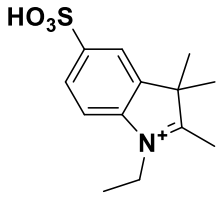

Synthesis of 1-ethyl-2,3,3-trimethyl-5-(sulfinooxy)-3H-indol-1-ium performed according to previously described methods.[16]

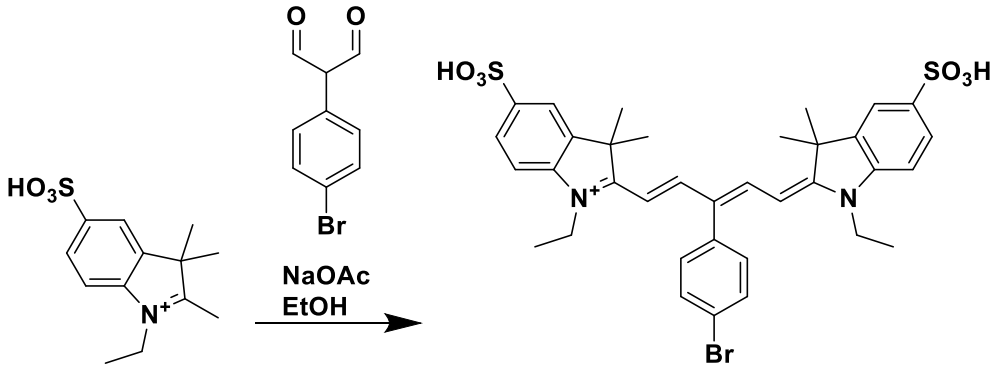

Synthesis of 2-((1E,3Z)-3-(4-bromophenyl)-5-((E)-1-ethyl-3,3-dimethyl-5-sulfoindolin-2-ylidene)penta-1,3-dien-1-yl)-1-ethyl-3,3-dimethyl-5-sulfo-3H-indol-1-ium

An oven dried 10 mL round bottom flask was charged with 1-ethyl-2,3,3-trimethyl-5-(sulfinooxy)-3H-indol-1-ium (50 mg, 0.187 mmol, 2 eq.), 2-(4-bromophenyl)malonaldehyde (20 mg, 0.094 mmol, 1 eq.), sodium acetate (15 mg, 0.187 mmol, 2 eq.), and ethanol (3 mL). The reaction vessel was then refluxed overnight and cooled to room temperature. The resulting dark blue solution was concentrated to dryness and taken up in minimal water. The blue solid was purified by preparative HPLC on a Luna C_{18} column with a gradient of 10% MeCN in H_2O with 0.05% TFA ramping to 90% MeCN in 20 minutes. The resulting material was concentrated to dryness to give a dark blue solid. HPLC-MS found [M^+] = 725.2

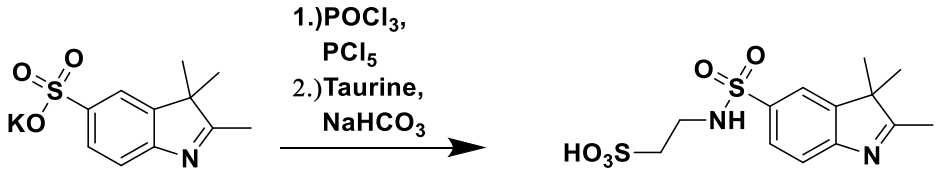

Synthesis of 2-((2,3,3-trimethyl-3H-indole)-5-sulfonamido)ethane-1-sulfonic acid

An oven dried 25 mL round bottom flask and condenser were charged with potassium 2,3,3-trimethyl-3H-indole-5-sulfonate (2g, 7.2 mmol, 1 eq.) and phosphorous pentachloride (1.5 g, 7.2 mmol 1 eq.). The apparatus was put under nitrogen and phosphoryl trichloride (10 mL) was added via syringe. The resulting dark purple solution was refluxed for 45 min and then cooled to room temperature and added to methylene chloride (10 mL). This solution was then added to 25% hexane in diethyl ether (50 mL) to give a deep purple solid that was filtered under vacuum. The sticky solid was taken up in methylene chloride and concentrated under vacuum to dryness. A solution of taurine (3.6 g, 29 mmol, 5 eq.) and sodium bicarbonate (7.3 g) in water (100 mL) was added dropwise at 0ºC to the sticky purple solid. Upon addition, the solution was heated to room temperature and stirred for 16 hours. Purification of product from salt was performed by an open reverse phase column first washing with water, then eluting with 1:1 water:MeCN mixture. The dark column band was collected and concentrated to dryness under vacuum to give product. (351 mg) HPLC-MS found [M^+] = 347.0

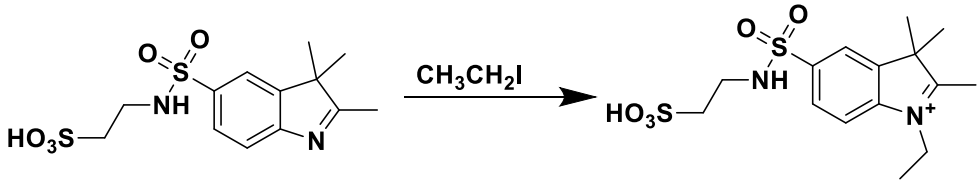

Synthesis of 1-ethyl-2,3,3-trimethyl-5-(N-(2-sulfoethyl)sulfamoyl)-3H-indol-1-ium

An oven dried 10 mL round bottom flask was charged with 2-((2,3,3-trimethyl-3H-indole)-5-sulfonamido)ethane-1-sulfonic acid (35 mg), MeCN (5mL), and ethyl iodide (5 mL) were refluxed for 48 hours. The reaction was then cooled to room temperature and concentrated to dryness. The purple solid was taken up in minimal acetonitrile and triturated with acetic acid to give product with no further purification. HPLC-MS found [M^+] = 375.1

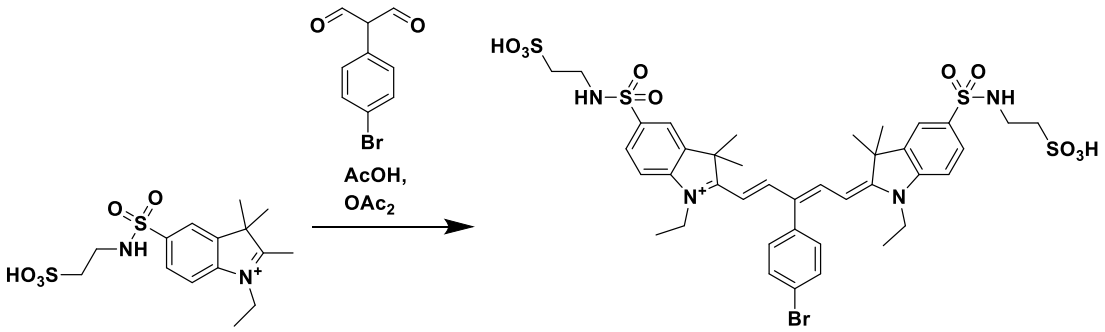

Synthesis of 2-((1E,3Z)-3-(4-bromophenyl)-5-((E)-1-ethyl-3,3-dimethyl-5-(N-(2-sulfoethyl)sulfamoyl)indolin-2-ylidene)penta-1,3-dien-1-yl)-1-ethyl-3,3-dimethyl-5-(N-(2-sulfoethyl)sulfamoyl)-3H-indol-1-ium

An oven dried 10 mL round bottom flask was charged with 1-ethyl-2,3,3-trimethyl-5-(N-(2-sulfoethyl)sulfamoyl)-3H-indol-1-ium (10 mg, 0.027 mmol, 2 eq.), 2-(4-bromophenyl)malonaldehyde (3 mg, 0.013 mmol, 1 eq.), acetic acid (0.3 mL) and acetic anhydride (0.3 mL). The round bottom was heated to 60°C and stirred overnight to give a dark blue solution. The reaction was cooled to room temperature and concentrated to dryness. The blue solid was taken up in a minimal water and acetonitrile mixture (1:1) and purified by preparative HPLC on a Luna C_{18} column with a gradient of 10% MeCN in H_2O with 0.05% TFA ramping to 90% MeCN in 20 minutes. The resulting material was concentrated to dryness under vacuum to give a dark blue solid. HPLC-MS found $[M^+]$ = 940.9

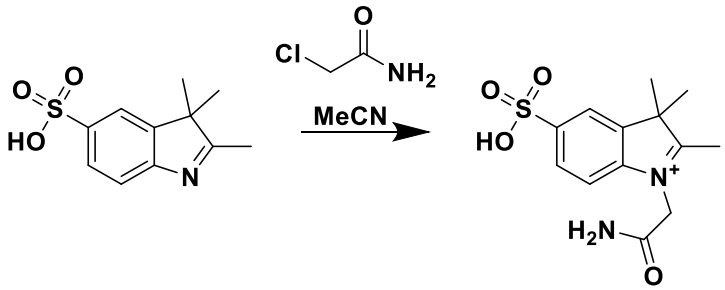

Synthesis of 1-(2-amino-2-oxoethyl)-2,3,3-trimethyl-5-sulfo-3H-indol-1-ium

An oven dried 5 mL round bottom flask was charged with 2,3,3-trimethyl-3H-indole-5-sulfonic acid (100 mg, 0.36 mmol, 1 eq.), chloroacetamide (334 mg, 3.6 mmol, 10 eq.), and acetonitrile (1

mL). The reaction was stirred at 80ºC for 5 days. Upon cooling to room temperature and concentrating under vacuum no further purification was performed. HPLC-MS found [M^+] = 297.0

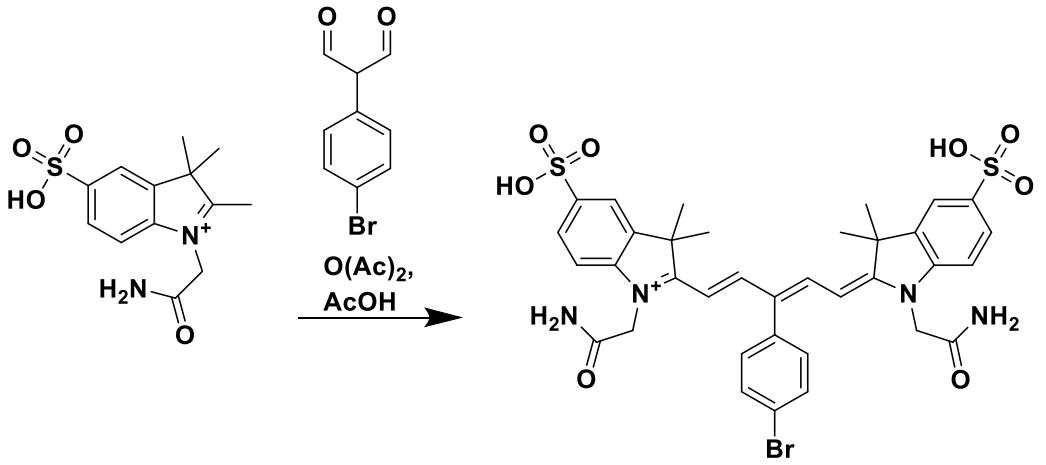

Synthesis of 1-(2-amino-2-oxoethyl)-2-((1E,3Z)-5-((E)-1-(2-amino-2-oxoethyl)-3,3-dimethyl-5-sulfoindolin-2-ylidene)-3-(4-bromophenyl-2-ylium)penta-1,3-dien-1-yl)-3,3-dimethyl-5-sulfo-3H-indol-1-ium

An oven dried 10 mL round bottom flask was charged with 1-(2-amino-2-oxoethyl)-2,3,3-trimethyl-5-sulfo-3H-indol-1-ium (40 mg, 0.135 mmol, 2 eq.), 2-(4-bromophenyl)malonaldehyde (15 mg, 0.068 mmol, 1 eq.), acetic anhydride (0.3 mL), and acetic acid (0.3 mL). The reaction vessel was heated to 80ºC and stirred for 16 hours to give a dark blue solution. Upon cooling to room temperature ethyl acetate was added to precipitate a blue solid. The suspension was then centrifuged for 2 minutes and the yellow supernatant was discarded. The resulting blue solid was washed 2 more times with ethyl acetate, taken up in water, and lyophilized to give 16 mg. HPLC-MS found [M^+] = 783.0

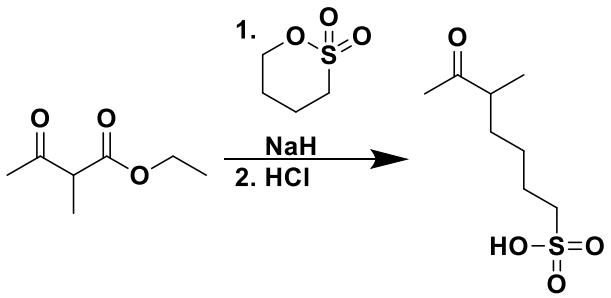

Synthesis of 5-methyl-6-oxoheptane-1-sulfonic acid

An oven dried 25 mL round bottom flask was charged with sodium hydride (278 mg, 6.94 mmol, 1 eq.) and put under nitrogen. Dimethylformamide (2 mL) was added via syringe and cooled to 0°C. In a separate dry 5 mL round bottom flask etheyl 2-methylacetoacetate(1g, 6.14 mmol, 1 eq.) was added, cooled to 0°C, and slowly transferred to the 25 mL round bottom causing vigorous bubbling and giving a yellow solution. After 15 minutes, the reaction vessel was warmed to room temperature until bubbling ceased. The reaction was then cooled to 0°C once more and 1,4-butanesultone (0.710 mL, 6.94 mmol, 1 eq.) was added dropwise over 15 minutes to give a bright yellow turbid solution that was then warmed to 50°C and stirred for 16 hours. The reaction was then cooled to room temperature and concentrated under vacuum to a yellow oil that was taken up in water (25 mL) and washed with diethyl ether (10 mL) two times. The aqueous layer was collected and concentrated under vacuum to give a light yellow solid that was added to concentrated hydrochloric acid (5 mL) to give a murky solution that was stirred at 90°C for 3 hours and then cooled to room temperature. It was then partially neutralized with sodium bicarbonate and purified by preparative HPLC on a Luna C_{18} column with a gradient of 10% MeCN in H_2O with 0.05% TFA ramping to 90% MeCN in 20 minutes.^{1}H NMR (400 MHz, DEUTERIUM OXIDE) δ ppm 0.90 (d, *J*=6.97 Hz, 3 H) 1.16 - 1.32 (m, 3 H) 1.43 - 1.60 (m, 3 H) 2.05 (s, 3 H) 2.47 - 2.56 (m, 1 H) 2.72 (t, *J*=8.40 Hz, 2 H)

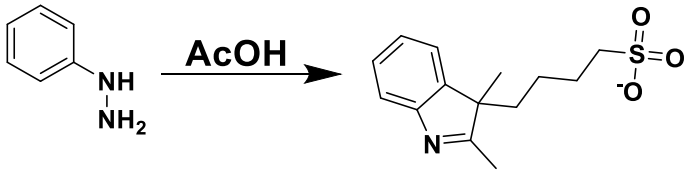

Synthesis of 4-(2,3-dimethyl-3H-indol-3-yl)butane-1-sulfonate

An oven dried 10 mL round bottom flask was charged with 5-methyl-6-oxoheptane-1-sulfonic acid(100 mg, 0.481 mmol, 1.2 eq.), phenylhydrazine (43 mg, 0.4 mmol, 1 eq.), and acetic acid (2 mL). The round bottom was heated to reflux for 2 hours and then concentrated under vacuum to a brown oil that was taken up in acetonitrile and purified by preparative HPLC on a Luna C_{18} column with a gradient of 0% MeCN in H_2O with 0.05% TFA ramping to 90% MeCN in 20 minutes. HPLC-MS found $[M^+] = 282.1$

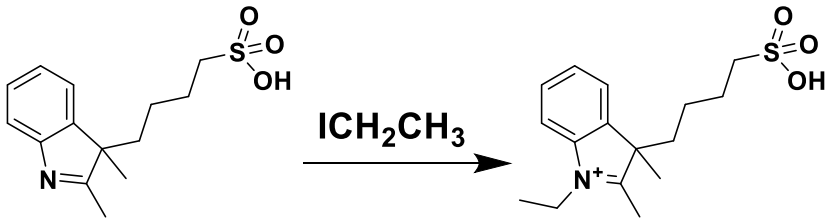

Synthesis of 1-ethyl-2,3-dimethyl-3-(4-sulfobutyl)-3H-indol-1-ium

An oven dried 5 mL round bottom flask was charged with 4-(2,3-dimethyl-3H-indol-3-yl)butane-1-sulfonic acid and refluxed in a large excess of ethyl iodide overnight. The resulting purple solid was concentrated to dryness and carried forward without any further purification. HPLC-MS found $[M^+] = 310.1$

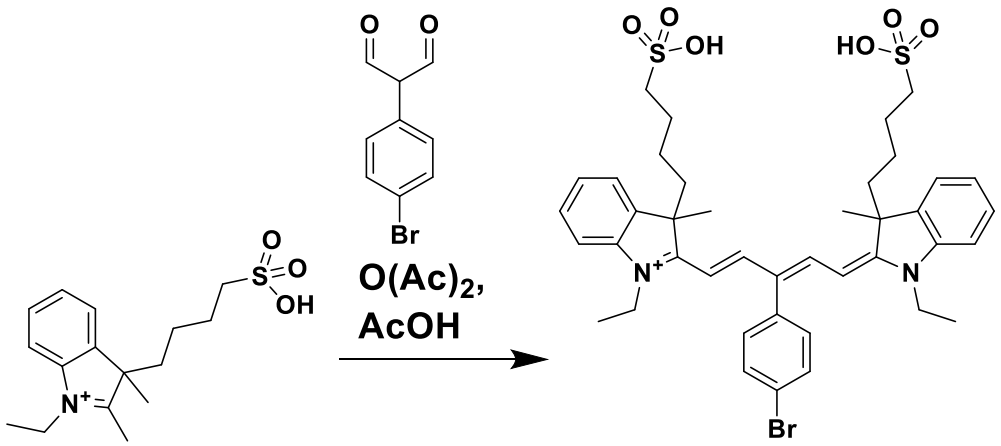

Synthesis of 2-((1E,3Z)-3-(4-bromophenyl)-5-((E)-1-ethyl-3-methyl-3-(4-sulfobutyl)indolin-2-ylidene)penta-1,3-dien-1-yl)-1-ethyl-3-methyl-3-(4-sulfobutyl)-3H-indol-1-ium

Same procedure as Cy5 synthesis previously described. HPLC-MS found [M^+] = 809.2

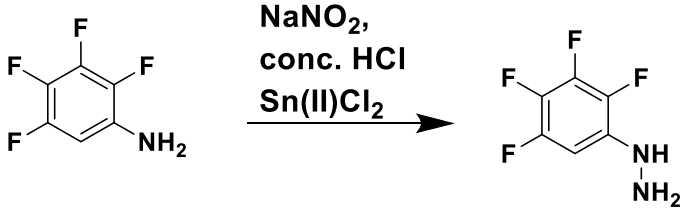

Synthesis of (2,3,4,5-tetrafluorophenyl)hydrazine

An oven dried 250 mL round bottom flask was charged with 2,3,4,5-tetrafluoroaniline (1g, 6 mmol, 1 eq.) and concentrated hydrochloric acid (160 mL) and cooled to 0^{o}C. Sodium nitrite (420 mg, 6 mmol, 1 eq.) in water (10 mL was added dropwise to give a bright yellow solution. Tin (II) chloride as dissolved in concentrated hydrochloric acid (23 mL) and then added dropwise. The reaction vessel was then warmed to room temperature and stirred for 10 hours. Upon completion, the solution was concentrated to dryness giving a white solid that was carried forward with no additional purification.

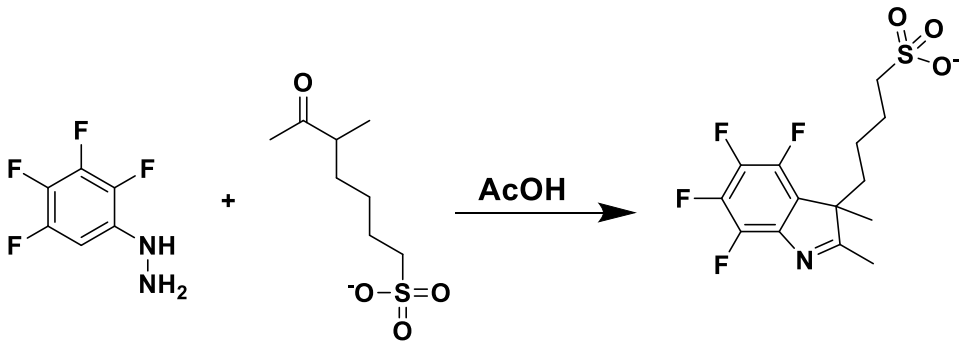

Synthesis of 4-(4,5,6,7-tetrafluoro-2,3-dimethyl-3H-indol-3-yl)butane-1-sulfonate was carried out according to the fischer indole synthesis described above. HPLC-MS found [M^+] = 354.3

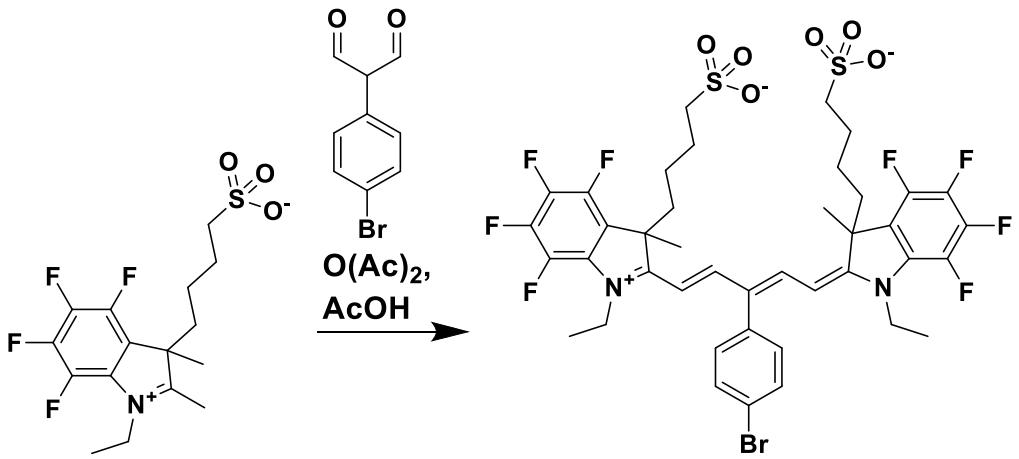

Synthesis of 4-(2-((1E,3Z)-3-(4-bromophenyl)-5-((E)-1-ethyl-4,5,6,7-tetrafluoro-3-methyl-3-(4-sulfonatobutyl)indolin-2-ylidene)penta-1,3-dien-1-yl)-1-ethyl-4,5,6,7-tetrafluoro-3-methyl-3H-indol-1-ium-3-yl)butane-1-sulfonate was carried out according to Cy5 synthesis described above. HPLC-MS found [M^+] = 955.2

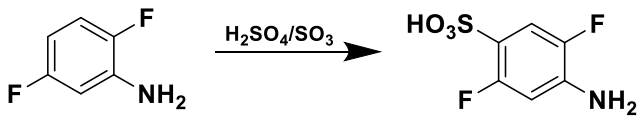

Synthesis of 4-amino-2,5-difluorobenzenesulfonic acid

An oven dried 10 mL round bottom flask was charged with 2,5-difluoroaniline and cooled to 0°C. Fuming sulfuric acid (2 mL) was added dropwise and then heated to 120°C for 1 hour. The reaction was then cooled to room temperature an poured over ice (100 mL). Barium carbonate was then

added with vigorous bubbling until the solution was neutralized giving a milky white solution that was passed through dowex 50w-x8 ion exchange resin (4 mL). The eluent was collected and concentrated to dryness to give an off-white wax. HPLC-MS found [M^+] = 209.9

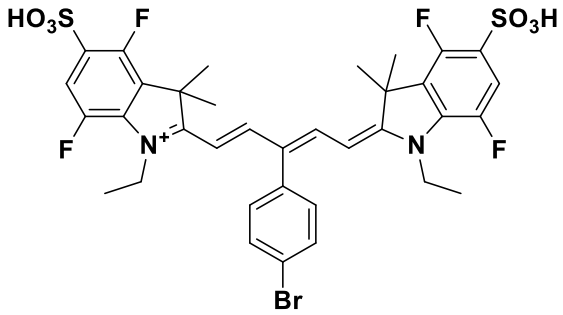

Synthesis of 2-((1E,3Z)-3-(4-bromophenyl)-5-((E)-1-ethyl-4,7-difluoro-3,3-dimethyl-5-sulfoindolin-2-ylidene)penta-1,3-dien-1-yl)-1-ethyl-4,7-difluoro-3,3-dimethyl-5-sulfo-3H-indol-1-ium was carried out as described in previously published methods and according to analogous syntheses described above.[16]

4.4 Discussion

4.4.1 All Optical Electrophysiology Applications of VF Red

All optical electrophysiology is an invaluable tool for a wide range of applications, but it is worth noting high throughput screens and *in vivo* experiments uniquely benefit from the technique. With regard to high throughput screens, Patch clamping neurons or electrical stimulation takes significantly longer or is more expensive than optical stimulation of channelrhodopsin expressing neurons. The use of optical activators of neurons vastly increases throughput for assays searching for pharmacological leads. However, the electrical signal must be recorded as well. Here again, optical recording is much faster and potentially cheaper than electrode based techniques. A red voltage sensor must be used since the only viable all optical electrophysiology approach requires a blue-only responsive electrical activator given no robust red-

only activator exists. Here, VF Red provides an ideal sensor that could be used to readout pharmacological effects on electrical activity rapidly with high fidelity. This type of experiment may open the door to new lead compounds capable of fighting neurological disease, an area in dire need of viable therapeutics.

In addition, coupling VF Red to optical electrical activators rather than electrodes provides a platform for a wide array of unique, previously inaccessible experiments. Optical electrical activators have the advantage of marking distinct neuronal populations with unique genetic, structural, and activity characteristics not possible otherwise. For example, it has been shown that hippocampal neurons activated during fear conditioning, can be manipulated to express channelrhodopsin and be reactivated with light to illicit the same fear response.[18] Stimulating this unique subset of hippocampal neurons could not be achieved with electrodes. This is just one exciting example of the many new experiments made possible by optical electrical activators. VF Red allows for VF dyes to be coupled with this powerful technique to read out the downstream electrical signals stimulated by optical electrical activators. Accordingly, VF Red provides a unique stepping-stone toward a new age of optical electrophysiology.

4.4.2 VF Red *In Vivo*

Far-red voltage sensors offer an exciting avenue for imaging voltage changes *in vivo* even without optical activity activators. Far-red voltage sensors make this type of work more accessible given than far red light interacts with biological molecules far less than shorter wavelength light. In addition, most *in vivo* recording of neural activity require a unique optical approach through two-photon microscopy which improves z-axis resolution and allows for much deeper imaging. While VF Red was not directly characterized by two-photon excitation, previous works has shown that Cy5 is a capable fluorophore for two-photon applications.[19] VF Red has very similar characteristic to Cy5 in one photon excitation which would suggest two-photon characteristics would align as

well. Two-photon microscopy is a valuable tool to be used in conjunction with VF dyes and further characterization of VF Red is certainly warranted once suitable lasers and hardware are made available either directly or through collaboration. While no application of VF Red *in vivo* has been made yet, there is currently no reason to suspect it would not perform better than fluorescein-based dyes of similar or even greater voltage sensitivity given the far red fluorescence and favorable two-photon characteristics of Cy5.

4.4.3 VF Red Fluorophore Derivatives

Given the success of the VF Red design and structural plasticity of the Cy5 fluorophore, further derivations built upon VF Red appeared to be an exciting area for future work. The prognosis of this line of work is far less optimistic given the poor showing of VF Cy5B through VF Cy5F that contained varying Cy5 structures. Seemingly, small changes to the structure of the Cy5 such as addition of two fluorine atoms appeared to drastically affect membrane staining in particular. It has been shown in this work that favorable membrane staining is an essential component to improved voltage sensors further discrediting the potential of future work on the Cy5 fluorophore. Notably, most of this work was performed in HEK cells, a fair model, but certainly different from the neuronal systems these dyes are intended for. It was shown that poor HEK cell staining did correlate with poor membrane staining with regard to VF Cy5.C3 in Figure 4.6, but this may not be the case for all dyes. Further exploration of neuron staining and recording of electrical activity would provide greater insight.

4.4.4 Non-Enzymatic Genetic Targeting of Cy5-based VF Derivatives

Some of the most promising derivatives of VF Red are covalently attached tags for targeting only to neurons expressing appropriate receptors. Here poorly staining dyes may provide a significant benefit. Voltage sensors like VF Cy5.C3 shown to not stain cells may be coerced to insert into the plasma membrane through a membrane bound covalent tag such as SNAP or

Halo.[20,21] Sparse expression of genetic tags in a subpopulation of neurons has the potential to dramatically limit background noise from neuropil and non-neuronal cells. Furthermore, teasing out signal from a single cell may be all but impossible *in vivo* where cells are packaged incredibly densely and there are significant motion artifacts. Sparse, targeted labeling alleviates this problem and opens up a wide range of interesting experiments.

Additionally, molecules like VF2.1OMe.H discussed in chapter 2 have a very high affinity for any membrane. In data not shown, VF2.1OMe.H was applied to a mouse brain for two-photon recording in a live mouse cortex. This dye was applied from a glass pipette to locally stain cortical cells for imaging. One of the main challenges was getting VF2.1OMe.H to diffuse throughout the cortical region. Upon ejection from the pipette, much of the dye immediately stuck to membranes found near the pipette tip with minimal diffusion. The high dye concentration near the tip eventually reached toxic levels without staining distal areas of the cortical region. Less sticky dyes that only insert into the membrane when covalently bound to tags expressed on a desired subset of neurons could potentially alleviate this issue.

In addition to simple covalent tags, Cy5-based VF dyes may be coupled to fluorogenic molecules like malachite green and thiazole orange derivatives that become fluorescent upon binding of fluorogen activating proteins.[22] This essentially turns the VF dye and fluorogen into a FRET pair that is only active when the malachite green or thiazole orange is bound to a cell expressing the fluorogen activating protein (FAP). Ideally, using an excitation wavelength for the fluorogen, only cells expressing the FAP will excite the bound fluorogen which can then transfer this excitation energy through FRET to the attached VF dye to report on electrical changes just as if it were directly excited by a photon rather than via FRET. Fluorescent signal would ideally be limited to the desired cells expressing the FAP with no background from glia or neuropil. However, this approach has the significant drawback of being photon inefficient. FRET is not a perfectly efficient process and many of the photons exciting the fluorogen may be lost to other relaxation

processes. As extensively discussed in chapter 1, when imaging voltage every photon is valuable, rendering this approach inherently flawed. The potential drastic reduction in background noise made possible through this approach may overcome this flaw though. To date, little work has been done to explore these important concerns in a potentially fruitful approach toward genetic targeting of Cy5 VF dyes.

4.4.5 Conclusion

Far-red fluorescent VF dyes represented an important goal for further refinement of PeT-based voltage sensors given their favorable wavelengths of fluorescence for biological application. *A priori*, VF dyes with a Cy5-like fluorophore in place of a fluorescein should be possible considering the universal physical chemical processes involved. Encouragingly, the lessons learned in VF dye development learned in chapters 2 and 3 proved invaluable toward realizing Cy5-based dyes with appreciable membrane staining and voltage sensitivities. Both tuning of the driving force for electron transfer and optimization of the bridge offered significant advancements in the development of VF Red, the best Cy5-based VF dye synthesized, just as they did in they did in the development of fluorescein-based VF dyes. There is no reason to think this rational design of probes cannot be applied to numerous other fluorophores if they offered meaningful improvements on VF Red or VF2.1OMe.H discussed in chapter 2. Increases to voltage sensitivity will always offer an avenue toward better sensors, but with a 25% ΔF/F per 100 mV, VF Red represents a valuable probe for many applications in its current form, and an important stepping stone for further development.

4.5 Bibliography

1. Jacques, S. L. Optical properties of biological tissues: a review. *Phys. Med. Biol.* **58,** R37–61 (2013).

2. Chung, K., Wallace, J., Kim, S.-Y., Kalyanasundaram, S., Andalman, A. S., Davidson, T. J., Mirzabekov, J. J., Zalocusky, K. a, Mattis, J., Denisin, A. K., Pak, S., Bernstein, H., Ramakrishnan, C., Grosenick, L., Gradinaru, V. & Deisseroth, K. Structural and molecular interrogation of intact biological systems. *Nature* **497,** 332–7 (2013).

3. Weissleder, R. A clearer vision for in vivo imaging Progress continues in the development of smaller , more penetrable probes for biological imaging . Toward the phosphoproteome. *Nat. Biotechnol.* **19,** 316–317 (2001).

4. Boyden, E. S., Zhang, F., Bamberg, E., Nagel, G. & Deisseroth, K. Millisecond-timescale, genetically targeted optical control of neural activity. *Nat. Neurosci.* **8,** 1263–8 (2005).

5. Ohkura, M., Sasaki, T., Sadakari, J., Gengyo-Ando, K., Kagawa-Nagamura, Y., Kobayashi, C., Ikegaya, Y. & Nakai, J. Genetically encoded green fluorescent Ca2+ indicators with improved detectability for neuronal Ca2+ signals. *PLoS One* **7,** e51286 (2012).

6. Zhao, Y., Araki, S., Wu, J., Teramoto, T., Chang, Y.-F., Nakano, M., Abdelfattah, A. S., Fujiwara, M., Ishihara, T., Nagai, T. & Campbell, R. E. An expanded palette of genetically encoded Ca^{2+} indicators. *Science* **333,** 1888–91 (2011).

7. Lin, J. Y., Knutsen, P. M., Muller, A., Kleinfeld, D. & Tsien, R. Y. ReaChR: A red-shifted variant of channelrhodopsin enables deep transcranial optogenetic excitation. *Nat. Neurosci.* **16,** 1499–1508 (2013).

8. Klapoetke, N. C., Murata, Y., Kim, S. S., Pulver, S. R., Birdsey-Benson, A., Cho, Y. K., Morimoto, T. K., Chuong, A. S., Carpenter, E. J., Tian, Z., Wang, J., Xie, Y., Yan, Z., Zhang, Y., Chow, B. Y., Surek, B., Melkonian, M., Jayaraman, V., Constantine-Paton, M., Wong, G. K.-S. & Boyden, E. S. Independent optical excitation of distinct neural populations. *Nat Meth* **11,** 338–346 (2014).

9. Lin, J. Y., Lin, M. Z., Steinbach, P. & Tsien, R. Y. Characterization of Engineered Channelrhodopsin Variants with Improved Properties and Kinetics. *Biophys. J.* **96,** 1803–1814 (2009).

10. Scanziani, M. & Häusser, M. Electrophysiology in the age of light. *Nature* **461,** 930–939 (2009).

11. de Silva, a. P., Gunnlaugsson, T. & Rice, T. E. Recent evolution of luminescent photoinduced electron transfer sensors. A review. *Analyst* **121,** 1759 (1996).

12. Kenmoku, S., Urano, Y., Kanda, K., Kojima, H., Kikuchi, K. & Nagano, T. Rational design of novel photoinduced electron transfer type fluorescent probes for sodium cation. *Tetrahedron* **60,** 11067–11073 (2004).

13. Schoutteten, L., Denjean, P. & Pansu, R. B. Photophysics of ‘Calcium Green 1’ in vitro and in live cells. *Pccp* **1,** 2463–2469 (1999).

14. Ueno, T., Urano, Y., Setsukinai, K., Takakusa, H., Kojima, H., Kikuchi, K., Ohkubo, K., Fukuzumi, S. & Nagano, T. Rational Principles for Modulating Fluorescence Properties of Fluorescein Fluorescence Quenching by the Electron-Deficient Ben-. 14079–14085 (2004).

15. Urano, Y., Kamiya, M., Kanda, K., Ueno, T., Hirose, K. & Nagano, T. Evolution of fluorescein as a platform for finely tunable fluorescence probes. *J. Am. Chem. Soc.* **127,** 4888–94 (2005).

16. Mujumdar, R. B., Ernst, L. a, Mujumdar, S. R., Lewis, C. J. & Waggoner, a S. Cyanine dye labeling reagents: sulfoindocyanine succinimidyl esters. *Bioconjug. Chem.* **4,** 105–111 (1993).

17. Peterka, D. S., Takahashi, H. & Yuste, R. Imaging voltage in neurons. *Neuron* **69,** 9–21 (2011).

18. Liu, X., Ramirez, S., Pang, P. T., Puryear, C. B., Govindarajan, A., Deisseroth, K. & Tonegawa, S. Optogenetic Stimulation of a Hippocampal Engram Activates Fear Memory Recall. *Nature* **484,** 381–385 (2012).

19. Patel, S. A., Richards, C. I., Hsiang, J. C. & Dickson, R. M. Water-soluble Ag nanoclusters exhibit strong two-photon-induced fluorescence. *J. Am. Chem. Soc.* **130,** 11602–11603 (2008).

20. Juillerat, A., Gronemeyer, T., Keppler, A., Gendreizig, S., Pick, H., Vogel, H. & Johnsson, K. Directed Evolution of O6-Alkylguanine-DNA Alkyltransferase for Efficient Labeling of Fusion Proteins with Small Molecules In Vivo. *Chem. Biol.* **10,** 313–317 (2003).

21. Los, G. V, Encell, L. P., Mcdougall, M. G., Hartzell, D. D., Karassina, N., Zimprich, C., Wood, M. G., Learish, R., Ohana, R. F., Urh, M., Simpson, D., Mendez, J., Zimmerman, K., Otto, P., Vidugiris, G., Zhu, J., Darzins, A., Klaubert, D. H., Bulleit, R. F. & Wood, K. V. HaloTag: A Novel Protein Labeling Technology for Cell Imaging and Protein Analysis. *ACS Chem. Biol.* **3,** 373–382 (2008).

22. Szent-Gyorgyi, C., Schmidt, B. F., Schmidt, B. a, Creeger, Y., Fisher, G. W., Zakel, K. L., Adler, S., Fitzpatrick, J. a J., Woolford, C. a, Yan, Q., Vasilev, K. V, Berget, P. B., Bruchez, M. P., Jarvik, J. W. & Waggoner, A. Fluorogen-activating single-chain antibodies for imaging cell surface proteins. *Nat. Biotechnol.* **26,** 235–40 (2008).

Chapter 5 Genetic Targeting of VF Dyes

5.1 Introduction

Recording fluorescent signal above the surrounding background noise is one of the great challenges of voltage sensitive probes in complex neuronal systems.[1] Small molecule sensors including VF dyes are generally designed to be broadly lipophilic, unable to distinguish between cells that are of interest for a given experiment, and those that are not. There are about 10 times more glial cells than neurons in a given brain.[2] These supporting cells generally have less interesting electrical signals for a vast majority of experiments, but they take up VF dye just as readily. Additionally, the brain has many different types of neurons with varying electrical signals in a given area that may not be relevant for a given experiment. Again, dye is taken up just as readily by these diverse types of neurons potentially confounding the desired recording. Combine these factors with probe that does not localize to the plasma membrane at all, and background noise can quickly drown out signal in the complex preparations most interesting for voltage sensor application.

Two main approaches toward addressing the issue of indiscriminate staining have been explored, either localizing probe only to membranes of interest, or turning on probe only in those membranes. Increasing affinity for cells of interest through covalent tags such as Halo has proven to be a challenge. In previous unpublished work, little difference was seen between cells with and without Halo tag given the already high affinity for all membranes VF dyes show.[3] The increased membrane affinity brought by Halo tag does not decrease the already high affinity for background cells inherent to VF dyes.

Masking the high affinity for membranes with hydrophilic groups to be removed for insertion into only membranes of interest is another potentially powerful approach. The use of

phosphate groups attached to di-4-ANEPPS and cleaved by phosphatases expressed on the surface of desired cells for selective membrane insertion was particularly interesting, but has stalled due to poor effective expression in neuronal systems.[4] Approaches like the phosphatase are attractive due to the catalytic nature of activation. A single enzyme can activate many individual molecules as opposed to a covalent tag which is forced to localize a single dye.

A second catalytic approach toward fluorescent VF dye localization acts by "turning on" fluorescence in only a select subset of cells or regions while other cells contain dye that has not been activated and cannot contribute to the background. Changes in FRET between two fluorophores where one is either quenched or never excited is a popular mechanism for targeting fluorescent signals when the probe itself may be more promiscuous.[5] As discussed earlier, FRET exhibits poor photon economy and is not a particularly efficient process for genetic targeting of voltage dyes. A related, more favorable avenue is to generate a highly fluorescent molecule from a non-fluorescent derivative via chemical modification. Cellular oxidation reporters are one successful example. Fluorophores such as fluorescein and Cy5 have been chemically reduced and applied to biological systems under oxidative stress capable of turning on fluorescence in either Cy5 or fluorescein via oxidation.[6,7] In addition to oxidative environments, enzymes such as horseradish peroxidase (HRP) and engineered derivatives like APEX2 are known to oxidize a range of molecules including fluorescein.[8,9]

VF dyes take advantage of favorable fluorescent characteristics of Cy5 and fluorescein to effectively report changes in potential. Additionally, VF dyes may be able to take advantage of the reactivity reduced Cy5 and fluorescein exhibit toward oxidizing enzymes like HRP to become active in a subset of cells and regions expressing these oxidizing enzymes.

VF dyes have been engineered as a lipophilic molecule containing a polar fluorophore electron acceptor and non-polar electron donor and bridge. These dyes have been shown to favorable localize to the plasma membrane when bath applied to brain slices and cellular

systems including HEK cells and cultured rat neurons in chapter 2. Perhaps the greatest challenge for applying VF dyes in more complex neuronal systems is the background noise generated by indiscriminate membrane staining. Reducing this noise would significantly improve the quality of data that could be collected through VF dyes in complex preparations.

In order to reduce background noise and improve VF dye performance toward broad application in neurobiology, reduced VF dyes were synthesized and shown to undergo reoxidation by HRP in combination with hydrogen peroxide in phosphate buffer. These dyes were then applied to cellular systems with no evidence of reoxidation under current preliminary experimental parameters. This initial work represents the first steps toward genetic targeting of VF dyes by enzymatically turning on fluorescence through oxidation.

5.2 Results

Reducing Cy5 to a stable, non-fluorescent species was an essential first step to test for potential reoxidation by HRP. The positively charged indolium moiety in the fluorophore represents a site for reduction by mild chemical treatment. Application of a relatively weak reductant, sodium borohydride, rapidly reduced Cy5 to a hydrogenated, non-fluorescent dye determined by UV-Vis and HPLC-MS in Figure 5.1. No NMR spectroscopy was performed to verify the location of reduction, but given literature precedent and the stark loss of absorbance in the far red, Cy5.DH shown in Figure 5.1a represents the likely product. Less than one equivalent was added at room temperature to generate spectra in Figure 5.1. Further addition of $NaBH_4$ generated numerous side products that were unidentifiable by HPLC-MS. A mixture of Cy5 starting material and Cy5.DH product that resulted from addition of less than one equivalent of $NaBH_4$ was not further purified given that this was a proof of concept experiment aimed at exploring whether Cy5.DH could be a potential substrate for HRP

oxidation. The additional Cy5 starting material was thought to have no impact on this reactivity and would give a static absorbance by UV-Vis seen in the initial measurement in Figure 5.1c.

Excitingly, once both HRP and hydrogen peroxide were added, the far-red absorbance increased at 650 nm where Cy5 absorbance is typically seen, indicating an oxidation of Cy5.DH back to fluorescent Cy5. This reaction appeared quite rapid, as the initial measurement resulted in a 3 fold increase in the fluorescent molecule. After 7.5 minutes, no further oxidation to product was observed indicating the reaction was nearing completion, thus further measurements were not performed.

A similar experiment with a chemically reduced Cy5-based VF dye was performed as well. Here again, less than one equivalent of $NaBH_4$ was added in order to prevent unknown side products. Synthesis of VF Cy5.BH was determined by UV-Vis spectroscopy and HPLC-MS which showed a similar stark drop in far red absorbance and a corresponding mass spectrum indicating the addition of two hydrogens to the fluorescent precursor. The mixture of VF Cy5.DH and VF Cy5.D was added to a cuvette and monitored for changes in absorbance. No change was observed until both HRP and hydrogen peroxide were added. After addition, a modest increase in absorbance was seen. Measurements 5 min., 10 min., and 15 min. after initial addition of HRP eventually gave a modest 1.2 fold increase in fluorescence at 650 nm that remained level after 10 min. of incubation with HRP and hydrogen peroxide.

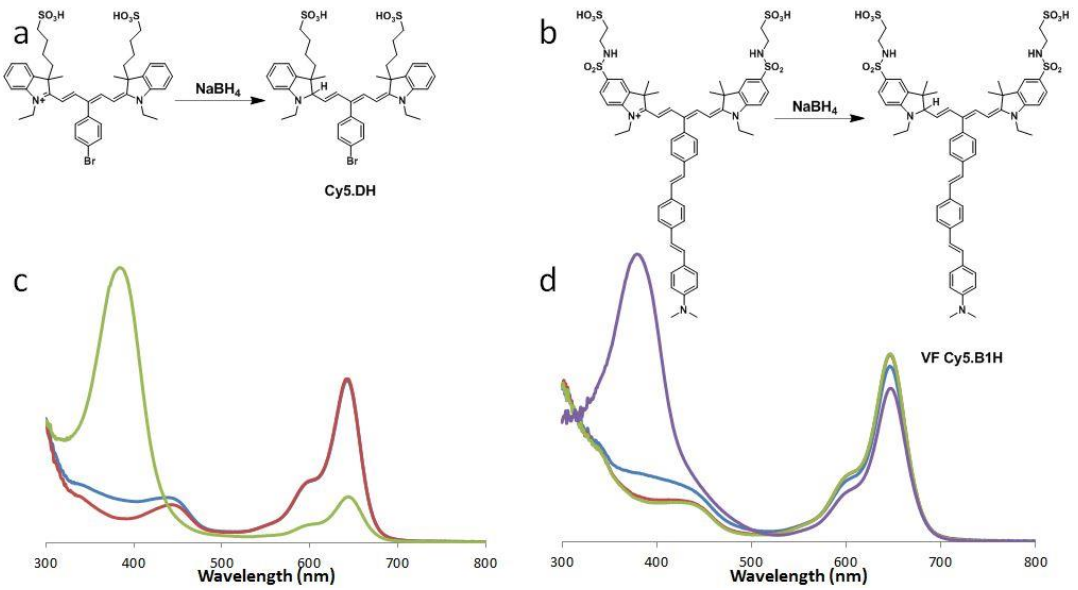

Figure 5.1 Synthesis of reduced Cy5 derivatives and oxidation by HRP with hydrogen peroxide. (a)Synthesis of Cy5.DH with sodium borohydride. (b) Synthesis of VF Cy5.B1H with sodium borohydride. (c) UV-Vis spectroscopy of Cy5.DH in 1M pH 7.4 phosphate buffer alone at room temperature (green). Spectra taken after the initial addition of H_2O_2 and HRP (red) and 7.5 min. after addition (blue). (d) The same set up as in (c) however VF Cy5.B1H was added (purple). Spectra taken after the initial addition of H_2O_2 and HRP (blue), 5 min. after addition (green), and 10 min. after addition (red) are shown as well.

Work *in vitro* indicated that VF Cy5.DH could potentially undergo oxidation by HRP in conjunction with hydrogen peroxide. Turning on fluorescence upon insertion into a biological membrane of interest was the next goal after showing proof of concept oxidation *in vitro*. VF dyes are generally synthesized in small quantities, and at times initial synthesis does not give sufficient dye to be applied in HEK cells. Synthesis of VF Cy5.DH was quite limited, and given the mixture of reduced product with fluorescent starting material, a new reduced VF dye was attempted. VF Cy5.A2 was made in much higher quantities after the initial experiments with VF Cy5.DH. It offered an ideal starting molecule given the strong membrane staining seen in Chapter 4. Reduction of VF Cy5.A2 proved to be more challenging as addition of sodium borohydride in any quantities curiously lead to the formation of numerous side products unidentifiable by HPLC-MS. Given the sensitivity to reduction, a still milder reductant, sodium cyanoborohydride, was applied. Addition of one equivalent of sodium

cyanoborohydride caused a color change from green to yellow indicating that reduction most likely took place. Upon exposure to atmospheric oxygen however, the characteristic green color of VF Cy5.A2 returned. In addition, no reduced product was observed by HPLC-MS. Further experiments using an excess of sodium cyanoborohydride gave a stable yellow product that did not change color upon exposure to atmospheric oxygen. This yellow product appeared to be doubly reduced VF Cy5.A1H2 as seen in Figure 5.2a. This over-reduction was unexpected, but appeared to be the only stable reduced form of the dye available. Unlike VF Cy5.DH, enough VF Cy5.A1H2 was made to be purified and applied to HEK cells. Staining of HEK cells appeared to have no effect on the health of HEK cells as they appeared normal in bright-field images seen in Figure 5.2b-d. Cells stained with VF Cy5.A1H2 appeared non-fluorescent as expected in Figure 5.2b. Addition of exogenous HRP and hydrogen peroxide to the cell bath did not increase fluorescence at all after incubation for 25 minutes and 60 minutes in Figure 5.2c and d. Importantly, HEK cells appeared healthy as seen under bright-field fluorescence even under longer exposer to HRP and peroxide.

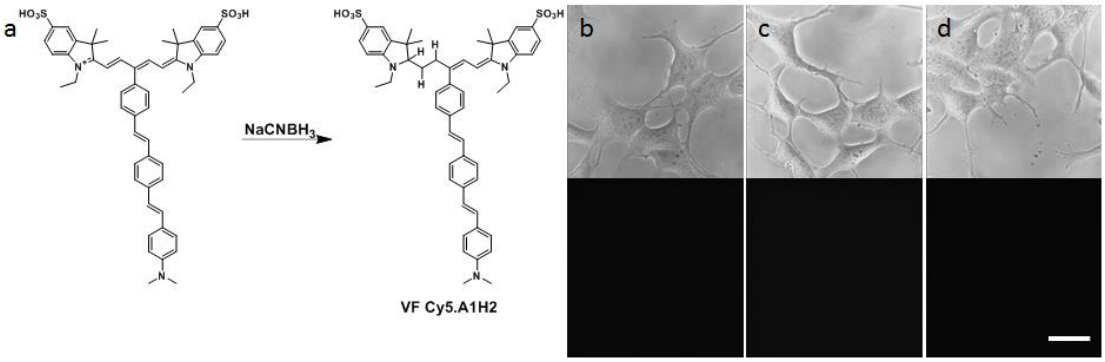

Figure 5.2 Synthesis and HEK cell characterization of VF Cy5.A1H2. (a) Synthesis of VF Cy5.A1H2 with sodium cyanoborohydride. (b) Brightfield (top) and epifluorescent (bottom) image of HEK cells stained with VF Cy5.A1H2. (c) Brightfield (top) and epifluorescent (bottom) image of HEK cells stained with VF Cy5.A1H2 and a 25 min. incubation with 2μM HRP and 100 μM hydrogen peroxide. (d) Same cell culture imaged in (c) after 1 hour.

Chemical reduction and enzymatic oxidation by HRP is potentially feasible for fluorescein-based VF dyes in addition to Cy5-based dyes. Reduction of fluorescein to a non-fluorescent molecule, FlH, was achieved by mild reduction with sodium borohydride almost quantitatively after an over-night reaction at room temperature as monitored by HPLC-MS. FlH was added to phosphate buffer where oxidation to fluorescein was monitored via UV-Vis spectroscopy. Initial measurements showed a significant amount of oxidized FlH in solution that remained stable in measurements not shown. Upon addition of both HRP and hydrogen peroxide a 1.3 fold increase in absorbance was observed. A small increase in absorbance was seen after a 5 minute incubation, but after 10 minutes a 2.1fold increase was seen which leveled off at a 2.5 fold increase in absorbance after 15 minutes. The absorbance spectra began widening and appeared to diverge from the absorbance spectrum of fluorescein more significantly at this point, where further measurement was stopped.

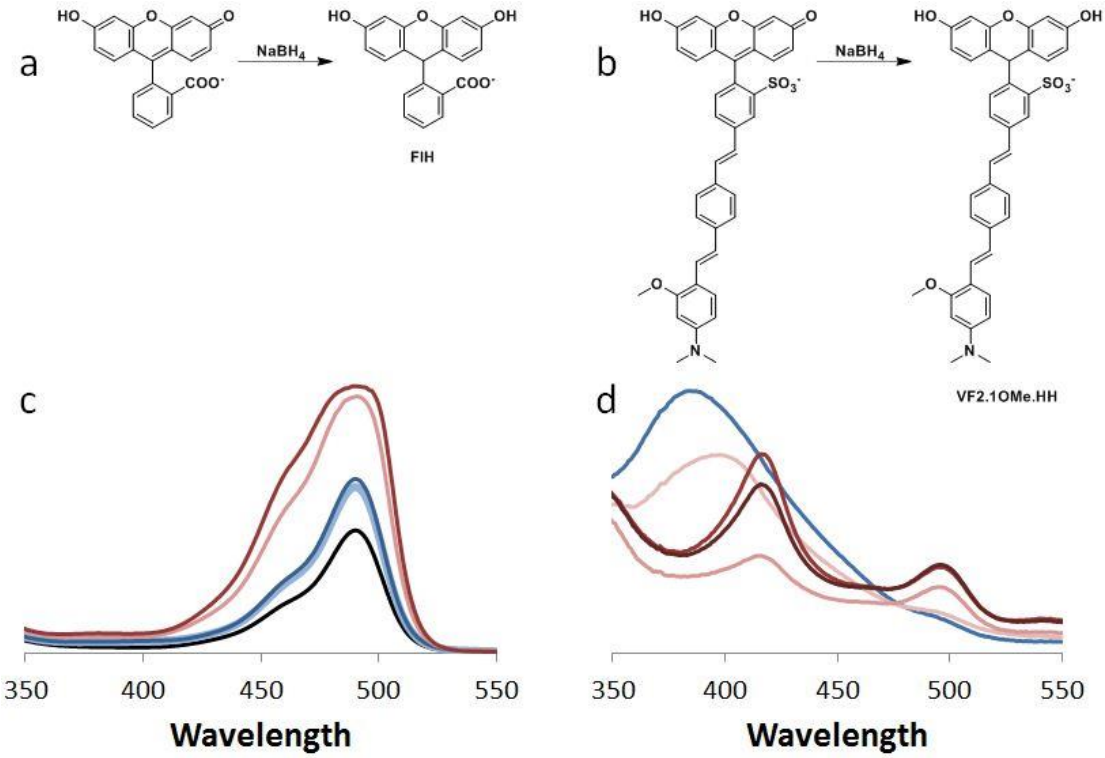

Figure 5.3 Synthesis of reduced fluorescein (FlH) and VF2.1OMe.HH followed by oxidation by HRP with hydrogen peroxide. (a) Synthesis FlH with sodium borohydride. (b) Synthesis of VF Cy5.B1H with sodium borohydride. (c) UV-Vis spectroscopy of FlH in 1M pH 7.4 phosphate buffer at room temperature (black). Spectra taken after the initial addition of H_2O_2 and HRP (light blue), 5 min. after addition (dark blue), 10 min. after addition (light red), and 15 min. after addition (dark red). (d) The same set up as in (c) however VF2.1.OMe.HH was added (blue). Spectra taken after the initial addition of H_2O_2 and HRP (light pink), 5 min. after addition (red), and 10 min. after addition (dark red) are shown as well.

With the successful oxidation of FlH, the focus was then shifted to fluorescein-based VF dyes. VF2.1OMe.H was shown to be an excellent voltage sensitive dye in chapter 2 with a 48% ΔF/F per 100 mV. VF2.1OMe.H was reduced by sodium borohydride just as FlH to give a non-fluorescent VF dye named VF2.1OMe.HH as shown in Figure 5.3b. The structure of VF2.1OMe.HH was inferred based on previous work reducing fluorescein and verified by UV-Vis Absorbance spectroscopy and HPLC-MS.

VF2.1OMe.HH was then oxidized by HRP in phosphate buffer. Addition of VF2.1OMe.HH alone showed minimal oxidation by UV-Vis absorbance and appeared stable in buffer. Addition of HRP and hydrogen peroxide lead to an increase in absorbance typical

for fluorescein moieties and a reduction in the absorbance seen near 400 nm wavelengths. After continuous incubation at room temperature for 10 minutes a 2.7 fold increase in absorbance was seen at 500 nm where sulfofluorescein shows strong absorbance.

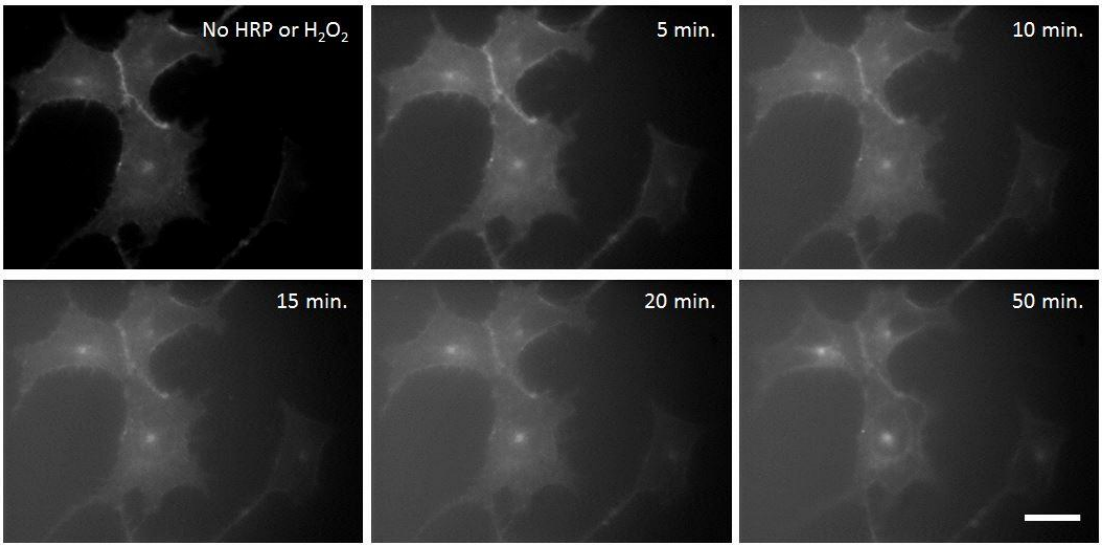

Figure 5.4 Epifluorescent images of VF2.1OMe.HH oxidation in HEK cells. Initial fluorescence of cells stained with VF2.1OMe.HH (top left) followed by addition of 1.5 μM HRP and 60 μM hydrogen peroxide at room temperature. Images of the same cells were taken over a 1 hour time course.

VF2.1OMe.HH was then applied to HEK cells to test for oxidation by HRP when localized to the plasma membrane. After a 15 minute incubation at 37°C, significant amounts of fluorescence around the cell membrane were observed even with no addition of HRP or hydrogen peroxide. Fluorescent images of HEK cells appeared similar to HEK cells stained with VF2.1OMe.H in chapter 2, though not quite as bright. Upon addition of HRP and hydrogen peroxide no measurable increase in fluorescence was observed. Over the course of one hour, membrane fluorescence remained steady. However, background fluorescence did begin to increase and qualitatively appeared to continue to increase over time. In addition, localization of fluorescent signal began to alter over the 1 hour time course. By the 50 minute

mark, internal membranes appeared to be stained as well with fluorescent signals clearly visible within single HEK cells.

5.3 Methods

5.3.1 General Synthetic and Analytical Measurements

As described in Chapter 2

5.3.2 Data Analysis

As described in Chapter 2

5.3.3 Patch Clamping Neurons and HEK Cells

As described in Chapter 2

5.3.4 Synthetic Scheme

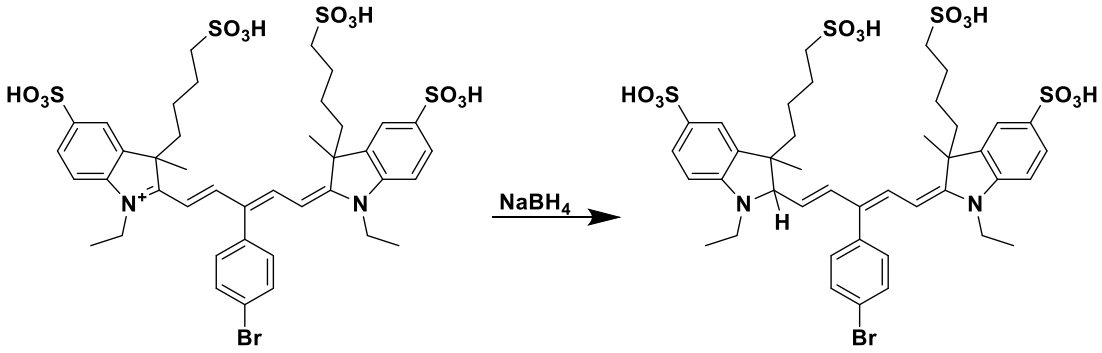

Synthesis of Cy5.DH

An oven dried 1.5 mL vial was charged with 2-((1E,3Z)-3-(4-bromophenyl)-5-((E)-1-ethyl-3-methyl-5-sulfo-3-(4-sulfobutyl)indolin-2-ylidene)penta-1,3-dien-1-yl)-1-ethyl-3-methyl-5-sulfo-3-(4-sulfobutyl)-3H-indol-1-ium (22 mg, 0.027 mmol, 1 eq.) and sodium borohydride (1 mg, .027mmol, 1 eq.) in methanol (0.1 mL) resulting in an immediate change in color from dark blue to a light green with bubbling. The solution was transferred to a UV-Vis cuvette for absorptivity analysis.

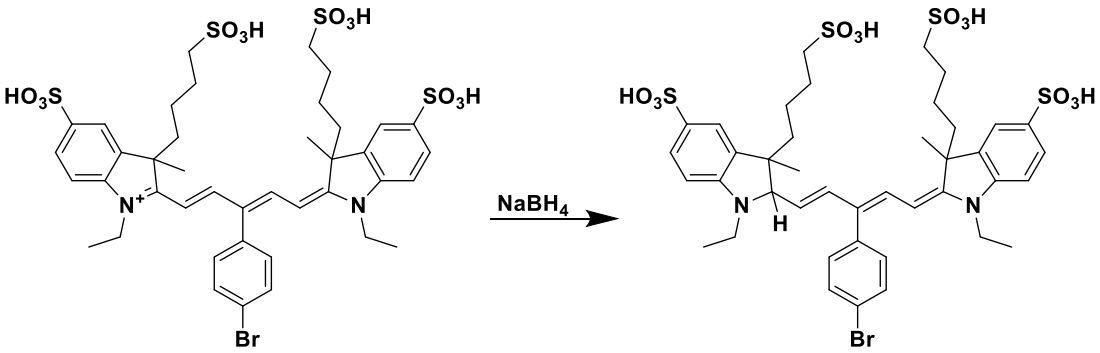

Synthesis of Cy5.DH

An oven dried 1.5 mL vial was charged with 2-((1E,3Z)-3-(4-bromophenyl)-5-((E)-1-ethyl-3-methyl-5-sulfo-3-(4-sulfobutyl)indolin-2-ylidene)penta-1,3-dien-1-yl)-1-ethyl-3-methyl-5-sulfo-3-(4-sulfobutyl)-3H-indol-1-ium (22 mg, 0.027 mmol, 1 eq.) and sodium borohydride (1 mg, .027mmol, 1 eq.) in methanol (0.1 mL) resulting in an immediate change in color from dark blue to a light green with bubbling. The solution was transferred to a UV-Vis cuvette for absorptivity analysis.

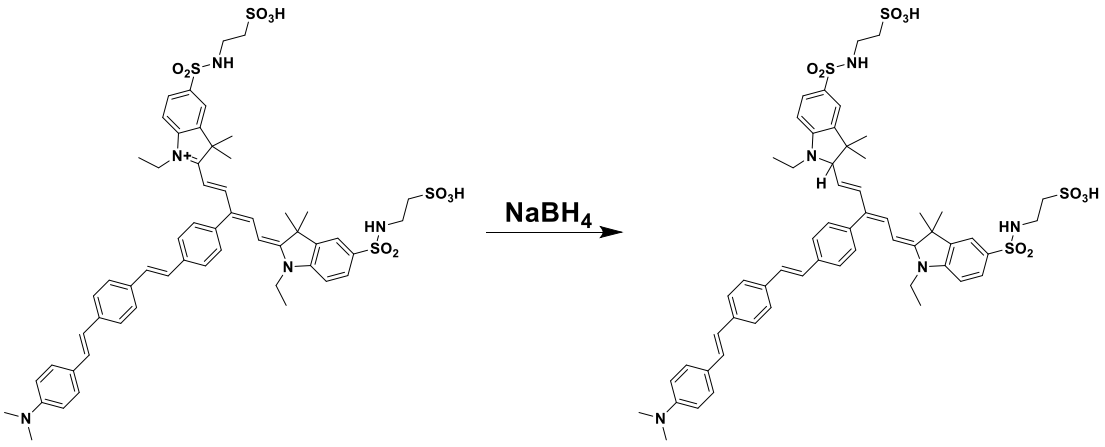

Synthesis of VF Cy5.B1H

An oven dried 1.5 mL vial was charged with VF Cy5.B1 (1 mg, 0.09 μmol, 1 eq.) and sodium borohydride (0.03 mg, .09mmol, 1 eq.) in methanol (0.02 mL) resulting in an immediate change in color from green to yellow. The solution was transferred to a UV-Vis cuvette for absorptivity analysis.

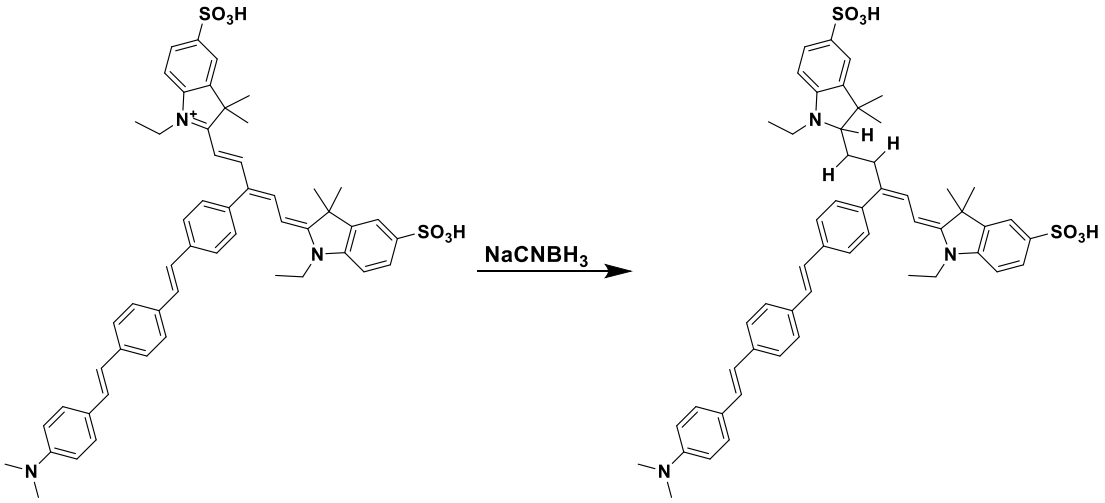

Synthesis of VF Cy5.A1H2

An oven dried 1.5 mL vial was charged with VF Cy5.A1H2 (1 mg, 1.12μmol, 1 eq.) and sodium cyanoborohydride (0.1 mg, 1.6 μmol, 1.4 eq.) in methanol (0.02 mL) and left overnight where a color change from dark green to yellow was observed. The solution was acidified with minimal acetic acid and purified by preparative HPLC on a Luna C_{18} column with a gradient of 10% MeCN in 1M triethylammonium acetate pH7 in H_2O ramping to 90% MeCN in 20 minutes. The resulting material was concentrated to dryness to give approximately 1 mg of a yellow solid. HPLC-MS found $[M^+] = 898.4$

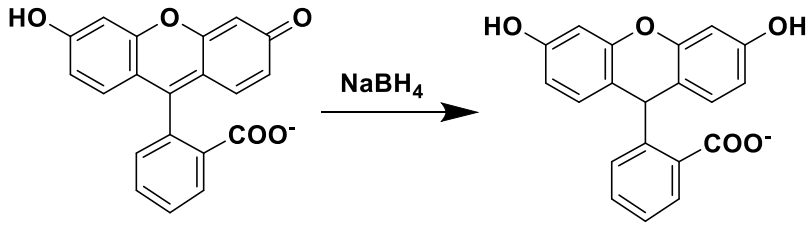

Synthesis of FlH

An oven dried round bottom flask was charged with fluorescein (100 mg, 0.3 mmol, 1 eq.) and sodium borohydride (11 mg, 0.3 mmol., 1 eq.) in methanol (1 mL). The reaction was left to stir at room temperature for 2 hours after which the solution was acidified with minimal acetic acid and purified by preparative HPLC on a Luna C_{18} column with a gradient of 10% MeCN

in 1M triethylammonium acetate pH7 in H_2O ramping to 90% MeCN in 20 minutes. The resulting material was concentrated to dryness to give approximately 1 mg of a yellow solid. HPLC-MS found [M^-] = 332.8

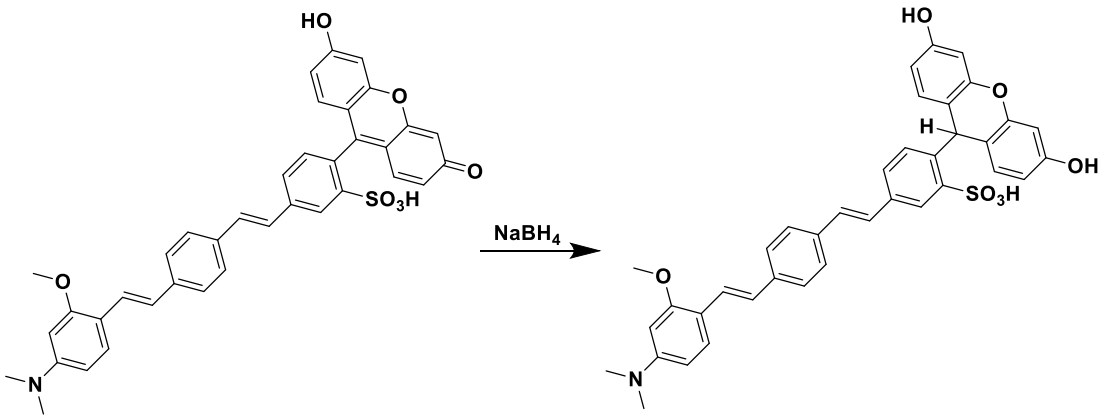

Synthesis of VF2.1OMe.HH

An oven dried round bottom flask was charged with VF2.1OMe.H (50 mg, 0.15 mmol, 1 eq.) and sodium borohydride (5 mg, 0.15 mmol., 1 eq.) in methanol (1 mL). The reaction was left to stir at room temperature overnight after which the solution was acidified with minimal acetic acid and purified by preparative HPLC on a Luna C_{18} column with a gradient of 10% MeCN in 1M triethylammonium acetate pH7 in H_2O ramping to 90% MeCN in 20 minutes. The resulting material was concentrated to dryness to give approximately 10 mg of a yellow solid. HPLC-MS found [M^-] = 648.3

5.4 Discussion

Ideally, VF dye fluorescence would be genetically targeted where only a subset of dye would be oxidized to a fluorescent VF dye for recording of membrane potentials. This is an important goal given that indiscriminate staining is perhaps the greatest weakness of VF dyes. Outlined above are preliminary results hinting that both Cy5 and fluorescein based dyes may

be amenable toward genetic targeting by oxidation to fluorescent voltage sensors in only membranes of interest. The experiments described were a first pass that need to be performed with greater precision before firm conclusions can be drawn from the data.

Synthesis and purification of reduced VF dyes requires revision as UV-Vis absorbance spectra showed high levels of starting material in many samples that convoluted imaging experiments. Even with the addition of oxidized fluorescent dyes, in all experiments performed inside a cuvette, increases in absorbance were observed commensurate with HRP oxidation of reduced dye back to fluorescent species. This was the first instance where VF dyes were shown to act as enzymatic substrates undergoing anywhere from a 1.2 fold increase in fluorescence seen in VF Cy5.B1H to a 3 fold increase seen in Cy5.DH. With regard to both fluorescein and Cy5, the VF dye showed a lower increase in absorbance relative to the fluorophore alone. This may be a result of the fluorophore alone being a better substrate for HRP. It is possible that the full VF dyes aggregated or crashed out of the phosphate solution making it inaccessible to HRP for oxidation as well. In both Figure 5.1 and Figure 5.3 there is a much more dramatic decrease in absorbance seen in the 350 nm to 400 nm range than increase in the 450 nm to 700 nm range. This could potentially indicate that much of the reduced dye is being oxidized to a range of other molecules that do not have fluorophore-like properties or high voltage sensitivities for voltage imaging experiments. Dye that is oxidized to these non-VF dye molecules would presumably contribute only to toxicity. Unfortunately, little can be done to control what the oxidation product generated by HRP is. Oxidation through other enzymes such as APEX2 could generate a different profile of products yielding more fluorescent dye. In an effort to more closely determine what the products of HRP oxidation are, HPLC-MS and NMR could be utilized.

Chemical reduction of Cy5-based dyes appeared to be less stable than fluorescein-based dyes. VF Cy5.A1H2 appeared to only undergo multiple reductions, where the single

reduced species appeared to oxidize back to VF Cy5.A2 upon exposure to atmospheric oxygen. Curiously, this was not seen with the Cy5.B and Cy5.D acceptors. There are no apparent chemical reasons this should be the case. Cy5 did appear more sensitive to chemical reduction as more than a single equivalent of reducing agent gave a wide range of products with varying optical properties. It is possible reduced Cy5 is too chemically labile to act as a reliable fluorogentic probe based on this result.

Fluorescein-based VF dyes such as VF2.1OMe.H appeared more amenable to chemical reduction giving minimal side products and no apparent stability issues when exposed to atmospheric oxygen. Auto-oxidation of VF2.1OMe.HH did appear to be of concern when applied to HEK cells however. When characterized in phosphate buffer solution, minimal absorbance in wavelengths beyond 450 nm was observed in VF2.1OMe.HH indicating very little auto-oxidation took place. Upon addition of VF2.1OMe.HH to HEK cells, significant levels of fluorescence were observed with no additional oxidizing agents or HRP indicating that HEK cells stained may have oxidized VF2.1OMe.HH back to VF2.1OMe.H. An additional possibility is the fluorescence is the result of VF2.1OMe.H and other fluorescent impurities present. This appears unlikely given the high purity seen by HPLC-MS. Dye stability with regard to fluorescein may be achieved by acetylation of the reduced fluorescein moiety which has been shown to limit auto-oxidation.[10]

Overall, a first pass in HEK cells appeared to require further optimization, while early experiments in phosphate buffer provided a bit more promise. Developing stable and reliable reduced VF dyes is the step toward exploring the viability of this approach to genetic targeting. The encouraging results seen *in vitro* appear to warrant further effort toward developing genetically targeted VF dyes.

5.5 Bibliography

1. Combs, C. A. Fluorescence microscopy: A concise guide to current imaging methods. *Curr. Protoc. Neurosci.* 1–19 (2010). doi:10.1002/0471142301.ns0205s00

2. Azevedo, F. A. C., Carvalho, L. R. B., Grinberg, L. T., Farfel, J. M., Ferretti, R. E. L., Leite, R. E. P., Filho, W. J., Lent, R. & Herculano-Houzel, S. Equal numbers of neuronal and nonneuronal cells make the human brain an isometrically scaled-up primate brain. *J. Comp. Neurol.* **513,** 532–541 (2009).

3. Los, G. V, Encell, L. P., Mcdougall, M. G., Hartzell, D. D., Karassina, N., Zimprich, C., Wood, M. G., Learish, R., Ohana, R. F., Urh, M., Simpson, D., Mendez, J., Zimmerman, K., Otto, P., Vidugiris, G., Zhu, J., Darzins, A., Klaubert, D. H., Bulleit, R. F. & Wood, K. V. HaloTag: A Novel Protein Labeling Technology for Cell Imaging and Protein Analysis. *ACS Chem. Biol.* **3,** 373–382 (2008).

4. Ng, D. N. & Fromherz, P. Genetic Targeting of a Voltage-Sensitive Dye by Enzymatic Activation of Phosphonooxymethyl-ammonium Derivative. *ACS Chem. Biol.* **6,** 444–451 (2011).

5. Savariar, E. N., Felsen, C. N., Nashi, N., Jiang, T., Ellies, L. G., Steinbach, P., Tsien, R. Y. & Nguyen, Q. T. Real-time in Vivo molecular detection of primary tumors and metastases with ratiometric activatable cell-penetrating peptides. *Cancer Res.* **73,** 855–864 (2013).

6. Miller, E. W., Bian, S. X. & Chang, C. J. A Fluorescent Sensor for Imaging Reversible Redox Cycles in Living Cells. *J. Am. Chem. Soc.* **129,** 3458–3459 (2007).

7. Kim, J. Y., Choi, W. Il, Kim, Y. H. & Tae, G. Highly selective in-vivo imaging of tumor as an inflammation site by ROS detection using hydrocyanine-conjugated, functional nano-carriers. *J. Control. Release* **156,** 398–405 (2011).

8. LeBel, C. P., Ischiropoulos, H. & Bondy, S. C. Evaluation of the probe 2',7'-dichlorofluorescin as an indicator of reactive oxygen species formation and oxidative stress. *Chem. Res. Toxicol.* **5,** 227–231 (1992).

9. Lam, S. S., Martell, J. D., Kamer, K. J., Deerinck, T. J., Ellisman, M. H., Mootha, V. K. & Ting, A. Y. Directed evolution of APEX2 for electron microscopy and proximity labeling_Supplementary. *Nat. Methods* **12,** 51–54 (2014).

10. Brandt, R. & Keston, A. S. Synthesis of Diacetyldichlorofluorescin: a Stable Reagent for Fluorometric Analysis. *Anal. Biochem.* **11,** 6–9 (1965).